

Elena Forcén Vázquez

Metal Citrate Cubanes: Synthesis, Characterization and Properties

Departamento
Química Inorgánica

Director/es

Falvello, Lawrence Rocco
Palacio Parada, Fernando

<http://zaguan.unizar.es/collection/Tesis>



Universidad
Zaragoza

Tesis Doctoral

METAL CITRATE CUBANES: SYNTHESIS, CHARACTERIZATION AND PROPERTIES

Autor

Elena Forcén Vázquez

Director/es

Falvello, Lawrence Rocco
Palacio Parada, Fernando

UNIVERSIDAD DE ZARAGOZA

Química Inorgánica

2014

Metal Citrate Cubanes: Synthesis, Characterization and Properties

Cubanos Metálicos con el Ligando Citrato:
Obtención, Caracterización y Propiedades



PhD Thesis
Elena Forcén Vázquez
Zaragoza 2014

University of Zaragoza
Faculty of Science
Department of Inorganic Chemistry



Universidad Zaragoza



FACULTAD DE CIENCIAS

DEPARTAMENTO DE QUÍMICA

INORGÁNICA

“Metal Citrate Cubanes: Synthesis, Characterization and Properties (Cubanos Metálicos con el Ligando Citrato: Obtención, Caracterización y Propiedades)”

Memoria presentada en la Facultad de Ciencias de la Universidad de Zaragoza para optar al grado de Doctor en Ciencias, Sección Químicas, por el Licenciado

Elena Forcén Vázquez



D. Fernando Palacio Parada, Profesor de Investigación del Consejo Superior de Investigaciones Científicas (CSIC) y D. Lawrence Rocco Falvello, Catedrático de Química Inorgánica de la Universidad de Zaragoza.

CERTIFICAN:

Que la Memoria de Tesis Doctoral titulada “Metal Citrate Cubanes: Synthesis, Characterization and Properties”, presentada por la Lcda. Elena Forcén Vázquez, ha sido realizada bajo su dirección, de acuerdo con el proyecto de tesis aprobado en su día, en el Departamento de Química Inorgánica de la Universidad de Zaragoza y el Instituto de Ciencia de Materiales de Aragón (ICMA), de la Universidad de Zaragoza y del Consejo Superior de Investigaciones Científicas (CSIC), y autorizan asimismo su presentación.

Zaragoza, 16 de Septiembre de 2014

Fdo.: Dr. Fernando Palacio Parada

Fdo.: Dr. Larry R. Falvello

Para ti, papá.

Acknowledgements

(Agradecimientos)

Con estas líneas me gustaría tener unas palabras de agradecimiento para todas aquellas personas que de una manera u otra han estado presentes durante estos años de esfuerzo y trabajo.

En primer lugar, a mis directores de tesis; Larry, a quien tuve la suerte de conocer como estudiante y el placer de poder asistir a sus clases. Gracias por todo lo que me has enseñado, por tu confianza, dedicación, tiempo y paciencia. Por todos esos días de trabajo y conversaciones sobre mil temas que sin duda alguna me han enriquecido como científico y persona. Y Fernando, gracias por confiar en mí desde el primer día, animarme y apoyarme en todo, por hacer que las cosas hayan sido “sencillas” y la gran cantidad de cosas que he podido aprender en estos años sobre ciencia y sobre la vida. Gracias a los dos por haber querido formar a esta “científica”, espero no defraudaros.

Mención especial merece Milagros, quien pese a no ser oficialmente mi directora siempre ha estado ahí ejerciendo como tal. Gracias por escucharme y estar dispuesta a lo que hiciera falta y dándome siempre buenos consejos e ideas. Sin duda has sido una parte imprescindible.

A Isabel, mi compi de laboratorio. Siempre preparada para todo y enseñándome infinidad de cosas que ni siquiera sabía que existieran. Todo esto no hubiera sido lo mismo sin ti. A Monika, mi rubia eslovaca, es imposible pensar en el laboratorio y no acordarse de ti y de tu buen humor (y de todas aquellas deliciosas recetas que nos preparabas). No puedo olvidarme tampoco de todos aquellos compañeros que han ido pasando por el laboratorio, de Gema, Nuha, Rubén, Rosa y de los múltiples visitantes que han ido llenando de vida el laboratorio.

De gran importancia para mí ha sido mi grupo, el M4 y todos aquellos que han formado y forman parte de él. Mención especial para Javier Campo quien ha estado siempre presente durante estos años. Gracias por todas esas charlas, reuniones, viajes, etc. Por estar siempre disponible para mí, ayudándome y dándome buenos consejos e ideas. A Cris, compañera de aventuras y de esas tardes que se hacían noches. Gracias por tu paciencia con la parte magnética y por contestar siempre con un “sí” a todas mis peticiones. A Germán y Emma por facilitarme la vida y estar siempre dispuestos a ayudarme con una sonrisa en la cara. A Ángel, Rafa, Javier, Clara, Lamiaa, Rodney, José Luis, a los compañeros de Grenoble y en general a todos los que habéis formado parte de este gran grupo. Siempre recordaré esas reuniones y viajes juntos. Gracias por hacerme sentir apoyada y arropada durante estos años.

Thanks to the Nottingham people, Stephen, Andrea, Irina, Simon, Victoria, Nic, Barry, Ben, etc. I really had a great time there. Thanks for making me feel at home and for everything I learnt during my stay. I take this opportunity to express my gratitude to Prof. Neil Champness for kindly accepting to my proposal and for the time he devoted to me.

Gracias a aquellos compañeros con los que he tenido la suerte de colaborar a lo largo de estos años. Gracias a Rosa Llusar (y a su equipo) por ser tan buena anfitriona y hacernos sentir como en casa en nuestras visitas a Castellón y echarnos un cable con las estructuras problemáticas. Gracias también a Garry, Silvia y Sax por todo su tiempo y dedicación durante las estancias en el ILL.

Me gustaría acordarme también de todas aquellas personas que desde mis comienzos como estudiante de química despertaron en mí esta vocación por la ciencia. Gracias entre otros a José Antonio Mayoral, Paco Martínez, María Pilar García, Miguel Ángel Esteruelas, etc.

Merecen mención todos mis compañeros de departamento, tanto los de Química Inorgánica como los de Física de la Materia Condensada, por todas esas charlas y debates de pasillo y a los miembros de los servicios de apoyo a la investigación de la universidad por su inestimable colaboración. Asimismo, me acuerdo de todas aquellos “colegas” que he tenido el placer de conocer en congresos y viajes, con quienes aprendí que trabajo y diversión no tienen por qué estar reñidos. Espero poder seguir compartiendo momentos con vosotros.

Por último pero no menos importante, un gracias muy especial a mi familia y amigos, por hacer que la vida sea mejor. Gracias a Susi, Nuri, Lore, Isabel, Vicky, Isa por vuestra amistad, por estar siempre ahí, tanto en los buenos como en los malos momentos. Espero poder seguir a vuestro lado muchos años más. Gracias a Jon, por estar siempre a mi lado animándome, escuchándome (aunque a veces te hable de cosas que te suenan a chino) y apoyándome en todo. Y finalmente gracias a mis padres y mis hermanas. Todo lo que soy os lo debo a vosotros. Soy afortunada por tener una familia tan maravillosa. Os quiero.

A todos y cada uno de vosotros, GRACIAS.

Table of contents

Preface

Part I: Transition metal citrate cubanes

Chapter 1: Two Different Linkage Isomers for the $[M_4(\text{citrate})_4]^{8-}$ Unit: Structural Study.

1.2 Introduction	2
1.3 Results and discussion	4
1.1 Summary and final remarks	20
References	22

Part II: Cobalt citrate cubanes

Chapter 2: Introduction II: Cobalt citrate cubanes

2.1 A brief overview of magnetism	27
2.2 Magnetism of Co(II) ions	32
2.3 Molecule-based Magnets	33
2.4 Single Molecule Magnets	36
2.4.1 What is a SMM?	36
2.4.2 Magnetic behaviour: requirements and characteristics	37
2.4.3 Synthesis of SMM: different approaches	40
2.4.4 Classification of SMMs	44
2.4.4.1 SMM based on Co(II)	47
2.4.4.2 SMM based on cubanes	49
2.5 Deposition of SMMs on surfaces	51
2.6 Further perspectives and future applications	55
References	57

Chapter 3: 0-D Cobalt citrate cubanes

3.1 Experimental	64
3.1.1 Synthesis	64
3.1.2 Single Crystal X-Ray diffraction	64
3.1.3 Powder X-Ray diffraction	64
3.1.4 FT-IR spectroscopy	65
3.1.5 Elemental analysis	66
3.1.6 Thermogravimetric analysis (TGA)	66
3.1.7 Magnetic characterization	67
3.2 Results and discussion	67
3.2.1 Synthesis	67
3.2.2 Single Crystal X-Ray diffraction	68
3.2.3 Powder X-Ray diffraction	77

3.2.4	Magnetic characterization	80
3.3	Conclusions	82
	References	84
Chapter 4: 2-D Cobalt citrate cubanes		
4.1	A Tetragonal 2-D Array of Single-Molecule Magnets with Modulable Collective Behaviour	
4.1.1	Experimental	87
4.1.1.1	Synthesis	87
4.1.1.2	Single Crystal X-Ray diffraction	87
4.1.1.3	FT-IR spectroscopy	88
4.1.1.4	Elemental analysis	89
4.1.1.5	Magnetic characterization	89
4.1.2	Results and discussion	90
4.1.2.1	Synthesis	90
4.1.2.2	Single Crystal X-Ray diffraction	91
4.1.2.3	Magnetic characterization	94
4.2	Rhombically distorted 2-D net of SMMs	
4.2.1	Experimental	96
4.2.1.1	Synthesis	96
4.2.1.2	Single Crystal X-Ray diffraction	97
4.2.1.3	FT-IR spectroscopy	98
4.2.1.4	Magnetic characterization	98
4.2.2	Results and discussion	98
4.2.2.1	Single Crystal X-Ray diffraction	98
4.2.2.2	Magnetic characterization	102
4.3	Square 2-D Cobalt polymer of SMMs with additional magnetically active centres	
4.3.1	Experimental	104
4.3.1.1	Synthesis	104
4.3.1.2	Single Crystal X-Ray diffraction	105
4.3.1.3	FT-IR spectroscopy	106
4.3.1.4	Magnetic characterization	106
4.3.2	Results and discussion	106
4.3.2.1	Single Crystal X-Ray diffraction	106
4.3.2.2	Magnetic characterization	109
4.4	Conclusions	110
	References	113
Chapter 5: 3-D Cobalt citrate cubanes		
5.1	High-dimensionality polymer with diamondoid topology	
5.1.1	Experimental	116
5.1.1.1	Synthesis	116

5.1.1.2	Single Crystal X-Ray diffraction	116
5.1.1.3	Powder X-Ray diffraction	117
5.1.1.4	FT-IR spectroscopy	117
5.1.1.5	Elemental analysis	118
5.1.1.6	Thermogravimetric analysis (TGA)	118
5.1.1.7	Magnetic characterization	119
5.1.2	Results and discussion	119
5.1.2.1	Single Crystal X-Ray diffraction	119
5.1.2.2	Powder X-Ray diffraction	122
5.1.2.3	Magnetic characterization	124
5.2	A neutral 3-D Cobalt polymer	
5.2.1	Experimental	127
5.2.1.1	Synthesis	127
5.2.1.2	Single Crystal X-Ray diffraction	128
5.2.1.3	FT-IR spectroscopy	128
5.2.1.4	Elemental analysis	129
5.2.2	Results and discussion	129
5.2.2.1	Synthesis	129
5.2.2.2	Single Crystal X-Ray diffraction	130
5.3	Conclusions	134
	References	136
<u>Part III: Manganese citrate cubanes</u>		
Chapter 6: Introduction: Manganese citrate cubanes		
6.1	Solid state reactivity	141
6.1.1	Types of solid state reactions	143
6.1.2	Single-crystal to Single-Crystal transformations	154
6.2	The Grotthüss mechanism	154
	References	160
Chapter 7: 0-D Manganese citrate cubanes		
7.1	Experimental	165
7.1.1	Synthesis	165
7.1.2	Single Crystal X-Ray diffraction	165
7.1.3	Powder X-Ray diffraction	166
7.1.4	FT-IR spectroscopy	166
7.1.5	Elemental analysis	167
7.1.6	Thermogravimetric analysis (TGA)	167
7.2	Results and discussion	168
7.2.1	Synthesis	168
7.2.2	Single Crystal X-Ray diffraction	169

7.2.3 Powder X-Ray diffraction	172
7.3 Conclusions	177
References	179
Chapter 8: 1-D Manganese citrate cubanes	
8.1 Experimental	184
8.1.1. Synthesis	184
8.1.2. Single Crystal X-Ray diffraction	184
8.1.3. Neutron diffraction	186
8.1.4. FT-IR spectroscopy	187
8.1.5. Elemental analysis	189
8.2 Results and discussion	189
8.2.1 Synthesis	189
8.2.2 Single Crystal X-Ray diffraction	190
8.2.3 Neutron diffraction	193
8.2.4 A model for the proton wire	194
8.3 Conclusions	205
References	207
Chapter 9: 2-D Manganese citrate cubanes	
9.1 Experimental	216
9.1.1 Synthesis	216
9.1.2 Single Crystal X-Ray diffraction	216
9.1.3 FT-IR spectroscopy	216
9.2 Results and discussion	218
9.2.1 Synthesis	
9.2.2 Single Crystal X-Ray diffraction	218
9.3 Conclusions	223
References	224
Spanish summary and conclusions: SMM basados en Cubanos Metálicos con el Ligando Citrato: Obtención, Caracterización y Propiedades	
Resumen y conclusiones de la memoria de tesis	229

Preface

Here I present the principal motivations and goals underlying the work reported in my thesis.

My work has been carried out immerse in a research group that has extensive experience in the fields of chemistry and magnetism. Physicists and chemists cooperate in the development of new lines of research with the aim of unifying efforts and knowledge so as to achieve advances in materials science. There is no question that there has been a substantial benefit and synergies derived from such environment.

Single-molecule magnetism, discovered in 1993, was the conceptual point of departure for the research described here, although many important results of this work are not directly related to magnetism. We began with the aim of designing and developing new magnetic materials with slow magnetic relaxation, as it is common rule in single-molecule magnet (SMM) behaviour. A follow-on goal, conditions permitting, would be the application of this behaviour to the development of devices. Earlier results^[1] had suggested that for future applications of SMMs, their ordered arrangement on surfaces would be required. For that reason we undertook the preparation of ordered polymer arrays of SMM with different dimensionalities.^[2]

Citric acid was chosen as the appropriate initial ligand due to its versatility in coordination chemistry and its pro-chirality, which together admit a large number of possibilities for coordination compounds and polymers. The three carboxylic acid functions of citric acid fit well with the fact that previous results in single-molecule magnetism involve carboxylates. At the same time, we began this work with Co(II) as the transition-metal center, because of its well-known magnetic properties, particularly its anisotropy.

So the concept of this research project at its outset could be described in this way: We would attempt to prepare and characterize Co(II) citrate compounds with SMM behaviour, and to arrange these compounds into ordered arrays of different dimensionalities in order to study the effect of environment on the SMM magnetic properties. Possible entry points into the development of new devices would be sought.

Apart from that, we considered that the utilization of another transition metal in the preparation of these materials could provide valuable and useful information. As the first material identified as an SMM was a mixed valence compound, commonly known as "Mn12," based on manganese, we chose Mn(II) for the preparation of compounds analogous to those

obtained with Co(II). Although Mn₁₂ was based on Mn(III), the use of Mn(II) ions presented two main advantages. The first one is to test whether it is possible to prepare clusters with axial anisotropy from isotropic ions; and the second was to enable the obtainment of mixed valence compounds as in the case of Mn₁₂ (in this case it would be Mn(II) Mn(III) instead of Mn(III) Mn(IV)).

In summary, after a careful study of the state of the art, and with an eye on future applications, our objectives in conducting the research described in this thesis were:

- The synthesis of new magnetic materials showing SMM behaviour.
- Their complete structural and magnetic characterization.
- The preparation of ordered polymeric arrays of such SMM.
- The study of the changes in the magnetic behaviour of SMMs when they are arranged into nets and how the environment of an SMM can influence the magnetic properties of the whole compound.
- Prepare analogous compounds based on Mn-cubanes.
- Study the structure and properties of these new derivatives.

In the way, unexpected features called my attention, which once investigated, opened new areas of interest. They are also reported in the thesis and can be summarized as:

- Solid state reactivity studied by single crystal X-Ray diffraction (single crystal to single crystal reactions - SC SC).
- Reversible dehydration-rehydration processes in non-porous materials.
- Proton transport within confined spaces in molecular crystals.

[1] F. Palacio, P. Oliete, U. Schubert, I. Mijatovic, N. Husing, H. Peterlik, *Journal of Materials Chemistry* **2004**, *14*, 1873-1878.

[2] J. Campo, L. R. Falvello, I. Mayoral, F. Palacio, T. Soler, M. Tomas, *Journal of the American Chemical Society* **2008**, *130*, 2932-2933.

Part I

Transition metal citrate cubanes

1

Two Different Linkage Isomers of the $[M_4(\text{citrate})_4]^{8-}$ Unit: Structural Study

The compounds presented in this thesis are all based on the same basic structural unit, a transition metal citrate cubane, with the transition metals cobalt and manganese.

Cubane-based compounds have been widely studied in different fields such as biochemistry, where they are of great interest due to the role they play in important processes such those involving electron transfer.^[1, 2] Moreover, in the last few years interesting magnetic properties have been found for compounds possessing this basic unit in their structures.^[3]

Citric acid is known to form cubane-based compounds. When it is quadruply deprotonated in the presence of a transition metal (TM), a transition metal citrate cubane can be formed. There are several examples in the literature of citrate cubanes of first transition series elements.^[4] In all of these examples the coordination environment around the cube is the same.

The work presented in the thesis is based on cobalt and manganese citrate cubanes. We have found that for some of the derivatives, the cubane unit is different from those reported to date. They are linkage isomers of the previously known TM-citrate cubane unit. In the present chapter, a full geometrical description of the structures of the cubanes will be given, along with a complete analysis of their structures in terms of the tetrahedral distortions of their constituent tetrahedra. Finally, a nomenclature system for this unit will be proposed.

1.2 Introduction

Originally, the term “cubane” was used as the common name of the compound Pentacyclo [4.2.0.0.2,5.0.3,8.0.4,7] octane (C_8H_8). This hydrocarbon was synthesized for the first time in 1964 by P. E. Eaton.^[5] The name cubane is based on its structure, in which the 8 carbon atoms are at the vertices of a cube, each bonding 3 neighbouring carbon atoms and one hydrogen.^[5]^[6] This cubic structure is observed for many different compounds, not only in organic chemistry but also in inorganic; and the use of this term has been extended to all derivatives containing this characteristic structural arrangement.

Of great importance is the $[Fe_4S_4]$ cubane cluster. It can be found as a part of complex biological systems, not least of all in proteins. Ferredoxins,^[7] isolated in 1962 by Mortenson and co-workers from the *Clostridium pasteurianum*, have an $[Fe_4S_4]$ cubane in their structure and are involved in electron transfer processes during metabolic reactions. High-potential iron-sulphur proteins (HiPIP) play an important role as electron carriers in the photosynthetic processes of bacteria.^[8] Another related cubane is present in nitrogenase, the enzyme involved in the reduction of dinitrogen to produce ammonia. This protein is divided in two parts, the Fe-protein containing an $[Fe_4S_4]$ cubane and the MoFe-protein formed by an $[Fe_3MoS_4]$ cubane (iron-molybdenum cofactor – FeMo cofactor).^[2]

Conceptually distant from biological processes, in 1993 a known compound based on manganese^[9] showed a new magnetic behaviour, described as single-molecule magnetism.^[3] A single molecule magnet (SMM) is a compound that shows superparamagnetism below a characteristic temperature. The magnetic properties of these compounds do not arise from collective long-range ordering; they have a molecular origin (this concept will be explained in more detail in Part II). Since the seminal discovery of single molecule magnetism, many compounds have been shown to possess this new magnetic behaviour. Some of them are based on cubane units.^[10]

Citric acid is an organic carboxylic acid with formula $C_6H_8O_7$, widely known because of its presence in many fruits, especially in citrus fruits such as oranges or lemons. It is a natural antioxidant,^[11] and is also involved in biological mechanisms, among which one of the most important is the citric acid cycle or Krebs cycle^[12].

Apart from its biological importance, citric acid has proved to be able to form cubanes when it is quadruply deprotonated in the presence of transition metals.^[4] Citric acid is formed by a central carbon atom substituted by a hydroxy group (-OH), one carboxylate (-COO⁻) and

two methylenecarboxylates ($-\text{CH}_2\text{COOH}$) (overall formula $\text{HOC}(\text{COOH})(\text{CH}_2\text{COOH})_2$, Figure 1.1). The pK_a values for the deprotonation of the three carboxylate groups ($-\text{COOH}$ and $2 \times -\text{CH}_2\text{COOH}$) are 3.15, 4.77 and 6.40 (these can be seen as the pH values at which the 1st, 2nd and 3rd protons of the carboxylate groups are sequentially lost). When citric acid is dissolved in water, it loses these three hydrogen atoms, giving an acidic solution in which the triply deprotonated citrate anion is present. To deprotonate the $-\text{OH}$ group is not as straightforward as for the carboxylic acid groups. The pK_a value for this deprotonation is not tabulated in any book. However, we have observed in this work that in the presence of a transition metal, the pH at which the hydrogen atom of the $-\text{OH}$ group is lost is in the range of 7 - 8. We believe that the presence of a transition metal is an enabling factor for this complete deprotonation, as the coordination of the quadruply deprotonated citrate anion to the transition metal produces a stable structure. This unit is sufficiently stable that, for all reactions published to date involving citric acid and a transition metal at a pH of 7 - 8, the same TM-citrate complex is obtained -- a cubane with general formula $[M_4(\text{citrate})_4]^{8-}$.

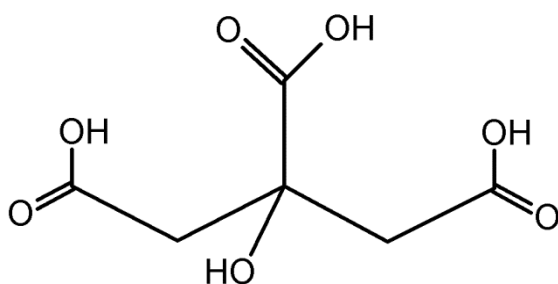


Fig. 1.1. Schematic representation of citric acid

Numerous examples of cubane-based compounds of first-transition-series metals, ranging from monomers (with guanidinium,^[4] Na^+ and $\text{NMe}_4^{+[13]}$ as counterions) to polymers (with Na^+ ,^[14] Rb^+ , Cs^+ ,^[15] $[\text{Co}(\text{H}_2\text{O})_6]^{2+}$,^[16] and $[\text{Mn}(\text{H}_2\text{O})_6]^{2+}$ ^[17] balancing the charge) have been studied. Most of the examples found in the literature to date all represent the same linkage isomer for the cubane unit; however, TM citrate cubanes with a distinct, novel linkage isomer for the cube are presented in this thesis.

Having obtained a new isomer for the basic cubane building block, a system of nomenclature is proposed in this chapter, not only for the isomers but also for the oxygen atoms forming the reactive periphery of the cubane. In addition, the geometry of the cubane core as well as that of its more complex periphery is analysed in terms of quadratic elongation parameters.^[18]

1.3 Results and discussion

A TM-citrate cubane is formed by four metal atoms and four quadruply deprotonated citrate ligands and has a general formula $[M_4(\text{citrate})_4]^{8-}$ (citrate = $(\text{C}_6\text{H}_4\text{O}_7)^{4-}$). The vertices of the cube are alternately occupied by the four TM atoms and the four oxygen atoms of the (deprotonated) –OH groups of the citrate ligands. Isele reviewed the geometries of different cubanes containing Co and Ni.^[19] Table 1.1 shows a comparison of some of the parameters used by Isele (such as the mean M-M and O-O distances (Å) or the ratio between these two values) with the ones calculated for our compounds classified by metal atom. Although Isele did not study Mn-containing cubanes, the results are comparable. Data obtained for our cubanes are in agreement with those found in Isele's review.

Table 1.1. Comparison of the average structural parameters of the compounds presented in this thesis, classified by metal atom, and the values obtained by Isele and co-workers for the M_4O_4 fragments (M = Co or Ni) found in the Cambridge Database (V5.27 with updates of January 2006).^[19]

	Reported by Isele and co-workers			Our compounds	
	Co(II)	Co(III)	Ni(II)	Co(II)	Mn(II)
Number of compounds	20	9	40	8	3
Mean M-M distance (Å)	3.14	2.80	3.11	3.169	3.314
Max, min M-M distance (Å)	3.368, 2.854	3.060, 2.641	3.269, 2.824	3.240, 3.091	3.438, 3.218
Mean O-O distance (Å)	2.747	2.510	2.698	2.746	2.856
Mean O-O/M-M ratio	0.875	0.898	0.869	0.866	0.861

The $[M_4O_4]$ unit has a cubic geometry which is sufficiently distorted that, for a geometric study, it can be viewed as two interpenetrating tetrahedra, one formed by four oxygen atoms and the other by four TM atoms (Figure 1.2).

The coordinated citrate has one deprotonated carboxylate and two deprotonated methylenecarboxylate groups (hereafter, short and long arms, respectively) and bonds to one TM atom in the cube through one of the oxygen atoms of each carboxylate group, forming 5- and 6-membered chelate rings, respectively (Figure 1.3). As only one oxygen atom of each carboxylate function is coordinated to a TM, there are 12 unbound oxygen atoms pointing outward from the cubane, forming a partially negatively charged shell around the cube. This

confers a high reactivity to this unit which, as will be described further on, allows the preparation of a diverse family of related compounds.

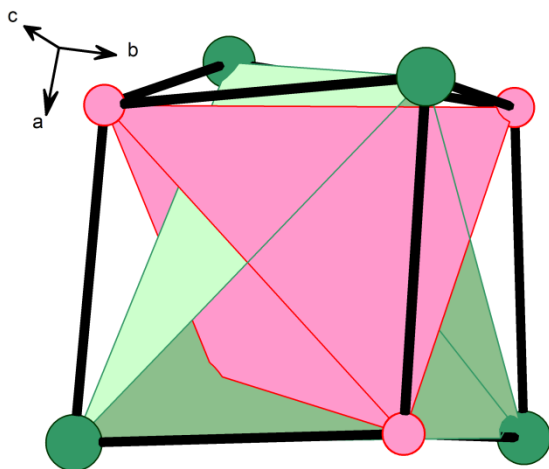


Fig. 1.2. Central cube seen as two interpenetrating tetrahedra O_4 (red) and M_4 (green).

All of the previously characterized transition-metal citrate cubanes present the same distribution of the chelate rings surrounding the M_4O_4 core, arranged in such a way that the whole structural unit has S_4 symmetry. Using a convenient but arbitrary definition of top and bottom ends of the cube, two 6-membered rings occupy opposite edges of the top and the bottom squares (Figure 1.4a), alternating with two 5-membered rings. The lateral edges are exclusively involved in 6-membered rings.

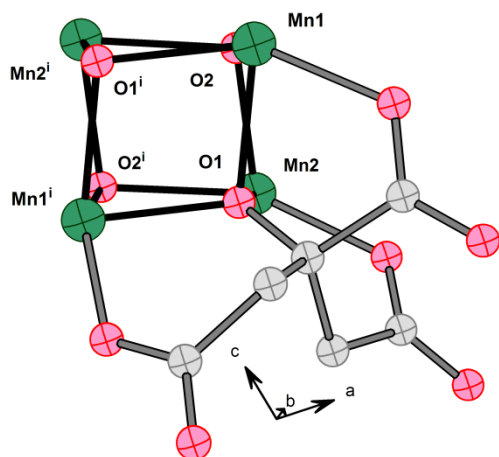


Fig. 1.3. Coordination mode of citrate in a cubane, forming one 5-membered and two 6-membered chelate rings. There are 3 unbonded oxygen atoms pointing outward. The drawing is based on compound **9**. i: (1-x, y, -z).

This arrangement can also be viewed as having lateral faces (left and right sides) formed by 6-membered rings while the central section is formed by the four 5-membered chelate rings.

We have synthesized new cobalt and manganese citrate cubanes. Some of them have the cubane structure described, while others present a new spatial distribution of the rings around the cube. This new cubane is a linkage isomer of the previously reported ones. For this unit, the top and bottom faces are also formed by two 6-membered rings alternating with two 5-membered rings. The difference is that they are rotated 90° in such a way that a 5-membered ring on the upper end is not eclipsed with a 5-membered ring on the bottom face (Figure 1.4b). Despite this difference, the cube preserves its S_4 symmetry.

Despite the differences, for both isomers, the five-membered ring has an envelope conformation with the fold at the metal atom. For the six-membered rings, one of them has a boat conformation and the other is a twist-boat.

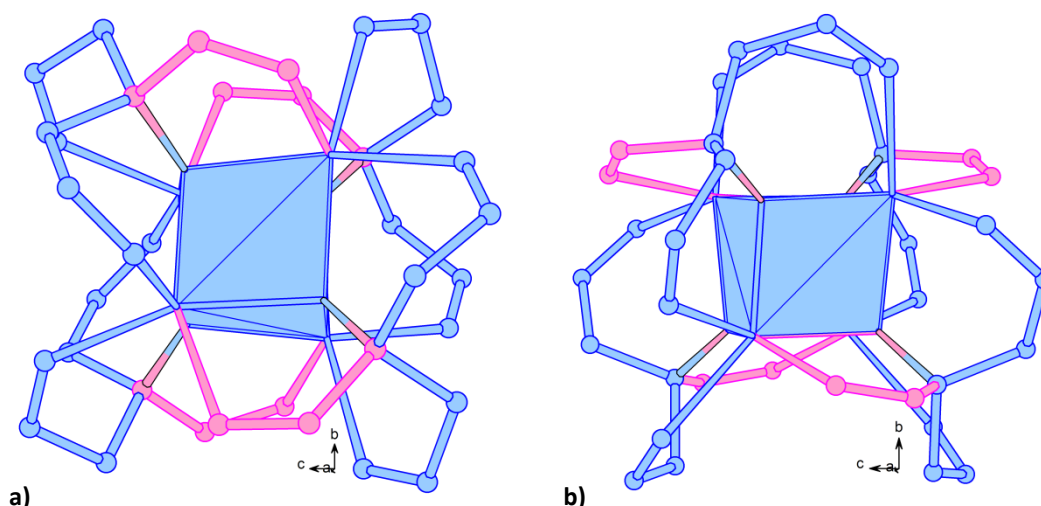


Fig. 1.4. Spatial distribution of the 5-membered (pink) and 6-membered (blue) rings around the cube for isomer A (a) and isomer B (b). Coordinates for isomer A are from compound **4** and those for isomer B are from compound **9**.

Citric acid is a prochiral reagent capable of forming chiral compounds if the two methylenecarboxylate fragments bind to different substituents; this renders the central carbon atom chiral. It is interesting that from a ligand with little symmetry, more complex structures with much higher symmetry can be obtained (*vide infra*). The symmetry of the cubane complexes obtained with citrate is not dependent on the presence of symmetry in the ligand itself. So this ligand, under the conditions used to prepare our compounds, has a latent symmetry, which means it can form structures with symmetry higher than its own. Chirality does indeed arise, at the central carbon atom, from the coordination of the species acting as counterions to the oxygen atoms of the methylenecarboxylate groups; this chirality is external

to the central cubane core; it is not dependent on the identity of the cubane linkage isomer, and it is not present for every central citrate carbon atom in a given structure. Table 1.2 presents the stereochemistry observed in the chosen crystallographic asymmetric unit, for each chiral centre in the TM-citrate cubanes presented in this work. The nomenclature used is that recommended by the IUPAC^[20] and is in accordance with the CIP (Cahn, Ingold and Prelog) system.^[21] Most of the structures reported here have achiral space groups, for which every chiral centre and its enantiomer are present in equal proportions.

Table 1.2. Stereochemistry at the central C atom of each citrate ligand (in the reference asymmetric unit) in the compounds presented in this thesis, classified by chapter and compound number. The nomenclature of the citrate ligands is in accordance with the nomenclature system proposed in this chapter (*vide infra*).

Chapter	Compound	Space group	Crystallographic point symmetry	Citrate			
				A	B	C	D
3	1	C2/c	2	S	S	S	S
	2	C2/c	2	Non chiral	Non chiral	Non chiral	Non chiral
4	3	P -42 ₁ c	-4	R	R	S	S
	4	P -42 ₁ c	-4	R	R	S	S
	5	C 2/c	2	S	S	Non chiral	Non chiral
	6	P -42 ₁ c	-4	S	S	R	R
5	7	I 4 ₁ /a	-4	R	R	S	S
	8	P -1	1	Non chiral	R	S	Non chiral
7	9	I2	1	R	R	R	R
8	10	P 2 ₁ /n	1	Non chiral	Non chiral	Non chiral	S
	11	P 2 ₁ /n	1	Non chiral	Non chiral	Non chiral	S
9	12	P 2 ₁ /n	1	Non chiral	Non chiral	S	Non chiral

The distortion of the cubanes has been studied in terms of their quadratic elongation parameters.^[18] For every tetrahedron considered (See Figure 1.2 and 1.5), a center (center of gravity - Cg) has been described at the unweighted average position of the four constituent atoms. For the $[M_4O_4]$ core two tetrahedra can be considered, namely those formed by the four metal atoms and by the four oxygen atoms. At the periphery of the extended cubane

fragment, three additional tetrahedra are considered, namely those formed by the 12 external oxygen atoms, divided into three groups of four topologically similar O atoms each.

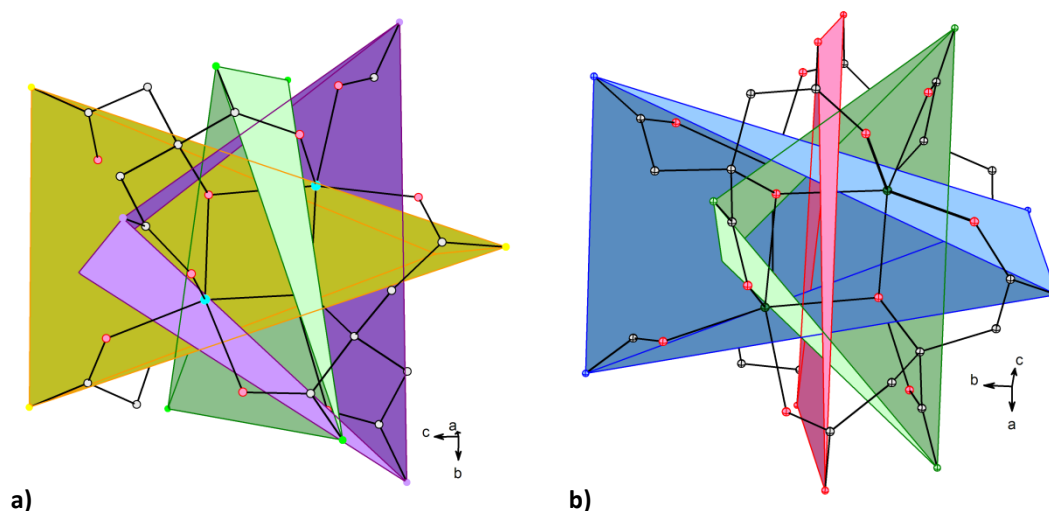


Fig. 1.5. Tetrahedra formed by the peripheral oxygen atoms when divided into three groups of symmetry relatives. The colours of tetrahedra are the same as those assigned to their constituent O atoms. For isomer A (a), there is one regular (violet-long arm), one elongated (yellow-long arm) and one compressed (green-short arm) tetrahedron. For isomer B (b) there is also one regular (green-short arm), one elongated (blue-long arm) and one compressed (red-long arm) tetrahedron. Data for isomer A are from compound 4 in chapter 4 and for isomer B from compound 9 in chapter 7.

The corresponding distortion parameters provide a quantitative measure of distortion in coordination and other polyhedra. Three parameters have been calculated for each tetrahedron (5 tetrahedra per compound, two for the core and three for the periphery) namely the tetrahedral volume (Vol) (\AA^3), quadratic elongation (λ) (dimensionless) and variance of the tetrahedral angles (var) (deg^2). Tetrahedral volume is the volume of the tetrahedron considered, calculated on the basis of the six vertex-to-vertex distances. With this value, the center-to-vertex distance for a tetrahedron with T_d symmetry whose volume is equal to that of the tetrahedron taken into account can be calculated (l_0 , defined as the length of a line from the center to a vertex in the unstrained state). Quadratic elongation (λ) is a convenient measure of distortion used in the analysis of strain independent of the size of the polyhedron (Equation 1). According to this definition, the mean quadratic elongation parameter (λ_{tet}) has been calculated (Equation 2). The variance of the tetrahedral angles is a similar variance calculated on basis the six vertex-center-vertex angles (Equation 3). Both the quadratic elongation and the variance of the tetrahedral angles reveal variations in both bond lengths and bond angles. They are linearly correlated for distorted tetrahedral coordination complexes.

$$\lambda \equiv \frac{l_i^2}{l_0} = \frac{l_0 + \Delta l^2}{l_0} \sim 1 + \frac{2\Delta l}{l_0} \quad \text{Eq. 1}$$

$$\lambda_{\text{tet}} = \frac{4}{i=1} \left(\frac{l_i}{l_0}\right)^2 \quad \text{Eq. 2}$$

$$\sigma_{\theta_{\text{tet}}}^2 = \frac{6}{i=1} \frac{(\theta - 109.47^\circ)^2}{5} \quad \text{Eq. 3}$$

For nearly regular tetrahedra, λ_{tet} should be almost 1 and $\sigma_{\theta_{\text{tet}}}^2$ should have a value near 0. Table 1.3. shows the results obtained for each compound reported in this thesis. They are classified by the chapter in which they are fully described. The linkage isomer is also indicated in the table. For both isomers, short arms are represented throughout this thesis in green. In isomer A, long arms are violet and yellow while in B they are blue and red (Figure 1.6).

The results show that for every compound the inner $[M_4O_4]$ core is nearly regular. Nonetheless, if both are considered as slightly distorted, when one tetrahedron is elongated with four vertex-center-vertex angles higher than the expected value for an ideal tetrahedron and two smaller, the other is slightly compressed. For only one of the examples presented in this thesis are both tetrahedra almost ideal (chapter 5 compound **8**). The geometries of 40 published $[\text{Co}^{\text{II}}_4\text{O}_4]$ cubanes have been studied, excluding structures such as fused cubanes. Results obtained from the Cambridge Database V5.31 are in agreement with those found for our compounds.^[22]

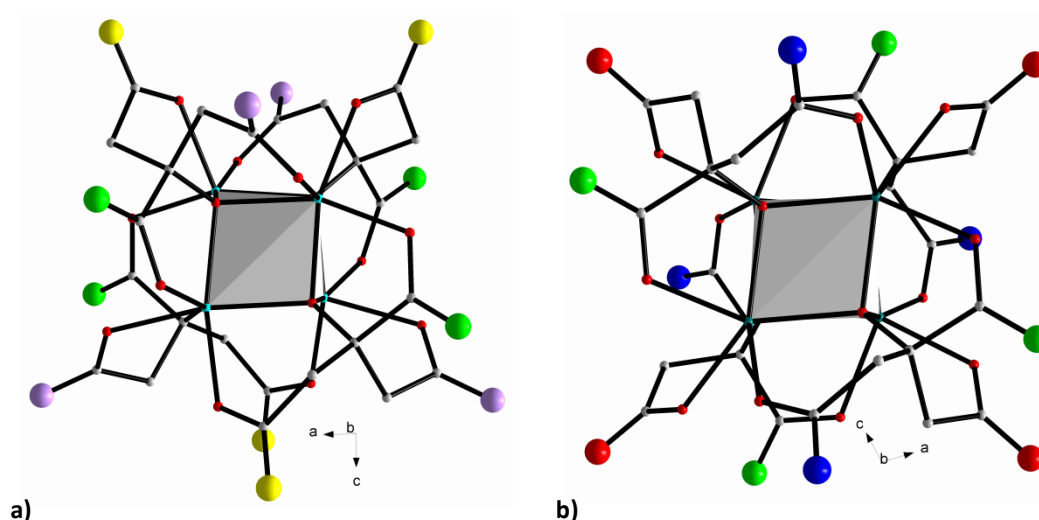


Fig. 1.6. Distribution of the 12 unbonded peripheral oxygen atoms into three groups. For isomer A (a) long arms are represented in violet and yellow while for isomer B (b) they are in blue and red. For both, short arms are green. Coordinates for isomer A are from compound **4** in chapter 4 and those for isomer B are from compound **9** in chapter 7.

Results for the peripheral tetrahedra are slightly different depending on the cubane isomer.

Table 1.3. Tetrahedral volume (\AA^3), quadratic elongation λ and variance of the tetrahedral angles, $\text{var}(\text{deg}^2)$ ^[18] for the two interpenetrating tetrahedra that form the M_4O_4 cube and for the three external O_4 tetrahedra formed by the twelve peripheral oxygen atoms of the citrate ligands. Colors refer to those used in Figure 1.6.

			<i>Vol</i>	λ_{tet}	<i>var</i> ($^{\circ}2$)
Chapter/compo und	Isomer	The cube			
Ch.3 / 1	B	O_4	2.3783	1.0009	3.2794
		M_4	3.7935	1.0009	5.9664
		Short arm (green)	58.7373	1.0277	201.0606
		Long arm (blue)	67.4527	1.1819	699.5810
		Long arm (red)	69.8864	1.1688	2267.0894
	Isomer	The cube			
Ch.3 / 2	B	O_4	2.4137	1.0008	3.0676
		M_4	3.7987	1.0012	4.6059
		Short arm (green)	60.4534	1.0270	192.3827
		Long arm (blue)	66.5075	1.2109	773.8930
		Long arm (red)	67.9506	1.1898	2160.5354
Chapter/compo und	Isomer	The cube			
Ch.4 / 3	A	O_4	2.4675	1.0007	2.9785
		M_4	3.7316	1.0004	1.6046
		Short arm (green)	40.6012	1.3809	877.1153
		Long arm (violet)	86.5643	1.0023	4.2747
		Long arm (yellow)	56.5295	1.2712	1044.7242
	Isomer	The cube			
Ch.4 / 4	A	O_4	2.4873	1.0006	2.3713
		M_4	3.7418	1.0002	0.8185
		Short arm (green)	39.9850	1.4101	919.2771
		Long arm (violet)	87.7062	1.0022	8.3156
		Long arm (yellow)	57.9820	1.2523	979.4550
	Isomer	The cube			
Ch.4 / 5	A	O_4	2.3976	1.0006	3.5860
		M_4	3.7351	1.0013	8.8817

		Short arm (green)	53.6087	1.1415	910.9779
		Long arm (violet)	83.6431	1.0148	56.3266
		Long arm (yellow)	63.5157	1.1821	674.1116
	Isomer	The cube			
Ch.4 / 6	A	O ₄	2.4577	1.0006	2.5727
		M ₄	3.7310	1.0015	5.7119
		Short arm (green)	42.4729	1.3484	827.5625
		Long arm (violet)	86.7781	1.0017	6.6298
		Long arm (yellow)	60.4213	1.2268	889.4217
Chapter/compo und	Isomer	The cube			
Ch.5 / 7	A	O ₄	2.4334	1.0023	9.1829
		M ₄	3.6872	1.0015	6.1162
		Short arm (green)	42.5360	1.3367	808.8883
		Long arm (violet)	86.5647	1.0079	32.1394
		Long arm (yellow)	60.7655	1.2301	901.2848
	Isomer	The cube			
Ch.5 / 8	A	O ₄	2.4666	1.0003	0.2382
		M ₄	3.7707	0.9985	0.1230
		Short arm (green)	56.7426	1.1090	992.8091
		Long arm (violet)	83.9355	1.0055	20.5611
		Long arm (yellow)	66.2122	1.1769	679.0147
Chapter/compo und	Isomer	The cube			
Ch.7 / 9	B	O ₄	2.7169	1.0013	8.8194
		M ₄	4.3039	1.0009	7.0464
		Short arm (green)	60.8311	1.0465	161.4144
		Long arm (blue)	69.1616	1.2182	827.9118
		Long arm (red)	72.9980	1.1846	2007,9353
Chapter/compo und	Isomer	The cube			
Ch.8 / 10	B	O ₄	2.7405	1.0025	11.5843
		M ₄	4.2627	1.0027	12.1990
		Short arm (green)	64.1551	1.0176	116.6813
		Long arm (blue)	68.5702	1.1953	782.5665
		Long arm (red)	70.7610	1.1750	2128.5806

	Isomer	The cube			
Ch.8 / 11	B	O ₄	2.7625	1.0016	9.4524
		M ₄	4.2825	1.0015	9.8333
		Short arm (green)	64.3982	1.0146	105.4807
		Long arm (blue)	73.5678	1.1264	507.7278
		Long arm (red)	71.3215	1.1609	2215.4775
Chapter/compound	Isomer	The cube			
Ch.9 / 12	B	O ₄	2.7288	1.0015	10.3244
		M ₄	4.2797	1.0018	11.7981
		Short arm (green)	63.4902	1.0186	131.4020
		Long arm (blue)	66.2795	1.2261	777.5401
		Long arm (red)	71.2618	1.1726	2159.8842

For isomer A, some of the compounds studied have a quarter of the cubane per asymmetric unit, so the separation of the peripheral oxygen atoms into 3 groups is clear; each group is formed by those related by symmetry. For the compounds with a half cubane or a complete cubane per asymmetric unit, an analogous classification of the external oxygen atoms is possible. The calculations show that the tetrahedron formed by the short arms is compressed, almost planar. One of the tetrahedra formed by the long arms (violet) is regular and the other (yellow) is elongated.

For isomer B, none of the examples has a quarter cubane per asymmetric unit, but some of them have half-cubanes, so for the classification of peripheral O atoms into tetrahedra, two topologically similar oxygen atoms and their congeners have been considered for each group. An analogous division into tetrahedra is possible for the compounds with isomer B, as for isomer A. In this case, however, the geometrical results are different. The short arms form a regular tetrahedron, while the tetrahedra formed by the long arms are both distorted, one of them (blue) by elongation and the other (red) by compression (almost planar) (Figure 1.5).

The periphery of both isomers can be described in general terms as an icosahedron (12 vertices, 20 faces). For isomer B, it is noteworthy that a small dihedral angle exists between two pairs of neighbouring faces (those sharing O10, O12 and their symmetry relatives – atom names correspond to those used for compound **9** of Chapter 7), so that the two can be regarded as single face, with the periphery more accurately described as a polyhedron with 12 vertices and 18 faces, an octakaidecahedron (Figure 1.7).

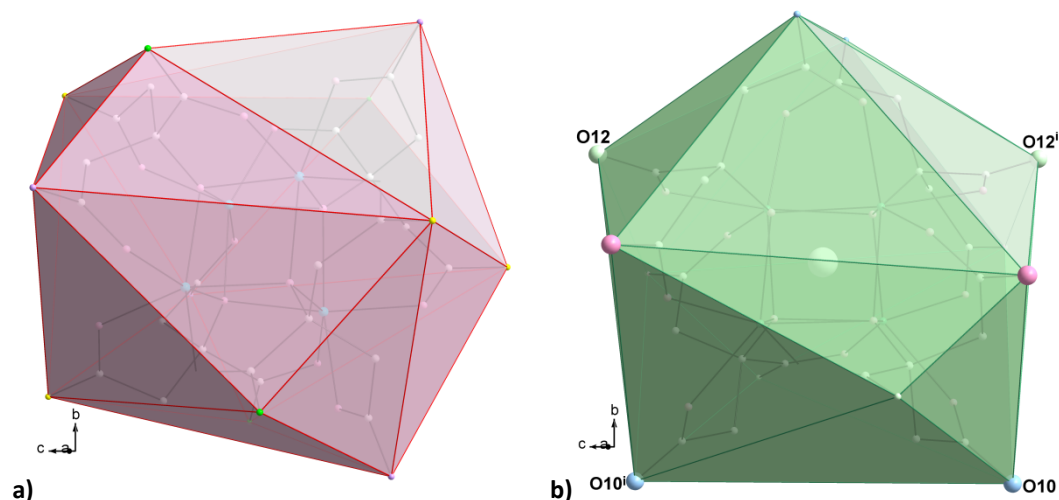


Fig. 1.7. External polyhedra formed by the twelve peripheral oxygen atoms for isomer A (a) and isomer B (b) viewing along the same direction. Both are an isocahedron with 12 vertices and 20 faces, however, for isomer A there is a small dehdral angle between two faces (those sharing O10 and O12 and congeners) that could be considered as one, having 12 vertices and 18 faces (octakaidecahedron). Data for isomer A correspond to compound **4** in chapter 4 and for isomer B to compound **9** in chapter 7. *i*: (1-*x*, *y*, -*z*).

As mentioned above, the coordination of additional species to the periphery of the cubane affects the overall symmetry of the unit, so a consistent system of nomenclature is needed to facilitate a description of the peripheral linkage sites in a common and unequivocal way. For this proposed nomenclature, two of the compounds, one per isomer, will be used as references. The nomenclature must be valid for both isomers (and in principle for any other isomer that might appear in the future); it will be fully explained here in a step-by-step fashion for the sake of clarity.

Aside from any crystallographic symmetry that might be present, the cubane presents chemical symmetry. As previously mentioned, for both isomers, A and B, this is S_4 symmetry, so there is a binary axis that relates two citrates. The remaining two citrates are obtained from the first one by a rotation of 90° plus inversion and by a 270° rotation plus inversion. These are the well-known components of S_4 symmetry. There are a total of 24 oxygen atoms surrounding the cube (8 from the carboxylates and 16 from the methylenecarboxylates). Half of these are coordinated to the metal atoms at the vertices of the cube, forming the chelate rings; the remaining carboxylate oxygen atoms point outward from the cube. The 24 oxygen atoms can be viewed as forming two shells around the cube, an interior one formed by the coordinated oxygens and an exterior layer formed by the uncoordinated ones. The system of nomenclature used in this thesis consists of components that describe the arm to which an oxygen atom pertains (short or long), and whether it is coordinated or not. A sequence number is then

assigned to each oxygen atom, giving a descriptor consisting of two letters and a number according to the following scheme:

First letter: S or L, depending on whether the atom belongs to a short (S) or long (L) arm.

Sequence number: 1-8, from 1 to 4 for short arms and from 1-8 for long arms. As described presently, the sequence number is assigned with the cubane orientated in a particular manner, established for each isomer with an example that acts as reference.

Second letter: i or e: i (interior) for coordinated O and e (exterior) for the uncoordinated O.

For isomer A, the reference compound is compound **4** (Chapter 4), while for isomer B the reference is compound **9** (chapter 7).

To establish the O-atom descriptors for a particular compound, the cubane is first orientated in such a way that in the front upper-left vertex is an oxygen atom. The ligand to which this oxygen atom belongs is called citrate A. The remaining ligands will be labelled in a clockwise order with respect to the drawing, that is:

Front upper-left vertex	A (light orange)
Back upper-right vertex	B (grey)
Front lower-right vertex	C (light blue)
Back lower-left vertex	D (pink)

For the cases in which the cubane has crystallographic symmetry, we prefer to place an oxygen atom from the chosen crystallographic asymmetric unit at the front upper-left vertex, for the sake of simplicity. In order to establish a uniquely defined orientation for the cube, a second condition is applied, with reference to the citrate containing the O atom at the front, upper-left vertex. One of the three edges that meet at this vertex is an edge of the five-membered chelate formed by this ligand. The cube is oriented so that this edge is in the plane of the drawing, pointing downward (Figure 1.8). In the figure, this bond is represented in red.

Once this orientation is fixed, citrates A, B, C and D can be assigned.

For short arms this is enough, and the names given to their oxygen atoms are:

Citrate A	S1i and S1e (for coordinated and uncoordinated O, respectively)
Citrate B	S2i and S2e (for coordinated and uncoordinated O, respectively)
Citrate C	S3i and S3e (for coordinated and uncoordinated O, respectively)
Citrate D	S4i and S4e (for coordinated and uncoordinated O, respectively)

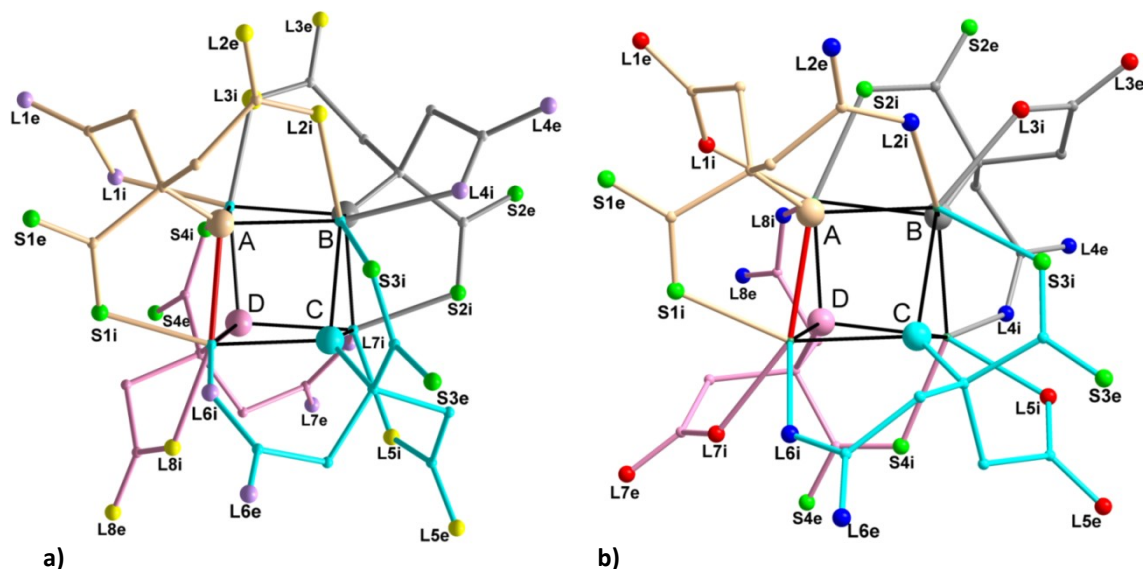


Fig. 1.8. Reference orientations for isomers A (a) and B (b). The reference oxygen atom is at the front upper-left vertex, and the reference edge, belonging to the five-membered chelate, is shown in red. Coordinates used in (a) are from compound **4**, and those for (b) are from compound **9**.

Long arms are numbered from 1 to 8, with 1-2 for citrate A, 3-4 for citrate B, 5-6 for citrate C and 7-8 for citrate D. Taking all requirements into account, the rule for assigning the corresponding number to each arm is as follows:

Viewing along the $C_{\text{central}} \text{---} O_{\text{cube}}$ bond, and starting from the short arm, numbers will be assigned clockwise in the case of citrates placed at the front face of the cube and anti-clockwise for citrates at the back.

This system gives rise to the names shown in Figure 1.8a and 1.8b, for an orientation chosen as described. Each citrate is shown in a different colour with its name (A, B, C, D) on the oxygen atom of the cube. Each of the 24 oxygen atoms forming the shells around the cube is represented with the colour of the group to which it belongs, according to the designation assigned to the O atom at the periphery. Inner oxygen atoms have the same colour as the external oxygen atom bonded to same carbon atom. This division is not necessary for using the proposed system, but it endows the whole procedure with a more visual aspect.

When one of the isomers is orientated in the manner described, with any one of the hydroxy oxygen atoms at the front upper-left vertex with the edge of its five-membered chelate ring pointing vertically downward, the direction of the binary axis in the drawing depends on the isomer. For isomer A, it is vertical, in the projection plane, while for isomer B is perpendicular to the picture. Further comparing the isomers, it can be seen that citrates A and C in both cases have their three arms similarly disposed with respect to three edges of the cube. The differences arise in citrates B and D, for each of which the position of the short arm

and the position of one of the long arms (light blue in the figure) are reversed in the two isomers.

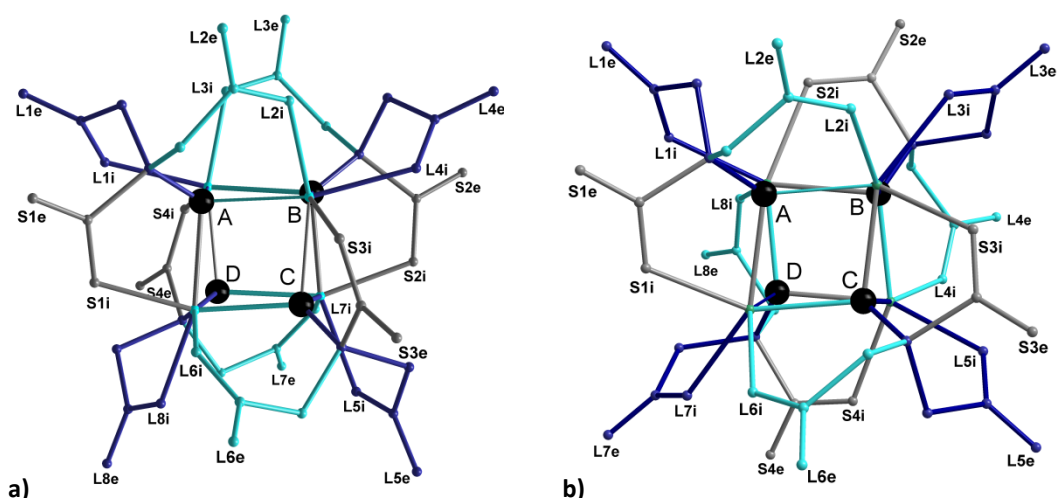


Fig. 1.9. Spatial distribution of the 5-membered (grey) and 6-membered (light and dark blue) rings around the cube for isomer A (a) and isomer B (b). Data for isomer A correspond to compound **4** and for isomer B to compound **9**.

This observation raises the question of the existence of other isomers. It is possible, for example, to conceive of an isomer in which the short legs in citrates B and D were interchanged with the other vicinal long leg (dark blue in the figure).

In what follows, we will refer to the coordination sites of the cubane, both internal and external, using the names given by this method.

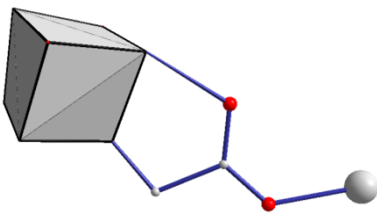
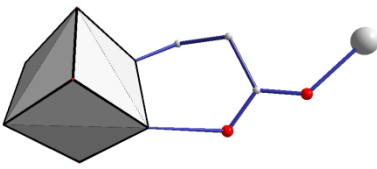
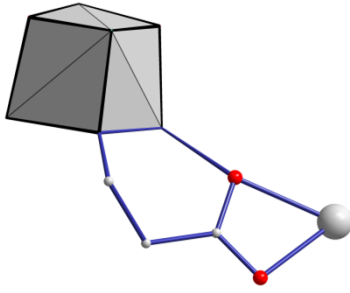
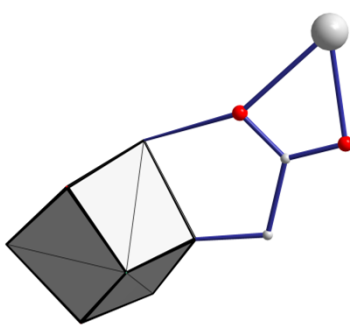
The information provided by this nomenclature system is:

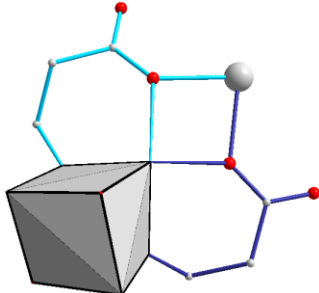
1. The nature of the citrate arm -- short or long -- to which a given O atom belongs. Whether an oxygen atom is internal, forming a chelate with a metal atom of the cube, or external, pointing outward.
2. Which oxygen atoms belong to a given citrate ligand, a useful distinction when more than one O atom binds an external metal centre.
3. For polymers, whether the propagation points are analogous points from different citrate ligands, or are related by symmetry, or are simply different.

This system of descriptors for the 24 carboxylate oxygen atoms of the four citrate ligands that participate in cubanes with transition metals permits us to present comparative descriptions of the diverse geometries found in the compounds that are the subject of this thesis. In addition to the inherent diversity of the compounds themselves, for a full consideration of their properties -- such as magnetic properties -- it is necessary to view the structures from two quite distinct points of view. Firstly, we consider the linkage points of

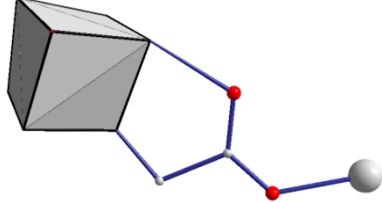
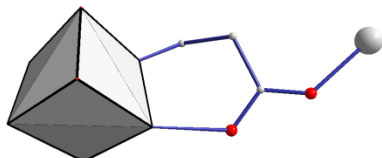
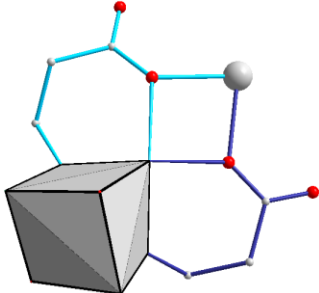
metal centres in terms of where they are attached to the periphery of the cube. It is for this respect that our system of O-atom descriptors is most useful. Secondly, it is also necessary to describe the peripheral metal atoms as coordinative centres in their own right. From this point of view, the cubane acts as a metalloligand, which it turns out has a large diversity of coordination modes.

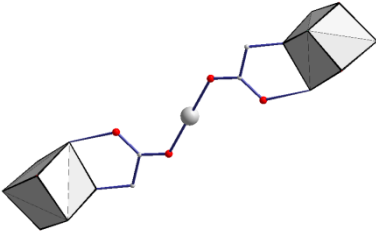
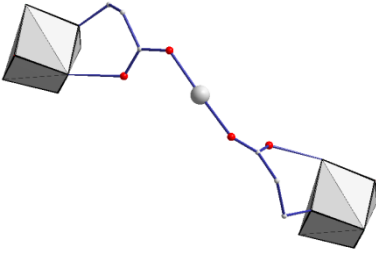
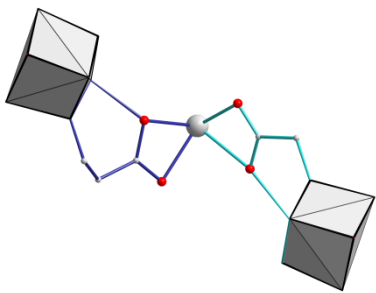
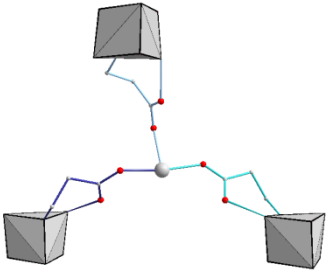
a) Coordination modes of the cubane (Table 1.4).

Description	Scheme	Compounds
Single bond through an external oxygen atom of a short arm (Sxe)		Chapter 3 compound 1 Chapter 4 compound 5 Chapter 8 compound 10, 11 ILUHUS (CDS refcode) MOBFEB (CDS refcode) MOBFIT (CDS refcode)
Single bond through an external oxygen atom of a long arm (Lxe)		Chapter 4 compounds 3, 4, 5, 6 Chapter 5 compound 7, 8 Chapter 7 compound 9 Chapter 8 compound 10 and 11 PUWYAI (CDS refcode) MOBFEB (CDS refcode) MOBFIT (CDS refcode)
κ^2 – Bidentate through two oxygen atoms of a citrate group (one interior and the other exterior) of a long arm (Lxe, Lxi)		MOBFIT (CDS refcode)
κ^2 – bidentate through two oxygen atoms of a citrate group (one interior and other exterior) of a short arm (Sxe, Sxi)		MOBFIT (CDS refcode)

κ^2 – bidentate through two internal oxygen atoms of long arms of different citrates (Lxi, Lxi)		Chapter 3 compound 1, 2 Chapter 7 compound 9
--	---	---

b) Coordination modes of the linking species coordinated to the periphery of the cubanes (Table 1.5).

Table 1.5. Coordination modes of the species coordinated to the periphery of the cubane.		
Description	Scheme	Compounds
TERMINAL		
Single bond to an external oxygen atom of a short arm (Sxe)		Chapter 3 compound 1 ILUHUS (CDS refcode) MOBFEB (CDS refcode)
Single bond to an external oxygen atom of a long arm (Lxe)		Chapter 7 compound 9 Chapter 8 compound 10 and 11 MOBFEB (CDS refcode)
Bidentate through two internal oxygen atoms of long arms of different citrates (Lxi, Lxi)		Chapter 3 compound 1, 2 Chapter 7 compound 9

BRIDGE		
Single bridge through single bonds to external oxygen atoms of short arms (Sxe-X-Sxe)		Chapter 4 compound 5 Chapter 8 compound 10, 11 MOBFEB (CDS refcode) MOBFIT (CDS refcode)
Single bridge through single bonds to external oxygen atoms of long arms (Lxe-X-Lxe)		Chapter 4 compound 3, 4, 5 and 6 Chapter 5 compound 7 MOBFEB (CDS refcode) MOBFIT (CDS refcode)
Single bridge through two oxygen atoms of a carboxylate group (one interior and other exterior) of long and short arms (μ -Lxe,Lxi-X- μ -Sxe,Sxi)		MOBFIT (CDS refcode)
TRIPLY BRIDGING		
μ_3 – triply bridging through single bonds to external oxygen atoms of long arms (X(Lxe) ₃)		Chapter 5 compound 8 PUWYAI (CDS refcode)

1.3 Summary and final remarks

The compounds presented in this thesis are all based on the same basic unit, commonly known as cubane due to the cubic shape of its core. They are TM citrate cubanes, with cobalt and manganese as the metal atoms. All previous examples have the same structure at their core, and differences arise from the relative arrangement of successive cubanes to form new derivatives. The cubic core is responsible for some of the properties that have been reported. However, we have obtained a new isomer of the $[M_4O_4]$ cubic core, so the preparation of new derivatives is not exclusively dependent on the coordination environment of the cube, but also on the linkage isomer.

In preparing these cubanes a first important consideration is the pH of the reaction medium necessary to obtain the compound. We have observed that cubanes are synthesized at $\text{pH} \geq 7$. This is in accord with previously reported results.^[13] At lower pH values a variety of subproducts are isolated in which the OH group is still protonated.

The characterization of a new linkage isomer of the previously known TM-citrate cubanes makes an in-depth geometrical study necessary, along with a classification of the compounds into groups. To this end, quadratic elongation parameters have been used as a quantitative measurement of the distortion of the cube and surrounding polyhedron. The M_4O_4 cube has been studied as two interpenetrating tetrahedra (M_4 and O_4). The 12 unbonded, partially negative oxygen atoms at the periphery of the cube have also been divided into three groups of symmetry relatives; and the geometries of the tetrahedra formed have been analysed in the same way. Results are the same for both isomers; the cube is regular for all of the compounds, but for the periphery there is one regular tetrahedron, one elongated and one compressed. For one isomer, the short arms form the compressed tetrahedron while for the other the regular peripheral tetrahedron is formed by short arms of citrate.

Citric acid is a prochiral reagent, with one OH, one COOH and two CH_2COOH groups coordinated to a central C atom. When forming a TM citrate cubane the two CH_2COO^- are stereochemically equivalent; so to obtain a chiral product an external atom or group should be bonded to the periphery of one of these fragments. The results of this study indicate that there is no preferential stereoisomer; some compounds have their citrates in the R configuration, other in S, some are achiral and one compound mixes the R and the S configurations (in the reference asymmetric unit chosen).

As mentioned before, apart from the cubane isomer, what determinates the molecular structure of each new derivative are the species that bond its periphery. A given product can be viewed as formed by two layers, the first one formed by the 12 carboxylate and methylenecarboxylate oxygen atoms coordinated to the cube and the other by the unbonded

carboxylate oxygen atoms. The TM citrate cubane thus structured can be seen as a reactive nano-ball surrounded by many nucleophilic sites. In order to simplify structural descriptions and to unify our terminology, for comparative purposes a nomenclature system for TM-citrate cubanes has been expounded. It is valid for all such compounds reported to date and in principle could be applied to new isomers.

Finally, coordination modes of the cubane as a metalloligand to peripheral metals have been presented (Table 1.4). The cubane can act as a monodentate ligand through an external oxygen atom from a long or short arm and as a chelate, bonding a central metal atom through two external oxygen atoms from long arms of different citrates. Inversely, Table 1.5 also presents the cubane viewed as a central unit and shows the coordination modes of the peripheral metal centers, considered as ligands. In this case there are three main possibilities, with the peripheral moiety as a monodentate ligand, as a double bridge or as a triple bridge.

Summing up, this part provides a complete analysis of cubane units and sets the basis for future studies and descriptions.

References

- [1] R. C. Valentine, R. S. Wolfe, R. L. Jackson, *Biochemical and Biophysical Research Communications* **1962**, *7*, 453-&; C. W. Carter, J. Kraut, S. T. Freer, R. A. Alden, L. C. Sieker, E. Adman, L. H. Jensen, *Proceedings of the National Academy of Sciences of the United States of America* **1972**, *69*, 3526-3529; D. Cummins, H. B. Gray, *Journal of the American Chemical Society* **1977**, *99*, 5158-5167; V. K. Shah, W. J. Brill, *Proceedings of the National Academy of Sciences of the United States of America* **1977**, *74*, 3249-3253.
- [2] L. M. Rubio, P. W. Ludden, *Annual Review of Microbiology* **2008**, *62*, 93-111.
- [3] R. Sessoli, D. Gatteschi, A. Caneschi, M. A. Novak, *Nature* **1993**, *365*, 141-143.
- [4] T. A. Hudson, K. J. Berry, B. Moubaraki, K. S. Murray, R. Robson, *Inorganic Chemistry* **2006**, *45*, 3549-3556.
- [5] P. E. Eaton, T. W. Cole, *Journal of the American Chemical Society* **1964**, *86*, 3157-&.
- [6] P. E. Eaton, T. W. Cole, *Journal of the American Chemical Society* **1964**, *86*, 962-&; E. B. Fleischer, *Journal of the American Chemical Society* **1964**, *86*, 3889-&.
- [7] L. E. Mortenson, J. E. Carnahan, R. C. Valentine, *Biochemical and Biophysical Research Communications* **1962**, *7*, 448-&.
- [8] S. Ciurli, F. Musiani, *Photosynthesis Research* **2005**, *85*, 115-131.
- [9] T. Lis, *Acta Crystallographica Section B-Structural Science* **1980**, *36*, 2042-2046.
- [10] M. Murrie, *Chemical Society Reviews* **2010**, *39*, 1986-1995.
- [11] C. C. Strachan, A. W. Moyls, *Food Technology* **1949**, *3*, 327-332.
- [12] H. D. Krebs, *Biochemical Journal* **1940**, *34*, 460-463.
- [13] M. Murrie, S. J. Teat, H. Stoeckli-Evans, H. U. Gudel, *Angewandte Chemie-International Edition* **2003**, *42*, 4653-4656.
- [14] K. W. Galloway, M. Schmidtman, J. Sanchez-Benitez, K. V. Kamenev, W. Wernsdorfer, M. Murrie, *Dalton Transactions* **2010**, *39*, 4727-4729.
- [15] E. Burzuri, J. Campo, L. R. Falvello, E. Forcen-Vazquez, F. Luis, I. Mayoral, F. Palacio, C. Saenz de Pipaon, M. Tomas, *Chemistry-a European Journal* **2011**, *17*, 2818-2822.
- [16] J. Campo, L. R. Falvello, I. Mayoral, F. Palacio, T. Soler, M. Tomas, *Journal of the American Chemical Society* **2008**, *130*, 2932-2933; L. R. Falvello, E. Forcen-Vazquez, I. Mayoral, M. Tomas, F. Palacio, *Acta Crystallographica Section C-Crystal Structure Communications* **2011**, *67*, M359-M363.
- [17] S. C. Capelli, L. R. Falvello, E. Forcen-Vazquez, G. J. McIntyre, F. Palacio, S. Sanz, M. Tomas, *Angewandte Chemie (International ed. in English)* **2013**, *52*, 13463-13467.
- [18] K. Robinson, G. V. Gibbs, P. H. Ribbe, *Science* **1971**, *172*, 567-&.
- [19] K. Isele, F. Gigon, A. F. Williams, G. Bernardinelli, P. Franz, S. Decurtins, *Dalton Transactions* **2007**, 332-341.
- [20] L. C. Cross, W. Klyne, *Pure and Applied Chemistry* **1976**, *45*, 13-30.
- [21] R. S. Cahn, C. K. Ingold, *Journal of the Chemical Society* **1951**, 612-622; R. S. Cahn, C. K. Ingold, V. Prelog, *Experientia* **1956**, *12*, 81-94; R. S. Cahn, C. Ingold, V. Prelog, *Angewandte Chemie-International Edition* **1966**, *5*, 385-&.
- [22] F. H. Allen, *Acta Crystallographica Section B-Structural Science* **2002**, *58*, 380-388.
- [23] L. R. Falvello, E. Forcen-Vazquez, F. Palacio, S. Sanz, M. Tomas, *Dalton transactions (Cambridge, England : 2003)* **2014**, *43*, 10700-10704.

Part II

Cobalt citrate cubanes

2

Introduction II: Cobalt citrate cubanes

After the first part of the thesis where the most relevant aspects of the cubanes are shown, this second part of the thesis is devoted to the study of a family of compounds based on cobalt citrate cubanes. The derivatives presented are all based on the same structural unit. What changes from one compound to another is the propagation path in the case of polymers, in which the cubane units are bridged by magnetically active Co(II) centres, the dimensionality, the counterion and the number of water molecules of crystallization.

Compounds based on cobalt citrate cubanes behave as single molecule magnets (SMMs),^[3] presenting an interesting magnetic behaviour first observed in 1993 by Sessoli and co-workers and which has attracted the interest and efforts of many scientists worldwide.^[5] The magnetic characterization and study of the samples comprised in this chapter has shown that slight modifications in the environment of the cube are translated into differences in the magnetism, giving rise to an ample variety of behaviours.

In the third chapter a reversible single-crystal to single-crystal transformation (SC-SC) is reported. Differences in magnetic behaviour are observed, with both of the discrete-molecular derivatives maintaining SMM properties. The first of the two products has a modulated crystal structure, which signals the possibility of one or more solid-state transitions in a nearby thermochemical regime.

Chapter 4 presents a family of 2-dimensional cobalt citrate cubanes. The nets formed in these samples are quite similar, with no dramatic changes. However, interesting differences in the magnetic response of the samples have been observed. In addition to the observation of the magnetic blocking of the cube that confirms the SMM behaviour, a striking extra peak has been observed in the AC magnetic measurements when data were collected at very low temperature.

Finally, two compounds with 3-D polymeric structures are presented in Chapter 5. Magnetic measurements could be done only for the first compound, a highly regular polymer with a diamondoid structure. In the solid state, this compound is marked by the interpenetration of symmetry related loops, which introduces modifications in the magnetic environment of the cube, with corresponding effects on the observed magnetism.

Throughout the present chapter, some useful concepts will be summarised with the aim of facilitating a more straightforward comprehension of the following chapters. We will begin by exploring single molecule magnets (the basic magnetic concepts and a general overview of the field). The chapter then continues with a review of synthetic procedures, the different types of SMMs and possible requirements for future applications.

2.1 A brief overview of magnetism ^{[B3][7]}

The *sine qua non* required characteristic of a magnetic material is the presence of unpaired electrons. The magnetic properties derive from the spins of these unpaired electrons and their interactions with each other.

The magnetism of a compound is its response to a magnetic field. It can be attractive or repulsive. In the first case the compound is called **paramagnetic** while in the second it is called **diamagnetic**.

If all of the electrons in a compound are paired, then it will be **diamagnetic** (*i.e.*, NaCl). No significant magnetic response would be expected. If on the contrary it presents unpaired electrons, different magnetic behaviours can be observed on the basis of the interactions among neighbouring electrons (Figure 2.1).

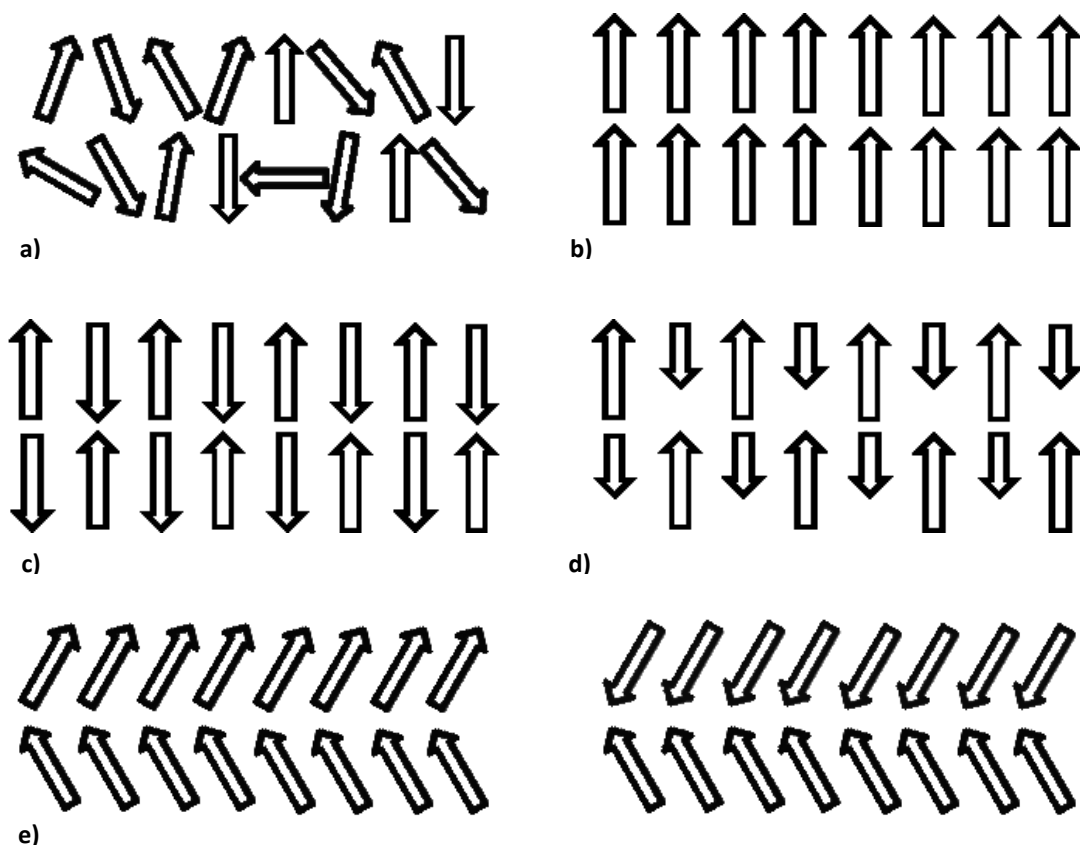


Fig. 2.1. Schemes for spin coupling behaviors in two dimensions. (a) Paramagnetic disordered spins. (b) Ferromagnetically ordered spins. (c) Antiferromagnetically ordered spins. (d) Ferrimagnetically ordered spins. (e) Canted antiferromagnetic spins. Note that the representation for a spin glass would be the same as for a paramagnetic material

Paramagnetism (*i.e.*, $\text{KCr}(\text{SO}_4)_2 \cdot 12\text{H}_2\text{O}$): when there is no interaction among spins moments or they are too weak to compete with thermal fluctuations. Spin moments can move freely within the sample, with random orientations as a result of thermal agitation and net magnetization, in the absence of an external magnetic field, is zero. When an external magnetic field is applied, the magnetization increases following a Brillouin law until it saturates to a value which is strictly proportional to the number of spins involved and the g-factor. At low magnetic fields and sufficiently high temperatures, the field dependence of the magnetization is quasi-linear and inversely proportional to the temperature. This results in the Curie Law (Equation 1 and 2)

$$M = C \cdot H(\text{Oe}) / T(\text{K}) \quad \text{eq. 1: Curie's Law where } M \text{ is the magnetization, } H \text{ is the magnetic field in Oesterd, } T \text{ is the temperature in Kelvin, } C \text{ is the Curie constant of the material}$$

$$\chi \propto 1/T \quad \text{eq. 2}$$

As the temperature is decreased the thermal energy decreases and the effects of the applied magnetic field are more effective rising the magnetization. The consequence is that the strength of the applied magnetic field to saturate the magnetization is lower. Differences arise when the spin moments interact with one another. At sufficiently high temperature, where thermal fluctuations overcome magnetic interactions, the material behaves like a paramagnet. Following a simplistic Mean-Field approximation, results in a simple correction of the temperature in the Curie law by a parameter "theta". This is the Curie-Weiss law given in equation 3. When the magnetic interactions are positive they tend to align the spin moments parallel and are called ferromagnetic; when they are negative, they tend to align the spin moments antiparallel to each other and are called antiferromagnetic. When reducing the temperature, the interaction energy can overcome thermal energy in which case interactions will extend over all the (interacting) spin moments in the material and the system will undergo a phase transition from a disordered (paramagnetic) state to a magnetically ordered one. The temperature at which the phase transition arises is known as critical temperature, T_c . If ferromagnetic interactions dominate, the material will order as a **ferromagnet**, their magnetic moments aligning all parallel to each other. If the interactions are antiferromagnetic, the material will order as an **antiferromagnet** with their magnetic moments aligned antiparallel to each other. This is

schematically represented in Figure 2.1. CrCl_3 would be a typical example of ferromagnetic compound while MnCl_2 would be an example of an antiferromagnetic one.

The behaviour of the magnetization is completely different in ferromagnets and in antiferromagnets. Below T_c , ferromagnets exhibit spontaneous magnetization with an external magnetic field will saturate rather easily. In the paramagnetic region of temperatures, the magnetic susceptibility will tend to be higher than expected for a Curie system (the magnetic susceptibility (χ_M) of a material is the ratio of the magnetization (M) within a given material to the applied magnetic field strength (H), $\chi_M = M/H$); however, it will undergo a dramatic increase below T_c to values orders of magnitude higher than paramagnetic ones. In the case of antiferromagnets, magnetization remains zero in the absence of an applied magnetic field, as the sublattice magnetization of moments with spin up will be compensated by the sublattice magnetization of moments with spin down. The presence of a magnetic field can induce complex field-induced magnetic phase transitions which description is beyond the scope of this thesis. In the paramagnetic region of temperatures, the magnetic susceptibility of an antiferromagnet will tend to be lower than expected for a Curie system reaching a maximum close to T_c . At T_c the susceptibility becomes anisotropic and its behaviour depends of the orientation of the crystal magnetic axes in the field, even if it is a small one. In the case of a powder sample, the susceptibility will show a maximum and then it will decrease with the temperature to a value 2/3 the maximum one.

$$\chi \propto (T-\theta)^{-1} \quad \text{eq. 3}$$

$\theta > 0$ for parallel alignment (ferromagnetism)

$\theta < 0$ for antiparallel alignment (antiferromagnetism)

θ results from the short range interaction of the spins and its magnitude is proportional to the strength of the interaction.

If the alignment of the spins is antiferromagnetic, but the sublattice magnetizations are not completely cancelled, the material is **ferrimagnetic** (*i.e.*, Fe_3O_4) and possesses a net magnetic moment.

These are the commonest magnetic responses; nevertheless, some others are also known. **Metamagnetism** is found when an antiferromagnet is transformed into a high moment state (*i.e.*, a field-induced “ferromagnet”) by applying a magnetic field. When the antiferromagnetic

coupling of the spins in a material is not exactly antiparallel it is called a **canted antiferromagnet** (*i.e.*, $\text{CsCoCl}_3 \cdot 2 \text{H}_2\text{O}$) or weak ferromagnet. Finally, there exist **spin glasses** (*i.e.*, $\text{La}_{1-x}\text{Sr}_x\text{CoO}_3$ ($0 < x \leq 0.18$)) where the spins are ordered randomly as in a paramagnet but without enough energy to move freely; they are fixed, or else move slowly.

Using the Brillouin Function, the magnetization of a paramagnet as a function of the applied magnetic field can be calculated as follows.

$$B_J(\xi) = \frac{2J+1}{2J} \coth\left(\frac{2J+1}{2J} \xi\right) - \frac{1}{2J} \coth\left(\frac{1}{2J} \xi\right) \quad \text{eq.4}$$

$$\xi = \frac{mB}{k_B T} = \frac{g \mu_B J B}{k_B T} \quad \text{eq.5} \quad \text{where } m \text{ is the}$$

magnetic moment of a particle, B is the magnetic field in Tesla, k_B is the Boltzmann constant, T is the temperature in Kelvin, g is the Landé factor, μ_B is the Bohr magneton

The magnetization is calculated by:

$$M = N g \mu_B J \cdot B_J(x) \quad \text{eq.6} \quad \text{where N is atoms per unit of volume.}$$

For a paramagnet, the magnetization increases with the field to reach an asymptotic value. This value is the saturation of the magnetization (M_s). For low magnetic fields, the susceptibility (χ) is M/H .

History dependent $M(H)$ behaviour is characteristic of materials with net magnetic moment (ferro-, ferri-, meta-, spin canted magnets and spin glasses) . This is because below T_c the spins are aligned in domains. The direction of the spins of adjacent domains may differ, but by applying a minimal magnetic coercive field (H_{cr}) they can be aligned. Depending on the magnitude of the magnetic coercive field required, two materials can be found:

Hard magnets $H_{cr} \gg 100 \text{ Oe}$ and significant remanent magnetization (M_r).

Soft magnets $H_{cr} < 10 \text{ Oe}$ and $M_r \rightarrow 0$.

When such materials are magnetised by an external field, they retain the magnetization and another external field in the opposite direction has to be applied to remove it. If an alternating magnetic field is applied, the magnetization of these materials follows a loop called hysteresis loop (Figure 2.2).

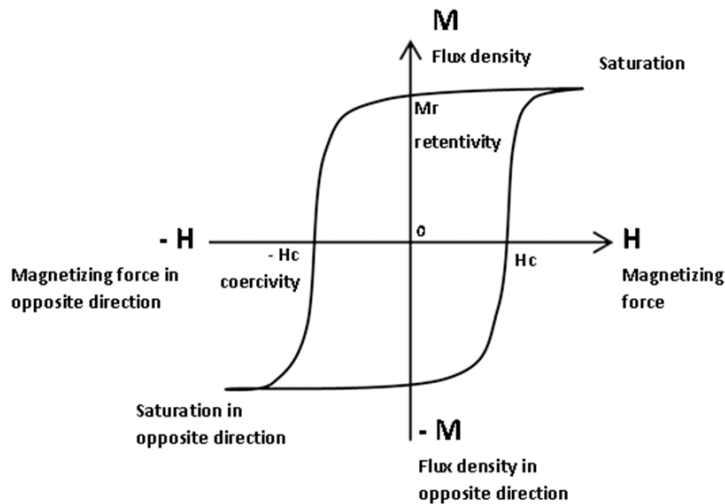


Fig. 2.2 Hysteresis loop.

The properties of the two types of magnets are different and so their uses are not the same. While hard magnets are used for magnetic storage, soft magnets are employed in magnetic shielding and transformers.

N.b., the properties described in here are not characteristic of the molecules but of the bulk material, as magnetism arises from a collective response of the spin moments.

Finally, **superparamagnets** are a new class of magnetic materials with subdomain size. It is observed for small particles which size is below ~ 20 nm. For a ferromagnet, there is a balance between the exchange interaction energy which tends to align neighbouring atomic moments, and the magnetostatic interaction energy that tries to break them into smaller antiparallel-aligned domains. The equilibrium between both forces determines the domain size. When the size of the magnetic material is reduced, there is a critical value below which is not possible to break the system into smaller domains. At this point, it is said that the material is composed by single domains.^[8]

The magnetic moment of the whole particle can be seen as the overall value of the magnetic moments of the atoms forming the nanoparticle. It is proportional to the saturation magnetization and the volume of the nanoparticle ($M_p = M_s V$).

Due to finite size of the particles is observed a preferential orientation for the alignment of their magnetic moment. If there is only one preferred orientation (the simplest case) it is called uniaxial anisotropy. The dipolar interactions and the spin-orbit coupling dictated the preferential orientation of the magnetic moments of the particles.

In these cases, the magnetization flips from one direction to the other by thermal effects. At very high temperatures, the effects of thermal energy dominates over the anisotropy, and

the magnetic moments can move freely and the sample behaves as a paramagnet ($k_B T \gg E_B$, with k_B the Boltzmann constant and E_B the blocking energy for the transition). For very low temperatures, the influence of the thermal energy is negligible and the magnetic moment of the particle remains along the anisotropy direction which is a local energy minimum ($k_B T \ll E_B$). The system is said to be in a blocked state. However, for intermediate temperatures an average time for thermal activation (τ) (first introduced by Néel) is needed. The average time of that flip is defined as the relaxation time.

$$\tau = \tau_0 \exp(E_B/k_B T) \quad \text{eq. 7}$$

The measuring time τ_m will be a determining factor for the magnetic state of the system. If the measuring time is much smaller than the relaxation time ($\tau_m \ll \tau$), a well-defined state is observed and the sample is blocked. On the contrary, if $\tau_m \gg \tau$ the sample is fluctuating and the average net magnetic moment results zero and the sample is at its superparamagnetic state.

The blocking temperature is the one at which $\tau_m = \tau$ and depends on both intrinsic particle parameters and on the measuring time.

$$T_B = \Delta E / k_B \ln(\tau_m / \tau_0) \quad \text{eq. 8}$$

2.2 Magnetism of Co(II) ions ^{[3] [9] [10] [11] [12]}

The study of the magnetic properties of cobalt (II) ions is not as straightforward as for other first-row transition metals due to its first-order orbital contribution. Co(II) is a d^7 ion, with 3 unpaired electrons and a significant orbital contribution at high temperatures. The magnetic moment of a Co(II) ion in an octahedral environment is around 4.7 - 5.2 μ_B and that for tetrahedral coordination is 4.6 μ_B .

A Co(II) ion in an octahedral environment has a ${}^4T_{1g}$ ground state and its magnetic behaviour is that expected for an ion with $S_i = 3/2$ at temperatures higher than 77 K and with a strong orbital contribution. However, the octahedral environment of the ion is rarely regular; it is commonly distorted. In this case, the degeneracy of the ${}^4T_{1g}$ term increases. If there is tetragonal distortion of the octahedron (elongation along a given axis), the ground state is split into two levels, ${}^4A_{2g}$ and 4E_g (excited state) with $M = \pm 1/2$ and $M = \pm 3/2$, respectively. The separation between these two levels can be considered the zero-field splitting (ZFS) of the state (Figure 2.3). Note that the D parameter for a Co(II) ion in a tetragonal environment is positive as the level $M = \pm 1/2$ is lower in energy than is the $M = 3/2$ level. The easy axis of a magnetically anisotropic material is the direction defined by the magnetocrystalline anisotropy. In ferro- or ferrimagnets this is the direction energetically favourable for its

magnetization. The magnetic moment of such materials will be aligned along that axis. The Hamiltonian of the system can be written as equation 9 where D is a negative constant for the system and H_z is the magnetic field strength in the direction of the easy axis. As the D value is negative, when the field is applied in parallel to the easy axis, the projection of the magnetization is antiparallel for those levels with a positive M_s and parallel for the ones with negative M_s . That makes the orientation of each ion in the cluster with respect the molecular easy axis of crucial importance to obtain an overall negative D value. The effective spin for a Co(II) ion is usually estimated as $S_i = 1/2$ as at low temperature only the lowest energy level is populated.^[13]

$$H_0 = D[S_z^2 - S(S+1)/3] + g\mu_B H_z S_z \quad \text{eq. 9}$$

In some systems the effect of the spin-orbit coupling that produces the level splitting implies a reduction of the structural symmetry that accompanies distortion. ZFS is of great importance, as it induces single-ion anisotropy. For Co(II), there is a marked anisotropy that makes this ion suitable for the preparation of single molecule magnets. (See section 2.1.4.2).

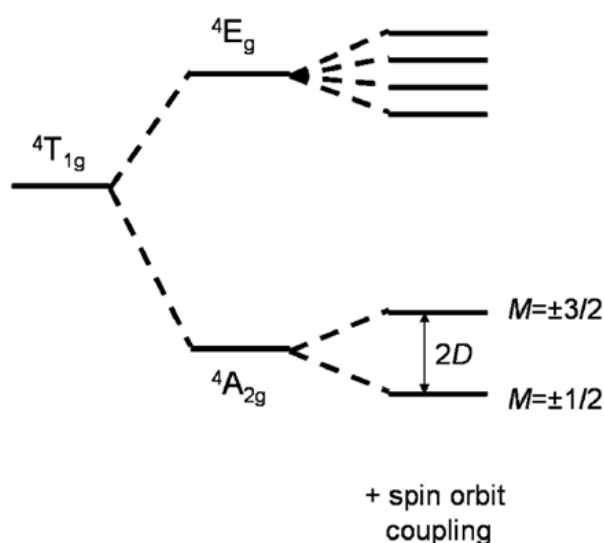


Fig. 2.3. The combined effect of a tetragonal distortion and spin orbit coupling on the energy levels of high-spin Co(II). Adapted from Galloway *et al.* 2010.^[1]

2.3 Molecule-based Magnet

Magnets are everywhere, on their own or as a part of more sophisticated devices. A typical magnetic material is based on pure metals (such as Fe or Co), alloys or metallic oxides (as CrO_2). Those materials are synthesized by the metal industry and usually present very high processing temperatures. The magnetic behaviour arises from the unpaired electrons residing

in the d or f orbitals of the metal atoms that interact throughout the whole material by quantum mechanical effects or by mediation, for example, of bridging oxide atoms. Despite the already high interest on magnets, the field is presently experiencing increased interest because of its possible broadening to new areas of such high societal impact as molecular spintronics and quantum computing. These new areas are related to molecule-based magnets.

Molecule-based magnets are a new class of magnetic materials presenting spontaneous magnetization. Their different nature with respect to conventional materials have made possible the combination of magnetic behaviour observed in classical magnets based on transition metals or rare-earth metals, with some other interesting properties mainly derived from their molecular nature. As these new magnets are molecular materials, they usually present at least one or more of the properties listed in Table 2.1, for example low densities, transparency or electrical insulation. Molecular based magnets with room-temperature ordering temperatures as well as with high and very low coercivities or significant remanent and saturation magnetizations have already been obtained. One of the principal advantages of these materials arises at the processing stage. They are commonly obtained from organic/inorganic chemical methodologies at lower temperatures than those used for metallurgic processing. This aspect of molecular materials not only permits simpler manufacturing processes but also permits new processing features for the preparation of technological devices.

Table 2.1. Typical properties found in molecule based magnets	
Mechanical flexibility	Low density
High strength	Low-temperature processability
Solubility	Modulation/tuning of properties by means of chemistry
Compatibility with polymers for composites	Low environmental contamination
High magnetic susceptibilities	Biocompatibility
High remanent magnetizations	High magnetizations
Transparency	Low magnetic anisotropy
Semiconducting and/or insulating dc electrical conductivity	

In these materials the magnetism arises from unpaired electrons that can reside not only in the d or f orbitals of the metal atoms but also in the s or p orbitals or on the organic ligand. They can be seen as a magnet where the building block is not an atom but a molecule. Interaction among the electrons can take place by different routes, commonly direct exchange, superexchange, dipolar interaction or orthogonal non-overlapping orbitals to mention some.

Some examples of the different types of molecule-based magnets are:

Organic-based ferromagnets: the first example is the ionic, non-covalently bonded 0-D compound with formula $[\text{FeCp}^*_2]^{2+}[\text{TCNE}]^-$ (Cp^* = pentamethyl cyclopentadienide; TCNE = tetracyanoethylene) with solubility in organic solvents. This is the first case in which the electrons residing in the p orbitals are involved in the magnetism.^{[14] [15] [16]}

Purely organic materials: the first example is a ferromagnet described in 1991 by Nakazawa *et al.* based on p-nitrophenyl nitroxide radicals^[17]. The organic magnet with the highest ordering temperature is a dithiadiazolyl radical which undergoes spontaneous magnetization at 36 K.^{[18] [19]} When pressure is applied to this weak ferromagnet, the transition temperature of this material is raised to 65K.^[20]

Hybrid organic/inorganic compounds: these hybrid materials are the result of the combination of molecular and solid state chemistry. Some of the efforts are focused on the preparation of metal-radical polynuclear complexes which show features such as exchange coupling between two spin carriers or the combination of two properties (conductivity and magnetism or optics and magnetism) as a result of the hybrid nature of the components of the samples.^{[21] [22]}

Inorganic cyanide-based network-structured magnets: layered double hydroxides (LDHs) are used as templates in the formation of 2-dimensional layers of cyanide-bridged coordination polymers.^[23]

Molecular ferromagnets: a Fe(III) complex with formula $\text{Fe}(\text{Cl})[\text{S}_2\text{CN}(\text{C}_2\text{H}_5)_2]_2$ which presents tetragonal pyramidal geometry at the Fe center is the first compound described as a molecular ferromagnet.^[24]

Single Molecule Magnets: Compounds in which the building block is a cluster formed by a number of magnetic centres. They can be considered as superparamagnets. The first compound presenting this behaviour is the well-known "Mn12," synthesized by Lis in 1980 and magnetically characterized by Sessoli and co-workers in 1993.^{[5] [25] [26] [27] [1] [28]}

Some examples of molecule-based magnets classified by their magnetic behaviour along with an example of an inorganic solid with the same behaviour are shown in Table 2.2.

Table 2.2. Some examples of inorganic solids and molecule-based materials classified by their magnetic behaviour. Adapted from Miller *et al.* 2000. ^[7]

Magnetic Behaviour	Network Inorganic Solid	Molecule-Based Material
Antiferromagnetic	MnO, VO ₂ , LaFeO ₃	[Mn ^{III} OEP][C ₄ (CN) ₆]
Metamagnetic	FeCl ₂ , MnP	[Fe ^{III} (C ₅ Me ₅) ₂ (TCNQ) Tanol suberate
Ferrimagnetic	Fe ₃ O ₄ , HoCo ₅	Mn ^{II} /Cu ^{II} chains Mn ^{II} nitronyl nitroxide chains [Mn ^{III} (porphyrin)] [TCNE] chains
Ferromagnetic	Fe, CrO ₂ , SmCo ₅ , Fe ₁₄ Nd ₂ B	[Fe ^{III} (C ₅ Me ₅) ₂][TCNE], NPNN, Fe(Cl)[S ₂ CN(C ₂ H ₅) ₂] ₂
Photomagnetic	FeBO ₃	K _{0.4} Co _{1.3} [Fe(CN) ₆] · xH ₂ O
Spin Crossover	LaCoO _{3.01}	Fe(<i>o</i> -phenanthroline) ₂ (NCS) ₂
Canted Antiferromagnetic/ Weak Ferromagnetic	α -Fe ₂ O ₃ , NiF ₂	4'-cyano tetrafluoro phenyl dithiadiazolyl, MnPc, Mn[N(CN) ₂] ₂
Spin Glass	α -Ho ₂ O ₃ ·B ₂ O ₃	V[TCNE] _x , [Mn ^{III} (porphyrin)] [TCNE]
Single-Molecule Magnet		Mn ₁₂ clusters

OEP = octoethylporphyrin; TCNQ = 7,7,8,8-tetracyano-p-quinodimethane; TCNE = Tetracyanoethylene; NPNN; 4-nitrophenyl nitronyl nitroxide

2.4 Single Molecule Magnets

2.4.1 What is a SMM?

As mentioned in this introduction, magnetic materials are widely used as information storage devices. However, there are some restrictions regarding size. The lower limit is set by the superparamagnetic size, below which the magnetization fluctuates freely and so, no information can be stored. At room temperature, this size is about 10-100 nm depending on the material. This problem can be overcome by working at low temperatures and/or by taking advantage of quantum size effects.

At this point, a new dilemma emerges: the magnetic properties of a material go with the size of the material; it is a bulk phenomenon. So, if nanomagnets are used, it is necessary to have ordered assemblies of identical particles or else to be able to address the particles individually at a specific position within the material.

It has been observed that some polynuclear TM complexes present superparamagnetic-like properties, as nanomagnets. They are called Single Molecule Magnets (SMMs). They are a

special sub-class of molecule-based magnets and consist of TM ions connected through intervening ligand donor atoms, forming clusters. The metal ions are exchange coupled and as a result, the cluster as a whole has a total spin. The magnetic properties arise from the overall spin of the cluster. The single-molecule magnets can be considered as an intermediate phase between isolated paramagnetic atoms and the extended nets of metal oxides or hydroxides that forms the conventional magnets.

2.4.2 Magnetic behaviour: requirements and characteristics ^[13] ^[27]

The magnetic properties of single molecule magnets, along with the requirements for considering a system to be an SMM will be presented in this section, along with a brief explanation of some concepts which are needed for a complete comprehension of these materials.

Spin ground state

The spins of the metal atoms forming the cluster are exchange coupled through the ligand donor atoms. As a result, the cluster has a net spin quantum number, S . The first condition to obtain a SMM is that the compound presents a large spin ground state. In addition, it is necessary to isolate the spin ground state from the excited states. As set out in previous sections, the separation between the ground and excited states depends on the strength of the exchange interaction. The stronger it is, the higher is the separation between levels.

Some synthetic approaches for obtaining molecules with large spin ground states have been studied. Most are focused on homometallic compounds. Although the chemistry is not always as predictable as might be desirable, some strategies have been employed successfully. These include the use of azides as ligands, giving ferromagnetic materials^[29] or the synthesis of compounds with bridging angles close to 90° , which makes the magnetic orbitals of two adjacent atoms orthogonal.^[30] ^[31]

The typical example of a mixed-valence compound exhibiting a large spin ground state is the Mn₁₂ compound.^[32]

Anisotropy

If the cluster has and $S \geq 1$, this ground state can be coupled with the excited states via spin-orbit coupling, giving a zero field splitting (ZFS). As explained in previous sections, this ZFS induces anisotropy on the metal atoms of the cluster, due to the distortion, which lowers the symmetry of the structure. In clusters, the main contribution to their magnetic anisotropy is

the tensor sum of the anisotropies of the single ions forming the cluster. The effects of the dipolar and exchange interaction on the magnetic anisotropy of the cluster are usually weak.

If there is no ZFS, the degeneracy of the M_s levels can be removed by the application of a magnetic field. If on the contrary, there is an axial ZFS, the levels are already split before the application of the magnetic field and the degeneracy is partially resolved. The levels are divided into $M_s = \pm 1/2$ and $M_s = \pm 3/2$, as in the case of $S = 3/2$, *e. g.* Co(II), and the separation of these two levels is $2D$, D being the axial ZFS parameter (Figure 2.3).

Given that the energy barrier between spin states up and down is directly proportional to the molecular magnetic anisotropy (see below), it is desirable for a SMM to present a large value of D .

Slow magnetic relaxation

When a SMM is exposed to a magnetic field it becomes magnetised and after removing the field there is a relaxation of the magnetization that follows an Arrhenius law characteristic of thermally activated processes in which is it necessary to overcome an energy barrier.

$$\tau = \tau_0 \exp(\Delta E / \kappa_B T) \quad \text{eq. 10}$$

τ is the experimental time, τ_0 is the relaxation time, ΔE the energy barrier, κ_B the Boltzmann constant, T the temperature.

By plotting $\ln(\tau)$ vs $1/T$ it is easy to obtain the corresponding values of τ_0 and ΔE .

The energy barrier for this process arises from the anisotropy of the molecular clusters that constitute the sample. At temperature above the blocking temperature, T_b , the thermal energy is enough to overcome that barrier and the compound will relax to the equilibrium state after the magnetic field is removed. On the contrary, below T_b , the system is blocked and the magnetization would be in principle retained. However, due to the particle size, quantum effects operate in these samples. They combine properties of the classical and quantum physics. It has been observed that SMMs relaxation processes are not only thermally activated, they can also relax via quantum tunnelling. It can be seen in the hysteresis loops where the characteristic steps observed are due to the tunnelling.

A single molecule magnet shows slow magnetic relaxation, observed when an oscillating magnetic field is applied (AC measurements). The dynamic susceptibility of the sample is dependant of the angular frequency of the applied field ($\omega = 2\pi\nu$).

Other considerations

Once the most important aspects of the magnetic behaviour of SMMs have been summarised, it is possible to set the key features to take into account in the design and preparation of new materials with enhanced properties.

Single molecule magnets are metal-organic compounds that exhibit slow magnetic relaxation below a certain temperature (blocking temperature T_B). Their magnetization has a preferential orientation along the "easy axis" of anisotropy which value is defined by the zero field splitting parameter. One of the principal problems for technological application of SMMs is that until now, the blocking temperatures have been too low. So, many efforts are focused on the development of new SMM with higher blocking temperatures. For that, it is necessary to increase the energy barrier in order to avoid the relaxation process.

$$T_B \propto \Delta E \quad \text{eq. 11}$$

$$\Delta E = |D| \cdot S^2 \quad \text{eq. 12}$$

Where ΔE is the energy barrier, D is the magnetic anisotropy parameter and S is the total spin of the molecule

From equations 11-12 it is clear that for increasing the energy barrier it would be necessary to prepare compounds with large spin ground states and also large anisotropies. As increasing S seems more practicable than increasing D , most efforts are focused on the synthesis of compounds with a large number of metal atoms. This in principle would have a quadratic influence on the energy barrier. However, some recent works have demonstrated that D and S are in some way related.^{[33] [34]} It was concluded from these studies that increasing S is not as efficient as suggested by eq. 12; in fact the results obtained by increasing D are much more promising than those observed when S is increased.^{[35] [36] [37]} There is an intrinsic relationship between D and S and the final results can be tuned by modifying D and S separately.

2.4.3 Synthesis of SMM: different approaches

A determining factor in the magnetic behaviour of SMMs is not only the metal atom but also its environment. In this context the election of the ligand is of crucial importance. Many families of SMMs are commonly given schematic names according to their nuclearities; this nomenclature, although simple, obscures relevant information.

So chemistry plays an important role in the production of new molecules with SMM behaviour. However, the synthetic procedure is not always predictable. There is a boundless array of variables involved in the process. The way in which each ligand coordinates the metal atoms, their oxidation state, the ratio ligand/metal atom, the stability of the final product, the reaction conditions (pH, temperature, time, etc.) are some of the relevant parameters. In addition, once a compound is isolated and characterised, there are some other problems. For instance, although there are some generalities that allow us to attempt to predict the magnetic behaviour of a sample and how to improve its properties, no prediction is accurate enough when a new derivative is obtained. An example is related to the discussion given in the previous section. It is accepted that to enhance the blocking temperature of an SMM it is necessary to increase the number of metal atoms in the cluster; in fact, most of the efforts are directed to that end, as the total spin should affect the energy barrier exponentially. However, experimental results show that for high nuclearity compounds the effects on the blocking temperature (energy barrier) are not as marked as expected. As a consequence, many authors consider this chemical task as a mixture of knowledge and experience with a bit of luck. The effects of serendipity can be controlled to some extent with the expertise gained working with specific types of compounds. Although tedious, the serendipitous approach has given important results along the way; one of the most relevant examples is the discovery of the compound commonly known as "Mn₁₂," the first compound identified as a single molecule magnet.

On the other hand, there are some other examples in which the results are much more predictable. Those normally involve the use of stable building blocks whose coordination modes are almost fixed. Rigid ligands can give certain geometries around the metal atom. An example is the ligand 1,3,5-triamino-1,3,5-trideoxy-*cis*-inositol (H₃taci), which has six coordination sites, three of which (the –OH groups) can act as bridges. It can force unexpected configurations around the metal groups, as in the case of a vanadyl complex with formula [V₈O₁₄(H₂taci)₂] where bridges four V(IV) ions forcing an orthogonal configuration around the V atoms giving an strong ferromagnetic interaction of the V spins. (Figure 2.4a).^[38] Other ligands

such as 1,4,8,11-tetraazacyclotetradecane (cyclam) can be used to block the equatorial plane of a metal atom, leaving the two axial positions available for other desired ligands (Figure 2.4b).

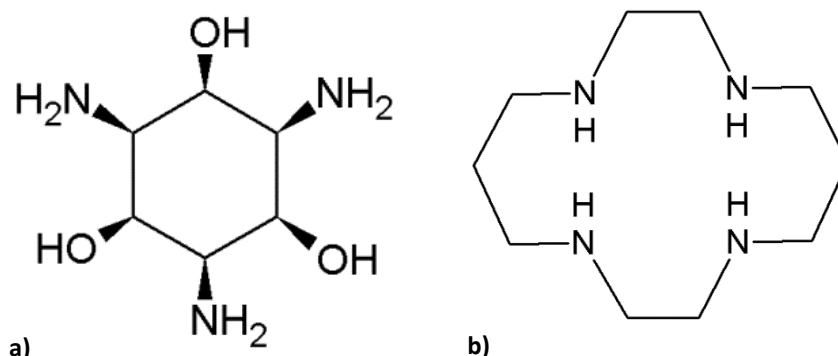


Fig. 2.4. Schematic representation of the ligand 1,3,5-triamino-1,3,5-trideoxy-cis-inositol (H₃taci) (a) and 1,4,8,11-tetraazacyclotetradecane (cyclam) (b).

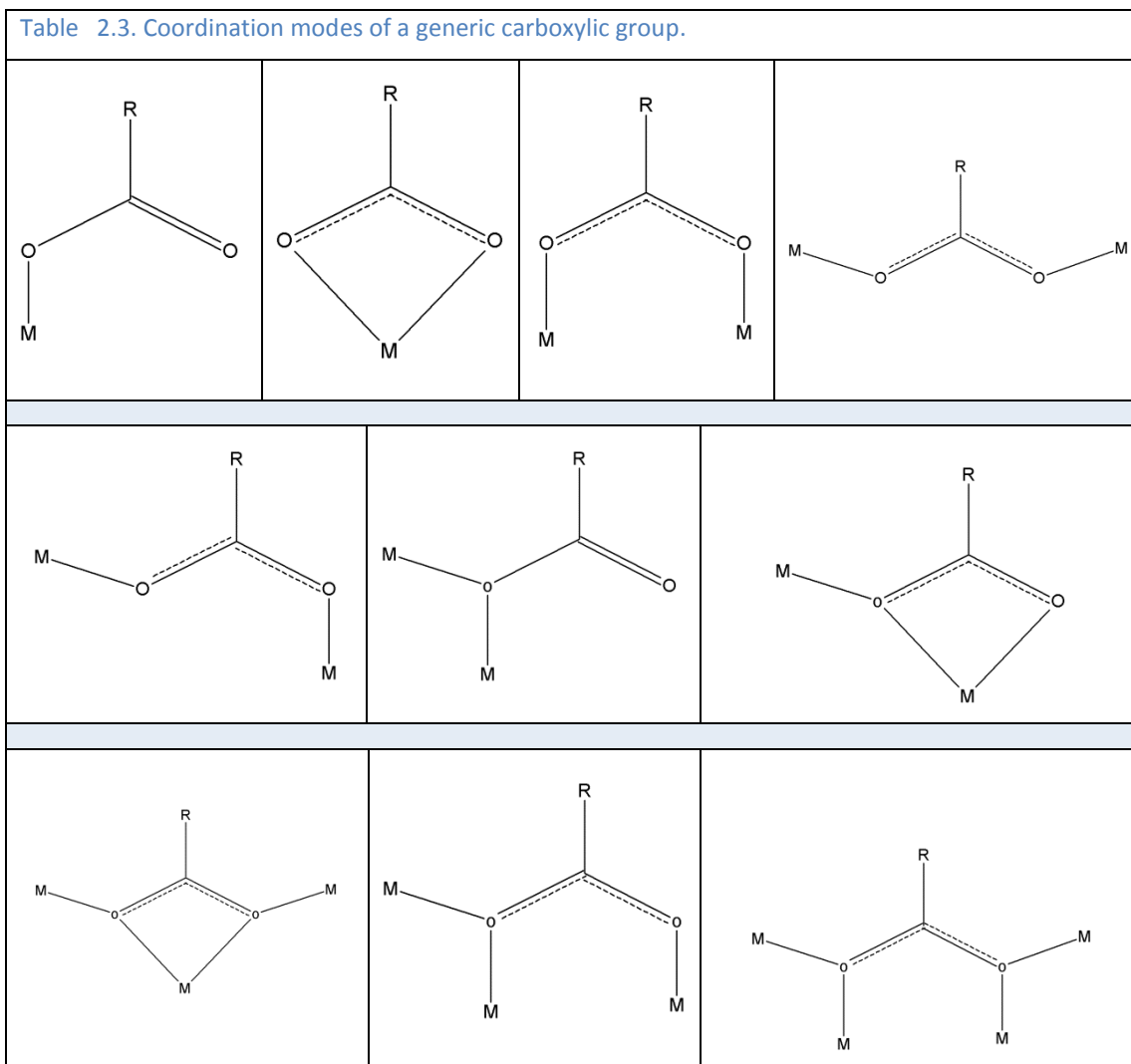
As mentioned at the beginning of this section, the environment of the metal atoms and also the nature of the ligand connecting them is what really determine the resulting magnetic behaviour.

Depending on the number of donor groups present in the ligand, they can be mono-, bi-, tri-, tetra- (and so on) dentate whether they bonds 1, 2, 3, 4 metal atoms respectively. In some cases, the same donor atom can coordinate more than 1 atom. In addition, some ligands can coordinate the same metal atom more than once, acting as chelates. That is thermodynamically favoured as there is a net gain in the entropy of the system when for instance six monodentate ligands are replaced by 3 bidentate (This is known as the chelate effect). It is also worth mention that the coordination number and geometry around an atom is affected by its nature and oxidation state. However, ligands can induce redox reactions, distorted geometries or can block some coordination sites, making others more accessible.

The commonest donor atoms in ligands are F⁻, Cl⁻, O²⁻, S²⁻, and OH⁻. Two different requirements can be distinguished when planning the synthesis of an SMM. Firstly, the ligand or part of a ligand connecting the metal atoms should impart an appropriate geometry to the cluster, one that favours the magnetic coupling of the metal centres. However, other ligands or part of the same ligand must isolate the cluster. They can optionally propagate the basic building block, forming polymers. What is compulsory is their function, isolating each magnetic unit from magnetic coupling with its neighbours; otherwise, the magnetism would be due to a bulk phenomenon.

It is known that when carboxylates are used as ligands, they induce a weak magnetic interaction between metal atoms. Nonetheless, they have been widely used as they offer other advantages such as an easy modification the lateral R groups which allow, for instance, the study of how the environment affects a given magnetic cluster. Changes in the R group also modify the solubility, the steric hindrance and the reactivity of the periphery of the cluster. Coordination modes of a generic carboxylate group are shown in Table 2.3.

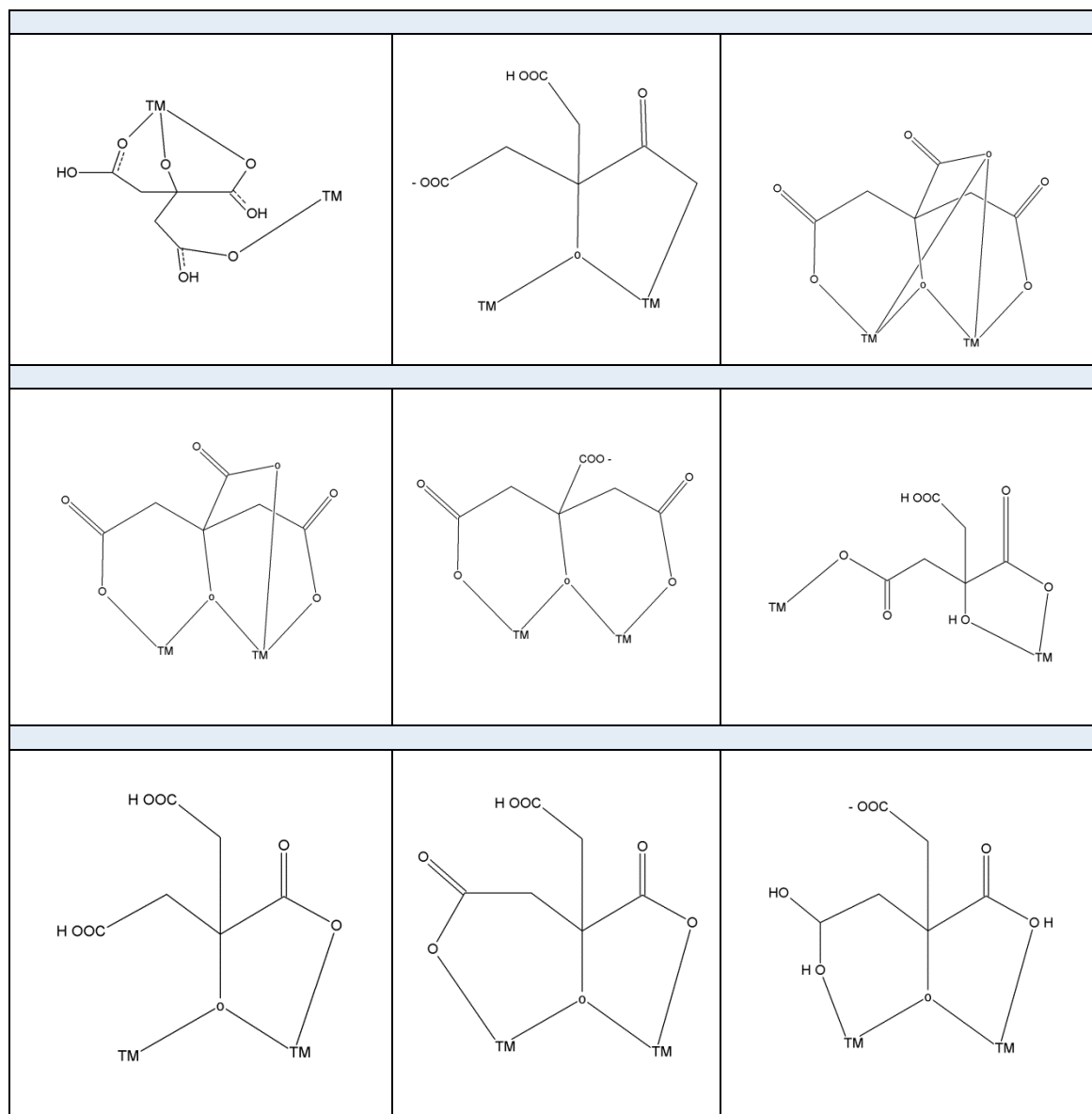
Table 2.3. Coordination modes of a generic carboxylic group.



The compounds presented in this thesis are all based in TM citrate cubanes. Citric acid has one hydroxyl group (-OH) and three carboxylate groups (two methylenecarboxylate and one carboxylate), and it can be deprotonated up to four times. So, it provides an ample variety of coordination modes and protonation states, which makes this ligand chemically unpredictable but reactive and versatile. A survey in the Cambridge Database System (CDS V.1.15) for coordination compounds presenting the citrate fragment, and considering any level of protonation of the hydroxy and carboxylate groups, produces about 350 results. Only those

involving transition metals were considered. Table 2.4 shows the commonest coordination modes of citric acid and its conjugate bases to TMs. Note that compounds in which citric acid is involved in the propagation of a polymeric structure have been omitted due to their complexity and the impossibility of classifying the results.

Table 2.4. Commonest coordination modes of citrates to transition metals. Data obtained from the Cambridge Database System V.1.15 for a citrate fragment. Examples in which the citric acid or citrate is coordinated to more than one TM atom, propagating a polymeric structure, have been omitted.



2.4.4 Classification of SMMs

Since single molecule magnetism was observed for the first time in 1993, a large number of compounds have been characterised as SMMs; still, most of the examples can be classified into families. In this section, a brief overview of the most-studied SMMs is given, with special attention to those examples based on either Co(II) ions or cubane-based compounds.

Mn₁₂-derivatives. The paradigmatic compound with formula $[\text{Mn}_{12}\text{O}_{12}(\text{CH}_3\text{COO})_{16}(\text{H}_2\text{O})_4] \cdot 2\text{CH}_3\text{COOH} \cdot 4\text{H}_2\text{O}$ (Mn₁₂)^[4] crystallises in the tetragonal system, space group I-4; it is formed by an Mn₁₂ cluster with S₄ symmetry (Figure 2.5a). Per asymmetric unit there are two Mn(III) and one Mn(IV). One of the Mn(III) ions completes its octahedral coordination sphere with 2 oxide ions and 4 acetate oxygen atoms and the other with 2 oxide ions, three acetate oxygen atoms

and 1 molecule of water. The Mn(IV) ion coordinates 5 oxide ions and one acetate ligand. The susceptibility observed at room temperature does not agree with the expected value for 8 Mn(III) and 4 Mn(IV) ions with spin of $S=2$ and $S=3/2$ respectively. Its smaller value suggests a ferrimagnetic coupling. A model in which the spins of the 8 Mn(III) ions are up and the spin of the Mn(IV) are down would give the observed total spin $S = 10$ for the cluster.

Mn₁₂ is one of the most studied SMMs, and despite much effort over the last two decades, it still presents the highest known blocking temperature ($\Delta E/k_B = 62$ K and $\tau_0 = 2.1 \cdot 10^{-7}$ s).^[39]

So not surprisingly, there is an active research field in the chemical vicinity of Mn₁₂. The result is the preparation of a rich family of related compounds. The most used approximation is the substitution of the acetate ligands by other carboxylates. It has been observed that when Mn₁₂ is dissolved in the presence of another carboxylic acid, the equilibrium for the displacement reaction is shifted towards the formation of the weakest acid. Most of the mixed ligand derivatives present substitution at both, the axial and equatorial positions.^{[40] [41] [42] [43]} Table 2.5 shows Mn₁₂ derivatives with reported structures. As the resulting total spin of the clusters is due to antiferromagnetic coupling, any modification of the strength of these interactions can be translated into changes in the final S value.^{[44] [45]}

An interesting group of compounds within the Mn₁₂ family are the reduced species. They are compounds in which some Mn atoms have been reduced.^[46] A relevant example was reported by Coronado *et al.* in which the acetate ligands were substituted by the positively charged ligand betaine.^[47] There are only 14 counterions, which mean that a two-electron reduction of the cluster has occurred. The results is a total spin of $S = 11$ but with a reduction of the resulting anisotropy due to the presence of the Mn(II) ions.^[48]

Fe₈ clusters: The compound with formula $[\text{Fe}_8\text{O}_2(\text{OH})_{12}(\text{tacn})_6]\text{Br}_8(\text{H}_2\text{O})_9$ (tacn = 1,4,7-triazacyclononane) is one of the most popular SMMs. It crystallises in the triclinic system, space group P1.^[6] There are eight Fe(III) ions per asymmetric unit, distributed over three different sites (Figure 2.5b). Two of them, at the inner part of the cluster, are bonded to two oxide atoms and two hydroxo bridges. The four Fe(III) ions at the external part of the cluster are coordinated by 3 nitrogen atoms from the tacn ligand and by three hydroxides. The two remaining Fe(III) ions bond 3 nitrogen atoms from the tacn, one oxide and two hydroxides. As happened with Mn₁₂, the susceptibility value at room temperature is smaller than that expected for eight $S = 5/2$. A total spin of $S = 10$ for the cluster is observed, which can be explained with six $S = 5/2$ up and two $S = 5/2$ down.^{[67] [68]}

Table 2.5. Mn12 derivatives with general formula $[\text{Mn}_{12}\text{O}_{12}(\text{RCOO})_{16}(\text{H}_2\text{O})_x]\cdot\text{Y}$. Only those with crystal structures reported are shown. Adapted from Gatteschi *et al.* 2006.^[B4]

R group / ^a L	x	Solvent molecules of crystallization	Space group	Reference
CH ₃	4	2 CH ₃ COOH · 4 H ₂ O	I-4	Lis 1980 ^[4]
CH ₂ CH ₃	3	4 H ₂ O	P-1	Eppley 1995 ^[49]
CH ₂ CH ₃	3	-	P2 ₁ /c	Aubin 2001 ^[50]
CH ₃ ; CH ₂ CH ₃	4	2 H ₂ O · 4 EtCOOH	I-4	Wei 1997 ^[51]
CH ₂ C(CH ₃)	4	CH ₂ Cl ₂ · CH ₃ NO ₂	P-1	Sun 1998 ^[52]
CH ₂ C(CH ₃)	4	CH ₂ Cl ₂ · CH ₃ CN	P-1	Soler 2003 ^[53]
C ₆ H ₅	4	-	P-1	Sessoli 1993 ^[54]
C ₆ H ₅	4	2 C ₆ H ₅ COOH	Fdd2	Takeda 1998 ^[55]
C ₆ H ₅ -pCH ₃	4	COOH-C ₆ H ₄ -pCH ₃	C2/c	Aubin 2001 ^[50]
C ₆ H ₅ -pCH ₃	4	3 H ₂ O	I2/A	Aubin 2001 ^[50]
C ₆ H ₄ -pCl	4	8 CH ₂ Cl ₂	C2/c	Aubin 2001 ^[50]
C ₆ H ₄ -mCl	4	COOH-C ₆ H ₄ -mCl	P-1	An <i>et al.</i> 2000 ^[56]
C ₆ H ₄ -oCl	4	CH ₂ Cl ₂ · 5 H ₂ O	Pnn2	Ruiz 1998 ^[57]
CH ₂ -C ₆ H ₅	4	-	P-1	Sun <i>et al.</i> 1998 ^[52]
CHCHCH ₃	4	H ₂ O	Ibca	Ruiz-Molina 2002 ^[58]
CF ₃	4	2.5 H ₂ O	P-1	Gomez-Segura 2005 ^[59]
CF ₃	4	2 CF ₃ COOH · 4 H ₂ O	I-4	Zhao 2004 ^[60]
CF ₃	4	CF ₃ COOH · 7 H ₂ O	P2 ₁ /n	Zhao 2004 ^[60]
CH ₂ Cl; CH ₂ C(CH ₃) ₃	3	CH ₂ Cl ₂ · H ₂ O	P-1	Soler 2001 ^[41]
CH ₂ Cl; CH ₂ CH ₃	3	CH ₂ Cl ₂	P-1	Soler 2001 ^[41]
CH ₂ Br	4	4 CH ₂ Cl ₂	I4 ₂ D	Tsai 2001 ^[61]
CH ₂ C(CH ₃) ₃ /NO ₃	4	CH ₃ NO ₂	C2/c	Artus 2001 ^[40]
CH ₃ /Ph ₂ PO ₂	4	12 CH ₂ Cl ₂	P4 ₂ /n	Boskovic 2001 ^[43]
CH ₃ /PhSO ₃	4	4 CH ₂ Cl ₂	P-1	Chakov 2003 ^[62]
CH ₃ /CH ₃ SO ₃	3	3 CH ₃ CN · 4 H ₂ O	Pbca	Kuroda-Sowa 2004 ^[63]
CH ₃ /Ph ₂ PO ₂	-	6.1 CH ₂ Cl ₂ · 0.4 H ₂ O	P2 ₁ /n	Bian 2004 ^[64]
C ₆ H ₄ -pSCH ₃	4	8 CHCl ₃	I-4	Zobbi 2005 ^[65]
C ₆ H ₅ / ^b adcb	4	8 CH ₂ Cl ₂	I4 ₁ /amd	Pacchioni 2004 ^[66]

^aWhere appropriate L indicates the non-carboxylate ligand.
^badcb = 10-(4-acetylsulfanylmethyl-phenyl)-anthracene-1,8-dicarboxylic acid.

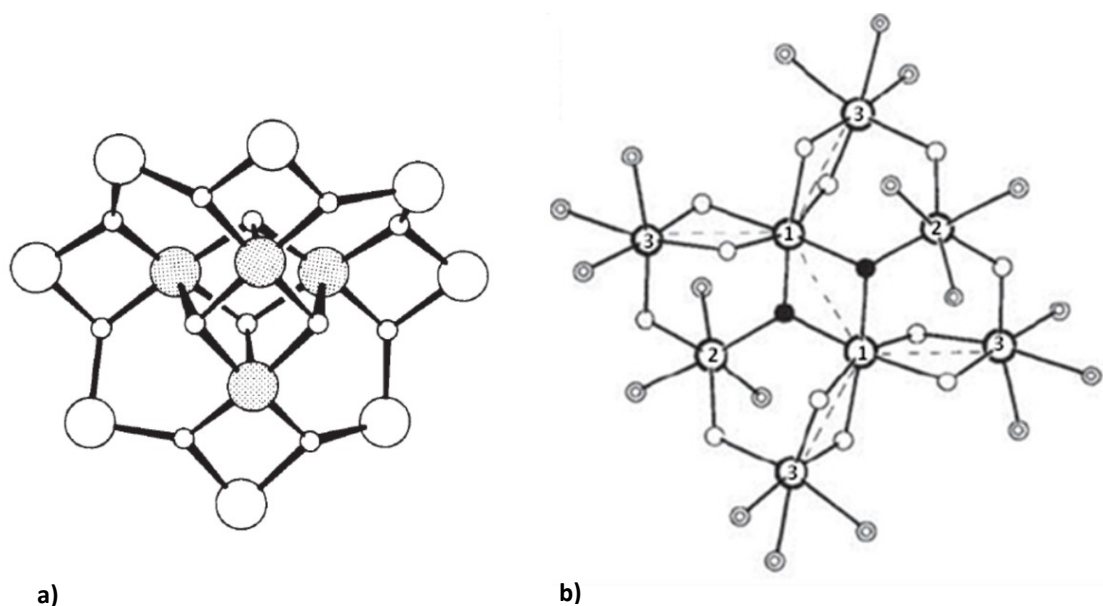


Fig. 2.5. (a) Schematic representation of the Mn₁₂ core. Large circles represent Mn(III) ions while the shaded shown Mn(IV). Bridging oxides are represented as small circles. The acetate bridging ligands and the four water molecules of the cluster have been omitted for clarity. (b) Scheme of the Fe₈ cation. Only Fe, O and N have been represented for simplicity. Large circles represent iron atoms, double circles are nitrogen and the others are oxygen atoms. Empty oxygen circles are for μ -OH and full circles for μ_3 -O. Reproduced from Lis 1980^[4] and Wieghardt *et al.* 1984.^[6]

Other examples of SMMs include lanthanide-based compounds and 3d- and 4d-cyanometallates.^{[69] [70]}

So the number of possibilities for the design of new SMMs is endless, due to the extensive number of metal atoms, ligands and their combinations. The aim of the examples presented here is to show the versatility of this field due to the chemical approach in the design of new molecules. The remainder of this chapter will focus on SMMs based on Co(II) and on those presenting a cubane based structure.

2.4.4.1 SMM based on Co(II)^[3]

There are many examples of SMMs based on Co(II); some of them are listed below. Schemes of the different ligands present in the examples given can be found in (Table 2.6).

Co₄-cubanes: the first example was reported in 2002. It was a compound with formula [Co₄(hmp)₄(MeOH)₄Cl₄] (hmp = monovalent anion of 2-hydroxymethylpyridine), which crystallises in the tetragonal system, space group I-42d. The Co(II) ions reside on the vertices of a cube with an octahedral environment for each. The cluster presents S₄ symmetry. Magnetic results show ferromagnetic coupling of the Co(II) centers with S = 2.^[71]

In 2008, a new derivative based on a cobalt citrate cubane, with formula $[\text{Guanidinium}]_8[\text{Co}_4(\text{citrate})_4] \cdot 8(\text{H}_2\text{O})$ was reported and studied simultaneously by two different research groups with $\Delta E/\kappa_B = 24 \text{ K}$ and $\tau_0 = 3.4 \cdot 10^{-8} \text{ s}$.^{[27] [26]} Since then many other examples of Co-cubanes have been reported.^{[25] [72] [73] [26] [27] [1] [3] [28] [74]} Although most of them present additional Co(II) atoms coordinated to the periphery of the cube, forming discrete molecules or polymers, magnetic measurements show that the cubane behaves as an isolated unit. The blocking temperature of the Co₄ clusters falls in the same range for all of those examples. The presence of additional Co(II) centres seems to introduce slight modifications in the energy barriers and to modify the magnetic behaviour after the blocking of the cubane.

Co₄ squares: compounds with general formula $[\text{Co}_4\text{L}_4]$. When L is N,N'-di[1-(2-hydroxyphenyl)ethylidene]-hydrazone, a compound in which the Co(II) ions are located at the vertices of a square is obtained. The environment of the cobalt atoms is a trigonal bipyramid with two N atoms at the axial positions and three O atoms at the apical sites. Magnetic results are in agreement with 4 spins of $S = 1/2$, ferromagnetically coupled, and show a $\Delta E/\kappa_B = 39 \text{ K}$ and $\tau_0 = 5.4 \cdot 10^{-9} \text{ s}$.^[75]

Co₅ square pyramids: The compound $[\text{Co}_5(\mu_4\text{-N}_3)(\text{piv})(\text{tbdea})_2(\mu\text{-pivalic})_4(\text{MeCN})_2]$ (tbdea = N-tertbutyldiethanolamine) presents a distorted structure in which the Co(II) atoms are at the vertices of a square pyramid. Those at the base of the pyramid have an octahedral environment formed by 4 O and 2 N atoms while at the apex there is trigonal prismatic coordination to 6 O atoms. Again, magnetic results show ferromagnetic coupling with $\Delta E/\kappa_B = 14 \text{ K}$ and $\tau_0 = 1.7 \cdot 10^{-7} \text{ s}$.^[76]

Co₇ disks: One of the most popular families of Co(II) based SMMs. These compounds can be mixed-valence and are obtained with many ligands. The structure is a central Co atom surrounded by a six-membered ring of Co atoms. The cluster presents S₆ symmetry. The first example exhibiting SMM behaviour was reported in 2006. It is a compound with formula $[\text{Co}_7(\text{bzip})_6(\text{N}_3)_9(\text{CH}_3\text{O})_3] [\text{ClO}_4]_2$ (bzip = 2-benzoyl pyridine) formed exclusively by Co(II) ions in octahedral environments. The metal atoms are coupled ferromagnetically.^[77]

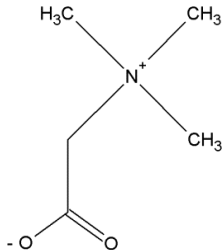
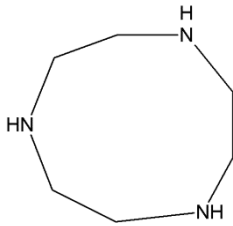
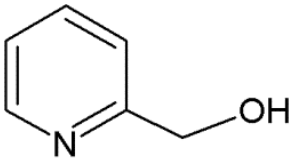
Co₁₂ clusters: The compound $[\text{Co}_{12}(\text{bm})_{12}(\text{NO}_3)(\text{O}_2\text{CMe})_6(\text{EtOH})_6][\text{NO}_3]_5$ (bm = benzimidazol-2-yl-methanol) presents a structure based on three cubanes connected by a central μ_6 -nitrate bridge. The Co atoms present octahedral environments, two of them formed by 6 O atoms and the remaining two by 2 N and 4 O atoms. The complete cluster presents C₃

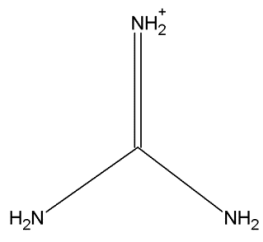
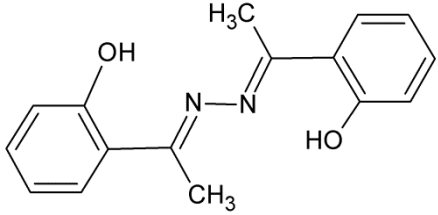
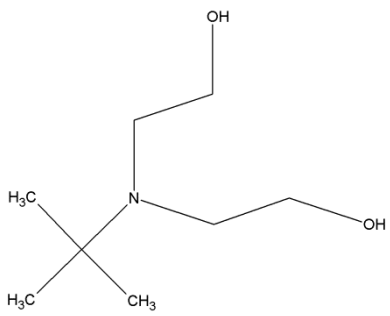
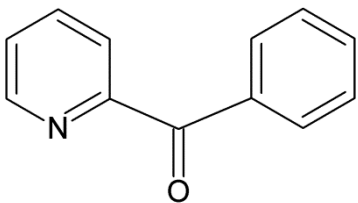
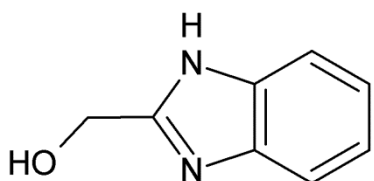
symmetry. The magnetic measurements are in accord with ferromagnetic coupling of the 12 S = 1/2 spins.^[78]

2.4.4.2 SMM based on cubanes

Finally, a survey on the commonest metal atoms used in SMMs based on cubanes has been done using the Web Of Science (WOS Version 5.13.1). Cubane-like structures presenting slow magnetic relaxation have been found for Co(II),^[3] Dy(III),^{[79] [80]} Fe(II),^[81] Ni(II),^{[82] [83]} Zn(II),^[72] Cu(II),^[84] homometallic mixed valence compounds^[85] and heterometallic derivatives containing Mn³⁺Ni²⁺, Mn³⁺Zn²⁺,^[86] Cu²⁺Y³⁺, Cu²⁺Gd³⁺.^[87]

Table 2.6 shows a schematic representation of the ligands present in the examples presented in section 2.4.4.

NAME	SCHEME
Betaine	
1,4,7-triazacyclononane (tacn)	
2-hydroxymethylpyridine (hmp)	

Guanidinium	 <chem>[NH2+]=NC(N)=N</chem>
N,N'-di[1-(2-hydroxyphenyl)ethylidene]- hydrazone	 <chem>C=C(O)c1ccccc1O=N=N/C=C(O)c1ccccc1O</chem>
N-tertbutyldiethanolamine (tbdea)	 <chem>CC(C)(C)NCCO</chem>
2-benzoyl pyridine (bzp)	 <chem>O=C(c1ccccc1)c2ccncc2</chem>
benzimidazol-2-yl-methanol (bm)	 <chem>OCc1nc2ccccc2n1</chem>

2.5 Deposition of SMMs on surfaces

The properties of SMMs, and of molecule-based magnets in general, are of great interest not only for basic research but also for technological applications, since SMMs admit interesting possibilities such as the design of hybrid materials or facile processing and modification. However, if the final aim is to produce a technological device, such a storage memories or sensors, it is compulsory to deposit the SMMs on a surface, and it is at this point that still-unresolved issues arise.

The requirements for getting a suitable deposition of SMMs on a surface are very demanding. Serendipity does not enter into this process; all components of the system and process must be carefully conceived. The first step is to choose an appropriate surface. Commonly gold or silicon are early choices because of their relevance in the computer industry. When a molecule is anchored to a surface it will interact with it. That interaction has to preserve the SMM properties and not allow the interaction of the molecule with its neighbours. In addition, there must be an information-transport-capable connection between the SMM molecule and the substrate in order to transfer the information that might be stored on the surface-bound molecules to another device as well. In addition, there are other prerequisites for the deposition. Firstly, the molecules have to be organized on the substrate in an ordered, addressable fashion. That is, the pattern of the SMM on the surface should be known, ordered and homogeneous. And secondly, the deposition process has to be reproducible in order to validate the procedure and to be useful for the preparation of analogous replicas.

There are many techniques for the deposition of molecules on different surfaces.

a. **Langmuir-Blodgett films (LB films)** ^[88] ^[89] ^[90]

LB films have generated great interest in recent years for preparing monolayers of a wide variety of compounds. Those examples related to our research are summarised below.

Polyoxometalates (POMs)

A schematic representation of these compounds shows them as negative spheres, so an analogy to our cubanes is easily established. The POMs form LB films when a cationic surfactant is used. The process is based on spreading an organic solution of the cationic surfactant onto a diluted aqueous solution of the POM, producing the adsorption of the

molecules on the positive side of the surfactant. Surfactants that could be used are DODA (Dioctadecylamine, $[\text{CH}_3(\text{CH}_2)_{17}]_2\text{NH}$) and behenic acid ($\text{CH}_3(\text{CH}_2)_{20}\text{COOH}$).^[91]

Magnetic results show that the clusters are magnetically isolated (results similar to those obtained when powder samples were measured) and that there is a restricted orientation of the clusters within the layer. There are some experimental results in which the counter-ions of the POMs have been replaced by cationic surfactants.^{[92] [93] [94]}

$[\text{Mn}_{12}\text{O}_{12}(\text{benzoate})_{16}]$

When chloroform solutions of this derivative are spread onto an aqueous solution the formation of an interface is not observed. It is necessary to prepare a mixture with behenic acid in order to obtain a monolayer. Only if the ratio cluster/lipid is high enough can the Mn12 monolayer be stable for a significant time.^[88]

Ferritin^{[95] [96]}

Ferritin molecules are negatively charged at pH higher than 5. Monolayers of ferritine are obtained when aqueous solutions of this compound at pH 5.7 are spread onto different surfactants, namely eicosylamine ($\text{C}_{20}\text{H}_{43}\text{N}$) and mixtures of DOMA (dioctadecyldimethylammonium bromide) and dimethyl stearate (SME). No ferritin adsorption is observed when pure SME is used. Ferritin shows a preferential bonding to eicosylamine as compared to DOMA films, despite the higher positive potential of DOMA. When DOMA is diluted in SME, ferritin adsorption increases up to a value similar to that obtained with eicosylamine. The results suggest an electrostatic-based mechanism. The superparamagnetic properties are preserved in the monolayer.

b. Laser ablation^[97]

Experiments performed for Mn12 samples with excimer lasers whose energies ranged from 200 to 450 mJ show a partial fragmentation of the molecules.^[98]

Pulsed laser deposition (PLD) experiments have been performed with a nitrogen laser that uses much lower pulsed energy for the ablation process (*e.g.*, a pulse frequency of 8 Hz with $E = 0.8$ mJ and a pulse frequency of 20 Hz with $E = 2$ mJ). The crystalline starting material is pressed to form a pellet at mounted in a high vacuum chamber. Glass, mica and Si/SiO₂ were the employed substrates. Results show that the structural and magnetic properties are preserved; however a partial loss of some acetate ligands and water molecules is observed

while the magnetic cores remain intact. The partial fragmentation of the ligands produces a new magnetic phase.

A random distribution of the molecules on the substrate was obtained and some differences in the magnetic behaviour were observed due to fragmentation.

c. **Self-assembly** ^[99] ^[100] ^[65, 101] ^[102]

Self-assembled monolayers (SAM) are formed when a substrate and a sample, with the appropriate reactive functional groups, are placed in contact, either in solution or in the gas phase.

The interaction between substrate and reagent can have several different origins -- covalent bonds, H-bonds, electrostatic interactions or van der Waals interactions.

There are two main approaches to this type of assembly.

- Direct deposition: when the sample with the appropriate functional groups bonds the surface.

An interesting example is Mn₁₂ – acetate films formed on Si/SiO₂ substrates by using the Dip&Dry method.^[103] A homogeneous and smooth film with a continuous coverage of the substrate was obtained. However, magnetic measurements of the samples could not be done due to the small quantity of material deposited and the high background signal from the substrate.

- Surface pre-functionalization: This is a two-step mechanism. Firstly, the substrate is functionalized with something that interacts in the way we want with the sample and then the sample and surface are put together (Figure 2.6).

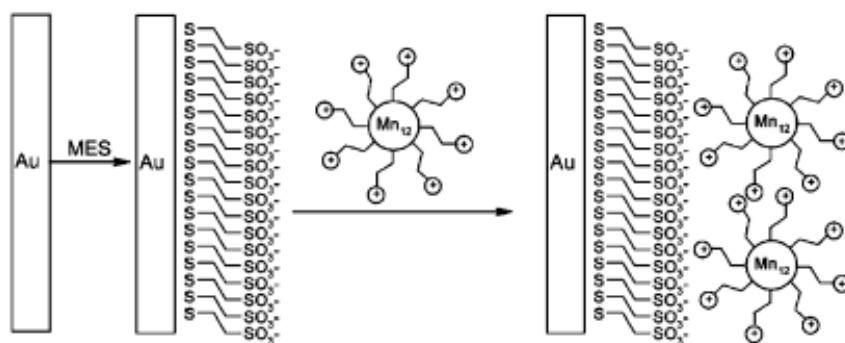


Fig. 2.6. Schematic representation of the pre-functionalization of an Au(111) surface with a layer of MES (sodium mercaptoethanesulfonate) followed by the formation of a monolayer of a positive charged derivative of Mn₁₂. Reproduced from Coronado *et al.* 2005.^[2]

It is possible to functionalize an Au surface with alkane derivatives whose free ends are positively charged head groups (Figure 2.7).^[104] ^[2] For using silicon as a substrate, hydrosilylation should take place between the molecules and the surface.^[105] ^[106] The SMMs thus deposited show a homogenous distribution and no order.

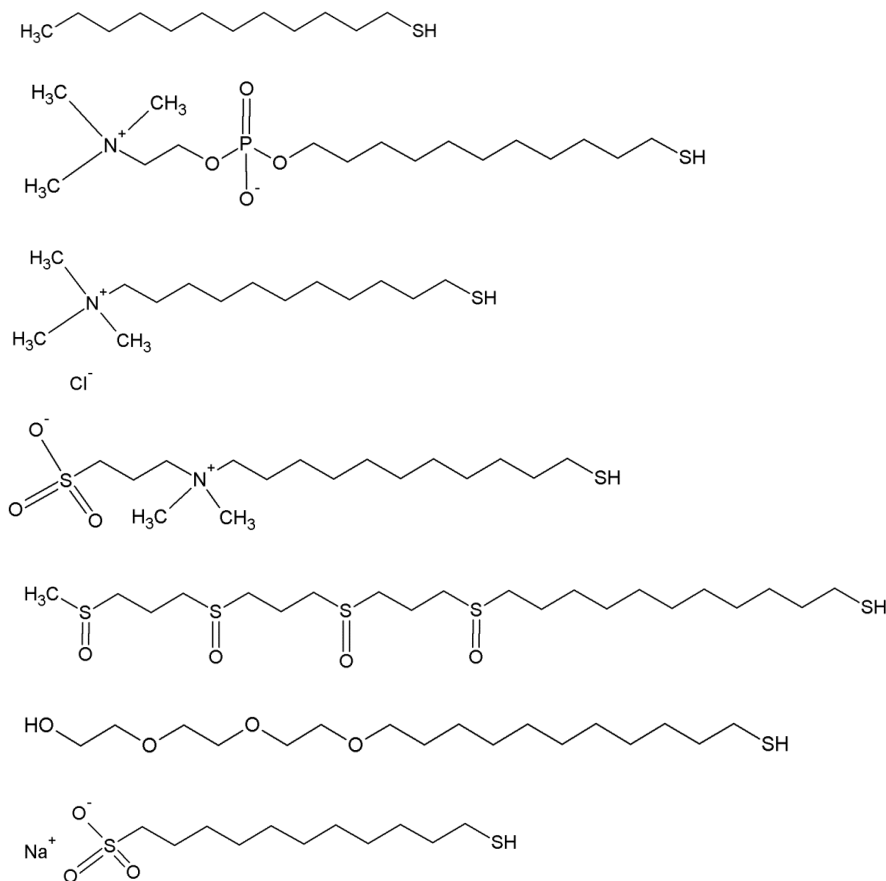


Fig. 2.7. Mercapto-alkane derivatives.

- Deposition on pre-patterned surface.^[107]

Some examples studied the deposition of the Mn12-betaine on a pre-patterned Si(100) surface covered with a APTES (3-Aminopropyl) triethoxysilane) Self Assembled Monolayer (SAM). Once the Si surface is covered with an APTES SAM, the silicon oxide nanopattern is produced by local oxidation nanolithography. The process is based on the preferential deposition of the SMM on the SiO_x pattern due to the attractive electrostatic interaction with the local oxides and the repulsive interaction with the unpatterned substrate.

Finally, a list of the most used substrates is shown in Table 2.7.

Table 2.7. An example of the most used substrates for the deposition of different compound on surfaces.

Substrate		Reference
Au (111) (110)		Ulman 1996 ^[108]
Si (100)		Ulman 1996 ^[108]
Silica (MCM 41)		Ulman 1996 ^[108]
^a SAMs on surfaces		Reference
SAM	Substrate	
1,4-bis(4-pyridyl)benzene	Cu (100)	Ulman 1996 ^[108]
4,4'-bis(4-pyridyl)biphenyl	Cu (100)	Ulman 1996 ^[108]
n-alkanoic acid	AgO	Allara 1985, ^[109] Allara 1985, ^[110] Ogawa 1985 ^[111]
	Al ₂ O ₃	Allara 1985, ^[109] Allara 1985, ^[110] Ogawa 1985 ^[111]
	CuO	Allara 1985, ^[109] Allara 1985, ^[110] Ogawa 1985 ^[111]
alkylchlorosilanes, alkylalkoxysilanes, and alkylaminosilanes	silicon oxide	Sagiv 1980, ^[112] Silberzan 1991, ^[113] Wasserman 1989, ^[114] Le Grange 1993, ^[115] Maoz 1984, ^[116] Gun 1986 ^[117]
	aluminum oxide	Gun 1984, ^[118] Tillman 1988 ^[119]
	quartz	Brandriss 1993 ^[120]
	glass	Gun 1986 ^[117]
	mica	Carson 1989, ^[121] Kessel 1991, ^[122] Schwartz 1992 ^[123]
	zinc selenide	Gun 1986, ^[118] Gun 1984 ^[117]
	germanium oxide	Gun 1986 ^[117]
	gold	Finklea 1986, ^[124] Rubinstein 1986, ^[125] Rubinstein 1986 ^[126]

2.6 Further perspectives and future applications

The field of single molecule magnetism is still at an early stage of development. Although it has been more than two decades since the phenomenon was observed for the first time, there is a great deal of scope for future development. There are uncounted potential applications. Currently, the most interesting applications are focused on the study of new magnetic phenomena. However, despite the fact that putative technological applications are promising, no innovative devices have been developed to date due to the difficulties in ordering and reproducibly anchoring SMMs onto surfaces, as was mentioned in the previous section.

Some possible applications would be:

Magnetic storage devices with higher data density in which each molecule would act as an individual quantum bit. The preparation of materials with high coercive fields will make these materials optimal for applications in which hard magnets are required.

Preparation of hybrid materials that combine slow magnetic relaxation with other properties --electrical or optical properties, for example. That could be achieved by chemical modification of a given material or by the preparation of layered compounds where a layer of an SMM is intercalated with layer of another compound with a different property.

Switchable magnets in which the magnetism could be changed or modulated by an external stimulus.

The versatility of these materials could conceivably allow the preparation of layered SMMs as well as liquid magnets. In addition, a chemical approach to the synthesis of SMMs can be focused on the design of biocompatible materials that could be considered for medical applications.

References

- [1] K. W. Galloway, M. Schmidtman, J. Sanchez-Benitez, K. V. Kamenev, W. Wernsdorfer, M. Murrie, *Dalton Transactions* **2010**, 39, 4727-4729.
- [2] E. Coronado, A. Forment-Aliaga, F. M. Romero, V. Corradini, R. Biagi, V. De Renzi, A. Gambardella, U. del Pennino, *Inorganic Chemistry* **2005**, 44, 7693-7695.
- [3] M. Murrie, *Chemical Society Reviews* **2010**, 39, 1986-1995.
- [4] T. Lis, *Acta Crystallographica Section B-Structural Science* **1980**, 36, 2042-2046.
- [5] R. Sessoli, D. Gatteschi, A. Caneschi, M. A. Novak, *Nature* **1993**, 365, 141-143.
- [6] K. Wieghardt, K. Pohl, I. Jibril, G. Huttner, *Angewandte Chemie-International Edition in English* **1984**, 23, 77-78.
- [7] J. S. Miller, A. J. Epstein, *Mrs Bulletin* **2000**, 25, 21-28.
- [8] D. Serantes, D. Baldomir, Vol. 4, *The Open Surface Science Journal*, **2012**, pp. 71-84.
- [9] F. Lloret, M. Julve, J. Cano, R. Ruiz-Garcia, E. Pardo, *Inorganica Chimica Acta* **2008**, 361, 3432-3445.
- [10] J. S. Miller, A. J. Epstein, in *Materials Chemistry: an Emerging Discipline*, Vol. 245 (Eds.: L. V. Interrante, L. A. Caspar, A. B. Ellis), **1995**, pp. 161-188.
- [11] D. Gatteschi, *Advanced Materials* **1994**, 6, 635-645.
- [12] P. Day, A. E. Underhill, *Philosophical Transactions of the Royal Society a-Mathematical Physical and Engineering Sciences* **1999**, 357, 2851-2853.
- [13] G. Christou, D. Gatteschi, D. N. Hendrickson, R. Sessoli, *Mrs Bulletin* **2000**, 25, 66-71.
- [14] J. S. Miller, P. J. Krusic, A. J. Epstein, W. M. Reiff, J. H. Zhang, *Molecular Crystals and Liquid Crystals* **1985**, 120, 27-34.
- [15] J. S. Miller, J. C. Calabrese, A. J. Epstein, R. W. Bigelow, J. H. Zhang, W. M. Reiff, *Journal of the Chemical Society-Chemical Communications* **1986**, 1026-1028.
- [16] J. S. Miller, *Pramana-Journal of Physics* **2006**, 67, 1-16.
- [17] M. Tamura, Y. Nakazawa, D. Shiomi, K. Nozawa, Y. Hosokoshi, M. Ishikawa, M. Takahashi, M. Kinoshita, *Chemical Physics Letters* **1991**, 186, 401-404.
- [18] A. J. Banister, N. Bricklebank, I. Lavender, J. M. Rawson, C. I. Gregory, B. K. Tanner, W. Clegg, M. R. J. Elsegood, F. Palacio, *Angewandte Chemie-International Edition in English* **1996**, 35, 2533-2535.
- [19] F. Palacio, G. Antorrena, M. Castro, R. Burriel, J. Rawson, J. N. B. Smith, N. Bricklebank, J. Novoa, C. Ritter, *Physical Review Letters* **1997**, 79, 2336-2339.
- [20] M. Mito, T. Kawae, K. Takeda, S. Takagi, Y. Matsushita, H. Deguchi, J. M. Rawson, F. Palacio, *Polyhedron* **2001**, 20, 1509-1512.
- [21] K. Awaga, E. Coronado, M. Drillon, *Mrs Bulletin* **2000**, 25, 52-57.
- [22] V. Laget, C. Hornick, P. Rabu, M. Drillon, R. Ziessel, *Coordination Chemistry Reviews* **1998**, 178, 1533-1553.
- [23] E. Coronado, C. Marti-Gastaldo, E. Navarro-Moratalla, A. Ribera, *Inorganic Chemistry* **2010**, 49, 1313-1315.
- [24] G. C. Defotis, F. Palacio, C. J. Oconnor, S. N. Bhatia, R. L. Carlin, *Journal of the American Chemical Society* **1977**, 99, 8314-8315.
- [25] M. Murrie, S. J. Teat, H. Stoeckli-Evans, H. U. Gudel, *Angewandte Chemie-International Edition* **2003**, 42, 4653-4656.
- [26] B. Moubaraki, K. S. Murray, T. A. Hudson, R. Robson, *European Journal of Inorganic Chemistry* **2008**, 4525-4529.
- [27] K. W. Galloway, A. M. Whyte, W. Wernsdorfer, J. Sanchez-Benitez, K. V. Kamenev, A. Parkin, R. D. Peacock, M. Murrie, *Inorganic Chemistry* **2008**, 47, 7438-7442.
- [28] E. Burzuri, J. Campo, L. R. Falvello, E. Forcen-Vazquez, F. Luis, I. Mayoral, F. Palacio, C. Saenz de Pipaon, M. Tomas, *Chemistry-a European Journal* **2011**, 17, 2818-2822.

- [29] G. S. Papaefstathiou, A. Escuer, R. Vicente, M. Font-Bardia, X. Solans, S. P. Perlepes, *Chemical Communications* **2001**, 2414-2415.
- [30] E. C. Yang, W. Wernsdorfer, L. N. Zakharov, Y. Karaki, A. Yamaguchi, R. M. Isidro, G. D. Lu, S. A. Wilson, A. L. Rheingold, H. Ishimoto, D. N. Hendrickson, *Inorganic Chemistry* **2006**, *45*, 529-546.
- [31] A. Ferguson, J. Lawrence, A. Parkin, J. Sanchez-Benitez, K. V. Kamenev, E. K. Brechin, W. Wernsdorfer, S. Hill, M. Murrie, *Dalton Transactions* **2008**, 6409-6414.
- [32] G. Chaboussant, A. Sieber, S. Ochsenein, H. U. Gudel, M. Murrie, A. Honecker, N. Fukushima, B. Normand, *Physical Review B* **2004**, *70*.
- [33] O. Waldmann, *Inorganic Chemistry* **2007**, *46*, 10035-10037.
- [34] E. Ruiz, J. Cirera, J. Cano, S. Alvarez, C. Loose, J. Kortus, *Chemical Communications* **2008**, 52-54.
- [35] N. Ishikawa, M. Sugita, W. Wernsdorfer, *Angewandte Chemie-International Edition* **2005**, *44*, 2931-2935.
- [36] C.-I. Yang, W. Wernsdorfer, G.-H. Lee, H.-L. Tsai, *Journal of the American Chemical Society* **2007**, *129*, 456-457.
- [37] C. J. Milios, A. Vinslava, W. Wernsdorfer, S. Moggach, S. Parsons, S. P. Perlepes, G. Christou, E. K. Brechin, *Journal of the American Chemical Society* **2007**, *129*, 2754-+.
- [38] K. Hegetschweiler, B. Morgenstern, J. Zubieta, P. J. Hagrman, N. Lima, R. Sessoli, F. Totti, *Angewandte Chemie-International Edition* **2004**, *43*, 3436-3439.
- [39] R. Bagai, G. Christou, *Chemical Society Reviews* **2009**, *38*, 1011-1026.
- [40] P. Artus, C. Boskovic, J. Yoo, W. E. Streib, L. C. Brunel, D. N. Hendrickson, G. Christou, *Inorganic Chemistry* **2001**, *40*, 4199-4210.
- [41] M. Soler, P. Artus, K. Folting, J. C. Huffman, D. N. Hendrickson, G. Christou, *Inorganic Chemistry* **2001**, *40*, 4902-4912.
- [42] N. E. Chakov, W. Wernsdorfer, K. A. Abboud, G. Christou, *Inorganic Chemistry* **2004**, *43*, 5919-5930.
- [43] C. Boskovic, M. Pink, J. C. Huffman, D. N. Hendrickson, G. Christou, *Journal of the American Chemical Society* **2001**, *123*, 9914-9915.
- [44] H. B. Heersche, Z. de Groot, J. A. Folk, H. S. J. van der Zant, C. Romeike, M. R. Wegewijs, L. Zobbi, D. Barreca, E. Tondello, A. Cornia, *Physical Review Letters* **2006**, *96*.
- [45] A. Caneschi, D. Gatteschi, C. Sangregorio, R. Sessoli, L. Sorace, A. Cornia, M. A. Novak, C. Paulsen, W. Wernsdorfer, *Journal of Magnetism and Magnetic Materials* **1999**, *200*, 182-201.
- [46] M. Soler, W. Wernsdorfer, K. A. Abboud, J. C. Huffman, E. R. Davidson, D. N. Hendrickson, G. Christou, *Journal of the American Chemical Society* **2003**, *125*, 3576-3588.
- [47] E. Coronado, A. Forment-Aliaga, A. Gaita-Arino, C. Gimenez-Saiz, F. M. Romero, W. Wernsdorfer, *Angewandte Chemie-International Edition* **2004**, *43*, 6152-6156.
- [48] A. Forment-Aliaga, E. Coronado, M. Feliz, A. Gaita-Arino, R. Llusar, F. M. Romero, *Inorganic Chemistry* **2003**, *42*, 8019-8027.
- [49] H. J. Eppley, H. L. Tsai, N. Devries, K. Folting, G. Christou, D. N. Hendrickson, *Journal of the American Chemical Society* **1995**, *117*, 301-317.
- [50] S. M. J. Aubin, Z. M. Sun, H. J. Eppley, E. M. Rumberger, I. A. Guzei, K. Folting, P. K. Gantzel, A. L. Rheingold, G. Christou, D. N. Hendrickson, *Inorganic Chemistry* **2001**, *40*, 2127-2146.
- [51] Y. G. Wei, S. W. Zhang, M. C. Shao, Y. Q. Tang, *Polyhedron* **1997**, *16*, 1471-1475.
- [52] Z. M. Sun, D. Ruiz, E. Rumberger, C. D. Incarvito, K. Folting, A. L. Rheingold, G. Christou, D. N. Hendrickson, *Inorganic Chemistry* **1998**, *37*, 4758-4759.
- [53] M. Soler, W. Wernsdorfer, Z. M. Sun, D. Ruiz, J. C. Huffman, D. N. Hendrickson, G. Christou, *Polyhedron* **2003**, *22*, 1783-1788.

- [54] R. Sessoli, H. L. Tsai, A. R. Schake, S. Y. Wang, J. B. Vincent, K. Folting, D. Gatteschi, G. Christou, D. N. Hendrickson, *Journal of the American Chemical Society* **1993**, *115*, 1804-1816.
- [55] K. Takeda, K. Awaga, T. Inabe, *Physical Review B* **1998**, *57*, R11062-R11064.
- [56] J. An, Z. D. Chen, J. Bian, J. T. Chen, S. X. Wang, S. Gao, G. X. Xu, *Inorganica Chimica Acta* **2000**, *299*, 28-34.
- [57] D. Ruiz, Z. M. Sun, B. Albelá, K. Folting, J. Ribas, G. Christou, D. N. Hendrickson, *Angewandte Chemie-International Edition* **1998**, *37*, 300-302.
- [58] D. Ruiz-Molina, P. Gerbier, E. Rumberger, D. B. Amabilino, I. A. Guzei, K. Folting, J. C. Huffman, A. Rheingold, G. Christou, J. Veciana, D. N. Hendrickson, *Journal of Materials Chemistry* **2002**, *12*, 1152-1161.
- [59] J. Gomez-Segura, E. Lhotel, C. Paulsen, D. Luneau, K. Wurst, J. Veciana, D. Ruiz-Molina, P. Gerbier, *New Journal of Chemistry* **2005**, *29*, 499-503.
- [60] H. H. Zhao, C. P. Berlinguette, J. Bacsá, A. V. Prosvirin, J. K. Bera, S. E. Tichy, E. J. Schelter, K. R. Dunbar, *Inorganic Chemistry* **2004**, *43*, 1359-1369.
- [61] H. L. Tsai, D. M. Chen, C. I. Yang, T. Y. Jwo, C. S. Wur, G. H. Lee, Y. Wang, *Inorganic Chemistry Communications* **2001**, *4*, 511-514.
- [62] N. E. Chakov, W. Wernsdorfer, K. A. Abboud, D. N. Hendrickson, G. Christou, *Dalton Transactions* **2003**, 2243-2248.
- [63] T. Kuroda-Sowa, T. Handa, T. Kotera, M. Maekawa, M. Munakata, H. Miyasaka, M. Yamashita, *Chemistry Letters* **2004**, *33*, 540-541.
- [64] G. Q. Bian, T. Kuroda-Sowa, H. Konaka, M. Hatano, M. Maekawa, M. Munakata, H. Miyasaka, M. Yamashita, *Inorganic Chemistry* **2004**, *43*, 4790-4792.
- [65] L. Zobbi, M. Mannini, M. Pacchioni, G. Chastanet, D. Bonacchi, C. Zanardi, R. Biagi, U. Del Pennino, D. Gatteschi, A. Cornia, R. Sessoli, *Chemical Communications* **2005**, 1640-1642.
- [66] M. Pacchioni, A. Cornia, A. C. Fabretti, L. Zobbi, D. Bonacchi, A. Caneschi, G. Chastanet, D. Gatteschi, R. Sessoli, *Chemical Communications* **2004**, 2604-2605.
- [67] C. Delfs, D. Gatteschi, L. Pardi, R. Sessoli, K. Wieghardt, D. Hanke, *Inorganic Chemistry* **1993**, *32*, 3099-3103.
- [68] E. Ruiz, J. Cano, S. Alvarez, *Chemistry-a European Journal* **2005**, *11*, 4767-4771.
- [69] R. Sessoli, A. K. Powell, *Coordination Chemistry Reviews* **2009**, *253*, 2328-2341.
- [70] J.-N. Rebilly, T. Mallah, in *Single-Molecule Magnets and Related Phenomena, Vol. 122* (Ed.: R. Winpenney), **2006**, pp. 103-131.
- [71] E. C. Yang, D. N. Hendrickson, W. Wernsdorfer, M. Nakano, L. N. Zakharov, R. D. Sommer, A. L. Rheingold, M. Ledezma-Gairaud, G. Christou, *Journal of Applied Physics* **2002**, *91*, 7382-7384.
- [72] T. A. Hudson, K. J. Berry, B. Moubaraki, K. S. Murray, R. Robson, *Inorganic Chemistry* **2006**, *45*, 3549-3556.
- [73] J. Campo, L. R. Falvello, I. Mayoral, F. Palacio, T. Soler, M. Tomas, *Journal of the American Chemical Society* **2008**, *130*, 2932-2933.
- [74] L. R. Falvello, E. Forcen-Vazquez, I. Mayoral, M. Tomas, F. Palacio, *Acta Crystallographica Section C-Crystal Structure Communications* **2011**, *67*, M359-M363.
- [75] D. Wu, D. Guo, Y. Song, W. Huang, C. Duan, O. Meng, O. Sato, *Inorganic Chemistry* **2009**, *48*, 854-860.
- [76] F. Kloewer, Y. Lan, J. Nehr Korn, O. Waldmann, C. E. Anson, A. K. Powell, *Chemistry-a European Journal* **2009**, *15*, 7413-7422.
- [77] Y.-Z. Zhang, W. Wernsdorfer, F. Pan, Z.-M. Wang, S. Gao, *Chemical Communications* **2006**, 3302-2006.
- [78] M.-H. Zeng, M.-X. Yao, H. Liang, W.-X. Zhang, X.-M. Chen, *Angewandte Chemie-International Edition* **2007**, *46*, 1832-1835.
- [79] Y. Gao, G.-F. Xu, L. Zhao, J. Tang, Z. Liu, *Inorganic Chemistry* **2009**, *48*, 11495-11497.

- [80] D. Savard, P.-H. Lin, T. J. Burchell, I. Korobkov, W. Wernsdorfer, R. Clerac, M. Murugesu, *Inorganic Chemistry* **2009**, *48*, 11748-11754.
- [81] H. Oshio, N. Hoshino, T. Ito, M. Nakano, *Journal of the American Chemical Society* **2004**, *126*, 8805-8812.
- [82] D. Venegas-Yazigi, J. Cano, E. Ruiz, S. Alvarez, *Physica B-Condensed Matter* **2006**, *384*, 123-125.
- [83] S. Hameury, L. Kayser, R. Pattacini, G. Rogez, W. Wernsdorfer, P. Braunstein, *Dalton Transactions* **2013**, *42*, 5013-5024.
- [84] C. Aronica, Y. Chumakov, E. Jeanneau, D. Luneau, P. Neugebauer, A.-L. Barra, B. Gillon, A. Goujon, A. Cousson, J. Tercero, E. Ruiz, *Chemistry-a European Journal* **2008**, *14*, 9540-9548.
- [85] S. M. J. Aubin, M. W. Wemple, D. M. Adams, H. L. Tsai, G. Christou, D. N. Hendrickson, *Journal of the American Chemical Society* **1996**, *118*, 7746-7754.
- [86] P. L. Feng, C. C. Beedle, W. Wernsdorfer, C. Koo, M. Nakano, S. Hill, D. N. Hendrickson, *Inorganic Chemistry* **2007**, *46*, 8126-8128.
- [87] C. Aronica, G. Chastanet, G. Pilet, B. Le Guennic, V. Robert, W. Wernsdorfer, D. Luneau, *Inorganic Chemistry* **2007**, *46*, 6108-6119.
- [88] M. Clemente-Leon, H. Soyer, E. Coronado, C. Mingotaud, C. J. Gomez-Garcia, P. Delhaes, *Angewandte Chemie-International Edition* **1998**, *37*, 2842-2845.
- [89] M. Clemente-Leon, E. Coronado, A. Soriano-Portillo, C. Mingotaud, J. M. Dominguez-Vera, *Advances in Colloid and Interface Science* **2005**, *116*, 193-203.
- [90] M. Cavallini, M. Facchini, C. Albonetti, F. Biscarini, *Physical Chemistry Chemical Physics* **2008**, *10*, 784-793.
- [91] M. Clemente-Leon, E. Coronado, C. L. Gomez-Garcia, C. Mingotaud, S. Ravaine, G. Romualdo-Torres, P. Delhaes, *Chemistry-a European Journal* **2005**, *11*, 3979-3987.
- [92] D. G. Kurth, P. Lehmann, D. Volkmer, H. Colfen, M. J. Koop, A. Muller, A. Du Chesne, *Chemistry-a European Journal* **2000**, *6*, 385-393.
- [93] D. G. Kurth, P. Lehmann, D. Volkmer, A. Muller, D. Schwahn, *Journal of the Chemical Society-Dalton Transactions* **2000**, 3989-3998.
- [94] D. Volkmer, A. Du Chesne, D. G. Kurth, H. Schnablegger, P. Lehmann, M. J. Koop, A. Muller, *Journal of the American Chemical Society* **2000**, *122*, 1995-1998.
- [95] M. Clemente-Leon, E. Coronado, A. Soriano-Portillo, E. Colacio, J. M. Dominguez-Vera, N. Galvez, R. Madueno, M. T. Martin-Romero, *Langmuir* **2006**, *22*, 6993-7000.
- [96] D. W. Britt, D. Mobius, V. Hlady, *Physical Chemistry Chemical Physics* **2000**, *2*, 4594-4599.
- [97] J. Means, V. Meenakshi, R. V. A. Srivastava, W. Teizer, A. Kolomenskii, H. A. Schuessler, H. Zhao, K. R. Dunbar, *Journal of Magnetism and Magnetic Materials* **2004**, *284*, 215-219.
- [98] V. Meenakshi, W. Teizer, D. G. Naugle, H. Zhao, K. R. Dunbar, *Solid State Communications* **2004**, *132*, 471-476.
- [99] A. Cornia, A. C. Fabretti, M. Pacchioni, L. Zobbi, D. Bonacchi, A. Caneschi, D. Gatteschi, R. Biagi, U. Del Pennino, V. De Renzi, L. Gurevich, H. S. J. Van der Zant, *Angewandte Chemie-International Edition* **2003**, *42*, 1645-1648.
- [100] M. Cavallini, G. Aloisi, R. Guidelli, *Langmuir* **1999**, *15*, 2993-2995.
- [101] A. Cornia, A. C. Fabretti, M. Pacchioni, L. Zobbi, D. Bonacchi, A. Caneschi, D. Gatteschi, R. Biagi, U. del Pennino, V. De Renzi, L. Gurevich, H. S. J. Van der Zant, *Journal of Magnetism and Magnetic Materials* **2004**, *272*, E725-E726.
- [102] C. D. Bain, E. B. Troughton, Y. T. Tao, J. Evall, G. M. Whitesides, R. G. Nuzzo, *Journal of the American Chemical Society* **1989**, *111*, 321-335.
- [103] D. M. Seo, V. Meenakshi, W. Teizer, H. Zhao, K. R. Dunbar, *Journal of Magnetism and Magnetic Materials* **2006**, *301*, 31-36.

- [104] R. E. Holmlin, X. X. Chen, R. G. Chapman, S. Takayama, G. M. Whitesides, *Langmuir* **2001**, *17*, 2841-2850.
- [105] G. G. Condorelli, A. Motta, I. L. Fragala, F. Giannazzo, V. Raineri, A. Caneschi, D. Gatteschi, *Angewandte Chemie-International Edition* **2004**, *43*, 4081-4084.
- [106] B. Fleury, L. Catala, V. Huc, C. David, W. Z. Zhong, P. Jegou, L. Baraton, S. Palacin, P. A. Albouy, T. Mallah, *Chemical Communications* **2005**, 2020-2022.
- [107] R. V. Martinez, F. Garcia, R. Garcia, E. Coronado, A. Forment-Aliaga, F. M. Romero, S. Tatay, *Advanced Materials* **2007**, *19*, 291-+.
- [108] A. Ulman, *Chemical Reviews* **1996**, *96*, 1533-1554.
- [109] D. L. Allara, R. G. Nuzzo, *Langmuir* **1985**, *1*, 45-52.
- [110] D. L. Allara, R. G. Nuzzo, *Langmuir* **1985**, *1*, 52-66.
- [111] H. Ogawa, T. Chihara, K. Taya, *Journal of the American Chemical Society* **1985**, *107*, 1365-1369.
- [112] J. Sagiv, *Journal of the American Chemical Society* **1980**, *102*, 92-98.
- [113] P. Silberzan, L. Leger, D. Ausserre, J. J. Benattar, *Langmuir* **1991**, *7*, 1647-1651.
- [114] S. R. Wasserman, Y. T. Tao, G. M. Whitesides, *Langmuir* **1989**, *5*, 1074-1087.
- [115] J. D. Legrange, J. L. Markham, C. R. Kurkjian, *Langmuir* **1993**, *9*, 1749-1753.
- [116] R. Maoz, J. Sagiv, *Journal of Colloid and Interface Science* **1984**, *100*, 465-496.
- [117] J. Gun, J. Sagiv, *Journal of Colloid and Interface Science* **1986**, *112*, 457-472.
- [118] J. Gun, R. Iscovici, J. Sagiv, *Journal of Colloid and Interface Science* **1984**, *101*, 201-213.
- [119] N. Tillman, A. Ulman, J. S. Schildkraut, T. L. Penner, *Journal of the American Chemical Society* **1988**, *110*, 6136-6144.
- [120] S. Brandriss, S. Margel, *Langmuir* **1993**, *9*, 1232-1240.
- [121] G. Carson, S. Granick, *Journal of Applied Polymer Science* **1989**, *37*, 2767-2772.
- [122] C. R. Kessel, S. Granick, *Langmuir* **1991**, *7*, 532-538.
- [123] D. K. Schwartz, S. Steinberg, J. Israelachvili, J. A. N. Zasadzinski, *Physical Review Letters* **1992**, *69*, 3354-3357.
- [124] H. O. Finklea, L. R. Robinson, A. Blackburn, B. Richter, D. Allara, T. Bright, *Langmuir* **1986**, *2*, 239-244.
- [125] I. Rubinstein, E. Sabatani, R. Maoz, J. Sagiv, *Journal of the Electrochemical Society* **1986**, *133*, C130-C130.
- [126] E. Sabatani, I. Rubinstein, R. Maoz, J. Sagiv, *Journal of Electroanalytical Chemistry* **1987**, *219*, 365-371.
- [B3] R. L. Carlin, *Magnetochemistry*, Springer-Verlag, Berlin Heidelberg New York Tokio 1986
- [B4] D. Gatteschi, R. Sessoli, J. Villain, Oxford University Press, 2006. ISBN: 9780199602261

3

0-D Cobalt citrate cubanes.*

A reversible chemical reaction and crystallographic phase transition provoked by dehydration in a discrete cobalt citrate cubane-based compound.

In this and related chapters a family of cobalt citrate cubane-based compounds with dimensionalities ranging from 0-D to 3-D are presented. As mentioned in the introduction, all of them behave as single molecule magnets (SMMs).

This chapter presents two compounds related by a reversible dehydration process. The first compound presents a modulated crystal structure and behaves as an SMM. Upon dehydration, the compound undergoes a reversible chemical transformation in the solid state, giving a discrete, neutral cubane which completes its coordination sphere with four pendant Co(II) units. The resulting compound is still an SMM; nevertheless, the structural transformation is accompanied by changes in the magnetic behaviour.

The two compounds have been fully characterised by single crystal and powder X-Ray diffraction, so that a complete description of the process can be given. In addition, there is clear evidence regarding the mechanism of interconversion of the two derivatives as well as for the reversibility of the transformation.

3.1 Experimental

3.1.1 Synthesis

All reactants were obtained commercially and were used as received. Manipulations were performed under ambient conditions.

The compound with formula $\{\text{Co}_4(\text{C}_6\text{H}_4\text{O}_7)_4[\text{Co}(\text{H}_2\text{O})_4]_2[\text{Co}(\text{H}_2\text{O})_4]_{5/4}[\text{Co}(\text{H}_2\text{O})_5]_{3/4}\} \cdot 4.75\text{H}_2\text{O}$ (**1**). To a stirred solution of citric acid (100 mL, 0.24 M) in deionized water was added $\text{CoCO}_3 \cdot x\text{H}_2\text{O}$ (7.1 gr, 52.34 mmol for $x = 1$). The reaction mixture was heated at 70 °C until no further reaction was observed. The dark red mixture was gravity-filtered and the supernatant was rapidly heated to 90 °C. After several hours heating, a fuchsia-coloured precipitate of **1** was observed and the suspension was filtered. Compound **1** was obtained as a microcrystalline powder whose colour ranges from pink to fuchsia depending on the grain size.

The second derivative, $\{\text{Co}_4(\text{citr})_4[\text{Co}(\text{H}_2\text{O})_4]_4\} \cdot 4\text{H}_2\text{O}$ (**2**), was obtained by dehydration of **1**. Any dehydration strategy can be used for this purpose. Some of the possible procedures are described in section 3.2.1.

3.1.2 Single Crystal X-Ray diffraction

Single crystal X-Ray diffraction data were collected on an Xcalibur S3 CCD-based four-circle diffractometer with a molybdenum source (Oxford Diffraction and Agilent Technologies) and on an Agilent SuperNova Atlas Dual diffractometer with a copper source (Agilent Technologies) at the University Jaime I in Castellon, Spain. The program CrysAlis Pro^[P1] was used for data collection and processing. The average structure of **1**, which was modulated, and the structure of **2** were solved *ab initio* by direct methods^[1] and refined by full-matrix least-squares analysis.^[2] Non-hydrogen atoms were refined with anisotropic displacement parameters. The methylene H atoms of the citrate ligands were placed at idealized positions and refined as riders with isotropic displacement parameters set to 1.2 times the equivalent isotropic U of their respective parent C atoms. For compound **1** no hydrogen atoms belonging to the water molecules were included in the structural model. For compound **2**, hydrogen atoms of the water molecules were found in a difference map and refined as riders on their parent oxygen atoms. Models of the modulation in the crystal of **1** were refined using the program Jana2006.^[P4] (Only the average structure is described here.) For the preparation of graphics and publication material the program Diamond^[P2] was used. Data collection and structure solution and refinement details are shown in Table 3.1.

3.1.3 Powder X-Ray diffraction

Powder X-Ray data were collected using a RIGAKU D/max 2500 diffractometer equipped with a copper rotating anode, operating at 40kV and 100 mA, with a graphite monochromator. Measurements were made for 2θ from 7° to 42° in steps of 0.03° with a rate of 3s/step.

Table 3.1. Crystallographic data for **1** and **2**.

	1 (average structure)	2
Formula	^a C ₂₄ H ₅₉ Co ₈ O _{49.5}	^b C ₂₄ H ₅₆ Co ₈ O ₄₈
fw (g mol⁻¹)	1611.15	1584.13
Radiation	X-Rays	
Wavelength (Å)	1.54184	0.71073
Crystal system	monoclinic	
Space group	C2/c	
Temp (K)	133	100
a (Å)	23.1931(5)	22.8070(17)
b (Å)	9.67387(19)	9.6745(4)
c (Å)	23.5335(5)	23.3079(14)
β (°)	111.076(2)	111.643(8)
V (Å³), Z	4926.93(19), 4	4780.2(5), 4
ρ_{calc} (Mg/m³)	2.172	2.201
μ (mm⁻¹)	21.794	2.841
F (000)	3260.0	3200.0
Crystal size (mm³)	0.17 x 0.12 x 0.04	0.15 x 0.12 x 0.07
θ (min,max) (°)	4.026, 72.218	4.10, 28.71
Reflns collected	23330	21305
Indep reflns	4794	5590
R(int), R(σ)	0.0228, 0.0165	0.0426, 0.0422
Completeness (θ)	0.987 (67.684)	0.905 (27.50)
Abs corr	multi-scan	
T (min,max)	0.205, 1.000	0.880, 1.000
Restraints/parms	0 / 415	0 / 423
Goodness-of-fit	1.048	1.087
R1, wR2 (obs)^c	0.0456 0.1261	0.0408, 0.0864
R1, wR2 (all)	0.0471, 0.1276	0.0599, 0.0912
Δ/σ(max,mean)	0.001, <0.001	0.002, <0.001
Δρ range (e Å⁻³)	1.062, -0.966	0.910, -0.552
^a {Co ₄ (C ₆ H ₄ O ₇) ₄ [Co(H ₂ O) ₄] ₂ [Co(H ₂ O) ₄] _{5/4} [Co(H ₂ O) ₅] _{3/4} }.4.75H ₂ O		
^b {Co ₄ (C ₆ H ₄ O ₇) ₄ [Co(H ₂ O) ₄] ₄ .4H ₂ O		
^c threshold I > 2σ(I).		

3.1.4 FT-IR spectroscopy

The FT-IR spectrum of compound **1** was measured on a Perkin-Elmer Spectrum 100 FT-IR Spectrophotometer with an ATR accessory, in the range of 4000 - 300 cm⁻¹. (Figure 3.1) Due to the instability of compound **2**, only the spectrum of **1** was collected.

IR (neat compound, cm^{-1}): $\nu(\text{OH})$ 3188.01 (w); $\nu(\text{C}=\text{O})$ 1560.23 (w); $\nu(\text{C}-\text{H})$ 1370.96 (w); $\nu(\text{CO})$ 1081.71 (t).

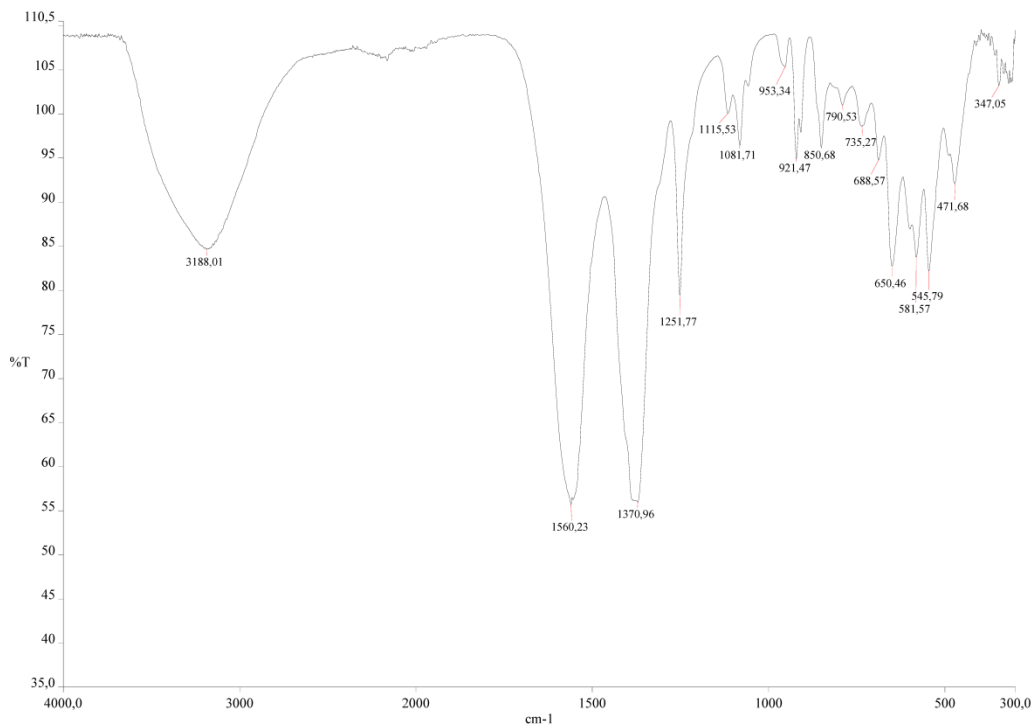


Fig. 3.1. IR spectrum of **1**.

3.1.5 Elemental analysis

Elemental analysis was performed on a Perkin Elmer 2400 CHNS/O analyser. Calculated analysis for $(\text{C}_{24}\text{H}_{59}\text{Co}_8\text{O}_{49.5})$ is: C, 17.98%; H, 3.71%; Results obtained were C, 17.91%; H, 3.16%.

3.1.6 Thermogravimetric analysis (TGA)

Thermogravimetric analysis (TGA) was carried out using a Universal V4.5A TA Instrument, model 2960 SDT V3.0F, in the temperature range 45 - 150 °C (Figure 3.2). The results pertain to measurements beginning with compound **1**, as it is the stable product under ambient conditions.

Dehydration of **1** is a continuous process. However, it can be seen as taking place in three steps. The first process, up to 60 °C, corresponds to the loss of 3 molecules of water. The second step takes place from 60 - 85 °C. It corresponds to a significantly greater weight loss and can be attributed to the egress of 8 molecules of water. Finally, the broadest signal, above 90 °C, corresponds to a loss of 5 molecules of water.

The dehydration process that relates compounds **1** and **2** affect a number of water molecules. In all likelihood, all of the non-coordinated molecules of water in **1** are the first to

leave the structure, provoking a reorganization of the sample that would involve the breaking and formation of covalent Co-O bonds. The point at which compound **2** is obtained falls between the first and the second TGA peaks. Nevertheless, as mentioned above, the dehydration process is continuous, so that although a weight loss corresponding to 3 molecules of water has not specifically been seen in the transformation of **1** into **2**, it is possible to stop the dehydration at this point, simply by using mild conditions.

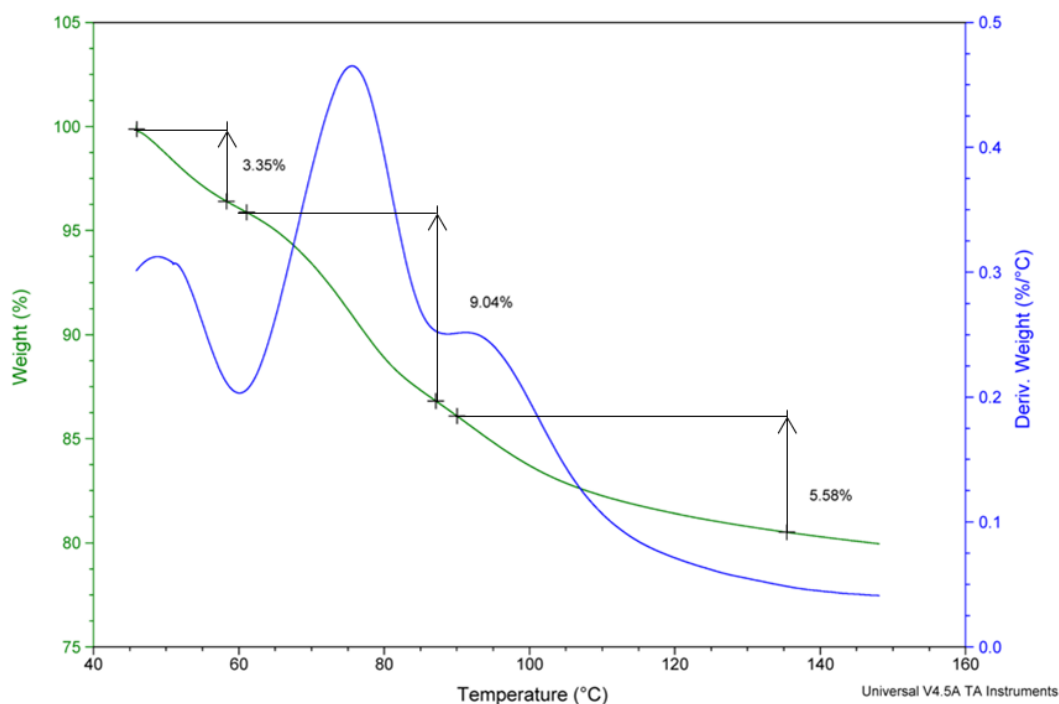


Fig. 3.2. TGA for **1**.

3.1.7 Magnetic characterization

Magnetic characterization of **1** and **2** was performed on a Magnetic Property Measurement System (MPMS), a Physical Property Measurement System (PPMS) from Quantum Design^[P3] and a SQUID magnetometer. To ensure the purity of the phases, the samples were isolated and sealed in Pyrex capsules.

3.2 Results and discussion

3.2.1 Synthesis

Most of the compounds presented in this thesis are obtained under ambient conditions after the addition of a base to the appropriate reactants to attain a pH above 7. Only one compound based on Mn (compound **9**, Chapter 7) and compound **1**, reported here, are crystallised at high temperatures. Small crystals of **1** precipitate from solution only when the reaction medium is heated at about 90 °C. Surprisingly, there is a close relationship between **1** and **2**, on one hand, and the Mn-based compound **9**. Compound **2** is topologically similar to compound **9**, with both possessing a discrete molecular structure; both present monoclinic crystal structures with similar *b*-axis repeats. In both cases the negative charge of the cubane is balanced exclusively by M(II) centres (with M = Co for **1** and **2** and M = Mn for **9**). These units

are doubly bridged to the periphery of the cube. Furthermore, although all of the other Co based compounds presented in this work belong to isomer A (Chapter 1) and those based on Mn to isomer B, the Co-based compounds **1** and **2** present isomer B at their cubane cores. Those analogies can be attributed to the synthetic procedure used.

Apart from that, as mentioned previously, the route for the preparation of **2** can be any process involving soft dehydration. Some of these are described in the following.

A single crystal of **1** can be dehydrated on the diffractometer using a flow of dry N₂. Maintaining a constant temperature of 60 °C for several hours can affect the transition. Alternatively, ramping the temperature from 100 K (a good temperature for measuring data for compound **1**) to a temperature as high as 90 °C will also provoke the transformation. When the transformation is conducted with a crystal on the diffractometer, it can be followed by determination of the unit cell and accompanying orientation matrix of the resulting phase.

When a bulk sample is needed, a microcrystalline powder of **1** can be dehydrated over silica gel beads at room temperature for several days in a desiccator. It is also possible to treat a sample of **1** with acetone inside a closed vial at ambient temperature. The acetone has to be replaced several times, and at the end of the process it is completely removed from the sample surface by placing the sample inside an oven at about 50 °C for several hours.

Some of the strategies described can be combined in order to guarantee the complete dehydration of the sample.

What should be taken into account is the high speed of the rehydration process. Just the humidity of the atmosphere at room temperature is enough to provoke the reversion to **1**. Meticulous care of the sample is required to preserve the integrity of compound **2**.

Finally, there is evidence of the existence of a third derivative, produced when the sample undergoes a massive dehydration. When the sample is heated beyond the point needed for obtaining **2**, it becomes purple. When the purple sample is exposed to a humid atmosphere, it recovers its initial fuchsia colour. This observation will be further described below, with reference to single crystal and powder X-Ray diffraction measurements.

3.2.2 Single Crystal X-Ray diffraction

Compound **1**, whose crystal structure is modulated (*vide infra*), crystallises with an average structure belonging to the monoclinic crystal system, space group C2/c. This compound presents an incommensurately modulated structure; that is, a fourth periodicity exists which is not a rational combination of the three principal periodicities *a*, *b* and *c*. When this additional periodicity is ignored, the resulting analysis gives a disordered model for the structure. The modulation produces additional Bragg diffraction in the form of satellite peaks, which can be observed, for example, in undistorted reciprocal lattice reconstructions (produced using CrysAlis Pro^[P1] in this case, Figure 3.3). The analysis of the structure of a modulated crystal such as **1** can be conducted in two steps. The first employs only the main diffraction peaks and gives the “average structure.” In this step the compound is treated as a disordered structure. In the second step, the main and satellite peaks are used in an attempt to characterise the

modulation, which can be described as the pattern of order in the parts of the structure that appear as disorder in the average structure. Here, the fourth periodicity enters into the analysis. (*N.b.*, other modulated structures can have a fifth and/or sixth periodicity.)

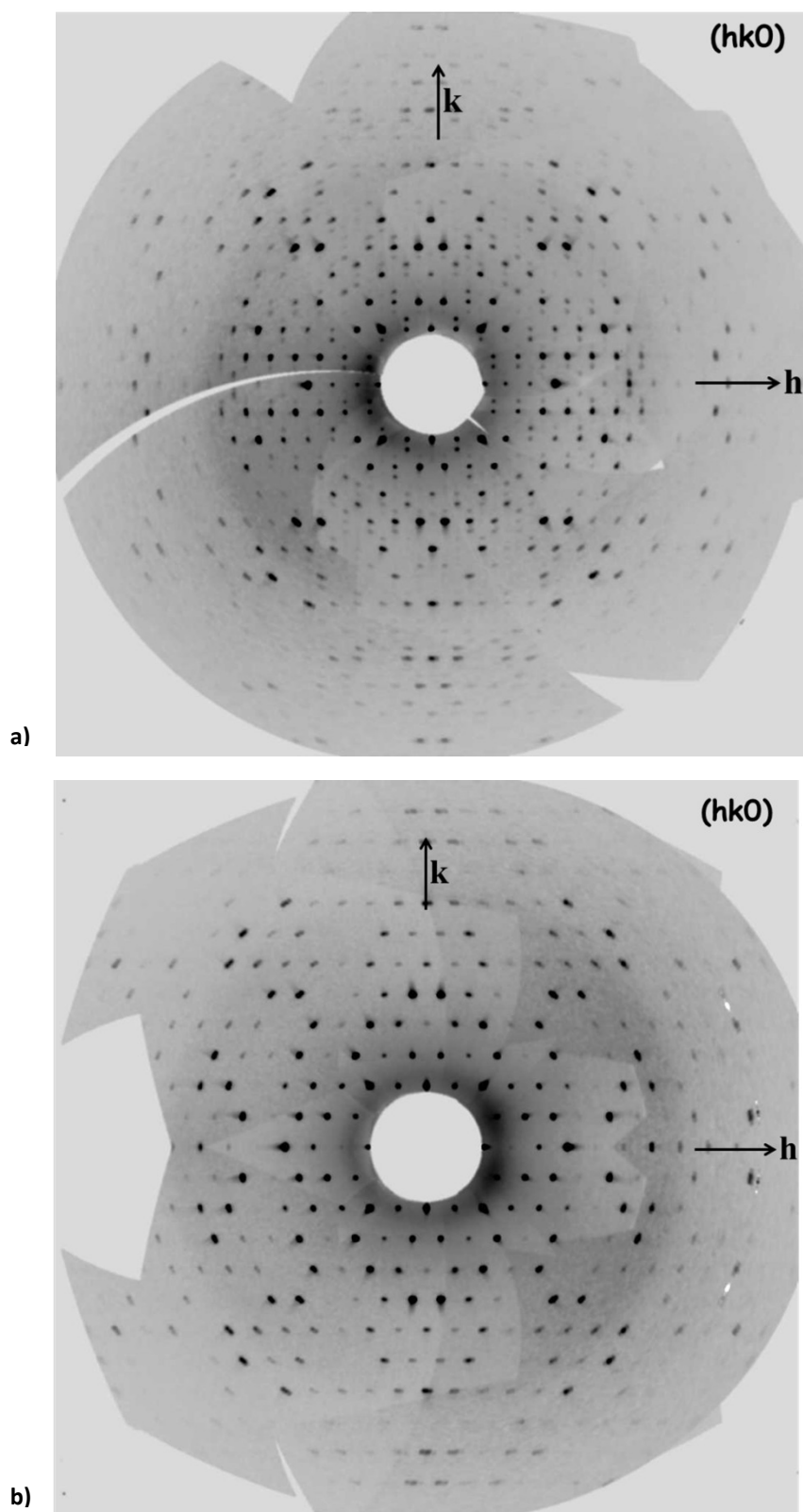


Fig. 3.3. Reciprocal lattice reconstructions, $(hk0)$ plane for 1 (a) and 2 (b).

When solving the “average structure” it is necessary to identify the different chemical entities that enter into the overall model. Once these entities have been defined, the disorder (and later, the modulation) can be described in terms that make chemical sense. It is important to note that in many cases the necessary chemical information can be seen in the average structure, obviating the need to conduct a full analysis of the modulation.

“AVERAGE STRUCTURE”

Compound **1** is based on a cobalt citrate cube, isomer B. In the reference asymmetric unit the absolute configuration of the central C atoms of the citrates is S. Per asymmetric unit there is a half cubane related to the other half by a crystallographic two-fold axis, a complete $[\text{Co}(\text{H}_2\text{O})_4]^{2+}$ unit, 5/8 of a Co(II) chemically formulated as $[\text{Co}(\text{H}_2\text{O})_4]^{2+}$ (Co4), 3/8 of another Co(II) ion formulated as $[\text{Co}(\text{H}_2\text{O})_5]^{2+}$ (Co5) and a total of 10.75 molecules of water distributed over 15 crystallographic sites, including those coordinated to Co3, Co4 and Co5 (Figure 3.4).

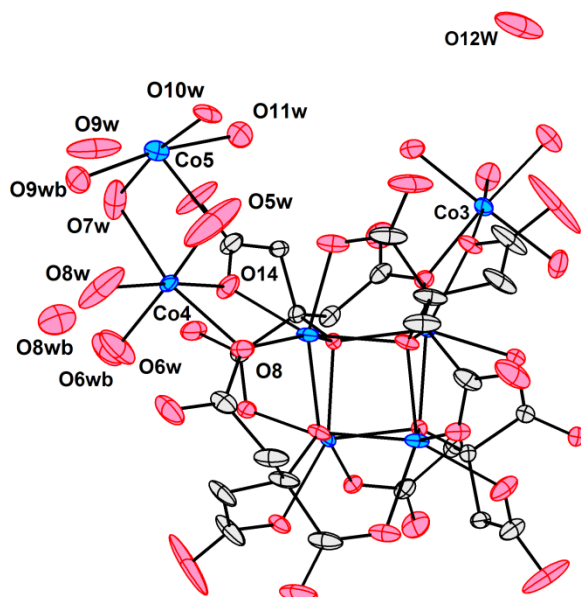


Fig. 3.4. Asymmetric unit for compound **1** with its pendant Co(II) units and free water, only the cubane has been grown. Displacement ellipsoids (probability 50%).

As mentioned before the compound is based on a cobalt citrate cubane, which resides on a two-fold axis. Attached to the periphery of the cube there are two symmetry related Co3 units, each attached to the cube by a double bridge through two internal oxygen atoms from long arms of different citrates (κ^2 -L1i-L8i and L4i-L5i). These units complete their coordination spheres with 4 molecules of water each. These two peripheral units are seen as the rear vertices in the upper left and lower right of Figure 3.5.

With reference to Figure 3.5a, in the upper right and lower left vertices (related by symmetry) the species are disordered. Co4 is doubly bridged to the cube through two internal oxygen atoms from long arms of different citrates (κ^2 -L2i-L3i and L6i-L7i), as is Co3, and completes its coordination sphere with 4 molecules of water. Co5 is singly bridged to the cube through an external oxygen atom of a short arm (S1e, S3e), and 5 molecules of water complete

its coordination sphere. Note that in Figure 3.5a, Co5ⁱⁱ and Co5ⁱⁱⁱ are the disordered congeners of Co4 atoms belonging to neighbouring cubane units, not of the Co4 and Co4ⁱ represented in the picture. Figure 3.5b shows the possible disordered situations in the region of Co4 and Co5. If Co4 is present, Co5 is absent and *vice-versa*.

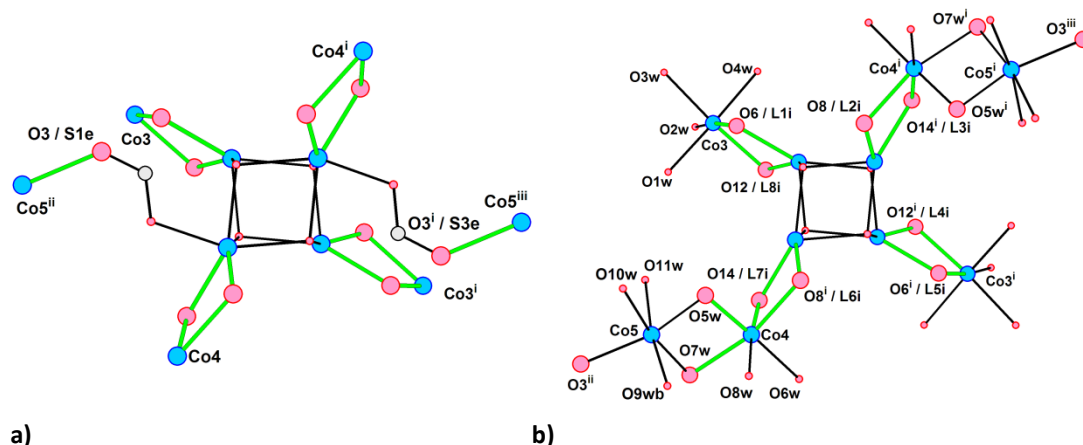


Fig. 3.5. Cubane unit of **1**. (a) Shows the anchoring sites of the peripheral Co(II) to the cubane unit. (b) presents the coordination environment of the Co(II) units along with the two possible disordered positions for Co4 and Co5. Further details are given in the text-. i: (1-x, y, 1.5-z), ii: (1-x, -y, 1-z), iii: (x, -y, 0.5+z).

Co4 and Co5 are not mutually compatible (Figure 3.5); they cannot both be present in the same asymmetric unit due to impossibly short contact between the water molecules present at the same time as each Co atom (O6w---O6wb, 0.835(0.012), O8w---O8wb, 1.120(0.013), O9w---O9wb, 0.719(0.009)). They have half occupancy in a given layer in the disordered model, which means that two species are equally possible, as will be shown further on; the only change is their spatial organization. Within a given layer, the occupancy of peripheral Co(II) must be 4 to balance the charge of the cube; and there will be either two units of Co4 per cubane, or one congener of Co4 and one of Co5, in addition to the constant two units of Co3. However, in the model described below for the modulation, the total occupancy refined is the average for 8 unit cells. Note that per unit cell there are two layers of cubanes related by a center of symmetry.

The experimentally determined modulation vector, the "q-vector," is: $q(1) \text{ } -0.0016(11) \text{ } 0.3759(4) \text{ } 0.0011(10)$ which is approximately $3/8$ of the b^* -axis. This can be interpreted as meaning that the structure is periodically homogeneous in the ac -plane, and that the differences that define the modulation are found upon traversing successive ac -levels, parallel to the b -axis. In fact, the cubane-centred molecules are arranged in rows in the ac -plane, forming a 2-D grid perpendicular to the b -axis. So, the crystal as a whole can be seen as formed by layers or levels in which the structure varies. That variation is periodic, a property which produces the extra diffraction peaks, the "satellite peaks," from which we derive the q -vector. In the average structure the different layers appear superposed, as a disorder assembly; nevertheless, in a modulated structure the components of the disorder can in principle be

distinguished and treated separately. The most complicated step is to conceive a description of the order and organization of the layers throughout the whole crystal.

Our model of the disorder proposes the existence of three different species.

1) A layer formed by a complete cubane with two Co3 and two Co4 centres doubly bridged to its periphery through two internal oxygen atoms from long arms of different citrates. The structure is analogous to that of **2**. Co3 would be coordinated to O1w and to O4w, and Co4 to O5w and O8w. Only two independent molecules of free water are present, namely O9w (hydrogen bonds with O5w, O7w and O8w – 3.092(0.010) Å, 3.300(0.008) Å and 2.977(0.011) Å respectively- and O12w (forming its shortest H-bond with O3w – 2.711(0.005) Å).

2-3) Layers in which a congener of Co4 migrates to a neighbouring cubane unit.

In these layers, when Co4 or Co5 is present in the reference asymmetric unit, it is absent in the asymmetric unit related to this by the two-fold axis, and *vice versa*. For example, if Co4 (x, y, z) is present, Co5 (x, y, z) cannot exist at the same time. On the other hand, when Co4 is present at (x, y, z), then Co4ⁱ (1-x, y 1.5-z) is not present and Co5ⁱ (1-x, y 1.5-z) instead occupies the symmetry-related asymmetric unit. As represented in Figure 3.5, there are two possible combinations, Co4 with Co5ⁱ and Co4ⁱ with Co5.

The chemical explanation of the disorder is a concerted migration of an external Co(II) centre from one cubane to the neighbouring one. The initial structure would be the one in which the four units around the cube are chemically equivalent, as they are in compound **2** (*vide infra*). That is, there are four Co(II) units doubly bridged to the cube in the manner described for Co3 and Co4. The disorder will arise from the migration of one congener of Co4 to a neighbouring cubane, from its parent cubane. The displaced Co4 is renamed as Co5 in our model. At the same time, the destination cubane will transfer one of its Co4 units to an adjacent cubane, and so on along a line of molecules in the same layer.

Co4 is coordinated by aqua ligands O5w through O8w and there are two independent molecules of free water (as described for layer 1), O9w and O12w.

Co5 is coordinated by waters centred on O5w, O7w, O9wb O10w and O11w. Three molecules of free water are present in this case, O6wb, O8wb (forming their shortest H-bond with O14 – 2.907(0.011) Å and O9wb – 2.944(0.015) Å respectively) and O12w.

The migration involves two sites on the cubane, for example the "origin" Co4ⁱ and the destination Co5ⁱ, and there are two possibilities for the direction of the "jump."

Layer 2) Co4 and Co5ⁱ are present and the migration occurs on the upper side of the cube as represented in Figure 3.6a. The direction of the concerted movement is from the left to the right in the figure. In this case, the peripheral Co centres on the molecule in the centre of Figure 3.6a are Co3, Co3ⁱ, Co4 and Co5ⁱⁱ.

Layer 3) The migration involves the lower side of the cube, as represented in Figure 3.6b. The molecule at the centre of the figure has Co3, Co3ⁱ, Co4ⁱ and Co5ⁱⁱⁱ at its periphery. The migration occurs from right to left in the figure.

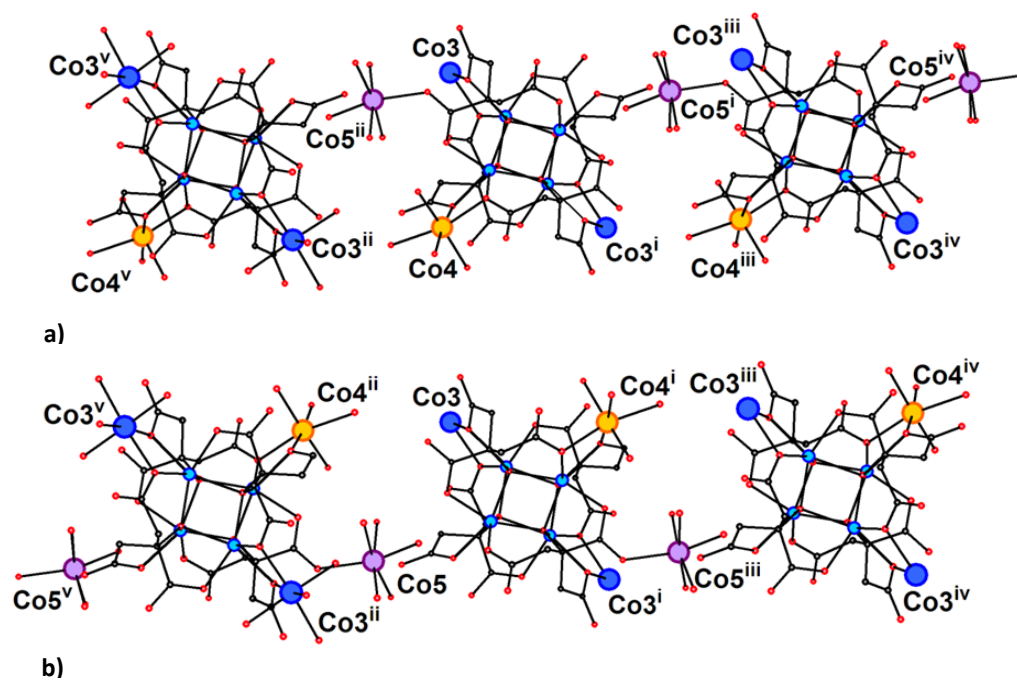


Fig. 3.6. Possibilities for the concerted “jump” of Co4 from one cube to an adjacent one at the upper (a) and the lower (b) sides of the molecule. i: $(1-x, y, 1.5-z)$, ii: $(1-x, -y, 1-z)$, iii: $(x, -y, 0.5+z)$, iv: $(1-x, -y, 2-z)$, v: $(x, -y, -0.5+z)$.

The proposed model for the modulation consists of a stack comprising three unit cells (six layers) formed by layers of 2, one unit cell of the derivative 1, three unit cells formed by layers of 3 and finally, one more unit cell of 1. That would give an overall occupancy for Co4 of $5/8$ ($12 \cdot 1/4 + 4 \cdot 1$) and of $3/8$ for Co5 ($12 \cdot 1/4$). The repetition of this sequence would give the observed satellite diffraction peaks.

The refined displacement parameters for Co4 and Co5, with occupancies of $5/8$ and $3/8$ respectively, are comparable in magnitude, which can be taken to indicate agreement with the proposed occupancies. Also, the occupancies of the water molecules were refined taking into account those of the cobalt atoms to which they are bonded and the necessity of avoiding a model with impossibly short contacts. In the final model the occupancies are mutually consistent and the displacement parameters involved have reasonable values.

In what follows, a detailed description of layers 2 and 3 is given.

LAYERS 2 AND 3

These layers are chemically identical. The only difference between them is the direction of the jump and the relative orientations of the resulting molecules in the crystal. A concerted “jump” of Co4 to occupy the site of Co5 propagated along the row formed by the cubanes is proposed. That supposes, as represented in Figure 3.7, the jump of Co4^i to the site of Co5^i at the same time that Co4^{iv} jumps to the site of Co5^{iv} . In this situation, Co4 and Co4^{iii} will be present and Co5 and Co5^{iii} absent. An alternative to this concerted jump could be the grouping of neighbouring cubanes into pairs. That situation is represented in Figure 3.7. It also involves the jump of Co4^i to the position of Co5^i . The difference is that Co4^{iv} does not jump to another

adjacent cubane unit occupying the site of Co5^{iv} . In this case Co4^{iv} is present and Co4^{iii} jumps to the site of Co^{iii} bonding the cubane unit in the asymmetric unit. The impossible short contacts between the water molecules coordinated to Co5^{i} and Co5^{iii} ($\text{O11w}^{\text{i}}\cdots\text{O10w}^{\text{iii}}$, 2.226(0.012) Å), invalidates this second explanation of the disorder, supporting the idea of the concerted jump.

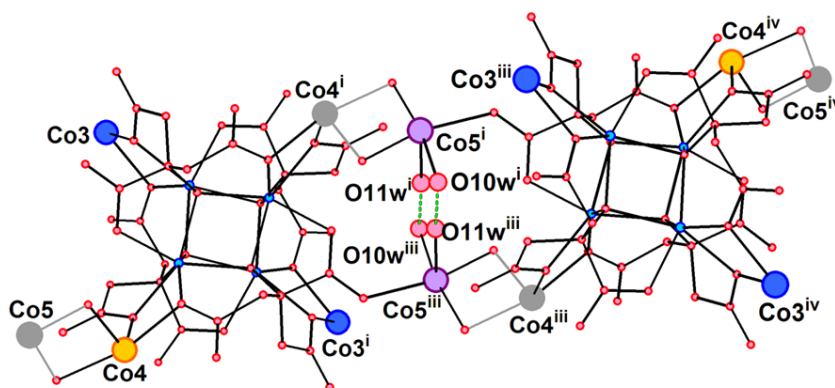


Fig. 3.7. Detailed view of the disordered zone where the proposed jump of the peripheral Co(II) units is observed. Color code for Co atoms: Co3, blue; Co4, orange; Co5, violet. Co4 and Co5 present in the situation proposed in our description of the disorder and previously explained (shown in Fig. 3.6) are represented in gray. Those in colour would be present in the putative second situation. Impossibly short contacts between water molecules coordinated to Co5 are represented as broken green bonds.

The disorder of the cobalt atoms and the water molecules is the same. Symmetry operations are not indicated in the following description of the disorder.

In both cases, when Co4 is present at a given vertex of the cubane, Co5 is absent and *vice versa*. So overall, Co4 is present 5/8 of the time, as layer 1 does not contain Co5, which is present 3/8 of the time. The water molecules merit a detailed analysis due to the diverse roles they play in the different layers.

O1w through O4w → complete occupancy. They are coordinated to Co3.

O5w and O7w → they coordinate 5/8 of the time Co4 and 3/8 of the time Co5, resulting in a total occupancy of 1. O5w has a short contact with O11w from the same unit cell (2.295(0.013) Å). This contact can be explained due to the elongated displacement parameters of O5w. This atom also presents short bond distances to the Co atoms (1.986(0.005) Å to Co4 and 1.8710 (0.0046) Å to Co5). This situation can be attributed to the fact that this water molecule is shared in the two possible congeners and as a result, O5w is placed at an averaged position. We prefer to keep this atom at this site as a unique congener as the refinement is acceptable so far instead of splitting the site into two congeners.

O6w → coordinated to Co4. Total occupancy of 5/8. Short contacts with O8wb (2.583(0.015) Å) from a neighbouring asymmetric unit. Symmetry operator: 1.5-x, 0.5+y, 1.5-z.

O6wb → Free water molecule when Co5 is present. It has short contacts with O8wb (1.969(0.016) Å) from a neighbouring asymmetric unit. Symmetry operator: 1.5-x, 0.5+y, 1.5-z. Total occupancy of 3/8.

O8w → coordinated to Co4. It has short contacts with O9wb (2.383(0.014) Å) of the same asymmetric unit. Total occupancy of 5/8.

O8wb → Free water molecule when Co5 is present. It has short contacts with O6w (2.583(0.015) Å) from a neighbouring asymmetric unit. Symmetry operator: $1.5-x, -0.5+y, 1.5-z$. Total occupancy of 3/8.

O9w → Free water molecule when Co4 is present. It has short contacts with O10w (2.411(0.012) Å) from the same asymmetric unit. Total occupancy of 5/8.

O9wb → Coordinated to Co5. It has a short contact with O5 from a neighbouring asymmetric unit (symmetry code $0.5+x, -0.5+y, z$) (2.497(0.010) Å) and with O8w (2.383(0.014) Å) from the same asymmetric unit. Total occupancy of 3/8.

O10w → Coordinated to Co5. It has a short contact with O11w (2.226(0.012) Å) from a neighbouring asymmetric unit (symmetry code $1-x, -y, 1-z$). Total occupancy of 3/8.

O11w → Coordinated to Co5. Total occupancy of 3/8.

O12w → Free water molecule. Total occupancy of 1.

In summary, water molecules can coordinate both cobalt atoms (O5w and O7w), can be free in both situations (O12w), can coordinate only one cobalt atom and be absent for the other (O10w, O11w) and can be free in the presence of one cobalt and coordinated in the presence of the other, being split (O6w/O6wb, O8w/O8wb, O9w/O9wb).

Compound **2** crystallises in the monoclinic system, space group C2/c. The cubane core corresponds to isomer B and the quaternary C atoms of the citrate ligands are not chiral. There is a half cubane per asymmetric unit, two $[\text{Co}(\text{H}_2\text{O})_4]^{2+}$ and 2 molecules of free water (Figure 3.8).

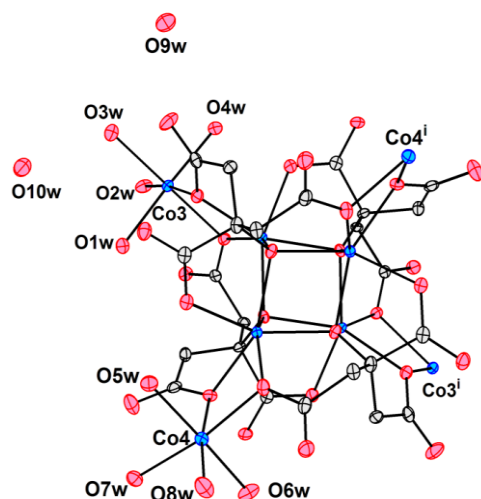


Fig. 3.8. Asymmetric unit of compound **2** with its pendant Co(II) centers and free water. Only the cubane has been grown Displacement ellipsoids (probability 60%). i: $(1-x, y, 1.5-z)$.

The compound, based on a cobalt citrate cubane, is a discrete neutral molecule. The cubane balances its negative charge with four peripheral Co(II) units. They are attached to the periphery of the cube through internal oxygen atoms of long arms from different citrates (K^2 -L1i-L8i, L2i-L3i, L4i-L5i and L6i-L7i) and each completes its coordination sphere with 4 molecules of water (Figure 3.9).

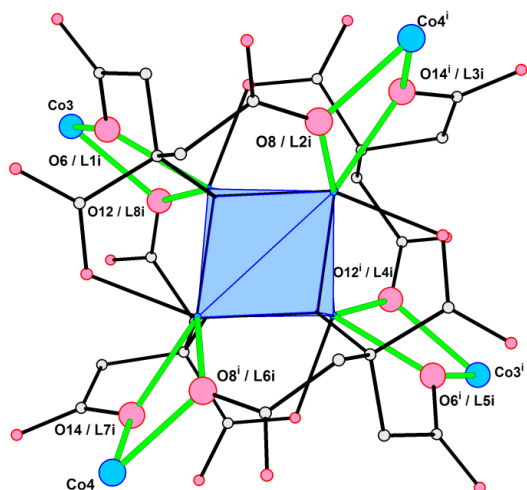


Fig. 3.9. A complete cubane unit of **2** with its four pendant Co(II) centers showing the connectivity of the peripheral units to the cube. i: (1-x, y, 1.5-z). Aqua ligands of the peripheral Co(II) centres have been omitted.

The extended structure of this compound can be seen as the same as in **1** but without disorder. The migration of Co4 to the Co5 site observed in **1** has been replaced here by an ordered Co4 unit with full occupancy.

When a single crystal of **1** is heated on the goniometer using a flow of gaseous N_2 , evidence of a new derivative is observed. The heating process consisted of a ramp from 42 °C to 87 °C (35 min. at 42 °C, 40 min. at 70 °C, 15 min. at 80 °C and 15 min. at 87 °C) followed by 16 hours at 60 °C. The unit cell of the crystal after this treatment is shown in Table 3.2.

Crystal system	monoclinic
Space group	C2/c
Temp (K)	100
a (Å)	22.3230(4)
b (Å)	9.5521(14)
c (Å)	19.9990(3)
β (°)	110.620(19)
V (Å³), Z	3991.2 (7), 4

3.2.3 Powder X-Ray diffraction

With the aim of fully characterising the thermal evolution of **1** and to clarify whether there is a third compound when heating is maintained after **2** has been obtained, a powder X-Ray diffraction study was conducted. Data for a fresh sample of **1** was first measured at 23 °C, then diffractograms at 30, 35, 40, 45, 50, 60, 70, 80 and 90 °C were collected, after heating the sample at each temperature for 20 minutes. A data collection takes about 20 min., so by the end of the experiment, the sample had been heated for a total of 6 hours (Figure 3.10).

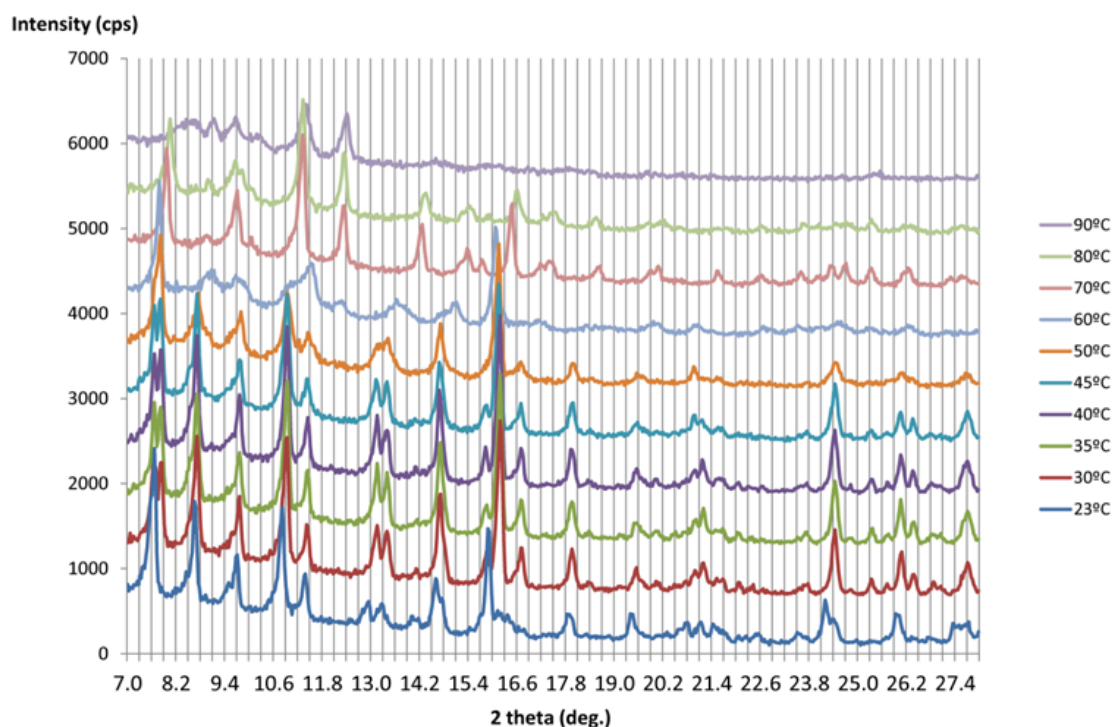


Fig. 3.10. Powder X-Ray diffractograms for the evolution of **1** from 23 °C to 90 °C. The sample was heated at each temperature for 20 minutes before data collection.

The spectrum at 23 °C (blue) corresponds to compound **1** (Figure 3.11a). At 30 °C (red) the powder pattern has already changed and remains stable until 50 °C (orange in Figure 3.10). The diffractogram at 40 °C matches the one simulated for compound **2** (Figure 3.11b). At 60 °C (light blue) the quality of the data deteriorates as a result of a second step in the evolution of the compound. At 70 °C (light pink) there is a new powder pattern that remains until 80 °C (light green).

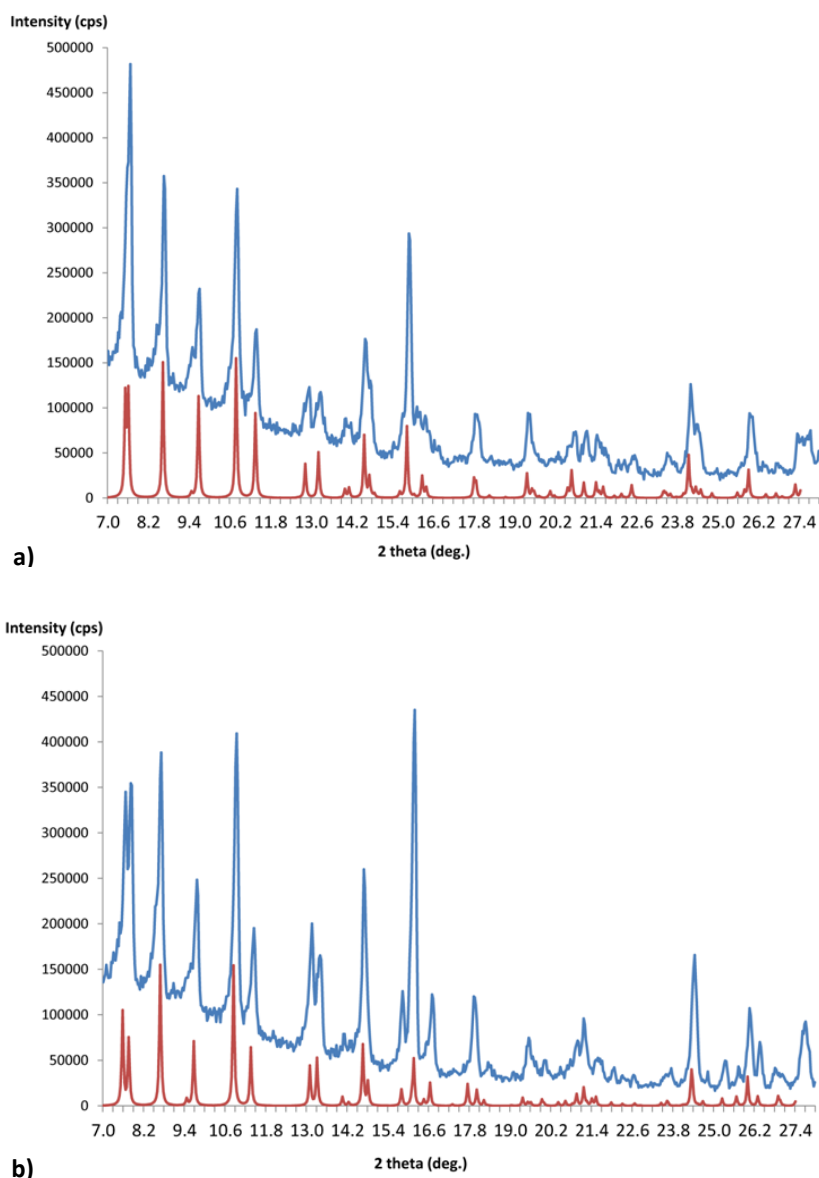


Fig. 3.11. Comparison of the Powder X-Ray diffractograms (a) **1** gathered at 23 °C (blue) during the heating process and the simulated pattern for **1** (red) and (b) **1** gathered at 40 °C (blue) during the heating process and the simulated pattern for **2** (red).

However, data at this temperature are of poor quality; and finally, at 90 °C (violet) the compound almost completely loses its crystallinity. When the diffractogram collected at 70 °C is compared to those simulated for compounds **1** and **2**, the profile does not match either of them (Figure 3.12). When the calculated powder pattern for the reflexions of the putative third compound (using Platon)^[3] is compared with the diffractogram at 70 °C a clear match is observed, even despite the low quality of the data (Figure 3.13). That supports the conclusion of the existence of a third compound that would evolve from compound **2** by a massive dehydration of the sample upon maintaining the heating for a longer period of time. Unfortunately, all attempts to characterise this species were unsuccessful; only partial and unsatisfactory structural information was obtained.

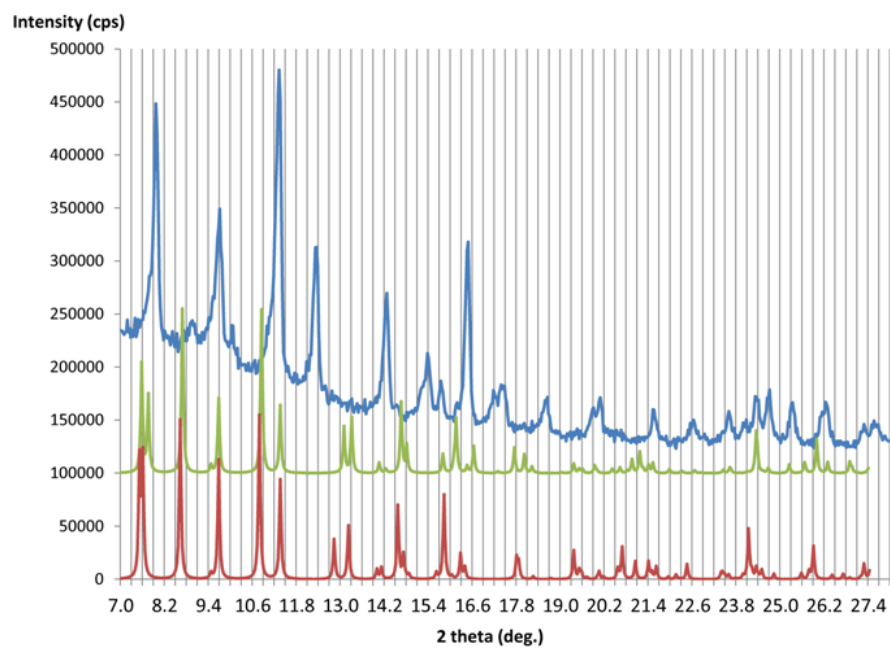


Fig. 3.12. Comparison of the Powder X-Ray diffractograms of **1** gathered at 70 °C (blue) during the heating process and the simulated patterns for compounds **1** (red) and **2** (green).

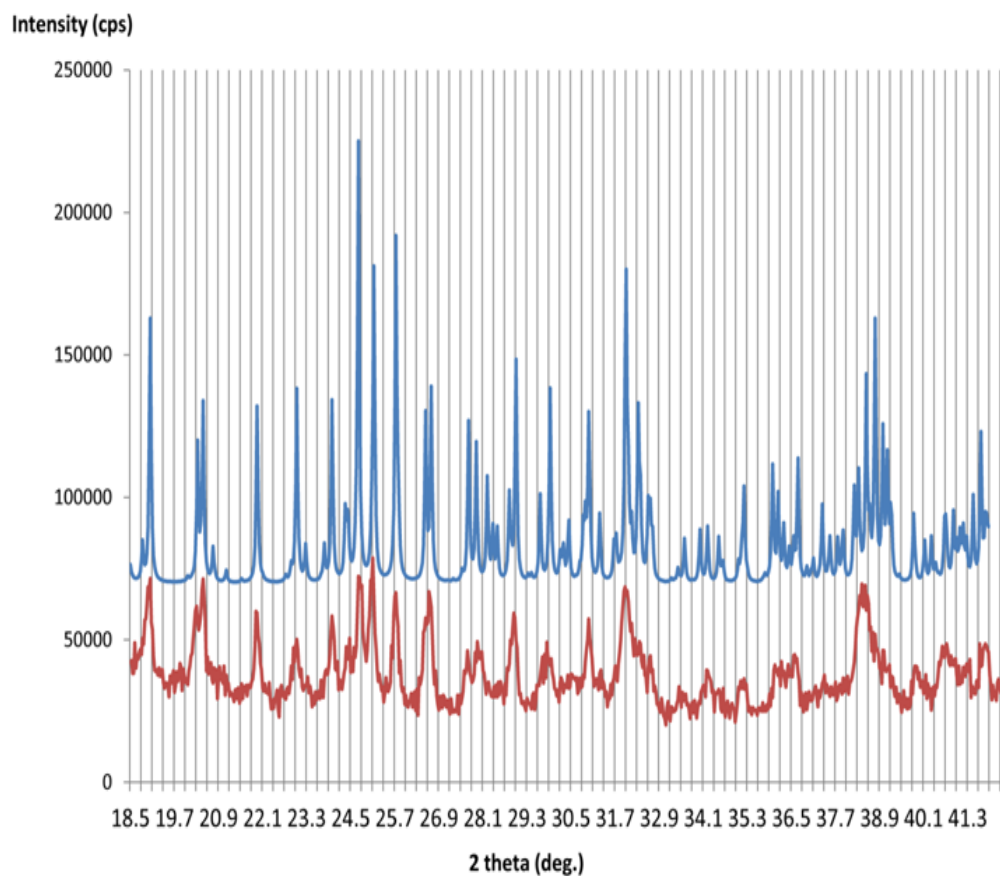


Fig. 3.13. Comparison of the Powder X-Ray diffractogram of **1** gathered at 70 °C (red) during the heating process and the simulated pattern for the putative third compound (blue).

3.2.4 Magnetic characterization

The magnetism of compounds **1** and **2** has been characterised by another member of this research group. (Thesis of Dra. C. Sáenz de Pipaón Soba^[B5]). The results of that study are reviewed here from a chemical point of view. Graphics have been extracted from the thesis of Dra. Sáenz de Pipaón Soba.

Special care was needed for the manipulation of the samples due to the reversible transformation observed under ambient conditions. The sample was isolated and sealed in Pyrex capsules to ensure its purity. It was observed that the vacuum applied in the purging process of the MPMS can partially transform compound **1** into **2**.

Initially, the sample corresponds to compound **1** which is stable under ambient conditions. The magnetization of the sample from room temperature to 1.8 K at a field of 500 Oe is shown in Figure 3.14. The $\chi_M \cdot T$ value at 300 K is in accord with the expected value for eight independent Co(II) ions with an effective magnetic moment of $4.77 \mu_B$ given by $S = 3/2$ and $g \geq 2.4$.

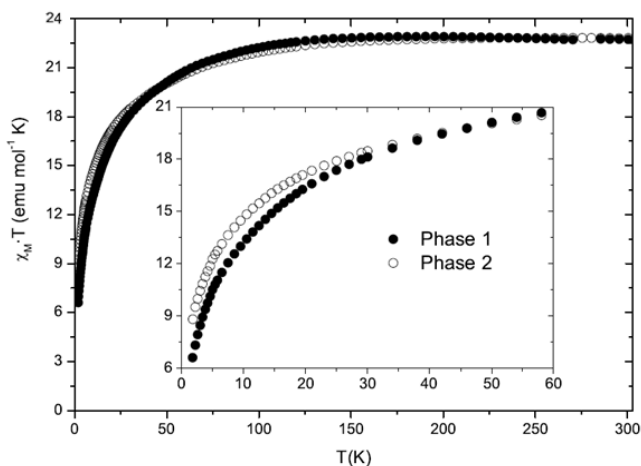


Fig. 3.14. $\chi_M \cdot T$ versus T plot for compound **1** (full circles) and **2** (open circles). The inset shows the low temperature region.

In order to establish the SMM nature of the sample, its AC susceptibility was measured at different temperatures within the range 8.0 – 1.8 K (Figure 3.15). There is a blocking phenomenon for both samples below 7.5 K which is only observable for frequencies higher than 10 Hz for compound **2**. Below the blocking temperatures, the in-phase and out-of-phase signals increase, although there is no isolated Co(II) ion to which the increase can be imputed. That can be due to the existence of another relaxation process or magnetic order arising from the modification in the environment of a cube introduced by adjacent units. Dipolar interaction could be also be responsible for this phenomenon, as observed in other compounds^[4]. A complete study of the sample at lower temperatures would need to be carried out in order to clarify the magnetic behaviour of the sample.

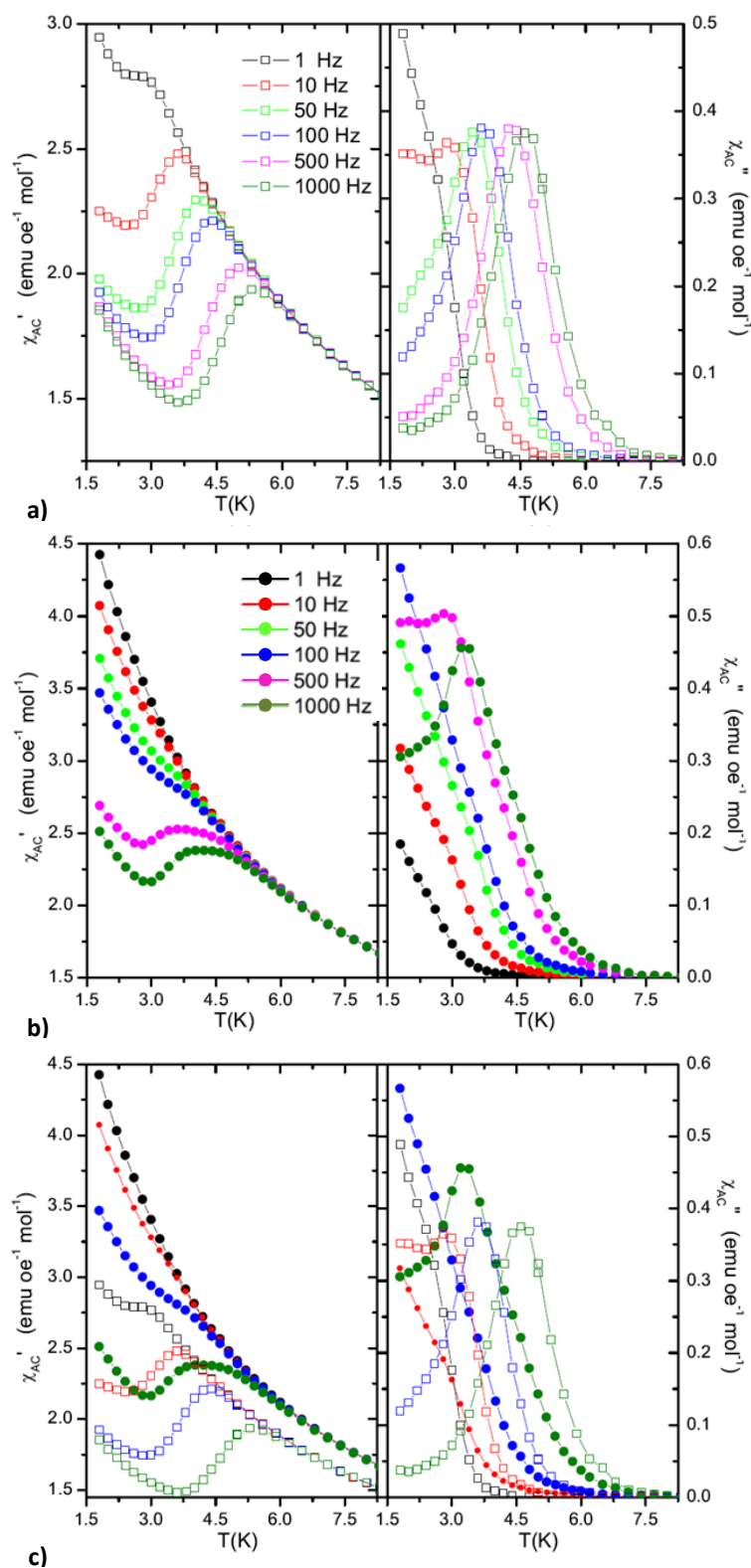


Fig. 3.15. χ_{AC} measurements at different frequencies for compound 1 (a) and compound 2 (b). The two are compared for some frequencies (c) (compound 1 – open squares and compound 2 – full circles).

Figure 3.15c shows a comparison of the AC signals for the two compounds. It can be seen that the sample corresponding to compound **2** is slightly contaminated with a trace of **1**. That explains the shoulder observed in the out-of-phase signal exactly at the same temperature as the blocking phenomenon in compound **1**.

The blocking phenomenon in **1** is observed at higher temperatures and lower frequencies than in compound **2**. That can be explained in terms of the environment of the cube. In compound **2** it is very symmetric, with four Co(II) units connected in the same way to the periphery of the cube and related by symmetry in pairs. However, in **1**, the “jump” of one Co(II) unit to a neighbouring unit breaks the symmetry and the environment of the cube is more anisotropic. That will also affect to the energy barrier and the relaxation times.

Energy barriers (ΔE) and characteristic relaxation times (τ_0) were calculated for both compounds. Values were $\Delta E = 39.8(11)$ K and $\tau_0 = 0.26(8) \cdot 10^{-7}$ s for **1** and $\Delta E = 9.2(3)$ K and $\tau_0 = 34(2) \cdot 10^{-7}$ s for **2**.

Several attempts to observe the phase transition *in situ* were made by heating and purging the sample chamber to obtain a pure sample of **2**. However, it was impossible to assure the purity of the samples and to characterise the phase present at each measurement. The best results obtained are those presented here.

3.4 Conclusions

In this chapter a compound with a modulated structure has been presented, along with a second compound that results from a reversible single-crystal-to-single-crystal transformation of the first product. The refinement of the average structure of the modulated crystal was completed and a model for the modulation has been proposed. The structure of the second product, which is not modulated, has also been presented. The initial compound is based on a cobalt citrate core surrounded by 6 Co(II) sites, of which four are bonded through a double bridge to the cube. Two of these are fully occupied and are related by symmetry. The remaining four are partially occupied and are mutually incompatible in pairs. The proposed model for the periodic disorder is based on two possible orientations of a layer of anisotropic molecular species propagated successively in an ordered fashion. If we consider the initial compound as the one formed by the cubane surrounded by the four doubly bridged Co(II) ions, the principal species involved in the modulated structure is formed by the migration of one of the peripheral Co(II) centres to an adjacent molecule. A given molecule would then consist of a cubane core surrounded by the three remaining doubly bridged peripheral Co(II) centres along with a fourth, singly bridged Co(II) which has migrated from a neighbouring molecule. Within a given layer of the structure, in the crystallographic *ac*-plane, the migration is concerted, affecting all molecules in the layer in a like fashion. The disorder model still gives a total of four peripheral Co(II) per cubane. One possible model for the modulation consists of an eight-unit cell stacking pattern which can be described as -AAABA'A'B-, in which A and A' are the modified layers, with A and A' related by two-fold rotation about the *b*-axis of the monoclinic cell. The B layer consists of a symmetrical species in which migration has not occurred.

The transformation of the first species to the second, which occurs non-destructively and reversibly in the crystal, has been fully characterised by single crystal and powder X-Ray

diffraction. The second compound is obtained by dehydration and as mentioned its structure corresponds to the cube with the four doubly bridged Co(II) units at its periphery. That is the structure taken as the starting point for an explanation of the modulation in the first compound. The transformation removes the disorder in two Co(II) units distributed over 4 crystallographic sites.

There is evidence for the existence of a third phase. It has been seen using both single crystal and powder X-Ray diffraction. Unfortunately, it was not possible to obtain a data set of sufficient quality for a single crystal structure analysis of the third phase, because of damage to the crystal during the heating process needed for the preparation of this species. However, a thermodiffraction study using a powder sample confirms the existence of the three different species. The process is completely reversible just by exposure of the sample to a humid atmosphere. This process can easily be followed by the change in the colour of the sample. In the third phase the compound becomes violet; and when the sample is placed in a humid atmosphere, the initial fuchsia colour is restored.

Because of the difficulties in the isolation of the third phase, only the first two have been characterised magnetically. They behave as single molecule magnets, with a blocking phenomenon below 7 K in each case. The energy barrier for the first phase is four times that for the second phase, which indicates that the increase of the anisotropy in the environment of the cube is translated into higher energy values and thus a higher blocking temperature. This is in accord with those synthetic approaches to the preparation of SMM with higher blocking temperatures which focus on increasing of the anisotropy of the cluster instead of its spin value.

This is the first example of a pair of SMM which are switchable through a reversible SC-SC transformation at room temperature involving a simple dehydration process.

Future efforts will be focused on the isolation and characterisation (structural and magnetic) of the third phase in order to complete the study of this novel crystalline material that undergoes two reversible SC-SC transformations with modification of the magnetism, preserving its SMM nature.

References

- [1] A. Altomare, G. Cascarano, C. Giacovazzo, A. Guagliardi, *Journal of Applied Crystallography* **1993**, *26*, 343-350.
- [2] G. M. Sheldrick, *Acta Crystallographica Section A* **2008**, *64*, 112-122.
- [3] A. L. Spek, *Acta Crystallographica Section D-Biological Crystallography* **2009**, *65*, 148-155.
- [4] A. Morello, F. L. Mettes, O. N. Bakharev, H. B. Brom, L. J. de Jongh, F. Luis, J. F. Fernandez, G. Aromi, *Physical Review B* **2006**, *73*.
- [P1] CrysAlisPro, Oxford Diffraction Ltd., Version 1.171.33.31
- [P2] Diamond. Klaus Brandenburg, Crystal Impact GbR, Bonn, Germany. Version 3.2i.
- [P4] Petricek, V., Dusek, M. & Palatinus, L. **2006**. Jana2006. The crystallographic computing system. Institute of Physics, Praha, Czech Republic.
- [B5] Sáenz de Pipaón Soba, Cristina. Contributions to Molecular Magnetism: Chiral Magnets and Networked SMMs. [on line]. Universidad de Zaragoza, 2013. <<http://http://zaguan.unizar.es/record/10403>>

4

2-D Cobalt citrate cubanes.*

This chapter continues with the study of compounds based on cobalt cubanes. The focus of this chapter is a series of 2-D polymers of cubanes. With appropriate variations in the reaction procedure, we have obtained a varied family of compounds based on the same Co-cubane core with different polymer geometries and propagation properties. All of them form anionic 2D nets in which the cubanes are bridged by octahedrally coordinated Co(II) ions. For all of them, the main building block is the cubane. Differences arise from how the cubanes are propagated and also from the counterions used for their crystallization.

This chapter is divided into three parts. The first describes two compounds with formulas $\text{Rb}_{4n}\{[\text{Co}_4(\text{C}_6\text{H}_4\text{O}_7)_4]\mu\text{-}[\text{Co}(\text{C}_2\text{H}_6\text{O}_2)(\text{H}_2\text{O})_2]_2\}_n \cdot 9.5n(\text{H}_2\text{O}) \cdot 2n(\text{C}_2\text{H}_6\text{O}_2)$ **3** and $\text{Cs}_{4n}\{[\text{Co}_4(\text{C}_6\text{H}_4\text{O}_7)_4]\mu\text{-}[\text{Co}(\text{C}_2\text{H}_6\text{O}_2)(\text{H}_2\text{O})_2]_2\}_n \cdot 4.5n(\text{H}_2\text{O}) \cdot 2.5n(\text{C}_2\text{H}_6\text{O}_2)$ **4**. The two are isomorphous and form tetragonal anionic nets. As the polymeric part of the compound is almost identical for both, differences are due to the counterions and molecules of free water between the polymeric nets.

The second part of the chapter presents a compound based on a rhombic anionic 2D net with formula $\text{Cs}_{4n}\{[\text{Co}_4(\text{C}_6\text{H}_4\text{O}_7)_4]\mu\text{-}[\text{Co}(\text{H}_2\text{O})_4]_2\}_n \cdot 16.5n(\text{H}_2\text{O})$ **5**. The only difference in the synthetic procedure between **5** and **4** is the ethylene glycol added to the reaction media in **4**. This simple modification brings the crystallization of a new compound with a different distribution of the bridging Co(II) units at the periphery of the cube. These modifications produce changes not only in the crystal structure but also in the magnetic behaviour of the solids.

Finally, in the third part of the chapter another 2D polymer is presented. This polymer with formula $\text{Cs}_{2n}[\text{Co}(\text{H}_2\text{O})_6]_n\{[\text{Co}_4(\text{C}_6\text{H}_4\text{O}_7)_4]\mu\text{-}[\text{Co}(\text{H}_2\text{O})_4]_2\}_n \cdot 12n(\text{H}_2\text{O})$ **6** presents a structure formed by tetragonal anionic nets, which resembles the polymeric net observed in **3** and **4**. The main distinctive feature of **6** is that balancing the negative charge of the polymeric net, there are

two different counterionic species, K^+ and $[Co(H_2O)_6]^{2+}$. Its magnetic characterization has also been conducted.

E. Burzurí, J. Campo, L. R. Falvello, E. Forcén-Vázquez, F. Luis, I. Mayoral, F. Palacio, C. Sáenz de Pipaón and M. Tomás, *Chem. Eur. J.*, **2010**, *17*, *10*, 2818-2822.

L. R. Falvello, E. Forcen-Vazquez, I. Mayoral, M. Tomas and F. Palacio, *Acta Crystallogr. C*, **2011**, *67*, M359-M363.

4.1 A Tetragonal 2-D Array of Single-Molecule Magnets with Modulable Collective Behaviour

4.1.1 Experimental

4.1.1.1 Synthesis

Reagents were commercial and used as received. No additional purifications were necessary.

Compounds **3** and **4** were obtained according to the following procedure. To a stirred aqueous solution of citric acid monohydrate (50 mL, 0.47 M) was added $\text{CoCO}_3 \cdot x\text{H}_2\text{O}$ (3.25 gr, 23.72 mmol, for $x=1$). After complete reaction, the mixture was gravity-filtered. An aqueous solution of MOH (0.5 M, $M = \text{Rb, Cs}$ for **3** and **4**, respectively) was added dropwise until a pH of 7-8 was reached. The resulting mixture was heated to restore the initial volume and cooled to ambient temperature. The addition of ethylene glycol to this solution (water / ethylene glycol 2 / 1) produces crystals of **3** or **4** depending on the alkali metal hydroxide used.

$\text{Rb}_{4n}\{[\text{Co}_4(\text{C}_6\text{H}_4\text{O}_7)_4]\mu\text{-}[\text{Co}(\text{C}_2\text{H}_6\text{O}_2)(\text{H}_2\text{O})_2]_2\}_n \cdot 9.5n(\text{H}_2\text{O}) \cdot 2n(\text{C}_2\text{H}_6\text{O}_2)$ (**3**) is obtained when MOH is RbOH. The procedure described gives 0.44 g. (0.22 mmol, 44% yield) of well-formed square fuchsia crystals after 8 days of standing at room temperature.

$\text{Cs}_{4n}\{[\text{Co}_4(\text{C}_6\text{H}_4\text{O}_7)_4]\mu\text{-}[\text{Co}(\text{C}_2\text{H}_6\text{O}_2)(\text{H}_2\text{O})_2]_2\}_n \cdot 4.5n(\text{H}_2\text{O}) \cdot 2.5n(\text{C}_2\text{H}_6\text{O}_2)$ (**4**) is obtained when CsOH is used. A quantity of 0.43 g (0.20 mmol, 40% yield) of well-formed square fuchsia crystals are obtained after 8 days of standing at room temperature.

4.1.1.2 Single Crystal X-Ray diffraction

Single crystal X-Ray diffraction was performed on an Xcalibur S3 CCD-based four-circle diffractometer (Oxford Diffraction and Agilent Technologies). The program CrysAlis Pro^[P1] controlled data collection and processing. The structure was solved *ab initio* by direct methods^[1] and refined by full-matrix least-squares analysis.^[2] Non-hydrogen atoms were refined with anisotropic displacement parameters. The methylene H atoms of the citrate ligands were placed at idealized positions and refined as riders on their respective parent C atoms with isotropic displacement parameters set to 1.2 times the equivalent isotropic U of the C atom. Analysing the difference map some hydrogen atoms of the water molecules were found, however, due to the high disorder of the species between the polymeric layers, their detailed assignment is not feasible. Graphical material was prepared using Diamond.^[P2] Data collection and structure solution information and refinement details are shown in Table 4.1.

Table 4.1. Crystallographic data for **3** and **4**.

	3	4
Formula	^a C ₃₂ H ₆₇ Co ₆ O _{49.5} Rb ₄	^b C ₃₃ H ₆₀ Co ₆ Cs ₄ O _{45.5}
fw (g mol⁻¹)	1939.32	2070.03
Radiation	X-Rays (Mo K α)	
Wavelength (Å)	0.71073	
Crystal system	tetragonal	
Space group	P -4 2 ₁ c	
Temp (K)	100(1)	100(1)
a (Å)	12.5307(2)	12.5873(2)
c (Å)	19.6730(5)	20.0623(8)
V (Å³), Z	3089.02(11), 2	3178.67(15), 2
ρ_{calc} (Mg/m³)	2.085	2.163
μ (mm⁻¹)	4.822	3.893
F (000)	1930.0	2008.0
Crystal size (mm³)	0.27 × 0.11 × 0.06	0.19 × 0.19 × 0.04
θ (min,max) (°)	3.78, 27.49	3.76, 27.49
Reflns collected	33233	32443
Indep reflns	3548	3652
R(int), R(σ)	0.0535, 0.0371	0.0583, 0.0348
Completeness (θ)	0.994, (27.49)	0.996, (27.49)
Abs corr	multi-scan	
T(min,max)	0.5189, 1.0000	0.4689, 1.00000
Restraints/parms	34 / 245	4 / 268
Goodness-of-fit	1.080	1.118
R1, wR2 (obs)^c	0.0579, 0.1516	0.0603, 0.1498
R1, wR2 (all)	0.0700, 0.1589	0.0647, 0.1514
Δ/σ(max,mean)	0.002, <0.001	0.001, <0.001
$\Delta\rho$ range (e Å⁻³)	0.832, -1.212	1.048, -1.119
^a Rb _{4n} {[Co ₄ (C ₆ H ₄ O ₇) ₄] μ -[Co(C ₂ H ₆ O ₂)(H ₂ O) ₂] ₂] _n ·9.5n(H ₂ O)·2n(C ₂ H ₆ O ₂) ^b Cs _{4n} {[Co ₄ (C ₆ H ₄ O ₇) ₄] μ -[Co(C ₂ H ₆ O ₂)(H ₂ O) ₂] ₂] _n ·4.5n(H ₂ O)·2.5n(C ₂ H ₆ O ₂) ^c threshold I > 2 σ (I).		

4.1.1.3 FT-IR spectroscopy

FT-IR spectra of **3** and **4** were measured on a Perkin-Elmer Spectrum 100 FT-IR Spectrophotometer with ATR accessory in the range of 4000 - 300 cm⁻¹. (Figure 4.1)

IR (neat compound **3**, cm^{-1}): $\nu(\text{OH})$ 3184.92 (w); $\nu(\text{C}=\text{O})$ 1547.62 (w); $\nu(\text{C}-\text{H})$ 1429.44 (w) and 1380.26 (w); $\nu(\text{CO})$ 1083.60 and 1058.18 (t).

IR (neat compound **4**, cm^{-1}): $\nu(\text{OH})$ 3190.69 (w); $\nu(\text{C}=\text{O})$ 1542.50 (w); $\nu(\text{C}-\text{H})$ 1375.47 (w); $\nu(\text{CO})$ 1084.80 and 1053.28 (t).

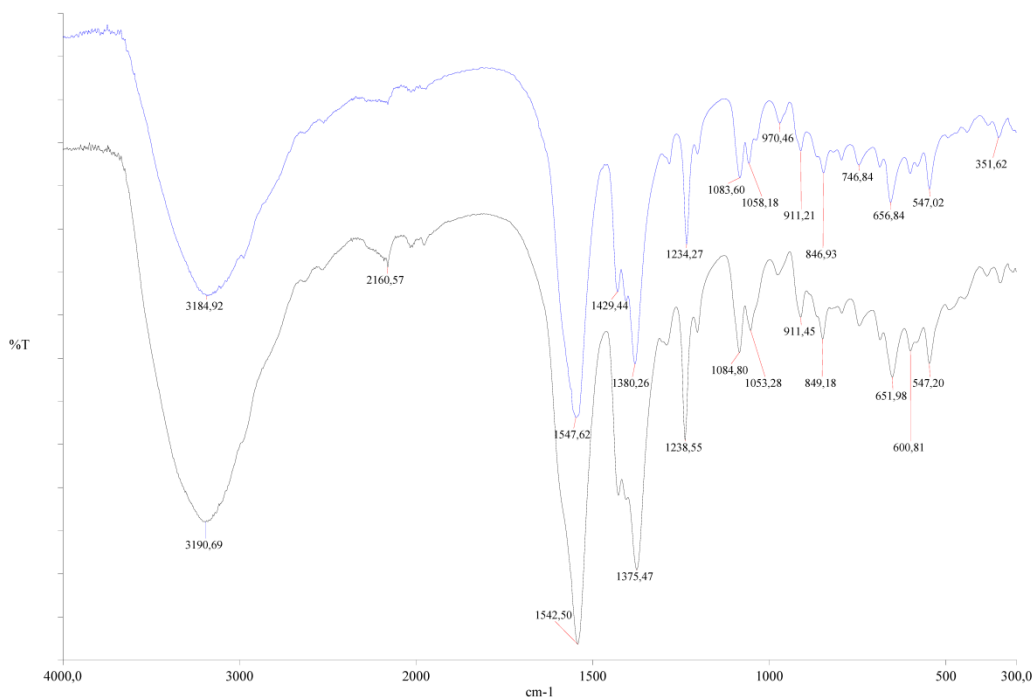


Fig. 4.1. IR spectra of **3** (blue) and **4** (black).

4.1.1.4 Elemental analysis

Elemental analyses of **3** and **4** were carried out on a Perkin Elmer 2400 CHNS/O analyser. Calculated analysis for $(\text{C}_{32}\text{H}_{67}\text{Co}_6\text{O}_{49.5}\text{Rb}_4)$ (**3**) is: C, 19.82%; H, 3.48%. Results obtained were C, 19.97%; H, 3.78%.

Calculated analysis for $(\text{C}_{33}\text{H}_{60}\text{Co}_6\text{Cs}_4\text{O}_{45.5})$ (**4**) is: C, 19.15%; H, 2.92%. Results obtained were C, 18.23%; H, 3.50%.

4.1.1.5 Magnetic characterization

Magnetic measurements on **3** and **4** were performed on a Magnetic Property Measurement System (MPMS) in the range of 300 - 1.8K, 0.1 - 1000 Hz, on a Physical Property Measurement System (PPMS) SQUID magnetometer from Quantum Design.^[P3]

4.1.2 Results and discussion

4.1.2.1 Synthesis

The synthetic procedures used for the compounds presented in this chapter are all very similar. As will be shown, there is no unique procedure for obtaining the corresponding TM citrate cubanes. As a general overview, the procedures can be summed up as follows. The key step is the preparation of an appropriate solution of a TM-citrate intermediate. There are two intermediates, the one when the ratio citrate/cobalt is 1/1 and the other when this proportion is 2/3. From an aqueous solution of either of them, by raising the pH to a value of 7-8, crystals of a wide variety of compounds based on citrate cubanes have been isolated.

More specifically, there are four general procedures that have been used interchangeably in the preparations of the four compounds that are presented in this chapter. Minor changes have been introduced in the last step (once the solution of the intermediate is ready) and these changes are responsible for the variety of compositions and structures found for the compounds.

Synthetic procedure 1: To a stirred solution of citric acid monohydrate in water (50 mL, 0.47 M), $\text{CoCO}_3 \cdot x\text{H}_2\text{O}$ (3.25 gr, 23.72 mmol, for $x=1$) is added. The mixture is stirred until the reaction is complete. It is possible, but not necessary, to heat the mixture slightly to speed up the reaction. Once the production of CO_2 has stopped, the mixture is gravity-filtered. The supernatant is a dark-red solution with a pH of 3.5 - 4 from which the first intermediate can be characterised. This is a compound with a ratio citrate / cobalt of 1 / 1.^[3] The quantity of MOH employed to obtain a solution with a pH of 7.5-8 will be higher than for the synthetic procedure 2.

Synthetic procedure 2: Another feasible procedure is to add 1.5 mol of $\text{CoCO}_3 \cdot x\text{H}_2\text{O}$ (4.89 gr, 35.69 mmol, for $x=1$) to a stirred solution of citric acid monohydrate (50 mL, 0.47 M) and filter the suspension by gravity after complete reaction. The reaction time is longer than in 1, as the quantity of cobalt carbonate reacting is larger. It is recommendable to add the cobalt carbonate little by little to speed up the reaction and avoid massive production of CO_2 . Under these conditions, the second intermediate, with a ratio citrate/cobalt 2/3 can be isolated.^[3] The pH of the resulting dark-red solution is around 4.5 - 5. So the quantity of MOH needed to reach a final pH of 7.5 - 8 will be smaller.

Synthetic procedures 3 and 4: Intermediates 1 and 2 (described in the preceding paragraphs) are obtained as microcrystalline solids following the synthetic route described in

the corresponding publication.^[3] When the solid has been purified and characterised, it is dissolved in water and the MOH is added to raise the pH.

For intermediate 1: 30 mL, 0.39 M and for intermediate 2: 30 mL, 0.20 M

As detailed in section 4.1.2.1 (*vide supra*) the synthetic procedure employed for the compounds in this chapter is number 1 because of its higher speed and the smaller quantity of $\text{CoCO}_3 \cdot x\text{H}_2\text{O}$ used. It is worth mentioning that every synthetic route described above is valid for all of the products.

Once a solution of the intermediate is obtained, the corresponding MOH is added dropwise until a pH of 7.5 - 8 is attained. The colour of the solution changes from dark red to fuchsia (sometimes slightly violet if the pH is closer to 8). The solution is stirred until reaction is complete and then gravity-filtered if needed (sometimes, small quantities of impurities, probably a metal hydroxide or mixed oxide, can appear). The solution is heated, allowing the evaporation of solvent to restore the initial volume. The solution is cooled to ambient temperature. Then, if something else such as ethylene glycol (for compounds **3** and **4**) or 3,3'-thiodipropanol (for compound **6**) is needed, it can be added. The resulting solution is placed in a closed vial and left at room temperature.

4.1.2.2 Single Crystal X-Ray diffraction

Compounds **3** and **4** are isomorphous and crystallise in the tetragonal system, space group P-42₁c. The same anionic polymer has been crystallised separately with Rb (**3**) and Cs (**4**) as counterions. Per asymmetric unit there is a quarter of cubane, a half of a $[\text{Co}(\text{C}_2\text{H}_6\text{O}_2)(\text{H}_2\text{O})_2]^{2+}$ bridging unit, molecules of water (2.375 for **3** and 1.125 for **4**), ethylene glycol (0.5 for **3** and 0.625 for **4**) and 1 alkali metal atom (Figure 4.2).

The cobalt citrate cubane corresponds to isomer A. The absolute configuration of the central C atom of the citrate in the reference asymmetric unit is R for two of them and S for the remaining; each cubane is racemic as the four citrates are related by a -4 symmetry element. The anion is a 2-D polymer in the form of a square net whose basic building block is the cobalt cubane, propagated through bridging octahedral Co(II) units. These units are coordinated to L1e (and L4e, L6e, L7e by symmetry) according to the nomenclature system proposed. The link is through an external oxygen atom of a long arm. The Co(II) nexus coordinates two carboxylate oxygen atoms in a mutually trans arrangement. It resides on a two fold axis and completes its coordination sphere with two molecules of water and one of ethylene glycol. (Figure 4.3).

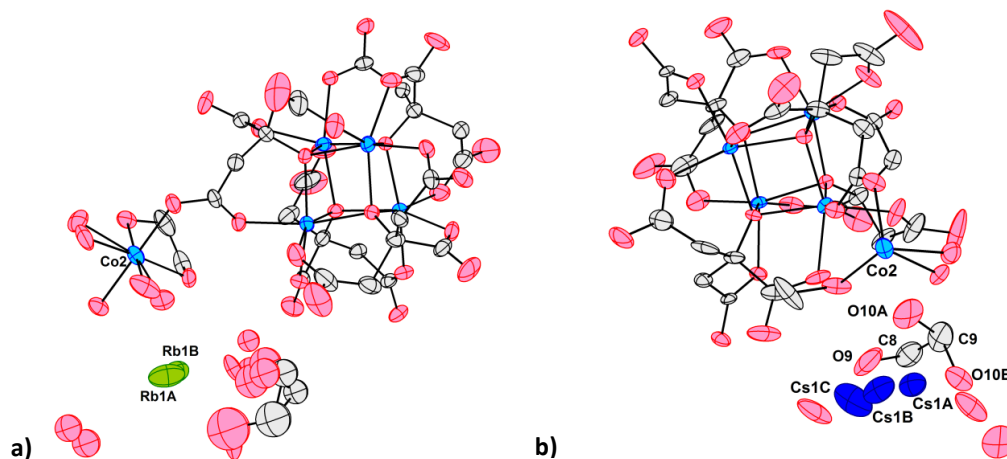


Fig. 4.2. A complete cubane unit with a Co(II) bridging unit, counterions and free water for compounds **3** (a) and **4** (b). Only free water molecules from one asymmetric unit have been represented for clarity. Displacement ellipsoids (probability 50%).

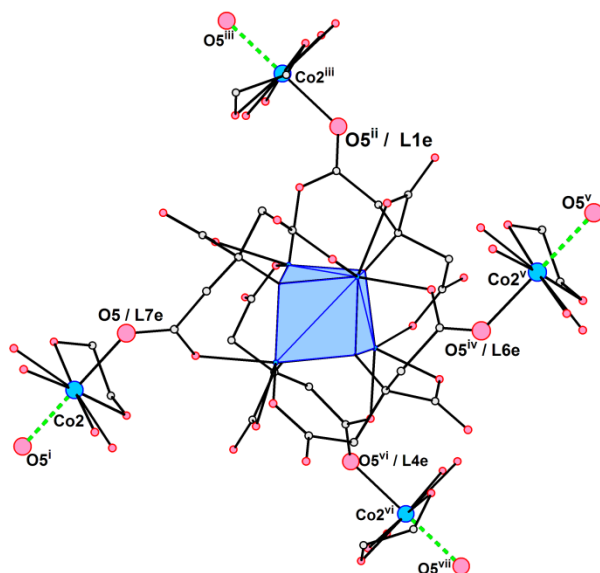


Fig. 4.3. A complete cubane unit of **3** with its four bridging Co(II) units, showing the propagation of the polymer. i: (1-x, -y, z), ii: (1-y, x, 1-z), iii: (1+y, 1-x, 1-z), iv: (1-x, 1-y, z), v: (x, 1+y, z), vi: (y, 1-x, 1-z), vii: (-y, x, 1-z).

Structurally, the compound is a square 2-D array of cobalt citrate cubanes bridged by Co(II) units. The layers are stacked perpendicular to the crystallographic *c*-axis following an ABAB pattern in such a way that the nodes of one layer are eclipsed with the cubanes of neighbouring layers (Figure 4.4). Looking at a single layer it has a crenelated structure. There are unbounded channels between the layers, along the *a*- and *b*-axis. The interlayer spacing is 0.5*c* (9.8365(3) for **3** and 10.031(2) for **4**). The space occupied by the channels, calculated using Platon,^[4] is 38.6 % for **3** and 39.2% for **4**. They are occupied by the alkali metal cations,

molecules of water and ethylene glycol. Those species are highly disordered in both structures (Figure 4.5).

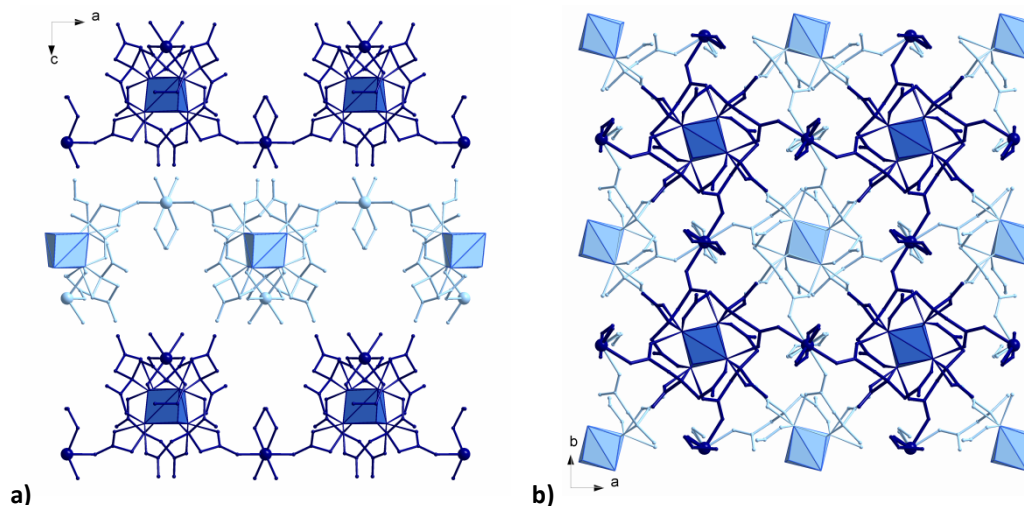


Fig. 4.4. View of the square 2-D anionic layers of **3** along the a -axis (a) and c -axis (b). ABAB packing. Counterions and free molecules of water have been omitted for clarity. A layers are represented in dark blue and B in light blue.

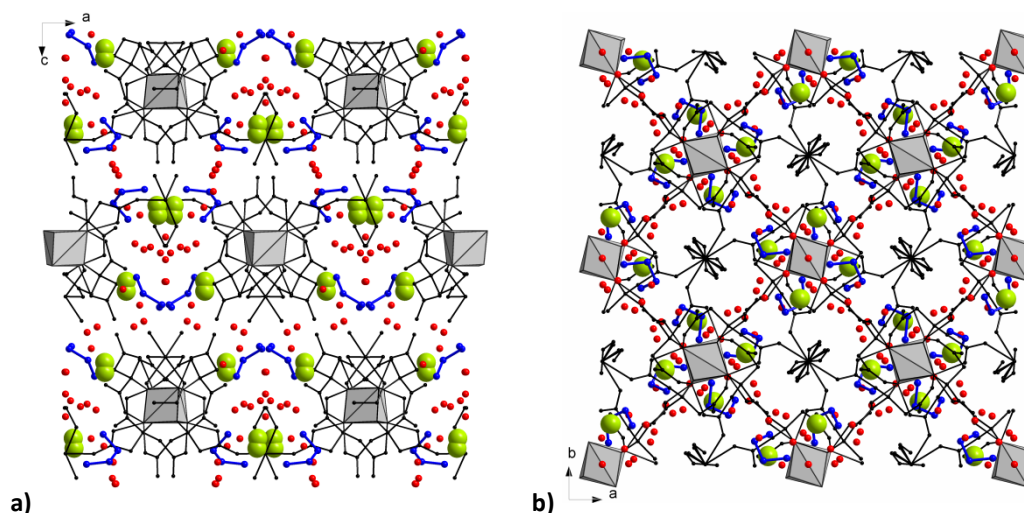


Fig. 4.5. View of **3** along the b -axis (a) and c -axis (b). The polymeric net is represented in black with the cubanes in grey. Counterions are represented in green and free molecules of water in red.

For compound **4**, the Rb atoms are distributed over two sites with a total occupancy of 1 per asymmetric unit. The relative occupancies for the two congeners were set to 0.75 and 0.25. Per asymmetric unit, there is a total of 2.375 molecules of water (9.5 per cubane) distributed over 8 crystallographic sites and 0.5 ethylene glycol (2 per cubane). Occupancies were refined and set in such a way as to maintain reasonable consistency among the displacement parameters of the atomic sites. The proximity of some of the disordered sites

obviated the possibility of refining the sites anisotropically with fully independent parameters. Geometrical restraints were applied to the ethylene glycol and similarity restraints were used for the displacement parameters of atomic sites within 1.7 Å of each other. Site occupancies were also set in such a way that sites which give impossible contacts are not simultaneously occupied. The final model is in accord with the elemental analysis of a bulk sample.

The Cs ion in compound **4** is disordered over 3 sites with occupancies of 0.6, 0.3 and 0.1. Per asymmetric unit, there is a total of 1.125 molecules of free water (4.5 per cubane at three unique sites) and 0.625 molecule of ethylene glycol (2.5 per cubane). All of the sites were refined with anisotropic displacement parameters. Geometrical restraints were used for the ethylene glycol fragment. The elemental analysis of a bulk sample agrees with the final structural model.

4.1.2.3 Magnetic characterization

Our group has magnetically characterised compounds **3** and **4** (Thesis of Dra. C. Sáenz de Pipaón Soba^[B5]). A description of the magnetism in chemical terms is presented in this section. Figures have been extracted from the thesis of Dra. Sáenz de Pipaón Soba.

Magnetization at different magnetic fields between 50000 - 500 Oe was measured from room temperature to 1.8 K (Figure 4.6).

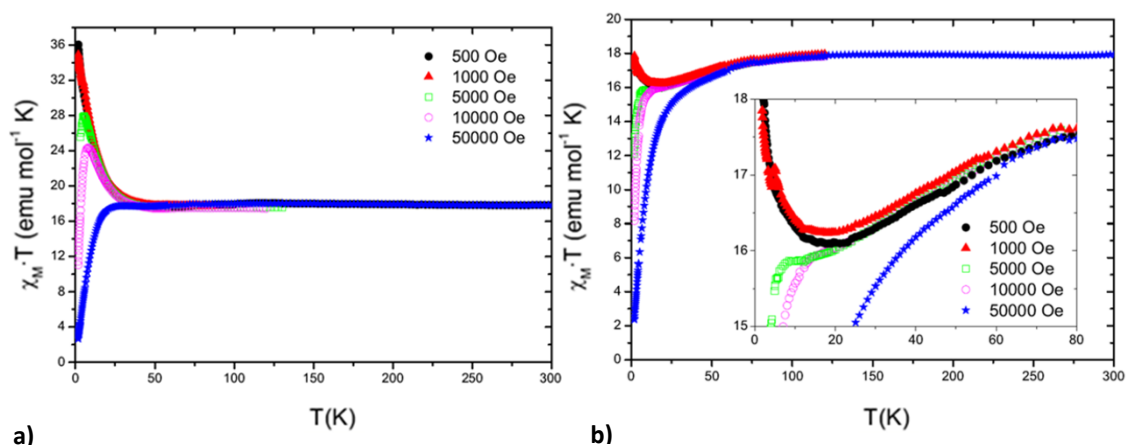


Fig. 4.6. $\chi_M \cdot T$ versus T plot for compounds **3** (a) and **4** (b). The inset shows in detail the low temperature region.

The $\chi_M \cdot T$ value remains constant at high temperatures. Below 60K the magnetic behaviour becomes field dependent due to the modification of energy levels and depopulation of high energy levels. Below this temperature, the signal decreases for high fields while for low fields it increases. The first difference between the magnetic behaviour of **3** and **4** is that in **3** for low fields at temperatures lower than 10K the magnetization is twice the value found for **4**.

This can be attributed to the existence of a stronger ferromagnetic interaction between the Co(II) ions in **3**.

At 300 K, the $\chi_M \cdot T$ value is around $18 \text{ emu} \cdot \text{mol}^{-1} \cdot \text{K}$ which is in accordance with the value expected for 6 independent Co(II) ions with an effective magnetic moment of $4.7 \mu_B$ ($S = 3/2$ and $g \geq 2.4$).

The AC behaviour of the samples was studied to determine their SMM nature. Magnetic susceptibility measurements were carried out at different frequencies below 1.8 K (Figure 4.7). These very low-temperature measurements were done in a dilution refrigerator.

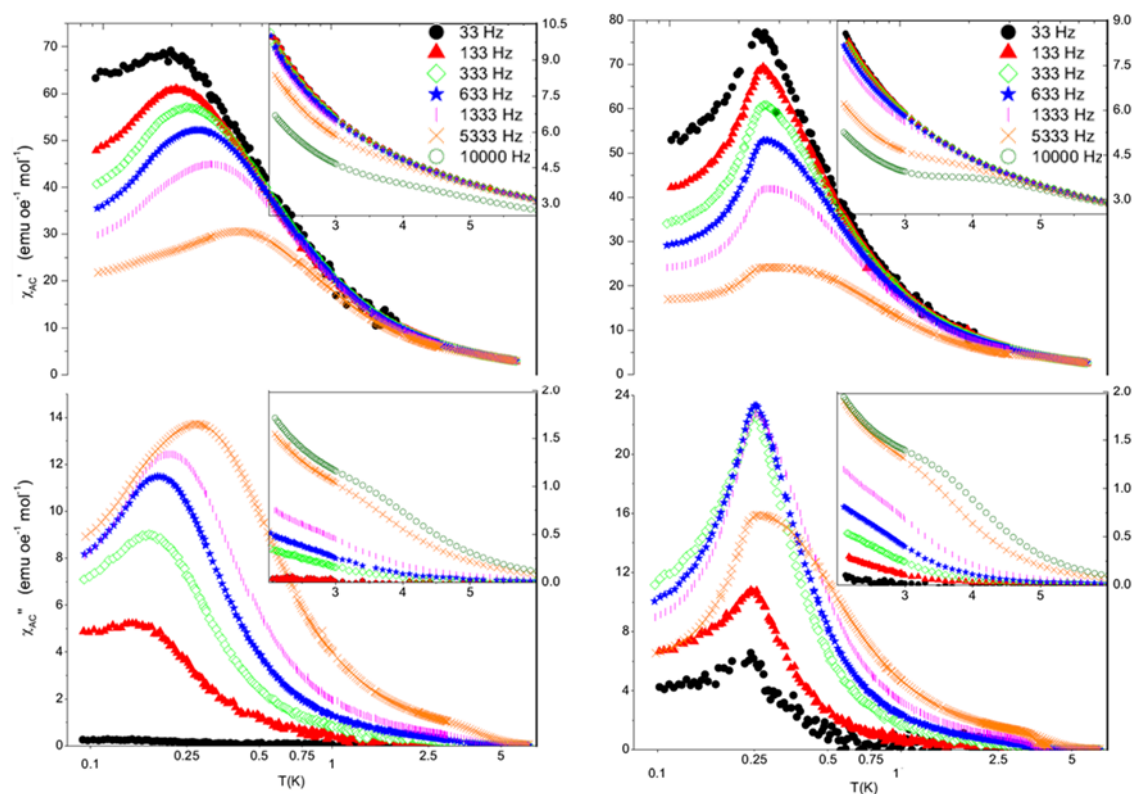


Fig. 4.7. χ_{AC} measurements at different frequencies for **3** (a) and **4** (b) in phase (up) and out of phase (bottom).

The signal becomes frequency dependent below 7 K. This signal is the result of the coexistence of two processes, a blocking phenomenon at around 4 K (a frequency-dependent peak), due to the superparamagnetic blocking of the cube (as has been seen for previously reported examples) and a frequency-independent peak near 0.2 K that could arise from a phase transition to an ordered magnetic phase. A critical temperature for this transition of 0.20 K for **3** and 0.25 K for **4** has been calculated from the data at very-low temperatures. Figure 4.8 shows the polymeric net in terms of the magnetically active centers, the cubanes and the Co(II) ions.

Energy barriers (ΔE) and characteristic relaxation times (τ_0) were calculated at high and low temperature for both compounds. Values at high temperature were $\Delta E = 13(2)$ K and $\tau_0 = 1.9(8) \cdot 10^{-7}$ s for **3** and $\Delta E = 14(1)$ K and $\tau_0 = 2.1(3) \cdot 10^{-7}$ s for **4**. Values at low temperature were $\Delta E = 0.459(5)$ K and $\tau_0 = 1.13(1) \cdot 10^{-5}$ s for **3** and $\Delta E = 0.554(7)$ K and $\tau_0 = 2.62(4) \cdot 10^{-5}$ s for **4**.

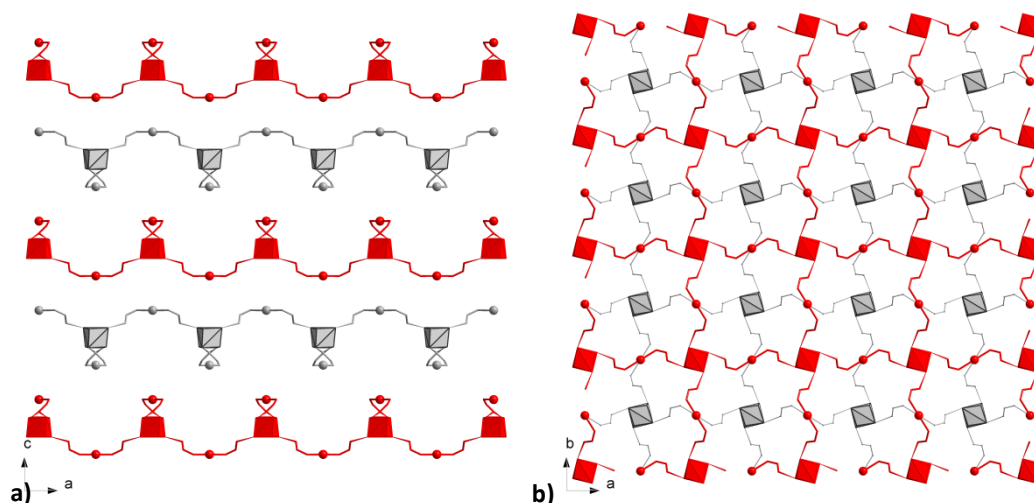


Fig. 4.8. View of **3** along the tetragonal *b*-axis (a) and *c*-axis (b). Only the magnetically active entities are shown. A layers are in red and B layers in grey.

4.2 Rhombically distorted 2-D net of SMMs

4.2.1 Experimental

4.2.1.1 Synthesis

Reagents were bought from commercial sources and used as received with no further purification.

The polymer $\text{Cs}_{4n}[\{\text{Co}_4(\text{C}_6\text{H}_4\text{O}_7)_4\}\mu\text{-}[\text{Co}(\text{H}_2\text{O})_4]_2\}_n \cdot 16.5n(\text{H}_2\text{O})$ **5** is directly obtained from the reaction medium as rectangular fuchsia crystals.

The reaction mixture was prepared by addition of $\text{CoCO}_3 \cdot x\text{H}_2\text{O}$ (3.25 g, 23.72 mmol, for $x = 1$) to a stirred aqueous solution of citric acid monohydrate (50 mL, 0.47 M). The suspension was stirred until reaction was complete and then gravity-filtered. An aqueous solution of CsOH ($\approx 1.8\text{M}$) was added dropwise to the resulting dark red supernatant until a pH of 7.5 - 8 was attained. The solution was heated, allowing the evaporation of the solvent to restore the initial volume, and then cooled to room temperature. After several weeks in a closed vial at room temperature, crystals of **5** were obtained.

Note the difference between this synthetic procedure and that previously described for **3** and **4**. For the preparation of **5** no ethylene glycol (ratio water/ethylene glycol 2/1) is added to the reaction medium. This, in principle minor modification produces a significant change in the structure of the compound as will be described presently.

4.2.1.2 Single Crystal X-Ray diffraction

Single crystal X-Ray diffraction was performed using an Xcalibur S3 CCD-based four-circle diffractometer (Oxford Diffraction and Agilent Technologies). The program CrysAlis Pro^[P1] controlled data collection and processing. The structure was solved *ab initio* by direct methods^[1] and refined by full-matrix least-squares analysis.^[2] Non-hydrogen atoms were refined with anisotropic displacement parameters. The methylene H atoms of the citrate ligands were placed at idealized positions and refined as riders on their respective parent C atoms with isotropic displacement parameters set to 1.2 times the equivalent isotropic U of the C atom. Some hydrogen atoms of the water molecules were found in a difference map. Their isotropic displacement parameters were set to 1.2 times the equivalent isotropic U of the respective neighbouring O atoms. The program Diamond^[P2] was used for graphical material. Data collection and structure solution information and refinement details are shown in Table 4.2.

Formula	^a C ₂₄ H ₆₅ Co ₆ CS ₄ O _{52.5}	Crystal size (mm³)	0.41 x 0.32 x 0.22
fw (g mol⁻¹)	2078.98	θ (min,max) (°)	4.180, 28.844
Radiation	X-Rays (Mo Kα)	Reflns collected	23851
Wavelength (Å)	0.71073	Indep reflns	7622
Crystal system	monoclinic	R(int), R(σ)	0.0330, 0.0335
Space group	C 2/c	Completeness, (θ)	0.891, (27.500)
temp (K)	105(1)	Abs corr	multi-scan
a (Å)	22.1271(6)	T(min,max)	0.74131, 1.00000
b (Å)	23.8783(8)	restraints/parms	0, 478
c (Å)	12.4763(4)	Goodness-of-fit	1.070
β (°)	97.556(3)	R1, wR2 (obs)^b	0.0399, 0.1046
V (Å³), Z	6534.7(4), 4	R1, wR2 (all)	0.0504, 0.1104
ρ calc (Mg/m³)	2.113	Δσ(max,mean)	0.019, <0.001
μ (mm⁻¹)	3.795	Δρ range (e Å⁻³)	2.155, -1.560
F (000)	4044.0		
^a Cs _{4n} {[Co ₄ (C ₆ H ₄ O ₇) ₄] _μ -[Co(H ₂ O) ₄] ₂ } _n ·16.5n(H ₂ O)			
^b threshold I > 2σ(I).			

4.2.1.3 FT-IR spectroscopy

FT-IR spectra of **5** were measured on a Perkin-Elmer Spectrum 100 FT-IR Spectrophotometer with ATR accessory in the range of 4000 - 300 cm^{-1} . (Figure 4.9)

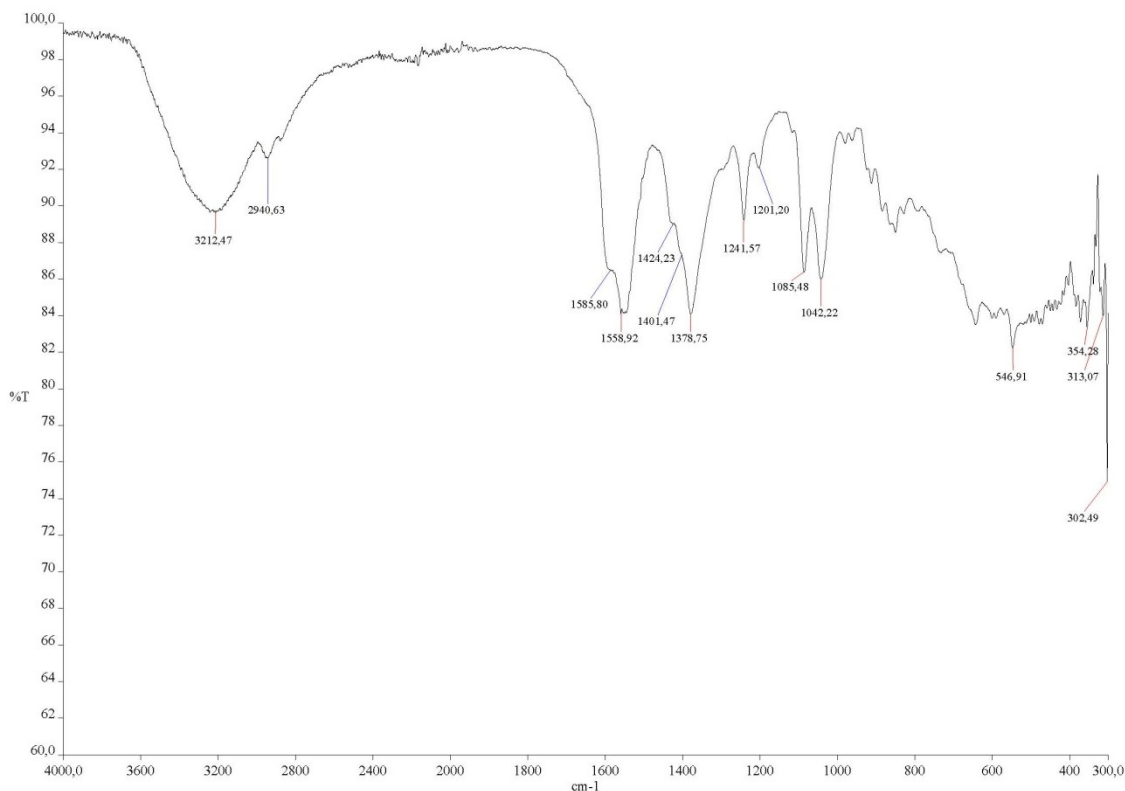


Fig. 4.9. IR spectrum of **5**.

IR (neat compound **5**, cm^{-1}): $\nu(\text{OH})$ 3212.47 (w); $\nu(\text{C}=\text{O})$ 1558.92 (w); $\nu(\text{C}-\text{H})$ 1378.75 (w); $\nu(\text{CO})$ 1085.48 and 1042.22 (d).

4.2.1.4 Magnetic characterization

Magnetic characterization of **3** was performed on a Magnetic Property Measurement System (MPMS) in the range of 300 - 1.8K, 0.1 - 1000 Hz, on a Physical Property Measurement System (PPMS) SQUID magnetometer from Quantum Design.^[P3]

4.2.2 Results and discussion

4.2.2.1 Single Crystal X-Ray diffraction

Compound **5** crystallises in the monoclinic system, space group $C2/c$. Per asymmetric unit there is one half of the cubane, relate to the other half by a two-fold axis, a complete $[\text{Co}(\text{H}_2\text{O})_4]^{2+}$ unit that propagates the polymer and 8.25 molecules of free water distributed over 13 crystallographic sites (Figure 4.10). The cubane core corresponds to isomer A. Two of

the citrates are not chiral while the remaining two (related by symmetry as there is a half-cubane per asymmetric unit) present an *S* configuration in the reference asymmetric unit by coordination of the $[\text{Co}(\text{H}_2\text{O})_4]^{2+}$ units to one of the long arms. Those units are coordinated, according to the nomenclature system proposed in Chapter 1, to the positions L1e and S4e (and symmetry related L4e and S3e). These units, acting as connecting nodes between two cubane units, reside on centres of symmetry, so that there is only one-half of each per asymmetric unit. The citrate oxygen atoms bonded to these connecting units are mutually *trans*. Their distribution around the cube is not as symmetrical as those in compounds **3** and **4** and the resulting anionic net is rhombic (Figure 4.11). The coordination mode of the bridging Co(II) unit to the cubane is through a single bond to an external oxygen atom of a long arm and propagates the polymer bonding an external oxygen atom of a short arm in a neighbouring unit (Lxe-X-Sxe). The anionic polymeric net is perpendicular to *b*-axis and counterions are placed in between the layers balancing the charge of the net (Figure 4.12 and Figure 4.13). For this compound there are 4 Cs^+ counterions per cubane (2 per asymmetric unit). An external oxygen atom from a short arm of the citrate (O11) had severely prolate anisotropic displacement, and was split into O11A and O11B with occupancy of 0.5 each.

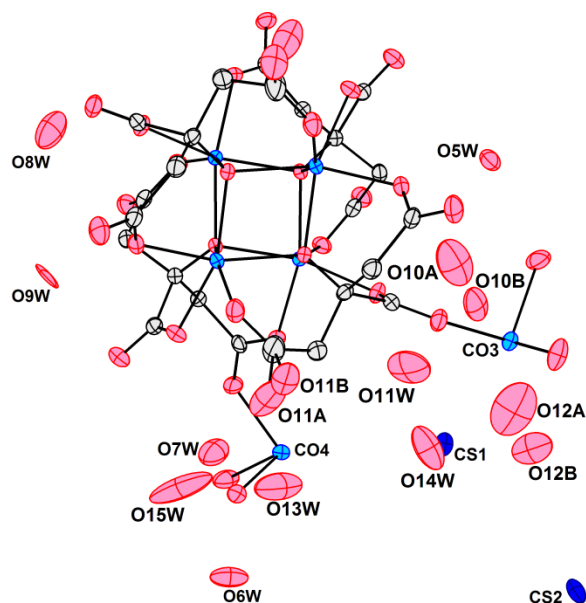


Fig. 4.10. Asymmetric unit of **5**. Only the cube has been grown. H atoms have been omitted for clarity. Displacement ellipsoids (probability 50%).

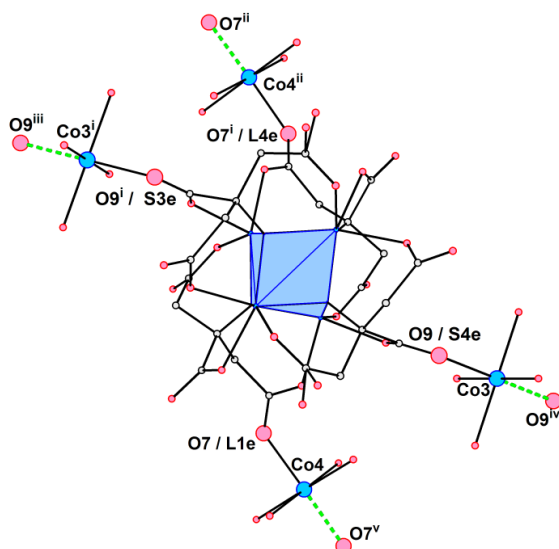


Fig. 4.11. A complete cubane unit with four appended Co(II) units showing the propagation of the polymer as well as the distorted environment of the cubane. i: $(1-x, y, 1.5-z)$, ii: $(x, y, 1+z)$, iii: $(-0.5+x, 0.5-y, 0.5+z)$, iv: $(1.5-x, 0.5-y, 1-z)$, v: $(1-x, y, 0.5-z)$.

There are 16.5 molecules of free water per cubane (8.25 per asymmetric unit distributed over 13 sites). Only 4 of them (O5w-O8w) have complete occupancy. The other has partial occupancy (given by the structural model (ShelX)) and only two of them (O10A/B and O12A/B) are split with a total occupancy for both congeners of one. These occupancies are in agreement with the model and no impossibly close contacts arise from its refinement. There is an extended H-bonding net involving molecules of free water that can act as a donor or acceptor and the oxygen atoms from the citrates as acceptors. Due to the high disorder within the layers, this H-bond net is crucial in the stabilization of the crystalline structure.

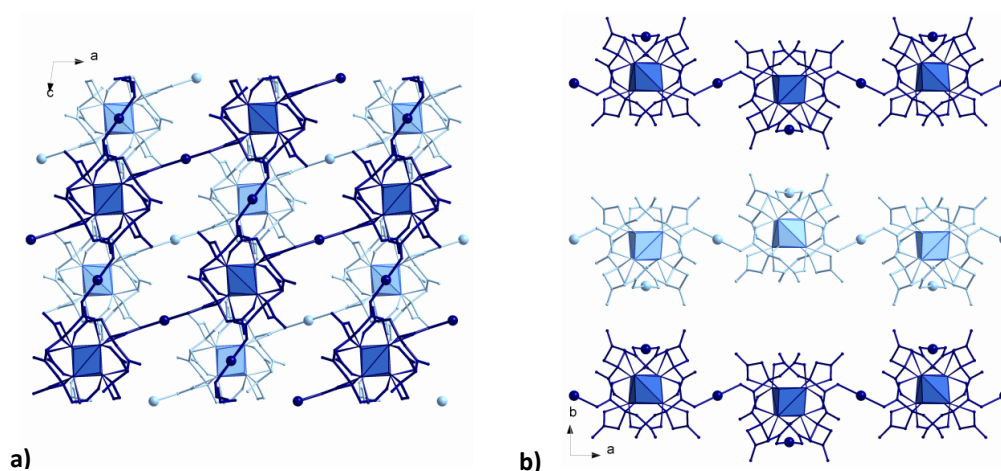


Fig. 4.12. The 2-D rhombic anionic layers in **5**, viewed along *b*-axis (a) and along the *c*-axis (b). Counterions and free molecules of water have been omitted for clarity. The cubanes are represented as a cube formed by Co1, Co2, O1, O2 and congeners. A layers have been represented in dark blue and B in light blue.

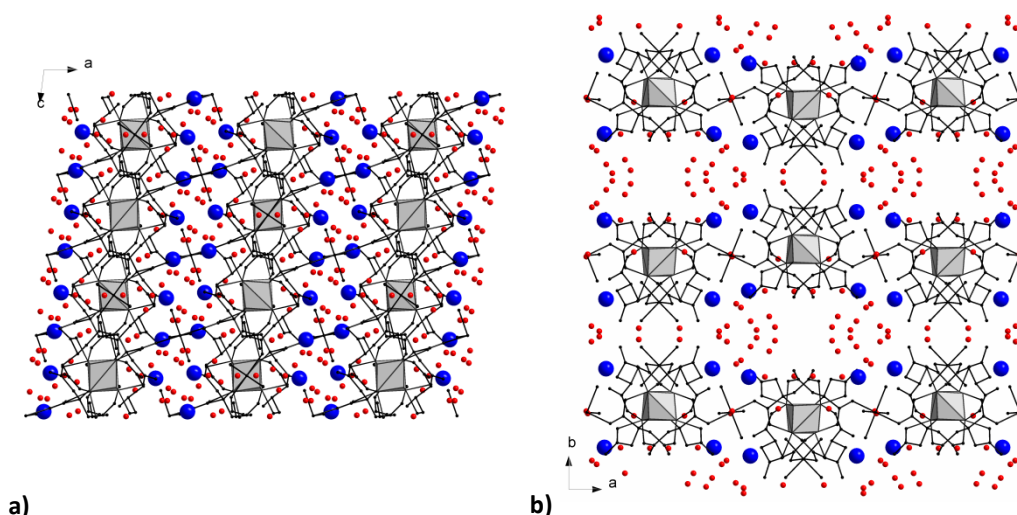


Fig. 4.13. Extended structure of **5**, viewed along the *b*-axis (a) and the *c*-axis (b). The polymeric net is represented in black with the cubanes in grey (see Fig. 4.12). Counterions are represented in dark blue and free molecules of water in red.

The layers have a crenelated structure with a packing pattern that does not follow the same ABAB pattern as for **3** and **4**. The nodes of one net are not eclipsed with the cubanes of a neighbouring layer, and the interlayer spacing is $0.5b$. As a consequence of this less efficient packing, there is a significant amount of space occupied not by the polymer but rather by the free water molecules and the counterions. However, the counterions are close to the polymer, for example, O3 is at $3.156(3)$ Å from Cs1ⁱ and $3.413(3)$ Å from Cs2ⁱ (*i*: $(1-x, y, 1/2-z)$). That fact leaves almost the complete space between layers available for the free molecules of water. The Kitaigorodskii packing index,^[B1] calculated using Platon^[4] gives a K.P.I. of 74.9%. The calculation is complicated for disordered structures, so the input to Platon (Shelx .res file) was modified giving O11A full occupancy and deleting its congener O11B. Something similar was done with the water molecules. For those that were split, (O10A/B and O12A/B) congener A was given full occupancy while congener B was omitted. For the others with partial occupancy, full complete occupancy was assigned for the calculation, so the K.P.I. value is slightly overestimated. The K.P.I. value could suggest the absence of pores or channels in the structure. Nevertheless, the partial occupancies of the water molecules as well as their elongated thermal ellipsoids cannot be overlooked. There is a kind of water movement within the layers what, together with the observation of channels in the crystal structure, make us think that these water molecules can be removed or replaced easily from the compound. Taking this into account, a K.P.I. calculation was done removing the free water from the input file. The K.P.I. value was 57.1% which is in agreement with the hypothesis of a porous material, with water molecules residing inside the channels.

The difference in the synthetic procedure of **4** and **5** is that for the preparation of **5**, no ethylene glycol is added to the reaction media. As these molecules do not play a crucial role in the structure of **4** (they just complete the coordination sphere of the Co(II) units acting as nexus and resides as free molecules of solvent within layers) it was expected to obtain an analogous polymeric net for **5** with the ethylene glycol substituted by two molecules of water each. However, the obtained compound was completely unexpected. To date there is no a rational explanation for this phenomenon since this slight modification does not seem significant enough to produce such a massive change in the crystalline structure.

4.2.2.2 Magnetic characterization

Compound **5** has been magnetically characterised by our group (Thesis of Dra. C. Sáenz de Pipaón Soba^[B5]). In this section, as in the previous ones about magnetism, the results are explained from a chemical point of view. Figures have been extracted from the earlier thesis.

Magnetization at different magnetic fields between 50000 - 500 Oe has been measured from room temperature to 1.8 K (Figure 4.14). The $\chi_M \cdot T$ value remains almost constant until about 75K as observed in compounds **3** and **4**. The main difference in comparison with the results described in the previous section is a peak observed at 75 K for 500 Oe and 1000 Oe. This peak is not present either at higher fields or in the other compounds. It was attributed to the environment of the cube. For compounds **3** and **4**, the distribution of the nexus Co(II) ions is symmetrical, and the cube has an S4 symmetry axis (parallel to the tetragonal *c*-axis) through the cube. However, for **5**, the distribution of the Co(II) bridges breaks the symmetry of the cube, which has only a C2 axis (parallel to the monoclinic *b*-axis) through the cube. The cube can be viewed as formed by two chemically different pairs of Co atoms, those proximal to the bridges between cubes and those which are distant from the bridges (Figure 4.15). This decrease in the symmetry of the environment of the cube affects the magnetism, which presents unexpected features not seen in the other compounds of this family.

of the cube (which is in accord with previously reported examples) and a crescent signal. As proposed for compounds **3** and **4**, this signal arises from the bridging Co(II) ions. If they form a net, it would have a blocking temperature lower than the one for the cube. If not, they could interact with the cubanes forming an extended net which blocks at very low temperatures.

Energy barriers (ΔE) and characteristic relaxation times (τ_0) for the blocking phenomenon at high temperature have been calculated giving a value of $\Delta E = 30(2)$ K and $\tau_0 = 0.4(3) \cdot 10^{-7}$ s.

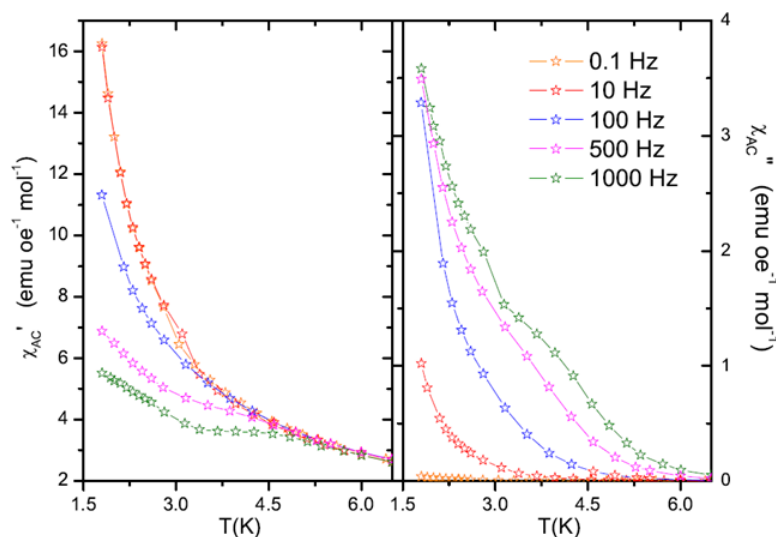


Fig. 4.16. χ_{AC} measurements at different frequencies for **5**.

4.3 Square 2-D Cobalt polymer of SMMs with additional magnetically active centres.

4.3.1 Experimental

4.3.1.1 Synthesis

All reactants and solvents were commercial and were used as received. No further purification was needed for any of them.

The polymer $\text{Cs}_{2n}[\text{Co}(\text{H}_2\text{O})_6]_n\{[\text{Co}_4(\text{C}_6\text{H}_4\text{O}_7)_4]_n\mu\text{-}[\text{Co}(\text{H}_2\text{O})_4]_2\}_n \cdot 12n(\text{H}_2\text{O})$ **6** was obtained as cubic-shaped, fuchsia crystals.

To a stirred solution of citric acid monohydrate in water (50 mL, 0.47 M) was added $\text{CoCO}_3 \cdot x\text{H}_2\text{O}$ (3.25 gr, 23.72 mmol, for $x = 1$). The mixture was stirred until reaction was complete and then gravity-filtered. An aqueous solution of CsOH ($\approx 1.8\text{M}$) was added dropwise to the resulting red solution until a pH of 7.5 - 8 was attained. The solvent was evaporated to restore the initial volume and the solution was cooled to room temperature. A commercial solution of 3,3'-thiodipropanol (98%) was added to the solution (water/3,3'-thiodipropanol 2/1) and the

final mixture was placed in a closed vial at room temperature. After several months a small number of crystals of **6** were obtained.

4.3.1.2 Single Crystal X-Ray diffraction

Single crystal X-Ray diffraction was performed using an Xcalibur S3 CCD-based four-circle diffractometer (Oxford Diffraction and Agilent Technologies). Data collection and processing were controlled by the program CrysAlis Pro.^[P1] The structure was solved *ab initio* by direct methods^[1] and refined by full-matrix least-squares analysis.^[2] Non-hydrogen atoms were refined with anisotropic displacement parameters. The methylene H atoms of the citrate ligands were placed at idealized positions and refined as riders on their respective parent C atoms with isotropic displacement parameters set to 1.2 times the equivalent isotropic U of the C atom. Most hydrogen atoms of the water molecules were found in a difference map and refined as riders on their respective parent O atoms. Their isotropic displacement parameters were set to 1.2 times the equivalent isotropic U of the respective O atoms. The program Diamond^[P2] was used for graphical publication material. Data collection and structure solution information and refinement details are shown in Table 4.3.

Formula	^a C ₂₄ H ₆₈ Co ₇ CS ₂ O ₅₄	Crystal size (mm³)	0.16 x 0.14 x 0.10
fw (g mol⁻¹)	1899.11	θ (min,max) (°)	4.16, 28.83
Radiation	X-Rays (Mo Kα)	Reflns collected	14807
Wavelength (Å)	0.71073	Indep reflns	3677
Crystal system	Tetragonal	R(int), R(σ)	0.0383, 0.0439
Space group	P -4 2 ₁ c	Completeness (θ)	0.933, (27.50)
temp (K)	100(1)	Abs corr	multi-scan
a (Å)	12.5738(1)	T(min,max)	0.79022, 1.00000
c (Å)	19.5895(3)	restraints/parms	0 / 203
V (Å³), Z	3097.11(6), 2	Goodness-of-fit	1.019
ρ calc (Mg/m³)	2.036	R1, wR2 (obs)^b	0.0374, 0.0923
μ (mm⁻¹)	3.106	R1, wR2 (all)	0.0455, 0.0940
F (000)	1886.0	Δ/σ(max,mean)	0.001, <0.001
^cFlack parameter	0.04(2)	Δρ range (e Å⁻³)	1.575, -0.452
^a Cs _{2n} [Co(H ₂ O) ₆] _n {[Co ₄ (C ₆ H ₄ O ₇) ₄] _n μ-[Co(H ₂ O) ₄] ₂] _n ·12n(H ₂ O) ^b threshold I > 2σ(I). ^c Flack, 1983. ^[5]			

4.3.1.3 FT-IR spectroscopy

FT-IR spectra of **6** were measured on a Perkin-Elmer Spectrum 100 FT-IR Spectrophotometer with ATR accessory in the range of 4000 - 300 cm^{-1} (Figure 4.17).

IR (neat compound **6**, cm^{-1}): $\nu(\text{OH})$ 3157.40 (w); $\nu(\text{C=O})$ 1541.66 (w); $\nu(\text{C-H})$ 1383.28 (w); $\nu(\text{CO})$ 1088.68 and 1060.93 (d).

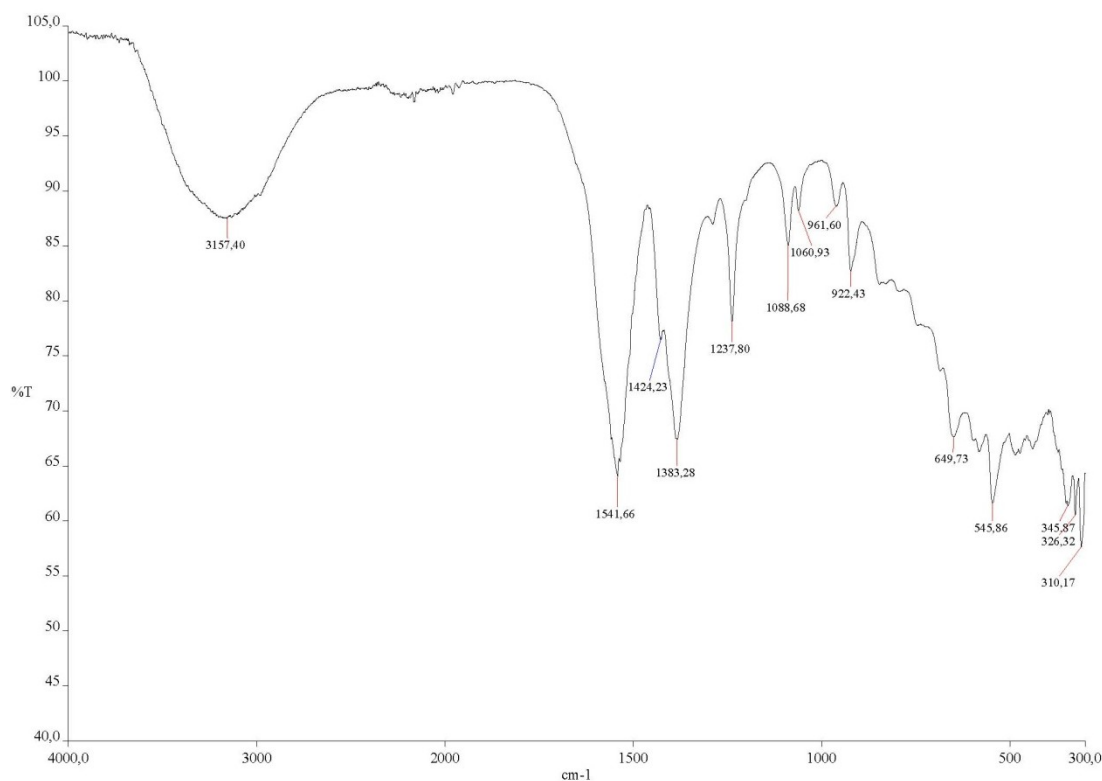


Fig. 4.17. IR spectrum of **6**.

4.3.1.4 Magnetic characterisation

Magnetic characterization of **6** was performed on a Magnetic Property Measurement System (MPMS) in the range of 300 - 1.8K, 0.1 - 1000 Hz, on a Physical Property Measurement System (PPMS) SQUID magnetometer from Quantum Design.^[P3]

4.3.2 Results and discussion

4.3.2.1 Single Crystal X-Ray diffraction

Compound **6** crystallises in the tetragonal system, space group $P-42_1c$. There is only a quarter of a cubane per asymmetric unit, sitting astride a -4 symmetry element, and half of a Co(II) unit acting as a nexus of union between cubanes. The bridge resides on a two-fold axis and completes its coordination sphere with 4 molecules of water, related in pairs by the

symmetry element. Balancing the charge of the polymer, there is a quarter of a Co(II) on a site of crystallographic symmetry -4 , that is, one of these per cubane, which completes its coordination sphere with 6 molecules of water related in groups of four and two by symmetry. There is also half of a Cs⁺ on a two-fold axis -- *i.e.*, two per cubane -- and 3 molecules of free water (Figure 4.18).

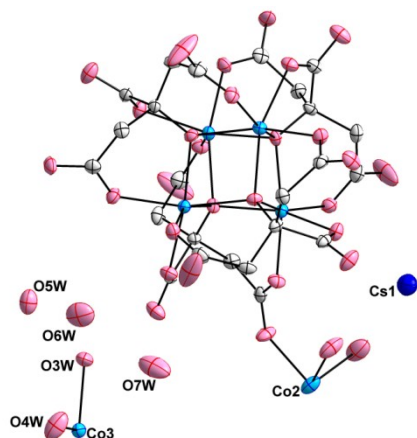


Fig. 4.18. A complete cubane unit of **6** with its Co(II) bridge and free water. Only free water molecules from one asymmetric unit have been represented for clarity. Displacement ellipsoids (probability 60%).

The cubane corresponds to isomer A and two of its citrates has S configuration and the remaining two are R in the reference asymmetric unit. Co(II) nexus units are coordinated to L1e, L4e, L6e and L7e according with the nomenclature system proposed. The coordination mode of the nexus unit is through a single bond connecting each of two external oxygen atoms from long arms (Figure 4.19).

The bridging Co(II) units mediate the propagation the polymer with the cubanes coordinated at mutually trans positions (Lxe-X-Lxe). The square 2-D polymeric net is a regular array of cubanes residing on -4 symmetry sites. The layers are anionic and run parallel to the *ab*-plane. The packing pattern of the layers is ABAB, in such a way that the nodes of one layer are eclipsed with the cubanes of neighbouring layers. The distance between layers is $0.5c$ as for **3** and **4**. There are channels in between the layers running parallel to the *a*- and *b*-axes (Figure 4.20).

The structure of **6** is a substitution isomorph of the structures of **3** and **4**. The substitution of half of the cations in either **3** or **4** by $[\text{Co}(\text{H}_2\text{O})_6]^{2+}$ is sufficient to produce a fully ordered structure instead of the severely disordered structures observed for **3** and **4**.

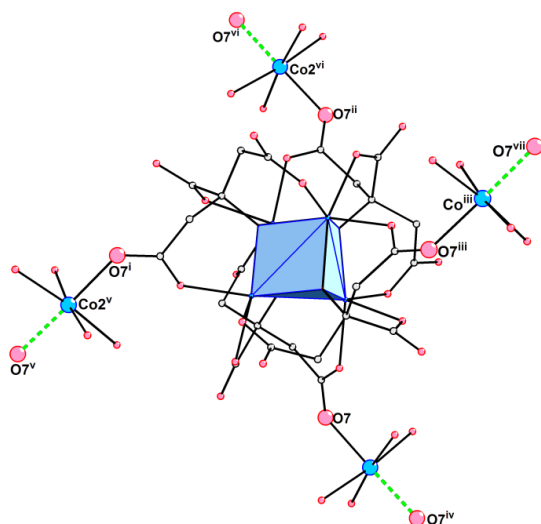


Fig. 4.19. A complete cubane unit of **6** with its four pendant Co(II) units showing the propagation of the polymer. i: (1-y, x, 1-z), ii: (1-x, 1-y, z), iii: (y, 1-x, 1-z), iv: (1-x, -y, z), v: (1+y, 1-x, 1-z), vi:(x, 1+y, z), vii: (-y, x, 1-z).

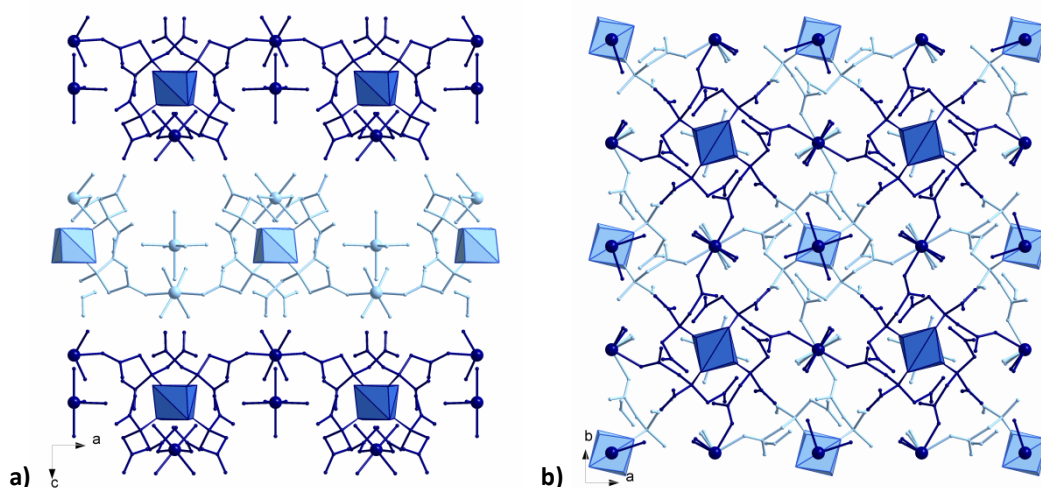


Fig. 4.20. Square 2-D anionic layers in **6** viewed along the *b*-axis (a) and *c*-axis (b). ABAB packing is seen in (a). Counterions and free molecules of water have been omitted for clarity; only the $[\text{Co}(\text{H}_2\text{O})_6]^{2+}$ cation is represented. A layers are represented in dark blue and B in light blue.

Free molecules of water form an extended H-bond net within the polymeric layers and also form hydrogen bonds with the oxygen atoms from the citrate and the coordinated water. There is a cyclic structure of covalent and hydrogen bonds encircling the cubane which involves the Co atoms not forming part of the cube and the molecules of water (7 per asymmetric unit, 4 coordinated and 3 unbonded). Hydrogen bonding is not a structure determining factor in this compound. As mentioned above, **6** is the unique example out of three with this structure type, in which no disorder is found for the counterions and species between the polymers. We attribute this to the larger size and hydrogen-bonding capacity of the $[\text{Co}(\text{H}_2\text{O})_6]^{2+}$ cation.

4.3.2.2 Magnetic characterisation

The magnetic properties of compound **6** were reported in the thesis of Dra. C. Sáenz de Pipaón Soba.^[B5] A brief review of the magnetic results is given here. Graphical material have been extracted from the thesis of Dra. Sáenz de Pipaón Soba.

Magnetization at different magnetic fields between 50000 - 500 Oe has been measured from room temperature to 1.8 K. The results were analogous to those obtained for compounds **1** - **5**. A comparison of the magnetization versus T at 500 Oe is shown in Figure 4.21.

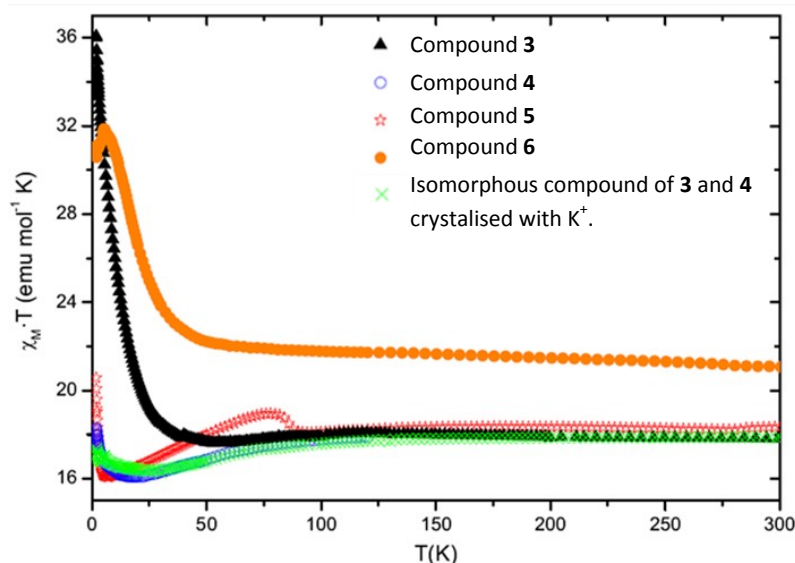


Fig. 4.21. $\chi_M \cdot T$ versus T plot for the the bidimensional networked compounds measured at 500 Oe.

At high temperature, the $\chi_M \cdot T$ value is around 21 $\text{emu} \cdot \text{mol}^{-1} \cdot \text{K}$ which is in accord with the value expected for 7 independent Co(II) ions with $S = 3/2$ and $g = 2.4$.

AC measurements were carried out to evaluate possible SMM behaviour of the sample at different frequencies at low temperatures (Figure 4.22). Once again, a blocking phenomenon around 4 K is observed. It is attributed to the superparamagnetic blocking of the cube.

Energy barriers (ΔE) and characteristic relaxation times (τ_0) at high temperature for the blocking have been calculated giving a value of $\Delta E = 23(1)$ K and $\tau_0 = 0.3(1) \cdot 10^{-7}$ s.

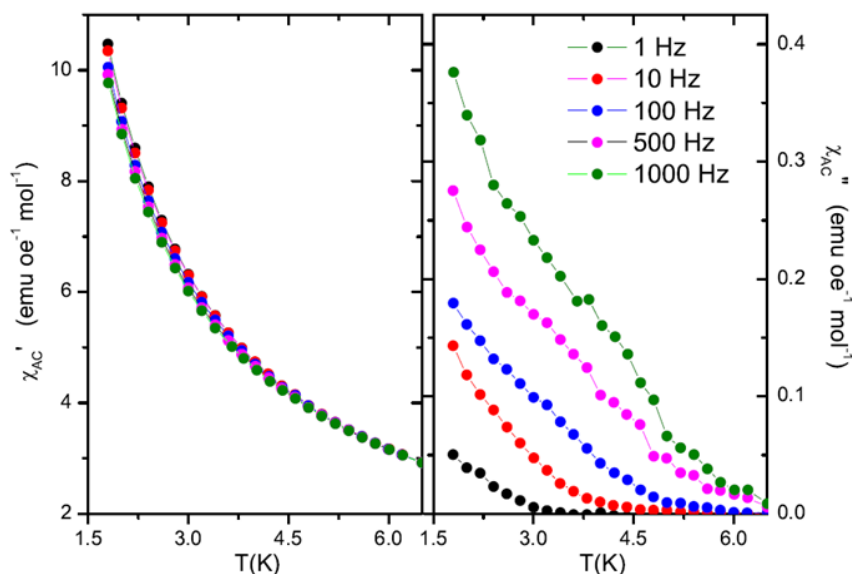


Fig. 4.22. χ_{AC} measurements at different frequencies for **6** in phase (right) and out of phase (left).

4.4 Conclusions

The objective of the work reported in this chapter was to prepare coordination polymers based on cubanes. Their rational synthesis would allow the preparation of ordered arrays of SMM. All of the resulting compounds are 2 dimensional. They present a layered structure which is in principle suitable for their putative future applications as, for example, technological devices because each layer can be envisaged as a single monolayer of a given compound deposited on a surface.

The second objective was to study the magnetism of the compounds obtained to see whether they preserve their SMM behaviour when ordered into nets. For the compounds presented in this chapter, frequency-dependent peaks are found in the χ_{AC} measurements at around 4 K, which are associated with the superparamagnetic blocking of the cube. That confirms the SMM nature of the sample and is in accord with previously reported results for similar compounds. The values of the energy barriers and relaxation times are in the same range for the four compounds and agree with values reported previously for other cubanes.^{[6][7][8][9]}

In the first section of this chapter, a pair of isostructural compounds, crystallised with different counterions, Rb^+ and Cs^+ , is presented. A third derivative, crystallised with potassium, was also obtained; but its highly disordered structure was not considered appropriate for presentation in the thesis. The layers are almost equal for the Rb^+ and Cs^+ derivatives. The details of the species residing between the layers are what change. In agreement with what

was expected due to its size, the Cs^+ compound presents a higher volume for the crystallographic unit cell. The axis parallel to the layers is almost equal for the two compounds; however, the cells vary along the axes perpendicular to the layers. In contrast to the stability of the polymeric net, the space between the layers is full of species in disorder. That suggests that it would be easy to remove the molecules of free water by soft dehydration and also to conduct ion exchange reactions.

The preparation of a family of related compounds opens the possibility of studying how small changes in their composition affect their magnetism. First of all, these compounds represent the first cases in which two relaxation processes with different energy barriers have been seen for these types of systems. That in turn suggests the study of several conceivable mechanisms for magnetic cooperativity. Despite the fact that the nets containing the magnetically active entities are almost identical, there are some interesting variations from one to another. There is a difference of 0.05 K in the critical temperature (T_c) for the second blocking process in **3** and **4** at very low temperature. It is difficult to find an explanation to this fact, it could be due to small differences in the alignment of the easy axis of the cubane Co(II) ions and the bridging Co(II). Changes in the alignment of the easy axis of the cube and the Co(II) bridge could be also be responsible for that difference. In general, it has been proved that it is not necessary to change the gross properties of the magnetic net in order to introduce modifications in the magnetism. Subtle structural modification can be sufficient.

A good example of this is compound **5**. It is the result of removing the ethylene glycol from the reaction medium used to prepare **4**. It was expected that the same polymer as in **4** would emerge, but without the ethylene glycol. Surprisingly, a new arrangement of the cubes was obtained. The resulting rhombic net, with a less symmetrical arrangement of the Co(II) units attached to the periphery of the cube, has modified magnetism. The energy barrier of the relaxation process increases due to the higher anisotropy around the cube.

In addition, compound **6** was obtained by substitution of the ethylene glycol used for **4** by 3,3'-thiodipropanol. The diol does not enter the structure, and the result is a square net nearly identical to that obtained in **3** and **4** but without ethylene glycol. This result was unexpected. We do not yet have a simple explanation for this finding: When the synthetic procedure used to obtain **3** is slightly modified to obtain the same compound but without the substance (ethylene glycol) removed from the reaction medium, a new polymer is obtained. When a different substance replaces the ethylene glycol, the result expected for the first modification is obtained; and the added reagent does not form part of the compound. A possible

explanation is that in solution, the cubes are formed when the pH is around 7.5 - 8. Whatever is added to the reaction medium modifies the environment of the sample (*i.e.*, dielectric constant, polarity) or is involved in the formation of intermediates that determine the final structure and composition of the derivatives obtained. This compound, with a $[\text{Co}(\text{H}_2\text{O})_6]^{2+}$ unit as counterion residing between the layers, has an energy barrier for the magnetic relaxation process which is two times that of compounds **3** and **4**. This fact is attributed to the interaction of the counterions with the molecular magnetic field of the cube.

Finally the fact that all these compounds present a layered structure with a significant amount of free space between the layers, sometimes filled with disordered molecules, makes these derivatives good candidates for the study of solvent sorption processes or ion exchange reactions, opening the possibility of obtaining multifunctional materials. These compounds can also serve as the starting point for an expanded study of the influence of chemical modification on their magnetic behaviour.

References

- [1] A. Altomare, G. Cascarano, C. Giacovazzo, A. Guagliardi, *Journal of Applied Crystallography* **1993**, *26*, 343-350.
- [2] G. M. Sheldrick, *Acta Crystallographica Section A* **2008**, *64*, 112-122.
- [3] Z. H. Zhou, Y. F. Deng, H. L. Wan, *Crystal Growth & Design* **2005**, *5*, 1109-1117.
- [4] A. L. Spek, *Acta Crystallographica Section D-Biological Crystallography* **2009**, *65*, 148-155.
- [5] O. Kennard, J. C. Speakman, J. D. H. Donnay, *Acta Crystallographica* **1967**, *22*, 445-&.
- [6] T. A. Hudson, K. J. Berry, B. Moubaraki, K. S. Murray, R. Robson, *Inorganic Chemistry* **2006**, *45*, 3549-3556.
- [7] B. Moubaraki, K. S. Murray, T. A. Hudson, R. Robson, *European Journal of Inorganic Chemistry* **2008**, 4525-4529.
- [8] M. Murrie, S. J. Teat, H. Stoeckli-Evans, H. U. Gudel, *Angewandte Chemie-International Edition* **2003**, *42*, 4653-4656.
- [9] K. W. Galloway, A. M. Whyte, W. Wernsdorfer, J. Sanchez-Benitez, K. V. Kamenev, A. Parkin, R. D. Peacock, M. Murrie, *Inorganic Chemistry* **2008**, *47*, 7438-7442.
- [B1] A.I. Kitaigorodskii, *Molecular Crystals and Molecules*, Academic Press, New York, 1973.
- [B5] Sáenz de Pipaón Soba, Cristina. Contributions to Molecular Magnetism: Chiral Magnets and Networked SMMs. [on line]. Universidad de Zaragoza, 2013. <<http://http://zaguan.unizar.es/record/10403>>
- [P1] CrysAlisPro, Oxford Diffraction Ltd., Version 1.171.33.31
- [P2] Diamond. Klaus Brandenburg, Crystal Impact GbR, Bonn, Germany. Version 3.2i.
- [P3] Quantum Design. <http://www.qdusa.com>

5

3-D Cobalt citrate cubanes.*

This chapter is devoted to a family of 3D polymers based on cobalt citrate cubanes. The basic unit of this polymer is the same as reported previously; in this case the isomer of the cube for the two compounds presented is isomer A.

The first polymer, with formula $K_{4n}\{[Co_4(C_6H_4O_7)_4]\mu-[Co(H_2O)_4]_2\}_n \cdot 8n(H_2O)$ **7** is a highly symmetrical 3-D net with a diamondoid structure. It has three interpenetrating 3-D nets in the solid state, related by symmetry and channels along the structure where the K^+ ions are located. A complete magnetic characterization of this compound has been made, with interesting results.

The second derivative has the formula $Ca_{2n}\{[Co_4(C_6H_4O_7)_4]\mu_3-[Co(H_2O)_3]_2\}_n \cdot 17.8n(H_2O)$ **8** and is the first example of a cubane polymer with an alkaline earth metal as counterion. The 3-D net is propagated through the Co(II) atoms resulting in a anionic polymer with a highly irregular 3-D structure.

J. Campo, L. R. Falvello, E. Forcén-Vázquez, F. Palacio, C. Saenz de Pipaon, M. Tomás (To be published).

L. R. Falvello, E. Forcén-Vázquez, F. Palacio and M. Tomás (To be published).

5.1. High-dimensionality polymer with diamondoid topology

5.1.1. Experimental

5.1.1.1. Synthesis

Reagents were commercial and used as received. No additional purifications were necessary.

The polymer $K_{4n}\{[Co_4(C_6H_4O_7)_4]_{\mu}\cdot[Co(H_2O)_4]_2\}_n\cdot 8n(H_2O)$ (**7**) was obtained by addition of $CoCO_3\cdot xH_2O$ (3.25 gr, 23.72 mmol, for $x = 1$) to a stirred aqueous solution of citric acid monohydrate (50 mL, 0.47 M). After the reaction was complete, the resulting mixture was gravity-filtered and then an aqueous solution of KOH (0.5 M) was added dropwise until a pH of 7-8 was reached. The solvent was evaporated at 90 °C to reach the initial volume. The addition of a commercial solution of 1,2-propanediol (99%, extra pure) ($H_2O/1,2$ -propanediol 2/1) gives well-formed red-pink cubic-shaped crystals of **7** after several days at room temperature.

As mentioned in Chapter 4 (section 4.1.2.1), any of the procedures given for the synthesis of the two different intermediates described therein are also valid for the preparation of the compounds presented in this chapter. The synthetic procedure is the same until the last step, where the appropriate MOH solution and any other reagent are added to the reaction mixture.

5.1.1.2. Single Crystal X-Ray diffraction

Single crystal X-Ray diffraction was performed in an Xcalibur S3 CCD-based four-circle diffractometer (Oxford Diffraction and Agilent Technologies). The program CrysAlis Pro^[P1] was used for data collection and processing. The structure was solved *ab initio* by direct methods^[1] and refined by full-matrix least-squares analysis.^[2] Non-hydrogen atoms were refined with anisotropic displacement parameters. The methylene H atoms of the citrate ligands were placed at idealized positions and refined as riders on their respective parent C atoms with isotropic displacement parameters set to 1.2 times the equivalent isotropic U of the C atom. Hydrogen atoms of the water molecules were found in a difference map. Their isotropic displacement parameters were set to 1.2 times the equivalent isotropic U of the corresponding O atom. Material for publication was prepared using Diamond^[P2] and Mercury^[3]. Data collection and structure solution information and refinement details are shown in Table 5.1.

Formula	^a C ₂₄ H ₄₈ Co ₆ K ₄ O ₄₄	Crystal size (mm³)	0.41 x 0.32 x 0.22
fw (g mol⁻¹)	1550.60	θ (min,max) (°)	4.385, 30.740
Radiation	X-Rays (Mo kα)	Reflns collected	13258
Wavelength (Å)	0.71073	Indep reflns	3514
Crystal system	tetragonal	R(int), R(σ)	0.0137, 0.0131
Space group	I 4 ₁ /a	Completeness (θ)	0.921 (27.500)
temp (K)	105(1)	Abs corr	multi-scan
a (Å)	20.7872(3)	T(min,max)	0.7458, 1.0000
c (Å)	11.3290(2)	restraints/parms	0, 223
V (Å³), Z	4895.35(13), 4	Goodness-of-fit	1.139
ρ calc (Mg/m³)	2.104	R1, wR2 (obs)^b	0.0294, 0.0730
μ (mm⁻¹)	2.451	R1, wR2 (all)	0.0301, 0.0734
F (000)	3128.0	Δσ(max,mean)	0.002, <0.001
		Δρ range (e Å⁻³)	0.661, -0.555
^a K _{4n} {[Co ₄ (C ₆ H ₄ O ₇) ₄] _n ·[Co(H ₂ O) ₄] ₂ } _n ·8n(H ₂ O)			
^b threshold I > 2σ(I).			

5.1.1.3. Powder X-Ray diffraction

Powder X-Ray data were collected by the X-Ray Diffraction and Fluorescence Analysis Service of the University of Zaragoza using a RIGAKU D/max 2500 diffractometer equipped with a copper rotating anode, operating at 40 kV and 100 mA with a graphite monochromator. Measurements were made at 2θ values from 5° to 50° in steps of 0.03° at a rate of 1s/step.

5.1.1.4. FT-IR spectroscopy

FT-IR spectra of **7** were measured on a Perkin-Elmer Spectrum 100 FT-IR Spectrophotometer with ATR accessory in the range of 4000 - 300 cm⁻¹ (Figure 5.1).

IR (neat compound, cm⁻¹): ν(OH) 3414.80 (w) and 3102.34 (w); ν(C=O) 1541.71 (w); ν(C-H) 1427.52 (w), 1410.84 (w) and 1382.12 (w); ν(CO) 1082.11 (t).

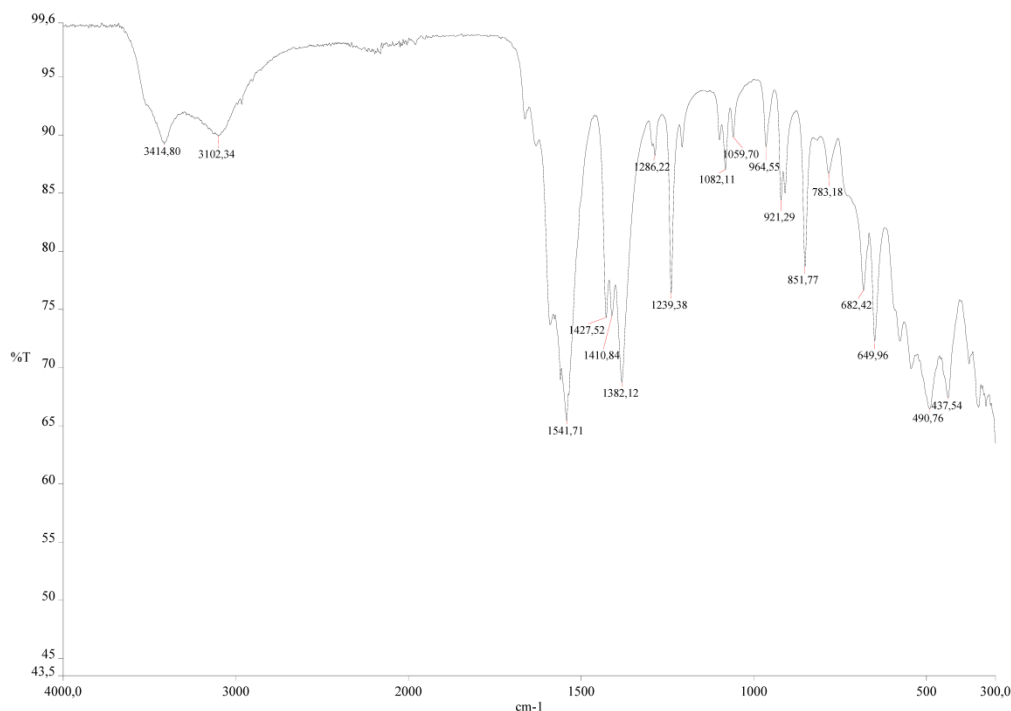


Fig. 5.1. IR spectrum of **7**.

5.1.1.5. Elemental analysis

Elemental analysis of **7** was carried out on a Perkin Elmer 2400 CHNS/O analyser. Calculated analysis for $(C_{24}H_{48}Co_6K_4O_{44})$ (**7**) is: C, 18.59%; H, 3.12%. Results obtained were C, 18.59%; H, 3.12%.

5.1.1.6. Thermogravimetric analysis (TGA)

Thermogravimetric analysis (TGA) was carried out using a Universal V4.5A TA Instrument, model 2960 SDT V3.0F in the range of 25 - 500 °C (Figure 5.2).

The result shows a slight weight loss starting at 25 °C that becomes more important at 75 °C, reaching its maximum at 100 - 125 °C. This is attributed to dehydration. A weight loss of 17.75% corresponds to a water loss of 15 molecules of water, which is almost the total number of water molecules in the compound. Peaks at higher temperatures are associated with decomposition processes.

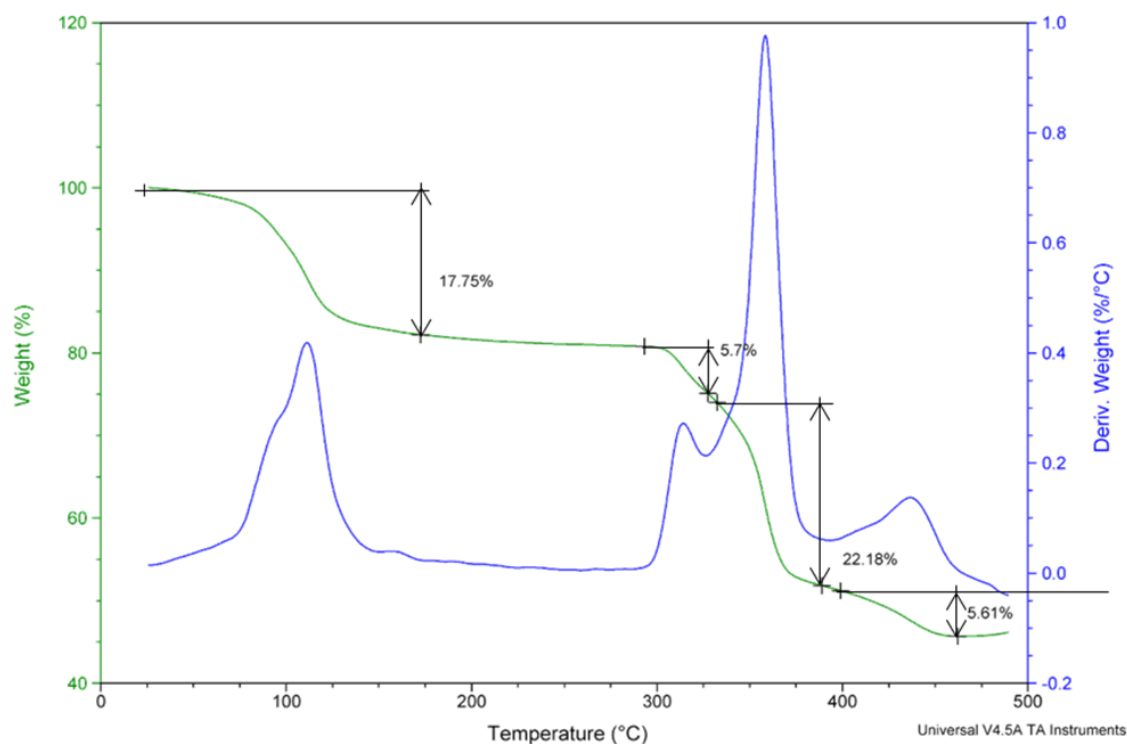


Fig. 5.2. TGA for **7**.

5.1.1.7. Magnetic characterization

Magnetic characterization of **7** was performed on a Magnetic Property Measurement System (MPMS) in the range of 300 - 1.8K, 0.1 - 1000 Hz, on a Physical Property Measurement System (PPMS) SQUID magnetometer from Quantum Design.^[P3]

5.1.2. Results and discussion

5.1.2.1. Single Crystal X-Ray diffraction

Compound **7** crystallises in the tetragonal system, space group $I4_1/a$. The asymmetric unit was chosen so as to permit the simplest possible description of the extended structure, with the Co_4O_4 cubane unit centred at $(1/2, 1/2, 1/2)$. For this purpose it was necessary to use Origin Choice 1 for this space group as given in the International Tables.^[B2]

The anionic polymer was crystallised with K^+ as the counterion. The content of an asymmetric unit is a quarter of cubane on a (-4) symmetry element, half of a Co(II) bridging unit, residing on an inversion centre, four molecules of water, two coordinated to the Co(II) unit and the others free, and one potassium cation disordered over two crystallographic sites, Figure 5.3.

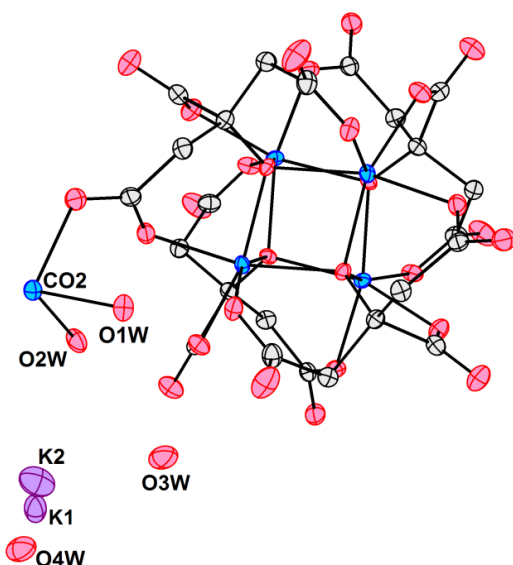


Fig. 5.3. A complete cubane unit with a Co(II) bridge, counterions and free water for compound **7**. Displacement ellipsoids (probability 60%).

The cobalt citrate cubane corresponds to isomer A. The asymmetric central carbon atom from the citrates, all of them related by symmetry, has R configuration for two of them and S for the remaining one (those related by the binary axis). The cubanes are propagated through the Co(II) units resulting in a 3-D anionic net with a diamondoid structure. The main building block of the net is the cubane, bridged by the four Co(II) units. These units are coordinated to four Lxe positions (L2e, L3e, L5e and L8e) according to the naming scheme described in Chapter 1. The bridge is through an external oxygen atom from a long arm (Figure 5.4).

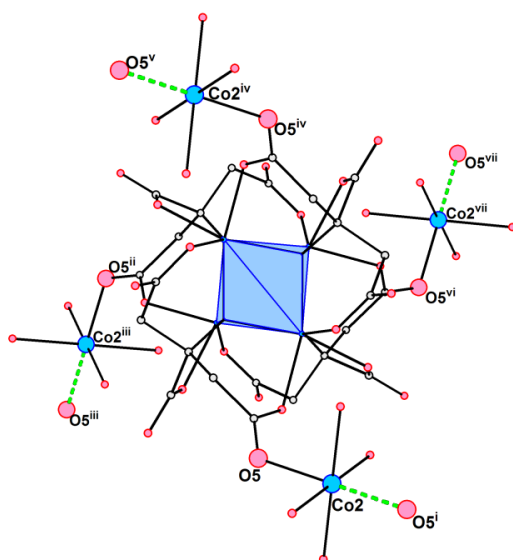


Fig. 5.4. A complete cubane unit of **7** with its four Co(II) satellites showing the propagation of the polymer (bonds in green). i: $(1-x, 0.5-y, 0.25-z)$, ii: $(1-y, x, 1-z)$, iii: $(0.5+y, 1-x, 0.75+z)$, iv: $(1-x, 1-y, z)$, v: $(x, 0.5+y, 0.25-z)$, vi: $(y, 1-x, 1-z)$, vii: $(0.5-y, x, 0.75+z)$.

The key factor for the difference in dimensionality between the polymeric net of **7** and those obtained previously is the distribution of the four Co(II) units around the cube. They describe a tetrahedron whose angles (subtended at their centre of gravity) vary from 101.5° to 113.6° (Figure 5.5). Tetrahedral distortion calculations indicate that this tetrahedron is almost regular (Vol = 152.98 \AA^3 , $\lambda_{\text{tet.}} = 1.0097$ and var = 39.3576 deg^2). The S_4 axis of the cube is parallel to the crystallographic c -axis producing a 3-D net with point symbol 6^6 . In the solid state, the crystal is formed by interpenetration of these diamond-like nets (Figure 5.6). Despite of the interpenetration there is a significant amount of space that is not filled by the cubanes. The compound presents channels along the quaternary axis, where counterions and free molecules of water are located (Figure 5.7).

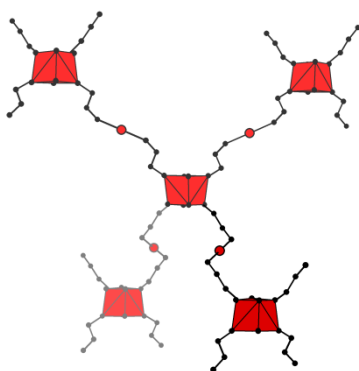


Fig. 5.5. Representation of the propagation of the polymeric net in terms of its magnetically active entities (red) showing the tetrahedral environment of each cubane. Each cubane is represented as a red $[\text{Co}_4\text{O}_4]$ cube. Red circles are the bridging Co(II) units. Only the Cube-O-C-O-Co bonds have been shown for the sake of simplicity (black bonds and circles).

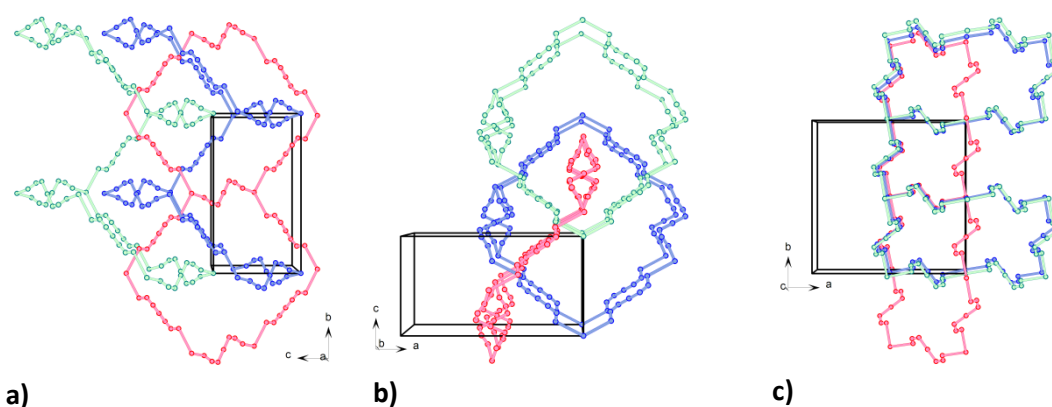


Fig. 5.6. Schematic representation of three 3-D polymeric nets showing the interpenetration, viewed along the a -axis (a), the b -axis (b) and the c -axis (c). Only the cubes, each represented by a point at its centre of gravity, the Co(II) units and the bridging O-C-O atoms are represented. Counterions and molecules of water have been omitted for clarity.

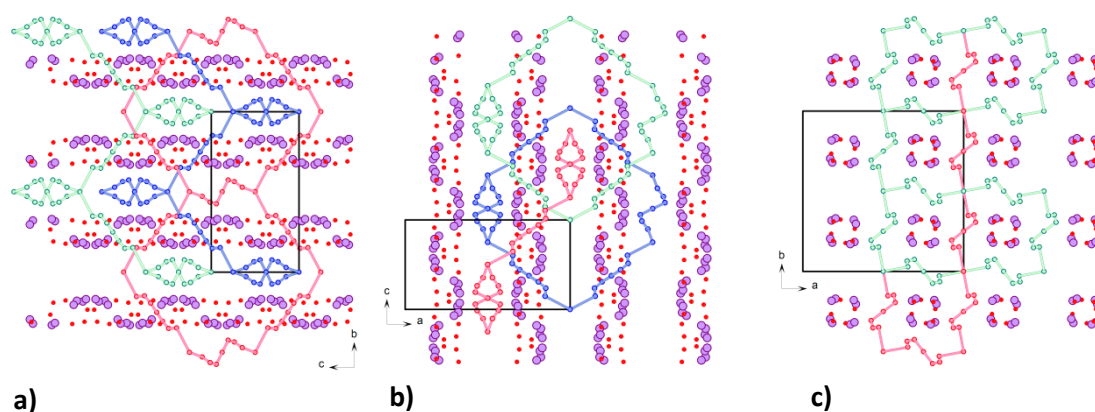


Fig. 5.7. Schematic representation of the polymeric nets as in Fig. 5.6 including counterions (violet) and free molecules of water (red) occupying the channels within the structure. Views along the a -axis (a), b -axis (b) and c -axis (c).

The Kitaigorodskii Packing Index,^[B1] calculated using Platon^[4] is 82.6%, which indicates that the compound is not porous, when all species are considered. However, if the contents of the channels, that is, K^+ and water molecules, are removed, the K.P.I. is 58.7%. So while the compound as prepared is not formally porous, there are occupied channels throughout the structure. Thus, there is a clear pathway for solvent and ionic interchange.

5.1.2.2. Powder X-Ray diffraction

A thermal study of the evolution of **7** was made in order to check if any dehydration process operates in the compound, as there are channels present with resident water. To this end, a powder sample of the compound was heated from 20 °C to 100 °C in steps of 10 °C, heating for half an hour at each temperature before X-Ray data collection. Each measurement takes about 20 minutes, so for each data point the compound was heated for approximately an hour. Figure 5.8 shows the evolution of **7** between 20 °C and 100 °C. There are no significant changes in the crystal structure of the compound until 60 °C. At 70 °C the intensity of the signal decreases a bit and finally, at 80 °C the compound starts losing its crystallinity. This could be caused by a massive water loss, in agreement with the results observed in the TGA. Below 100 °C the compound undergoes dehydration. There is a threshold temperature, 60 °C, below which there are no changes. Above this threshold temperature there appears to be a kinetic factor in play, because more rapid heating produces more rapid water egress. The fact that the diffraction pattern retains its integrity to higher temperatures suggests that water molecules do not exit the sample easily. Experiments at temperatures above 80 °C are needed. That matches with the TGA results where the main peak attributed to dehydration appears

between 75 - 150 °C. When water molecules leave the structure, its crystallinity is lost. The colour of the sample after the heating process changes from pink to violet.

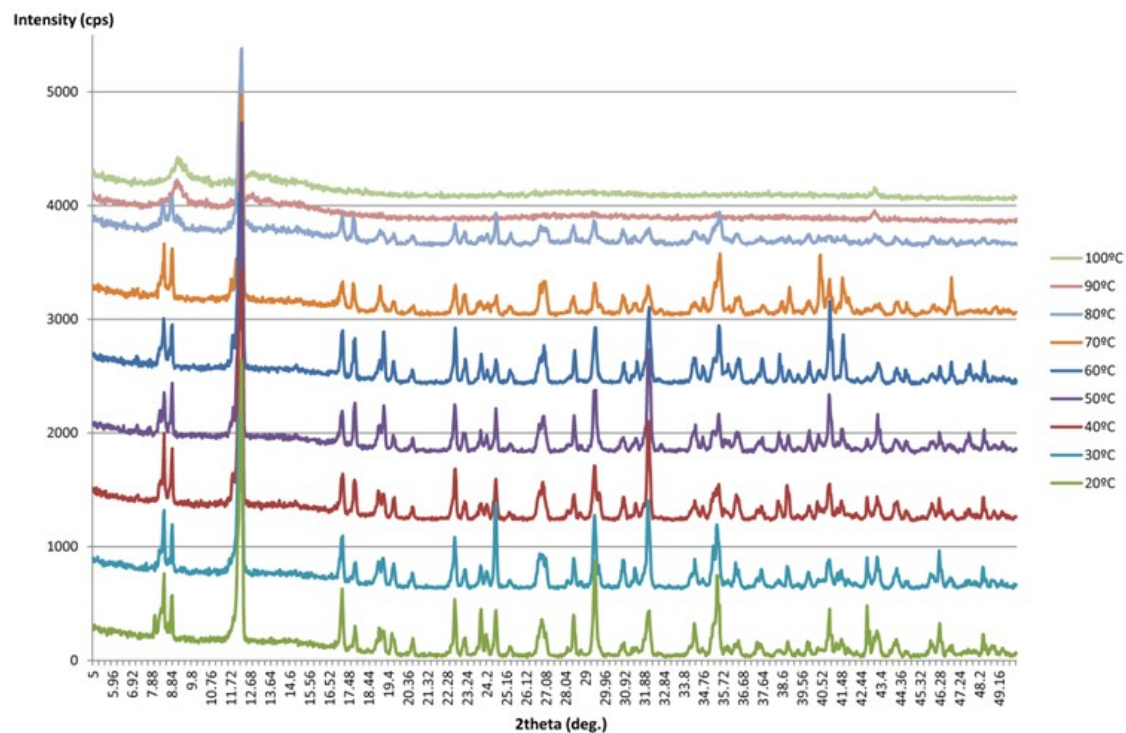


Fig. 5.8. Powder X-Ray diffractograms for the evolution of **7** from 20 °C to 100 °C in steps of 10 degrees, heating the sample for 30 minutes at each temperature before data collection.

Once the sample is removed from the diffractometer, it is placed in a humid atmosphere for a week at room temperature. After that, the sample recovers its pink colour and a diffractogram collected at 20 °C shows that the initial pattern is nearly restored, suggesting the reversibility of the dehydration. Figure 5.9, presents the initial diffractogram, the one at 90 °C and finally the diffractogram after rehydration, measured at 20 °C.

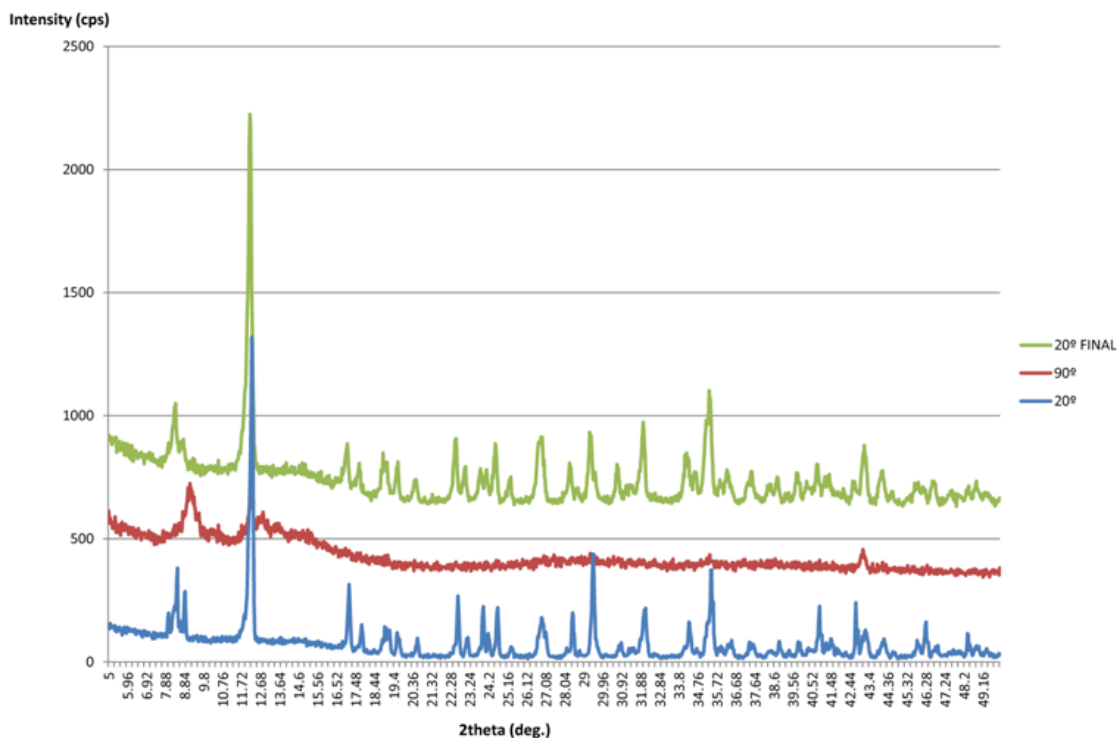


Fig. 5.9. Comparison of the powder X-Ray diffractograms of **7** at 20 °C, 90 °C and 20 °C after exposure of the sample to a humid atmosphere.

5.1.2.3. Magnetic characterization

Our group has magnetically characterised compound **7** (see Thesis of Dra. C. Sáenz de Pipaón Soba^[B5]). A brief analysis of the results will be given in this section. Figures have been extracted from the mentioned thesis.

The magnetization versus temperature at 500 Oe was measured from room temperature to 1.8K (Figure 5.10). The $\chi_M \cdot T$ value obtained from the curve at 300 K is 17 $\text{emu} \cdot \text{mol}^{-1} \cdot \text{K}$ which is in accord with the results expected for six independent Co(II) ions with $S = 3/2$ and $g = 2.4$.

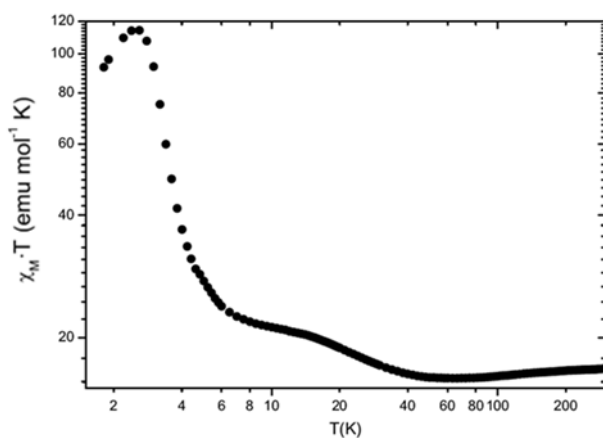


Fig. 5.10. $\chi_M \cdot T$ versus T plot of **7** measured at 500 Oe.

The AC behaviour of the samples was studied at different frequencies from room temperature to 1.8 K (Figure 5.11). As expected, there is a blocking phenomenon at around 4K attributed to the superparamagnetic blocking of the cubes. In addition and in accord with previous results, a frequency-independent peak appears at 2.7 K due to the presence of a phase transition.

Energy barriers (ΔE) and characteristic relaxation times (τ_0) have been calculated at low temperature for frequencies between 100 Hz and 1000Hz, giving values of $\Delta E = 44.04(18)$ K and $\tau_0 = 1.62(6) \cdot 10^{-8} \text{ s}^{-1}$.

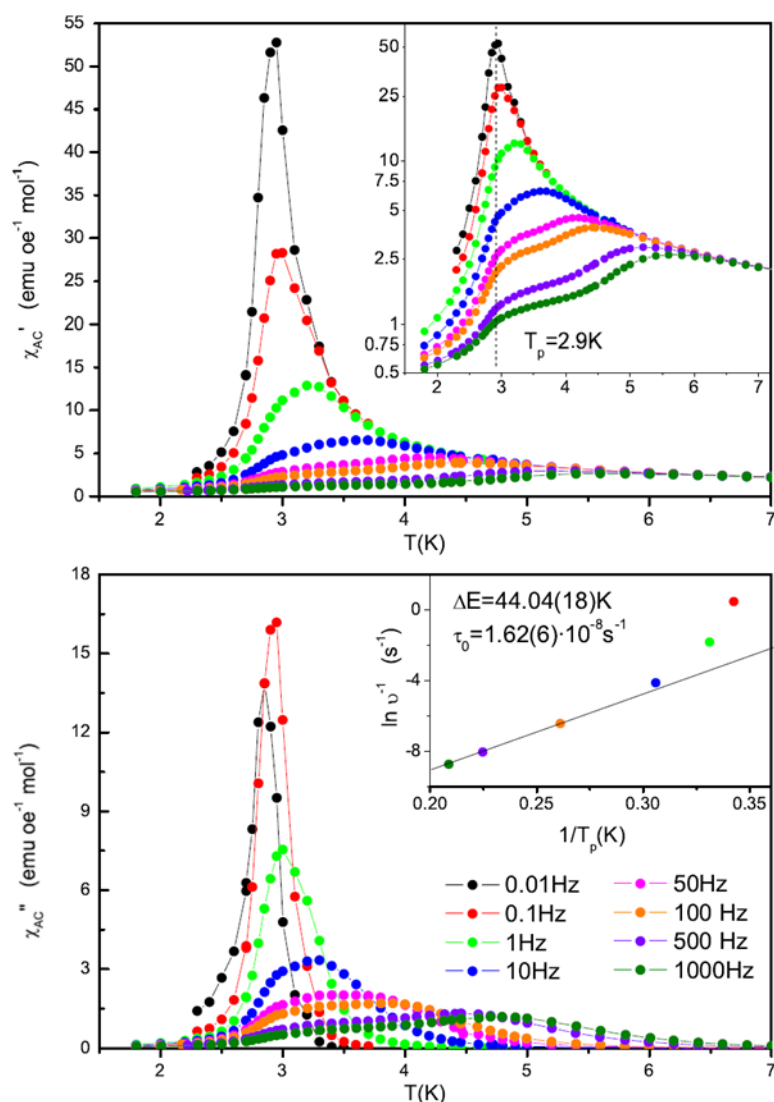


Fig. 5.11. χ_{AC} measurements at different frequencies for **7**. In the top, χ' versus T and a logarithmic inset that reflects the existence of two peaks, one frequency-dependent and one at 2.9K. At the bottom, χ'' versus T and an inset with an Arrhenius fit.

Heat capacity measurements were carried out to confirm the existence of magnetic order (Figure 5.12). A sharp peak at low temperatures indicates the existence of a magnetic order transition at 2.7K.

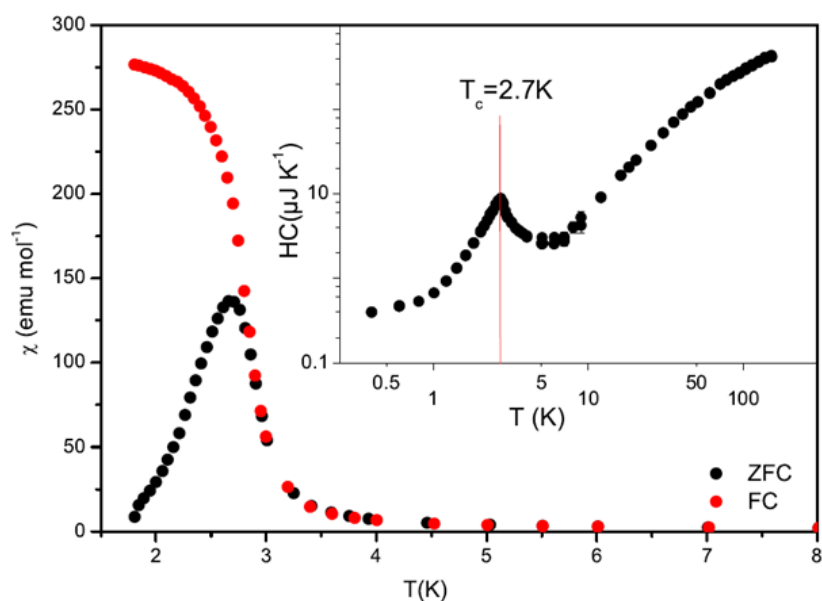


Fig. 5.12. χ_M versus T at the zero field-cooled (ZFC) and field-cooled (FC) at 500e cycles for **7**. The inset shows the heat capacity versus temperature curve. A phase transition is observed at 2.7K.

It is worth noting the peculiarities of the net arising from its diamondoid structure and the interpenetration of the polymers. Figure 5.13 shows the distances between a given cubane of a net and its congeners and Co(II) from its own net (a) and the neighbouring nets (b). It can be seen that the shortest distance is the one between a given cubane and the Co(II) directly bonded to it. The remaining distances within the same net are longer than those with neighbouring nets. The shortest distances between cubes and bridges not connected by direct bonds are between nets. Each cubane meets a cube from each of the two neighbouring nets at 10.7726(1) and 11.3290(2) Å and two Co(II) bridges (related by symmetry) per net at 8.7831(1) and 11.7064(1) Å. So the magnetic environment of a cube is not only affected by the magnetically active entities from its own net but also by those in the neighbouring ones. That means that the magnetism is not only determined by the polymeric structure; the spatial distribution of the polymer also affects its behaviour.

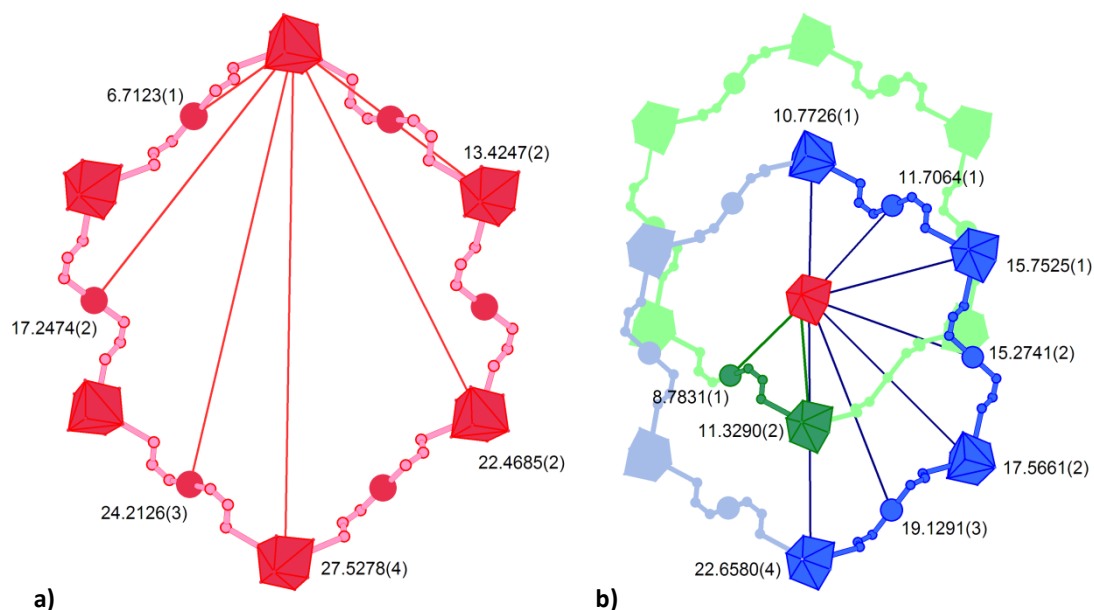


Fig. 5.13. Distances from a given cubane (from its center of gravity) to the other magnetic entities (cubanes represented as cubes and Co(II) bridges as balls) in the same net (a) and between neighbouring nets (b).

5.2. A neutral 3-D Cobalt polymer

5.2.1. Experimental

5.2.1.1. Synthesis

All reactants were commercial and were used as received. No further purification of the reagents was required.

The neutral polymer $\text{Ca}_{2n}\{[\text{Co}_4(\text{C}_6\text{H}_4\text{O}_7)_4]_{\mu_3}\text{[Co}(\text{H}_2\text{O})_3]_2\}_n \cdot 17.8n(\text{H}_2\text{O})$ **8** is obtained from a mixture of two different solutions (solutions A and B).

Solution A is obtained by addition of $\text{CoCO}_3 \cdot x\text{H}_2\text{O}$ (3.25 gr, 23.72 mmol for $x = 1$) to a stirred solution of citric acid monohydrate (25 mL, 0.47 M). The mixture was filtered and an aqueous solution of $\text{Ca}(\text{OH})_2$ (0.5 M) was added to the supernatant until a pH of 8 was reached.

Solution B is prepared by dissolving compound **1** (chapter 3) with formula $\text{C}_{24}\text{H}_{59}\text{Co}_8\text{O}_{49.5}$ in water (25 mL, 0.1 M). This solution has a pH of 6.

To obtain compound **8**, solution B was added dropwise to A (10 mL) until a pH of 7.5 was attained. The resulting fuchsia solution was kept inside a closed vial at room temperature. After several months, small rectangular fuchsia crystals of compound **8** were obtained.

5.2.1.2. Single Crystal X-Ray diffraction

Single crystal X-Ray diffraction data were collected on an Xcalibur S3 CCD-based four-circle diffractometer (Oxford Diffraction and Agilent Technologies). The program CrysAlis Pro^[P1] was used to control data collection and processing. The structure was solved *ab initio* by direct methods^[1] and refined by full-matrix least-squares analysis.^[2] Non-hydrogen atoms were refined with anisotropic displacement parameters. The methylene H atoms of the citrate ligands were placed at idealized positions and refined as riders on their respective parent C atoms with isotropic displacement parameters set to 1.2 times the equivalent isotropic U of the adjacent C atom. No further hydrogen atoms were included in the model. Diamond^[P2] was used to prepare graphical material. Table 5.2 presents data collection and structure solution and refinement details.

Table 5.2. Crystallographic data for 8			
Formula	^a C ₂₄ H _{63.6} Ca ₂ Co ₆ O _{51.8}	F (000)	1648.0
fw (g mol ⁻¹)	1614.89	Crystal size (mm ³)	0.10 x 0.08 x 0.04
Radiation	X-rays (Mo K α)	θ (min,max) (°)	4.131, 24.999
Wavelength (Å)	0.71073	Reflns collected	30077
Crystal system	triclinic	Indep reflns	9748
Space group	P-1	R(int), R(σ)	0.1039, 0.1167
temp (K)	295(1)	Completeness (θ)	0.995, (25.00)
a (Å)	12.3803(9)	Abs corr	multi-scan
b (Å)	12.5544(9)	T(min,max)	0.6937, 1.0000
c (Å)	18.4206(11)	restraints/parms	0, 793
α (°)	85.333(5)	Goodness-of-fit	1.034
β (°)	77.247(6)	R1, wR2 (obs) ^b	0.0716, 0.1913
γ (°)	90.086(6)	R1, wR2 (all)	0.1095, 0.2190
V (Å ³), Z	2782.6(3), 2	Δ/σ (max,mean)	0.006, < 0.001
ρ_{calc} (Mg/m ³)	1.927	$\Delta\rho$ range (e Å ⁻³)	0.989, -0.770
μ (mm ⁻¹)	2.058		
^a Ca _{2n} {[Co ₄ (C ₆ H ₄ O ₇) ₄] μ_3 -[Co(H ₂ O) ₃] ₂ } _n ·17.8n(H ₂ O)			
^b threshold I>2 σ (I).			

5.2.1.3. FT-IR spectroscopy

The FT-IR spectrum of compound **8** was measured on a Perkin-Elmer Spectrum 100 FT-IR Spectrophotometer with ATR accessory, in the range of 4000 - 350 cm⁻¹. (Figure 5.14).

IR (neat compound, cm⁻¹): ν (OH) 3215.62 (w); ν (C=O) 1547.86 (w); ν (C-H) 1429.87 (w) and 1384.84 (w); ν (CO) 1088.10 (t).

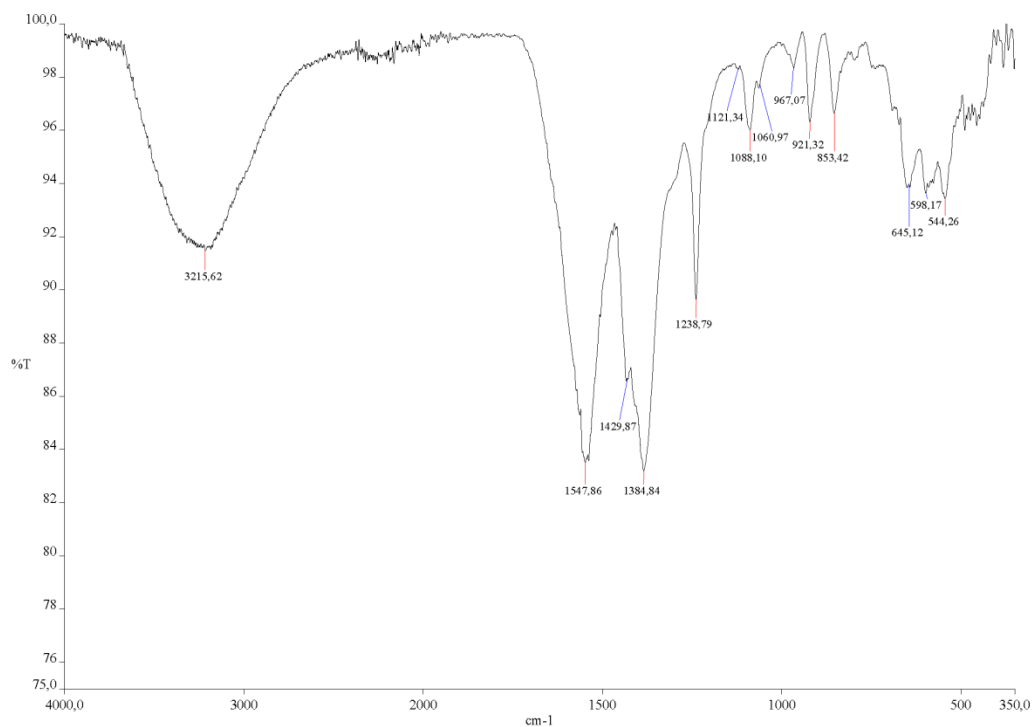


Fig. 5.14. IR spectrum for **8**

5.2.1.4. Elemental analysis

Elemental analysis was performed on a Perkin Elmer 2400 CHNS/O analyser. Calculated analysis for $(C_{24}H_{63.6}Ca_2Co_6O_{51.8})_n$: C, 17.85%; H, 3.97%. Results obtained were C, 17.85%; H, 3.97%.

5.2.2. Results and discussion

5.2.2.1. Synthesis

The neutral polymer $Ca_{2n}\{[Co_4(C_6H_4O_7)_4]_{\mu_3}-[Co(H_2O)_3]_2\}_n \cdot 17.8n(H_2O)$ **8** is obtained by mixing two different solutions to obtain a final mixture with a pH of 7.5. From those solutions separately, crystals of different cobalt citrate compounds are obtained.

Solution A is prepared by adding $CoCO_3$ to an aqueous solution of citric acid to obtain a cobalt citrate polymer^[5] with a ratio Co/citr of 1/1. The mixture obtained is filtered and then $Ca(OH)_2$ is added until a pH of 8 is attained.

Solution B is an aqueous solution of **1**, previously reported in chapter 3. This solution has a pH of 6. This compound has a formula of $C_{24}H_{59}Co_8O_{49.5}$.

Solution B is added dropwise to A until a pH of 7.5 is reached.

By itself, solution A would be expected to produce compound **5** reported in chapter 4 but with Ca^{2+} instead of Cs^+ , as the synthetic procedure is almost the same. For its part, solution B gives the complex derivative presented in the chapter 3.

On the basis of the observed reaction behaviour, we conclude that, once the cubane is formed, the number of new derivatives attainable is incalculable. Any slight modification of the reaction medium is translated into new coordination environments for the cube and, as a consequence, new products.

5.2.2.2. Single Crystal X-Ray diffraction

Compound **8** crystallizes in the triclinic system, space group P-1. There are two units of the polymer repeated per unit cell. The polymer is based on a $[\text{Co}_4(\text{citr})_4]^{8-}$ cubane core corresponding to isomer A. The cubane still has S_4 symmetry. About the isomerism of the central carbon atom of the citrate ligands, two of them are not chiral, one is S and the other is R. Per asymmetric unit there is a complete cubane unit, two $[\text{Co}(\text{H}_2\text{O})_3]^{2+}$ units which complete their coordination sphere with three carboxylate oxygen atoms. There are also two Ca^+ ions balancing the charge of the cube and 17.8 molecules of free water distributed over 22 crystallographic sites (Figure 5.15).

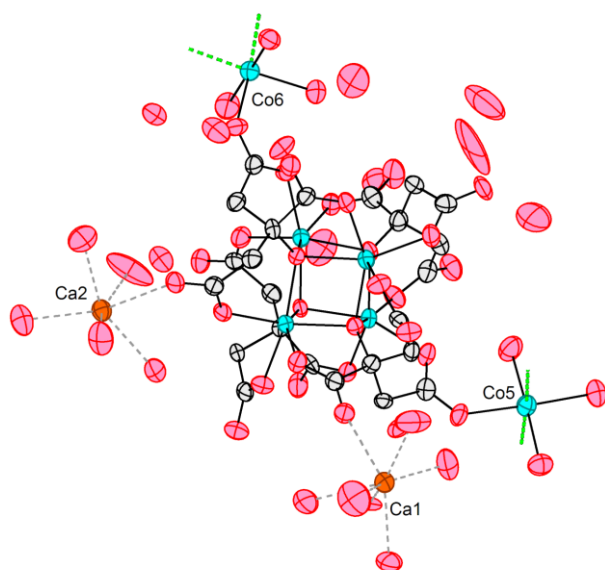


Fig. 5.15. A complete cubane unit, a Co(II) unit, counterions and free water for compound **8**. Coordination environment of the Ca^+ ions is represented as broken grey bonds. Bonds through which the polymer is propagated are represented in green. Displacement ellipsoids (probability 50%). i: (2-x, 1-y, 1-z), ii: (1-x, 1-y, 2-z).

The distribution of the Co(II) centres around the cube is not symmetrical. Co5, Co6 are attached to peripheral oxygen atoms of methylenecarboxylate groups (L2e, L7e) and act as

triple bridges, connecting three different cubane units in a *mer*- configuration. Two of these positions are mutually *trans* about the bridging Co centres (Figure 5.16). Co5 and Co6 complete their coordination spheres with three molecules of water. The Ca atoms are very close to the periphery of the cubane. Ca1 presents a coordination sphere formed by 6 molecules of water and 2 carboxylate oxygen atoms from neighbouring cubane units. The distances to the eight oxygen atoms are between 2.3879(2) – 2.5937(2) Å; the distances for the carboxylate oxygens are 2.4704(2) Å and 2.5777(3) Å. The coordination environment around Ca2 is formed by 5 molecules of water and two carboxylate oxygen atoms from different cubanes. Distances vary from 2.3376(2) Å to 2.5048(2) Å and those for the two carboxylate oxygen atoms were 2.3550(2) Å and 2.5048(2) Å.

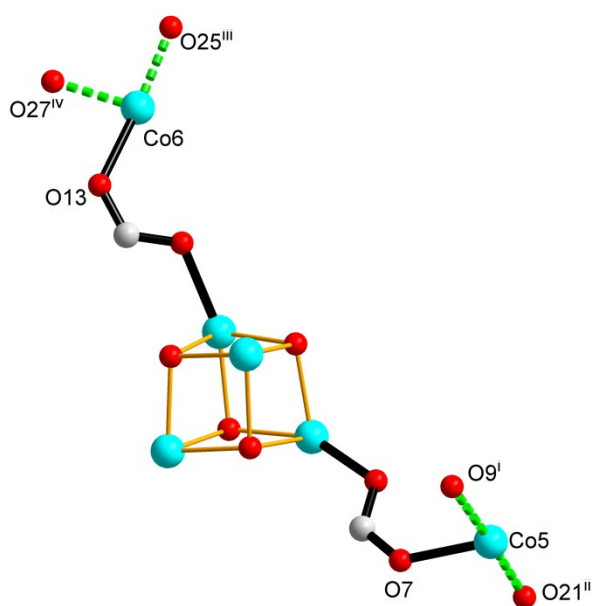


Fig. 5.16. Schematic representation of a cubane unit of **8** with two Co(II) bridges showing the propagation of the polymer (green). i: (1-x, 1-y, 2-z), ii: (2-x, 1-y, 2-z), iii: (x, 1+y, z), iv: (2-x, 2-y, 1-z).

In addition to this, there are 6.8 molecules of free water per cubane, distributed over 11 crystallographic sites. There are three pairs of water sites that cannot coexist at the same time. They are O19w with O20w, O22w with O25w and O24w with O26w. The refinement of their occupancies was carried out maintaining the thermal parameters within reason. No impossible contacts are present in the final model; those water molecules that cannot coexist are not present at the same time.

The propagation of the polymer is not as symmetrical as in compound **7**, so that its description is more complex. There are two molecules per unit cell. The shortest way to

connect those individual molecules is through a cubane of a neighbouring cell. This path involves two carboxylate groups and two opposite oxygen atoms in a cube and goes through Co5 and Co6 (Figure 5.17). Each cubane is directly connected to 8 neighbouring units. However, not every pathway between cubanes is linear; some of them describe circular patterns, ending at the starting point passing through several adjacent units. The whole structure can be seen as composed of layers connected by covalent bonds. The packing pattern of the layers is approximately ABAB perpendicular to the *c*-axis (Figure 5.18). Ca^+ ions and free molecules of water lie within the spaces left by the polymeric net, which form channels through the structure.

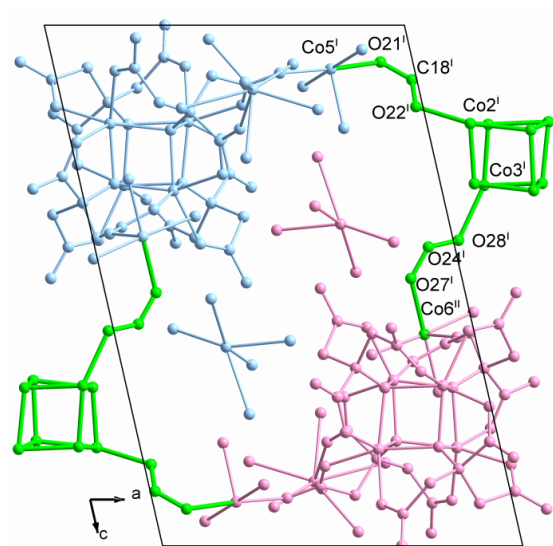


Fig. 5.17. Two molecules of **8** per unit cell showing the shortest connection of two independent molecules per asymmetric unit through neighbouring cubane units i: $(2-x, 1-y, 1-z)$, ii: $(x, -1+y, z)$.

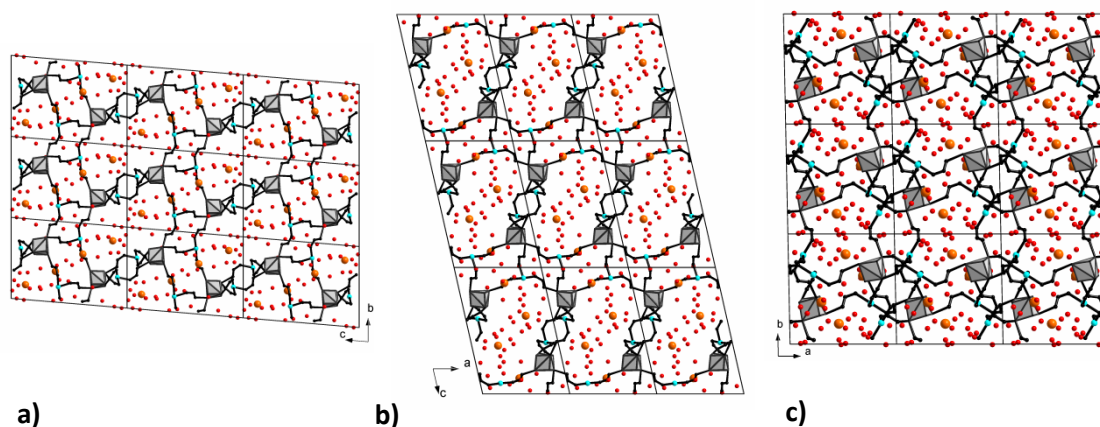


Fig. 5.18. Schematic representation of the polymeric net of **8** including counterions (orange) and free molecules of water (red) occupying the channels through the structure. Views along the *a*-axis (a), *b*-axis (b) and *c*-axis (c).

The Kitaigorodskii packing index^[B1] (K.P.I.) has been calculated using Platon^[4]. For the purpose of this calculation the structural model was modified to represent one plausible component of local content, rather than the disordered average structure derived from the least-squares refinement. That is, (using IUCr terminology) for each disorder assembly one disorder group was selected and given full occupancy. The K.P.I. value for this structure is 69.9. It is generally accepted that if the K.P.I. value of a structure is about 65-70% there are no significant voids or channels. However, since the space between the polymeric nets contains nothing but free water molecules, the K.P.I. value for the completely dehydrated derivative has also been calculated. The resulting value is 51.7%. Thus, once the unligated molecules of water have been removed, there will be a significant amount of free space inside the structure. Furthermore, if the Ca⁺ ions are also removed from the calculation, the K.P.I. value is 48.7%. This amount of free space will never be completely available; however, the calculation gives a good estimation of the space that other counterions and solvent molecules could in principle occupy in this compound.

Compound **8** is isostructural with the first 3-D cubane-based compound reported by Murrie *et al.*^[6] with cationic substitution (PUWYAI as its Refcode in the CCDS). Table 5.3 shows the unit cells for the two compounds. There is a clear relationship between the cells; nevertheless, a transformation is needed in order to have the same setting for the purposes of comparison. The unit cell of PUWYAI after its transformation by the following matrix

$$\begin{bmatrix} 0 & -1 & 0 \\ -1 & 0 & 0 \\ 0 & 0 & -1 \end{bmatrix}$$

results in a similar cell and setting as those for compound **8** (Table 5.3 shows the PUWYAI before and after transformation). The transformed structure was very similar to that of **8**, with complete concordance except for the counterions. No calcium atom position in **8** matches the location of sodium in PUWYAI, and the water positions O8w, O25w and O26w are not present in PUWYAI. Figure 5.19 shows the superposition of the two structures.

Table 5.3. Comparison of the unit cell of PUWYAI, compound **8** and PUWYAI after transformation.

	PUWYAI	Compound 8	PUWYAI after transformation
a	12.260(5)	12.3803(9)	12.366(6)
b	12.366(6)	12.5544(9)	12.260(5)
c	19.101(9)	18.4206(11)	19.101(9)
α	78.180(16)	85.333(5)	84.625(16)
β	84.625(16)	77.247(6)	78.180(16)
γ	89.511(17)	90.086(6)	89.511(17)
Vol.	2822(2)	2782.7(4)	2821(2)

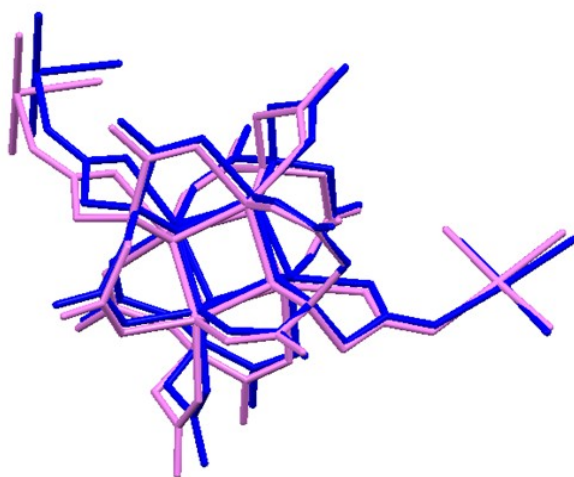


Fig. 5.19. Superposition of compound **8** (dark blue) and PUWYAI (violet). Only the cubane and the Co(II) units have been represented.

5.3. Conclusions

In this chapter two new derivatives of the cubane-based compounds are presented. Both have 3-D polymeric structures. The first is a highly symmetrical polymer with a diamondoid topology. The second presents an irregular structure formed by the crosslinking of layers. This chapter serves as an example of the versatility of the cubanes as building blocks for the preparation of new derivatives. They combine high stability with reactive behaviour. It is also worth mention that there is only one prior example in the literature reporting a 3-D Co-citrate polymer.

Commonly, interpenetration of polymeric nets is a stabilization mechanism for the compounds in the solid state. It usually entails the reduction of the free space between the polymer nets. Interpenetration and porosity might thus be expected to be mutually exclusive.

However, in some situations it is possible to integrate the two in a single solid as that is the case for compound **7**. In the solid state, it is formed by the interpenetration of equivalent 3-D nets, but there is also a significant amount of space occupied by counterions and molecules of water, possibly accessible to other ions and solvent molecules through interchange processes.

Magnetic measurements for **7** show that there is a significant interaction of the magnetic entities. This is the first case in which there is clear evidence of the coexistence of a magnetic blocking process and a magnetic phase transition. This has been attributed to the interpenetration of the nets, which positions the cubanes of one net closer to others in neighbouring nets. From a magnetic point of view, the closer the magnetic entities are, the stronger is the observed interaction. This is contrary to the goal when a porous material is wanted. In that case, a larger separation between the nodes of the nets is desired. Compound **7** is an example in which porosity is combined with stronger interaction of the magnetic entities due to closer contacts of the magnetic centres in distinct polymers.

The high stability of the water molecules of compound **7** is also interesting. The compound remains intact when it is heated, until approximately 80 - 90 °C. Then a dehydration process takes place with the corresponding loss of crystallinity. The reversibility of this process has been proved, as the diffraction pattern is almost completely restored after exposure of the sample to a humid atmosphere for a week at room temperature.

Finally, compound **8** is the first case where an alkaline earth metal acts as the counterion for a citrate cubane polymer. To date, there are only examples with alkali metals or with complex counterions such as $[M(H_2O)_6]^{2+}$, guanidinium or tetramethyl ammonium. The structure of **8** is isomorphous with the first reported 3-D cobalt citrate cubane polymer, which was a sodium salt. Magnetic measurements have not been done yet because of sample requirements. However, as the magnetism is provided by the polymeric net, the magnetic behaviour of **8** is expected to be analogous to that reported for PUWYAI. No significant modifications of the magnetic response of the compound due to the isomorphous substitution of Na^+ for Ca^{2+} are predicted.

Some additional experiments should be carried out in order to study the ability of these compounds to undergo solvent and ion exchange reactions.

References

- [1] A. Altomare, G. Cascarano, C. Giacovazzo, A. Guagliardi, *Journal of Applied Crystallography* **1993**, *26*, 343-350.
- [2] G. M. Sheldrick, *Acta Crystallographica Section A* **2008**, *64*, 112-122.
- [3] C. F. Macrae, I. J. Bruno, J. A. Chisholm, P. R. Edgington, P. McCabe, E. Pidcock, L. Rodriguez-Monge, R. Taylor, J. van de Streek, P. A. Wood, *Journal of Applied Crystallography* **2008**, *41*, 466-470.
- [4] A. L. Spek, *Acta Crystallographica Section D-Biological Crystallography* **2009**, *65*, 148-155.
- [5] Z. H. Zhou, Y. F. Deng, H. L. Wan, *Crystal Growth & Design* **2005**, *5*, 1109-1117.
- [6] K. W. Galloway, M. Schmidtman, J. Sanchez-Benitez, K. V. Kamenev, W. Wernsdorfer, M. Murrie, *Dalton Transactions* **2010**, *39*, 4727-4729.
- [B1] A.I. Kitaigorodskii, *Molecular Crystals and Molecules*, Academic Press, New York, 1973.
- [B2] International Tables for Crystallography, Vol. A: Space-group Symmetry, 5th Edition. (Ed: Th. Hahn), Springer, Dordrecht, The Netherlands 2005.
- [B5] Sáenz de Pipaón Soba, Cristina. Contributions to Molecular Magnetism: Chiral Magnets and Networked SMMs. [on line]. Universidad de Zaragoza, 2013. <<http://http://zaguan.unizar.es/record/10403>>
- [P1] CrysAlisPro, Oxford Diffraction Ltd., Version 1.171.33.31
- [P2] Diamond. Klaus Brandenburg, Crystal Impact GbR, Bonn, Germany. Version 3.2i.
- [P3] Quantum Desing. <http://www.qdusa.com>

Part III

Manganese citrate cubanes

6

Introduction III: Manganese citrate cubanes

A family of compounds based on manganese citrate cubanes is presented in this part of the thesis. Their dimensionalities range from 0-D to 2-D. In this case, the cubane unit corresponds to isomer B for all of the compounds.

The classification of the compounds presented is based not only on the composition of the compounds but also on the different properties observed. While cobalt-containing derivatives behave as single molecule magnets, presenting interesting magnetic features, the compounds described throughout this part, all based on manganese, are of little interest from a magnetic point of view. Many examples of Mn clusters have been proved to behave as single molecule magnets; this is because of the magnetic anisotropy of the cluster where the major contribution arises from the single-ion anisotropy of Mn(III) ions. In the compounds reported in this thesis, the manganese atoms have an oxidation state of +2. As d^5 ions are isotropic, no anisotropy is expected for a cluster formed exclusively by Mn(II) ions; and as a consequence they do not show slow magnetic relaxation. That does not mean that samples based on manganese citrate cubanes will not be magnetically active, as a Mn(II) ion has $S_i = 1/2$ in low-spin complexes and $S_i = 5/2$ for the high-spin case. Magnetic measurements carried out with one of the Mn-based samples showed that the compound behaves as a conventional paramagnet.

Despite the fact that Mn derivatives do not present interesting magnetic responses, other properties and reactivity have been observed. It is worth noting that contrary to what was observed for the Co-containing compounds reported in the previous part of the thesis, the Mn compounds do not contain ions of elements other than Mn balancing the charge of the cubane unit; hexa-aquo manganese complexes will be seen to act as counterions in all cases.

The first chapter of this section is devoted to a discrete compound with formula $[\text{Mn}_8(\text{C}_6\text{H}_4\text{O}_7)_4(\text{H}_2\text{O})_{18}]\cdot(\text{H}_2\text{O})$, **9**. For the many TM-citrate compounds found in the scientific

literature, it has been observed that discrete molecular moieties are anionic while polymeric compounds are neutral. The compound reported in Chapter 7 is to our knowledge the first example of a discrete neutral compound based on Mn-citrate cubanes. In addition, it undergoes a reversible dehydration-rehydration process under mild conditions in the absence of pores in its structure. This transformation has been characterised by powder X-Ray diffraction.

In the second chapter of this section, Chapter 9, an anionic 1-D polymer is presented (**10**). This undergoes a reversible single crystal to single crystal transformation (SC-SC) -- partial dehydration -- under ambient conditions, which was studied by single crystal X-Ray diffraction. As the compound was not porous, the sample was rehydrated using D₂O instead of H₂O and neutron diffraction experiments were carried out, in an attempt to elucidate the mechanism of the transformation. The unexpected results revealed the working of an interesting mechanism operating within this non-porous molecular crystal when it is exposed to a humid atmosphere for rehydration.

Finally, the third chapter of this section describes an anionic 2-D polymer, **13**, which presents a structure nearly identical to that of the 1-D polymer mentioned above. In this compound the polymeric 1-D chains of **10** have been crosslinked by molecules of ethylene glycol, giving 2-D layers in compound **13**. This result demonstrates the reactivity and versatility of the citrate cubane as a building block for the preparation of an ample variety of related compounds.

In what follows, some concepts that will be helpful in understanding the subsequent chapters will be presented. These concepts are related to the reactivity of the samples to be described. There are two distinct sections, one devoted to solid-state reactivity and the other about the so-called Grotthüss Mechanism.

As our Mn-citrate derivatives undergo reversible single-crystal to single-crystal transformations (SCSC), a general view of solid-state reactivity is presented, with special attention to those processes that occur in the crystalline state.

Then, in the second section, some concepts related to the proton transport mechanisms operating in confined spaces as well as a brief review of the most important features and examples will be presented.

6.1 Solid-state reactivity^[3] ^[4]

For chemists, one of the most important properties of molecules is their reactivity. Molecules can react in any of the different aggregation states of matter. Liquid-phase reactions are widely known and used, while those taking place in the solid state have been less widely explored. The main difference between the two is that in the solid state the relative disposition of the reactive groups is fixed, and the molecules cannot move freely as in solution. Thus, the reactivity of a sample depends not only on its constituent molecules but also on their periodic assemblies. An external stimulus is required for a solid state reaction to take place; in general, these need to be activated by light, heat or any other mean. The restricted motion of the molecules in a solid-state reaction offers a degree of stereocontrol over the final products, enabling the preparation of derivatives that cannot be prepared by processes in solution. However, in many cases a prediction of the nature of the final product is still uncertain as the activation of the reagent involves the breaking and formation of weak interactions (van der Waals interactions, hydrogen bonds, etc.) and covalent bonds.

These reactions present some attractive advantages with respect to conventional chemistry. From the point of view of green chemistry, since they are solvent-free processes, problems related to the storage and disposal of solvents are avoided. In addition, the obtainment of solvated subproducts is also obviated. As mentioned above, there are some products that cannot be prepared by other reactions and others that would be entirely unexpected in a liquid-phase reaction.^[4] ^[5] ^[6] ^[7] It has been observed that many solid-to-solid reactions give near-quantitative yields of only one product in a reasonable amount of time. Finally, in many cases these reactions require only simple equipment: a UV lamp for photochemically activated reactions, a mortar and pestle for mechanochemical processes or a heat source such an oven or an IR lamp for thermal activations.^[3]

Solid-state reactions are those that occur between or within solid reactants. The initial and final products can be amorphous, microcrystalline or single crystals. In some cases, intermediate liquid phases can be formed, such as eutectic phases or a melt. There is some controversy in such cases, which cannot be considered as direct solid-to-solid processes. The same occurs when the complete destruction of the crystal structure is needed before reaction, for example by grinding the starting powder, as such mechanical activation may provoke the local melting of the interphase of the solids involved in the reaction. Reactions where a minimal quantity

of solvent is used can be considered solvent-free reactions but not solid-to-solid processes.

The techniques employed in the elucidation of the composition and structure of the final products must necessarily be solid-state techniques. Some of the most commonly used are solid-state NMR, differential scanning calorimetry (DSC), thermogravimetric analysis (TGA), infrared spectroscopy (IR), X-Ray powder diffraction (XRD) and single crystal diffraction (XSCD).

It is desirable to isolate single crystals of the final product so that a complete description of the three-dimensional structure can be obtained by diffraction analysis. The structural detail revealed by this means can provide important clues about the mechanism of the reaction. However, this is quite uncommon and the products are usually amorphous solids or microcrystalline powders. An alternative option is to grow single crystals of such compounds separately by other techniques (*i.e.*, by another reaction that preserves the crystallinity of the starting sample or by recrystallization of the products using appropriate solvents and methods). A comparison of the powder diffractograms of both samples -- the product of the solid-state transformation and the sample prepared by other means -- can be used to confirm the nature of the former (Figure 6.1). In some cases, "*ab initio*" refinement of the X-Ray powder diffraction data can succeed in the resolution of the structure of a product. Recent advances have enabled *in-situ* studies of these processes. Although quite complicated, these experiments are of great utility in determining the mechanisms that operate in solid-state transformations. Not only do the results serve to explain a specific process, but the accumulated knowledge of such processes is an aid in predicting the results of other reactions.

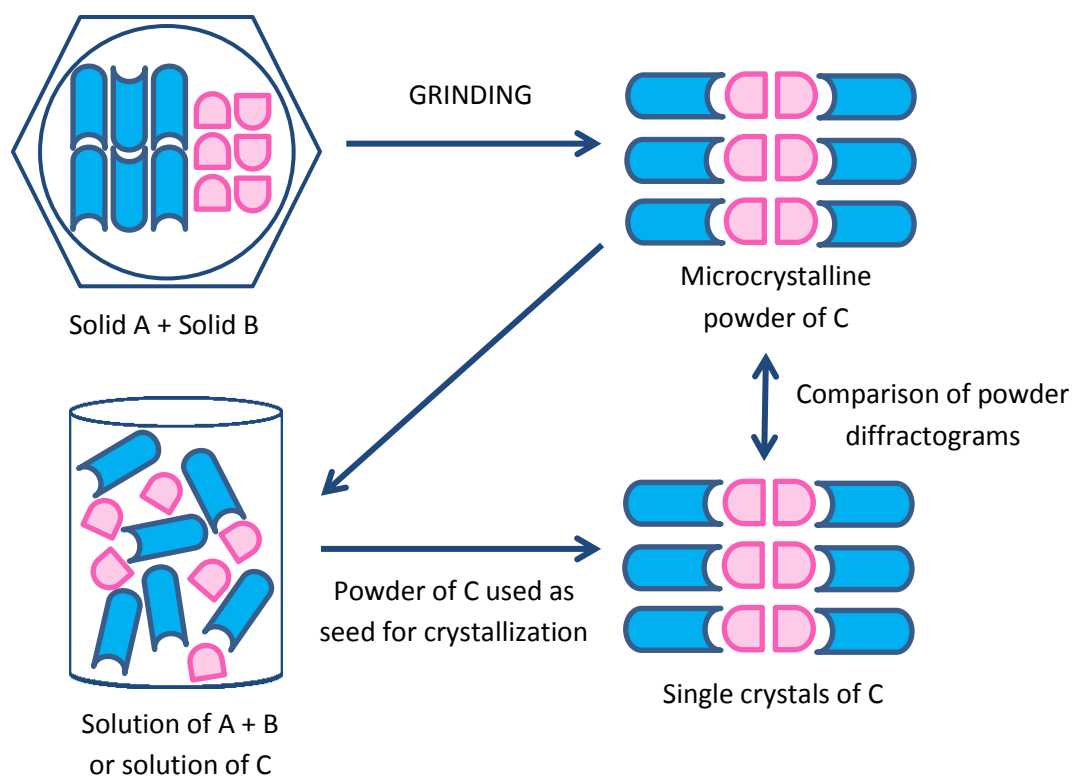


Fig. 6.1. Schematic representation of a plausible method for elucidating the structure of a final product after a solid-to-solid reaction, when the product is obtained as a microcrystalline powder instead of as single crystals. Adapted from Braga *et al.* 2004^[3]

6.1.1. Types of solid state reactions

Gas-solid reactions: These represent the first examples of solvent free reactions, first reported in 1884 by Pellizzari and studied in depth by Paul and Curtin in the 1970's.^[8] Most of the currently known examples are related to the study of physi- and chemi- sorption of gases by a solid matrix or to host-guest processes. Metal Organic Frameworks (MOFs) and Porous Coordination Polymers (PCPs) present interesting properties in selective gas sorption and storage and in catalysis. Some other examples of complex gas-solid reactions are shown in Table 6.1 (adapted from Ramachandran *et al.* 1982^[9]).

Intersolid reactions: These are reactions that involve molecules of different crystalline samples. In most cases the synthetic procedure is quite simple. Just by putting the reagents together in a recipient and by applying the appropriate external stimulus (*i.e.*, grinding the mixture or irradiating it with UV light), the final product is obtained. It has been proved that in some cases, the supramolecular assembly of the reagents is faster under solvent free conditions than in solution; 2- and 3-dimensional compounds as well as double helicates have been obtained in the solid state with a significant reduction of the reaction time.^[23] For example, the reaction between [(ethylenediamine)Pt(NO₃)₂] and 4,4'-

bipyridine lasts more than 4 weeks at 100 °C in solution, while the same product is obtained from reaction of the solid components in 10 minutes.

The potential of these reactions is shown using some examples.

- Preparation of inclusion compounds. These are characteristic of host-guest chemistry. The “host” compound forms a matrix in whose cavities the molecules of the “guest” compound are located. The definition found in the IUPAC Gold book for “inclusion compound (inclusion complex)” is: “A complex in which one component (the host) forms a cavity or, in the case of a crystal, a crystal lattice containing spaces in the shape of long tunnels or channels in which molecular entities of a second chemical species (the guest) are located. There is no covalent bonding between guest and host, the attraction being generally due to van der Waals forces. If the spaces in the host lattice are enclosed on all sides so that the guest species is 'trapped' as in a cage, such compounds are known as clathrates or 'cage compounds'.”^[P7]

Inclusion compounds are readily obtained from solution or from a melt. However, Nakai *et al.* has obtained clathrates of tri-O-methyl- β -cyclodextrin (TMCD) and benzoic acid (BA) by two solid state procedures. One of them consists of heating a physical mixture of the two components at 84 °C, while the other involves grinding at room temperature. In both cases the inclusion compound was obtained. The effects of grinding the starting materials are to increase the reaction surface and amorphize the material by the applied mechanical energy.^{[24] [25]}

- Reaction between molecular crystals. An interesting example is the charge-transfer complex obtained by mixing tetrathiafulvalene and tetracyanoquinodimethane. The compound, commonly synthesized by conventional crystallization from solution, has been obtained by grinding the corresponding powders together. The compound thus obtained shows similar electrical conductivity to that obtained by conventional means. The fact that the donor and acceptor molecules form the charge-transfer stack suggests that they can move freely in the solid state.^{[26] [27]} (Figure 6.2.)

Table 6.1. Examples of complex gas-solid reactions (Adapted from Ramachandran *et al.* 1982^[9])

Reaction	Scheme	Example	Reference
Consecutive reaction of the solid	$B + A \rightarrow G_1 + A \rightarrow G_2$	Reduction of Haematite Reduction of Manganese Oxide	Spitzer 1966 ^[10] De Bruijin 1980 ^[9]
Consecutive reaction of the gas	$A_1 + B \rightarrow P + B \rightarrow G_2$	Reaction of Iron Sulfide with Oxygen	Tseng 1980 ^[11]
Reaction of 2 gases with the same solid	$A_1 + B \rightarrow \text{Products}$ $A_2 + B \rightarrow \text{Products}$	Reduction of Iron Ore with a Mixture of CO and H ₂ Reaction of UO ₂ F ₂ with a mixture of F ₂ and BrF ₅	Tsay 1976 ^[12] Anastasi 1971 ^[13]
Reaction of 2 solids with the same gas	$A + B_1 \rightarrow \text{Products}$ $A + B_2 \rightarrow \text{Products}$	Chlorination of Ilmenite Regeneration of Coked Catalyst Sulfation of Dolomite Reduction of a Mixture of Nickel Oxide and Iron Oxide	Doraiswamy 1959 ^[14] Ramachandran 1975 ^[15] Hartnan 1976 ^[16] Szekely 1976 ^[17]
Gaseous product of first reaction reacting with a second solid	$A_1 + B_1 \rightarrow G + P$ $P + A_2 \rightarrow \text{Products}$	Reduction of cobalt sulfide in presence of CaO Oxidation of metal sulfide in presence of CaO	Fahim 1978 ^[18] Bartlett 1973 ^[19]
Solid product of first reaction with a second gas	$A_1 + B \rightarrow G + P$ $G + A_2 + \nu_{A1}A_1 \rightarrow \text{Products}$	Simultaneous oxidation and sulfation of cuprous oxide Direct removal of H ₂ S(A ₂) from hot synthesis gas (A ₁ = CO; A ₂ = H ₂ S, B = Fe ₂ O ₃ ; G = Fe)	Bourgeois 1974 ^[20] Tamhankar 1981 ^[21]
Homogeneous heterogeneous reactions	$A_g + B_s \rightarrow G + P$ $B(s) \rightarrow B(g)$ $A_g + B_g \rightarrow G + P$	Reduction of metal chlorides with hydrogen	Rao 1981 ^[22]

A = species A or concentration of A at position y; A₁, A₂ = gaseous reactant species; A_g = concentration of A in the bulk gas; B = concentration of B at position y; B₁, B₂ = reactants present in the solid; G = product solid formed in the reaction; P = product gas species; n = stoichiometric coefficient for the species indicated in the subscript.

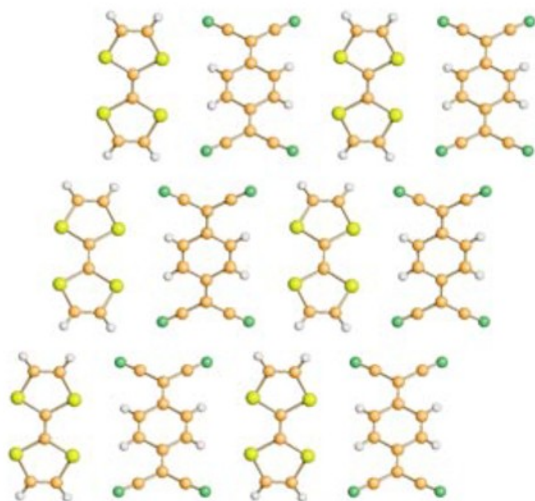


Fig. 6.2. Crystal packing of the charge-transfer compound formed by tetrathiafulvalene and tetracyanoquinodimethane. Colour code: C, orange; N, green; S, yellow; H, grey. Reproduced from Braga *et al.*

- Formation of covalent bonds: *cis*-Diammine dichloroplatinum (II) ($\text{Pt}(\text{NH}_3)_2(\text{Cl})_2$), commonly known as *cis*-platinum or cisplatin is widely known due to its anti-carcinogenic properties. Many different derivatives have been synthesized since its effectiveness in the inhibition of cell division in *Escherichia Coli* was observed in 1969.^[28] Recently, Balema has succeeded in the preparation of some different *cis*-platinum derivatives in the solid state. *Cis*- $[(\text{PPh}_3)_2\text{PtCl}_2]$ is obtained with a 98% yield simply by grinding PtCl_2 and Ph_3P in a ball-mill.^[29]

Another example of the formation of covalent bonds is the reactivity of fullerenes (C_{60}) in the solid state. They present low solubility in solvents, which is a handicap in the preparation of related compounds. It has been demonstrated that fullerenes can react in the solid state to give, in some cases, compounds different from those obtained from solution. For instance, when C_{60} reacts with KCN in solution, a simple cyanation takes place, while when the reaction is conducted in the solid state, the [2+2] dumbbell-shaped dimer C_{120} is obtained.^{[30] [31]}

Intrasolid reactions: reactions that involve molecules within a crystal. Most of the examples of this type of reaction are topotactic. So this section is focused on topochemical reactions.^{[32] [4]}

According to the IUPAC Gold book,^[P7] a topotactic or topochemical reaction is “A reversible or irreversible reaction that involves the introduction of a guest species into a host structure and that results in significant structural modifications to the host, for

example, the breakage of bonds.” In terms of crystallography, they can be seen as reactions in which the starting material is a crystalline solid in which the reactive groups are almost at bonding distances from each other within the lattice. By an external stimulus, commonly light or heat, the rupture and formation of bonds involving these groups occur.

As the position of the reactive groups of the molecules is fixed in the crystal lattice, the organization of the reactants determines the stereochemistry of the resulting products. That makes these reactions highly selective, allowing the preparation of compounds that cannot be obtained by any other means. Recent investigations in this area have made possible the preparation of solids with the appropriate spatial distribution of the reactive groups for obtaining specific target products.^[6]

These reactions have typically been regarded in terms of minimal movement of the atoms in the crystal. In 1918, Kohlschutter enunciated the “Topochemical Postulate,” which states that reactions in crystals proceed with a minimum of atomic and molecular movement.^[33] This postulate was subsequently supported by the studies of Schmidt and co-workers in the early 1960’s on photodimerization of cinnamic acids.^{[34] [35] [36]}

Kohlschutter proposed that due to the restrictive conditions under which the reaction takes place, the nature and properties of the final products are dominated by the three-dimensional periodic environment of the crystal. The basis of topochemical control of uni- and bi- molecular reactions is the following (Reproduced from Schmidt 1964^[37])

- The intrinsic reactivity of a molecule is less important than the nature of the packing of neighbouring molecules around the reactant.
- The separation distance, mutual orientation, and space symmetry of reactive functional groups are crucial.
- In crystalline solids there are very few (usually just one) conformations taken up by molecules which, in the dispersed state, are very flexible.
- Molecular crystals (into which category the vast majority of organic solids fall) display a rich diversity of polymorphic forms, in each of which a particular conformer or particular symmetry and separation of functional groups prevails.

According to this postulate, it is possible to predict whether a solid-state reaction will take place. The crystal lattice will determine the reactivity of the sample and the molecular structure of the final products. One of the corollaries of this postulate is

that the process will take place among neighbouring groups of molecules in the crystal. There are some empirical rules to predict topochemical reactions. Schmidt observed that for a [2 + 2] photoreaction, the double bonds of the reagents should be parallel to each other and separated by a distance smaller than 4.2 Å, in such a way that the p(z) orbitals of the double bonds are collinear and overlapped enough for the reaction to take place.^[B6]

Although this postulate provides useful geometric criteria for the prediction of topochemical reactions, it does not take into account the molecular movement when the shape of the final product is different from that of the starting material.

It was clear that some modifications of the postulate as well as the introduction of new concepts were needed to explain many reactions that violate, in principle, the rules. The postulate does not consider two important points regarding the course of a topochemical reaction. First of all, the influence of the neighbouring atoms and molecules is omitted. Their role is downgraded to that of simple spectators. Secondly, the effects of the molecular excitation on the crystal are not considered.

Craig and co-workers studied the effects of the electronic excitation in topochemical reactions. They introduced a model to describe the effects on the lattice when a crystal absorbs a photon. They proposed that the initial unstable lattice can relax via two mechanisms, one giving a new symmetric equilibrium and the other a metastable intermediate which could be the precursor of the photochemical reaction. This “dynamic preformation” helps in the understanding of the mechanisms of many photoreactions.^{[38] [39] [40] [41]}

Cohen emphasised the importance of the neighbouring molecules, introducing the term “reaction cavity,” which was used to explain the geometries of excimers of polyaromatics.^{[42] [43]} It considers that the atoms or molecules involved in the reaction occupy a space with a concrete shape and size. Such a cavity is surrounded by other molecules in the lattice. The atomic movements that take place during the reaction will cause pressure on the walls of the cavity, which may tend to become distorted. There would be a decrease of the attractive forces and/or increase of the repulsive forces. As the reaction takes place in the solid state, the distortion of the cavity is restrained by the packing of the crystal lattice. Only those processes that involve minimum changes in the external contacts of the cavity will be energetically favoured. Figure 6.3 shows a schematic representation of the concept “reaction cavity” in terms

of the activation energy for the different intermediates. For a case in which more than one product can be obtained, only the process with the lowest-energy transition states will be energetically and geometrically favoured by the crystal lattice.

The postulate can thus be re-stated as “reactions proceeding under lattice control do so with minimal change or distortion of the surface of the reaction cavity.”

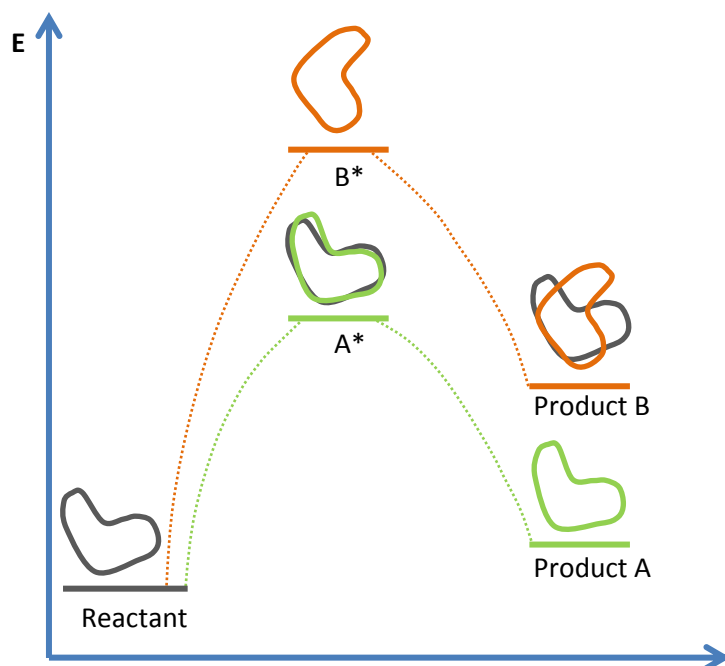


Fig. 6.3. Representation of the “reaction cavity” concept in terms of relative energies of the transition states (A^* and B^*) which lead to the final products. The mechanism which involves the least perturbation by the reaction cavity on its crystalline surroundings (A^* in this case) will be favoured by the neighbouring molecules in the crystal lattice.

In what follows, some examples of topochemical reactions are given, showing the versatility of the processes that can take place in the solid state.

- a. [2+2] Photocycloaddition: These reactions are among the most studied in the solid state. They allow the preparation of cyclobutane, a substance quite complicated to obtain by other methods. In addition, the process in the solid state is more efficient and selective than in solution. Pioneering studies by Schmidt in the 1960's and 1970's were focused on the [2 + 2] photocycloaddition of cinnamic acids. Only light irradiation is needed to provoke the reaction. An example of the mechanism of these cycloadditions is shown in Figure 6.4. As mentioned previously, the double

bonds have to be arranged in such a way that the p(z) orbitals are collinear and overlapped to interact when irradiated.^{[35] [36]}

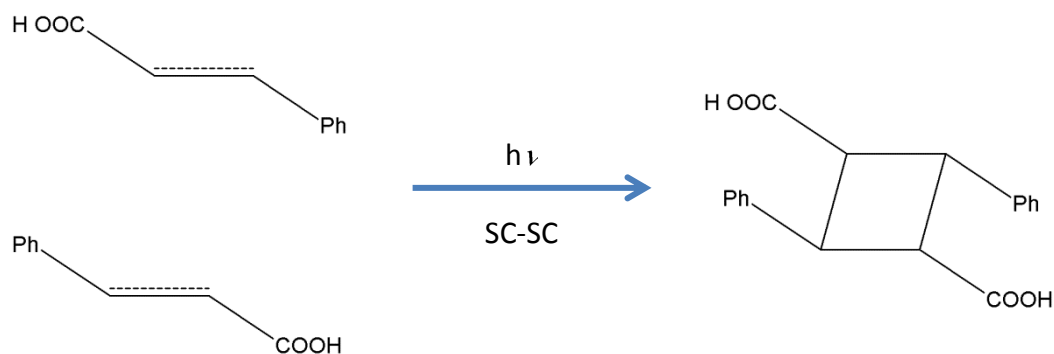


Fig. 6.4. [2 + 2] photocycloaddition of α -cinnamic acid.

- b. Polymerizations: One of the most significant examples of this type of reaction is the 1-4 polymerization of diacetylene.^[44] In some cases, the only feasible method of preparing these compounds is a thermal- or photo-activated solid-to-solid reaction. However, it only takes place if the arrangement of the monomers in the solid state is appropriate for the polymerization to take place; that is, the dispositions and distances of the reactive groups should be correct. Although polydienes can be found in nature, polymers of small conjugated diacetylenes, trienes and triacetylenes are still unknown or are simple laboratory curiosities. Lauher and co-workers have developed a strategy to establish the necessary structural parameters for a series of diacetylene monomers to undergo the expected polymerizations.^{[45] [1]} The host-guest method consists of a previous determination of the structural parameters and distances needed for the formation of the desired polymer. A host molecule that can impose the correct distance and molecular arrangement is chosen. Then a monomeric structure is built up around the host molecules and the final solid is irradiated or heated to provoke the polymerization. An example of molecules that self-assemble in a predictable way is the oxalamide prepared from glycine (Figure 6.5). In the solid the molecules form a 2-D packing arrangement mediated by H-bonds, consisting of an α -network of amide H-bonds with a characteristic distance of 5 Å between neighbouring chains (vertical in Figure 6.5), and a second α -network of dicarboxylic acids (horizontal in Figure 6.5). The key point is that when using longer-chain ω -amino acids, the distance of 5 Å between chains remains intact; changes are only observed along the horizontal directions (referred to the orientation of the

molecule in Figure 6.5). That allows the corresponding polymerization to take place.

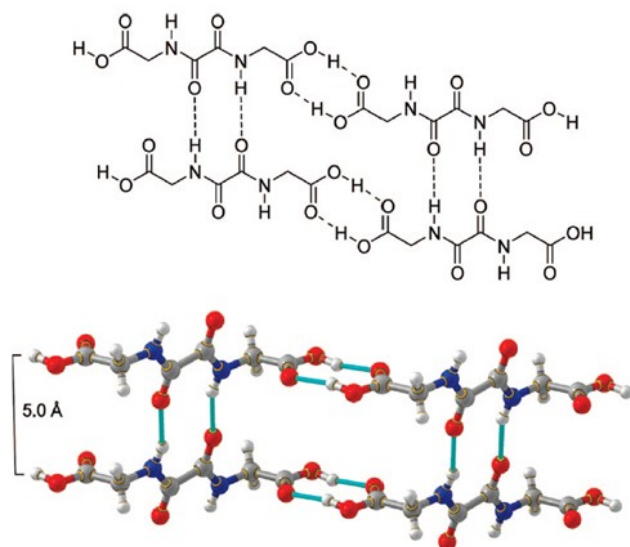


Fig. 6.5. Schematic representation and crystal structure of the oxalimide of glycine, showing the 2-D H-bonded packing. Image Reproduced from Lauher *et al.* 2008^[45]

- c. **Polymorphism:** This phenomenon is observed when a solid material can present more than one crystal structure. Many examples of interconversion between two polymorphs through single-crystal to single-crystal transformations have been observed. One of them involves lead monoxide. It can crystallise in two different forms. One gives yellow orthorhombic crystals at high temperature whose structure is formed by corrugated Pb-O-Pb-O chains running along [100] but in antiparallel directions in neighbouring (010) planes. The second form exists at low temperature and consists of red tetragonal crystals formed by zig-zag Pb-O-Pb-O chains in the (100) and (010) planes (Figure 6.6).

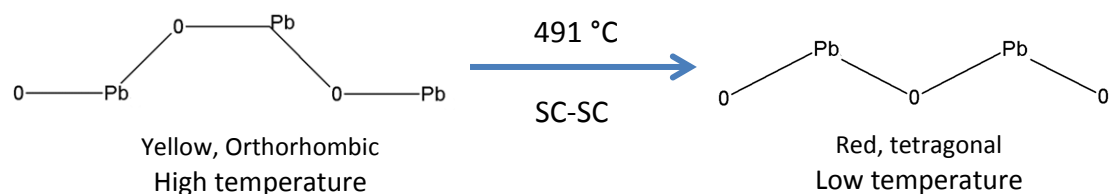


Fig. 6.6. Polymorphic transformation of PbO at 491 °C through a spontaneous SC-SC transformation.

Both present layered structures parallel to (001). The starting material is obtained at high temperature as the orthorhombic structure. Such crystals are metastable

and in a few hours they spontaneously undergo the transition to the tetragonal structure with a transition temperature of 491 °C.^[46]

- d. Dehydration: This term refers specifically to a loss of water molecules. Generally speaking, this term can be re-defined as solvent loss. At this point it is necessary to distinguish between two different ways of losing solvent molecules. The simpler case occurs when these molecules are not bonded to the skeleton of the compound. They are connected by weak interactions (H-bonds, van der Waals forces, etc.). In this case the removal of solvent molecules is more straightforward and does not cause dramatic changes in the crystal structure. On the other hand, when solvent molecules are covalently bonded to other parts of the structure, their exit provokes significant changes in the crystal structure. The destruction of the crystal lattice is common in these cases. In this section, we will talk about the second type of dehydration, the one that involves a cooperative contribution of the lattice to the solvent egress.

One example is the transformation of brucite [$\text{Mg}(\text{OH})_2$] with the hexagonal CdI_2 layered structure to give periclase (MgO) with the cubic rock-salt structure, which takes place at 250 - 300 °C, through a spinel intermediate in which Mg ions are at both octahedral and tetrahedral sites. The transformation can be explained in terms of a donor-acceptor model. The acceptor regions of brucite gain Mg(II) ions from the donor regions and lose protons. Those protons are combined with the OH groups of the acceptor regions and the resulting molecule of water exits the structure (Figure 6.7). This mechanism also explains the pores observed in the structure.^[47]

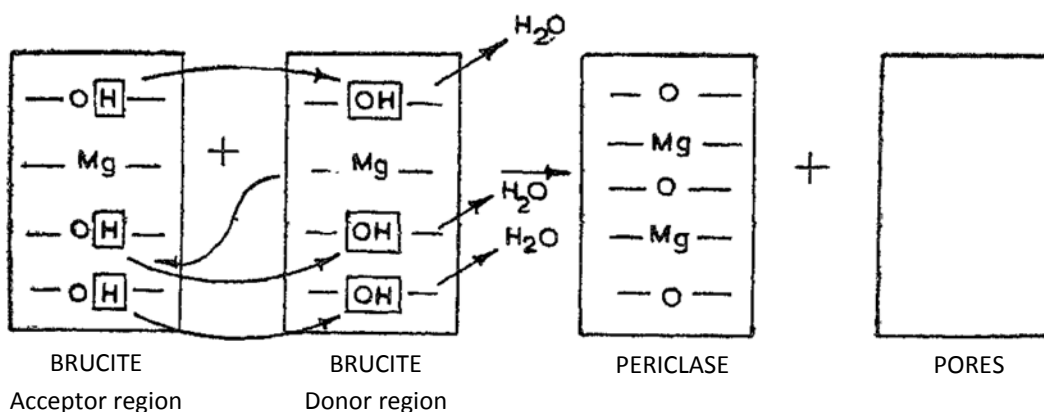


Fig. 6.7. Representation of the dehydration process from brucite to periclase. Adapted from Manohar 1975^[1]

- e. Decomposition. The example given in this section is the decomposition of anthracene peroxide to anthraquinone and anthrone. The process preserves the crystallinity of the sample as the two products are isomorphous, with similar unit cells; they are obtained as twins. The process is induced by heat or by X-Ray irradiation. Figure 6.8 shows the three compounds involved in this reaction.^[48]

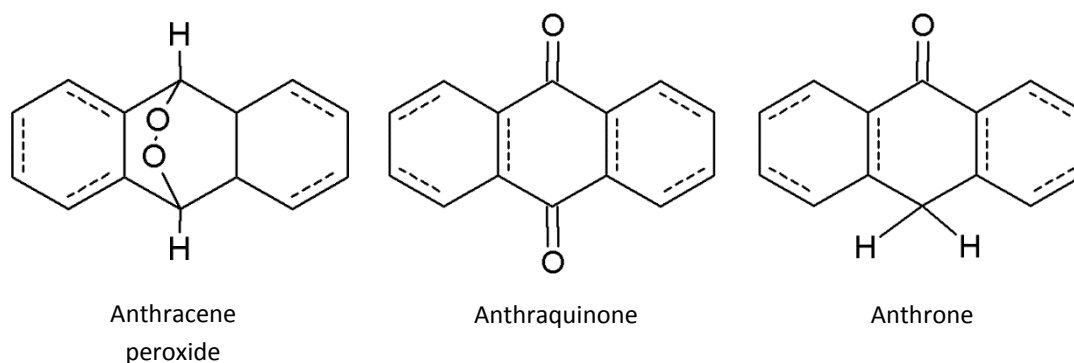


Fig. 6.8. Structure of anthracene peroxide, anthraquinone and anthrone; the decomposition of anthracene peroxide gives twinned crystals of the other two compounds.

- f. Electron-ion transfer (redox): Intercalation compounds can be obtained by a topotactic electron-ion transfer when the reagents have the appropriate structure and electronic properties. These compounds are formed by a host lattice and guest molecules. Two types of lattices can be used, insulators and conductors. The former have an effective matrix charge that remains constant during the reactions while for the latter it may be altered, so that the uptake of ions and electrons is simultaneous. Examples of insulator lattices are zeolites, sheet silicates and polyphosphates, and of conducting lattices are graphite, molybdenum sulphide and tungsten trioxide. The guests can range from protons and metal ions to large organic and inorganic molecular ions.

Among the earliest systems studied were solid oxygen-carrying metal chelates. Red-to-brown crystals of [2,2'-ethylene bis(nitrilemethylidene) diphenolato] cobalt (II) become black when exposed to air due to reversible uptake of O_2 . The crystal structure of the compound presents channels through which the O_2 molecules diffuse. The Co(II) ions are oxidised during the process but the final oxidation state is still uncertain. This and related compounds are used in welding for the generation of pure oxygen from air.^[49]

6.1.2. Single-crystal to single-crystal transformations^{[32] [50] [51] [52]}

In concluding this part of the chapter, some brief ideas and comments about single-crystal to single-crystal transformations are given.

As stated throughout this section, when a transformation of a single crystal occurs, preserving the long-range order in every direction in the solid -- that is, preserving its integrity -- the process is called single-crystal to single-crystal (SC-SC). Thus, there is not a specific type of reaction that can be defined as SC-SC.

Initially, it was believed that reactivity within molecular crystals that preserves their crystallinity was limited to topotactic reactions. However, studies of SC-SC transformations using atomic force microscopy (AFM) revealed that anisotropic long-range molecular movement inside a crystal was also possible.^{[53] [54]} There is some controversy over this fact due to the complexity of the mechanism involved in such processes, as the whole lattice has to cooperate in the arrangement of the atoms to form the final structure. This atomic rearrangement takes place with a minimum distortion of the crystal lattice; otherwise, the crystal would be destroyed. That is of crucial importance for the cases in which the removal or uptake of guest molecules occurs in non-porous crystals.

Although uncommon due to the restrictive prerequisites for a reaction to take place in an SC-SC fashion, these processes are highly desirable due to their advantages. The fact that the initial and final structures of the compounds can be determined reveals the details of the transformation and allows the explanation of the mechanism in terms of the resulting changes, the interactions within the structure and the modification of the properties of the crystal. Recent advances in instrumentation permit the obtainment of high quality analytical data in a reasonable period of time. That makes possible the “in situ” study of some processes as well as the refinement of disordered molecules, which is especially important in porous materials such as metal organic frameworks (MOFs) and porous coordination polymers (PCPs).^{[55] [56] [57]}

6.2 The Grotthuss Mechanism

Protons are at the centre of many chemical reactions (acid-base, redox, enzymatic catalysis, etc.), as well as biological and technological processes. Their presence is crucial in hydrogen fuel cells, atmospheric chemistry, corrosion processes or biological ATP synthesis. It is known that proton mobility in liquid water is around 4.5 times higher than the mobility of

any other cation in solution. Understanding the concepts behind the simple mechanism of this mobility is vital to shedding light on some other complicated phenomena.^{[58] [59] [2]}

It has been observed that the presence of 1-D hydrogen bonded chains allows transport through membranes, in a process in which the molecules remain static while an excess proton is transported along the chains. This is called a “water wire,” and the materials showing this behaviour are known as “protonic semiconductors.” The excess proton or charge defect transport can involve many different configurations of the Eigen and Zundel cations (Figure 6.9). (When a proton reacts with water, different hydrates can be formed. They are commonly known as hydrogen ions. Eigen (H_9O_4^+) and Zundel (H_5O_2^+) are two of these cations and play important roles in proton transport via the Grötthuss mechanism).

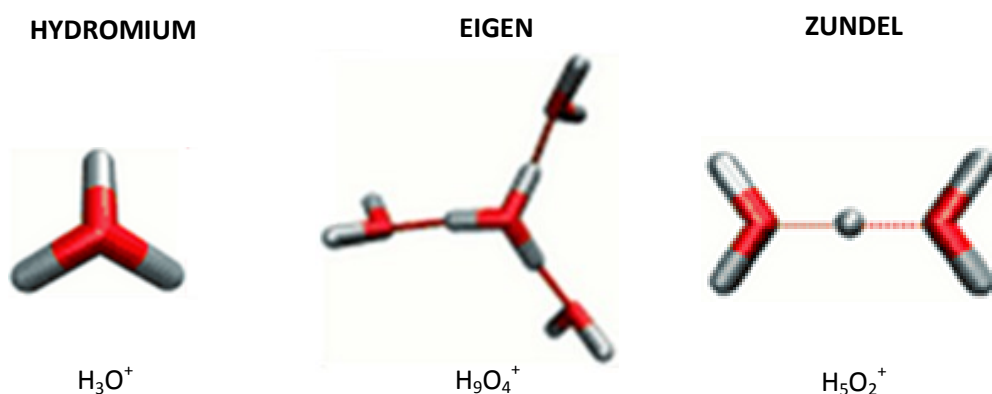


Fig. 6.9. Structure of Eigen and Zundel cations. Adapted from Kirchner 2007.^[2]

The proton jump from one molecule to another in its surroundings, both embedded in an infinite H-bonded net, can take place via the “Grotthuss Mechanism.” This is the commonest way of explaining proton conduction in liquid electrolytes and solids.

Another feasible mechanism for proton transport within confined spaces is the “Vehicle Mechanism,” by which the protons travel on a host molecule, called the carrier, not as an H^+ but rather as an H_3O^+ , NH_4^+ , etc. unit, where the vehicles or carriers would be H_2O , NH_3 , etc. (Figure 6.10).^{[60] [61]} Diffusion coefficients correspond to proton conduction and the substance behaves as a Brønsted base. Almost every good proton conductor is a good ion exchanger in such a way that protons are always exchanged as an oxonium ion. As an infinite H-bonded net is not required, stronger basic species such as NH_3 can be used for proton transport. This concept has helped in the preparation of new proton conductors based on zeolites.



Fig. 6.10 Models for proton conduction via (a) Grotthuss Mechanism (protons jump from one molecule to a neighboring one within an extended hydrogen-bond net) and (b) Vehicle Mechanism (a vehicle molecule or carrier assists the movement, and the proton is transferred as a complex ion). Reproduced from Kreuer *et al.* 1982.^[60]

In 1805 F. C. J. D. Theodor Von Grotthuss published his paper entitled “Mémoire sur la décomposition de l'eau et des corps qu'elle tient en dissolution à l'aide de l'électricité galvanique.”^[62] ^[63] The galvanic process was interpreted not from an electrostatic point of view but rather as a process based on physical-chemical phenomena. Grotthuss considered the electrolytic processes as polarised systems constituted by particles of opposed electrical natures. Note that at the time this paper was published, the modern concepts of molecule and bonding, as understood today, had not been developed.. In this paper, Grotthuss gave an answer to questions that had been unexplained until that moment, *i.e.*, why hydrogen was generated at one pole of an electrostatic cell and oxygen at the other instead of throughout the solution.

He studied the electrolysis of various salts in solution, confirming that certain metals are deposited at the negative pole of the cell while oxygen can be observed at the positive pole. He proposed that the battery was not only a simple galvanic generator, but also that it acts as a dynamic polarised system of particles. He also observed that the molecules of water were affected by the action of attractive and repulsive forces in the direction of the galvanic current. He postulated that water molecules were polarised during the electrolytic process, forming extended parallel polar chains. The molecules of water are split into their constituent components, which are continuously interchanged between neighbouring molecules giving recombination. Only the molecules at the end of the chains, in contact with the electrodes, underwent electrolysis.

This novel view of the electrolysis of water set the principles for new concepts such as atomism, divisibility or discreteness of materials, and attributed a dynamic nature to matter.

Currently, the modern interpretation of the Grotthuss mechanism is a bit more detailed.^{[64][65][66]} Initially, there are H-bonded water chains (water or proton wires) and an electrochemical gradient that favours the movement of the protons (from the left to the right in Figure 6.11).^[67]

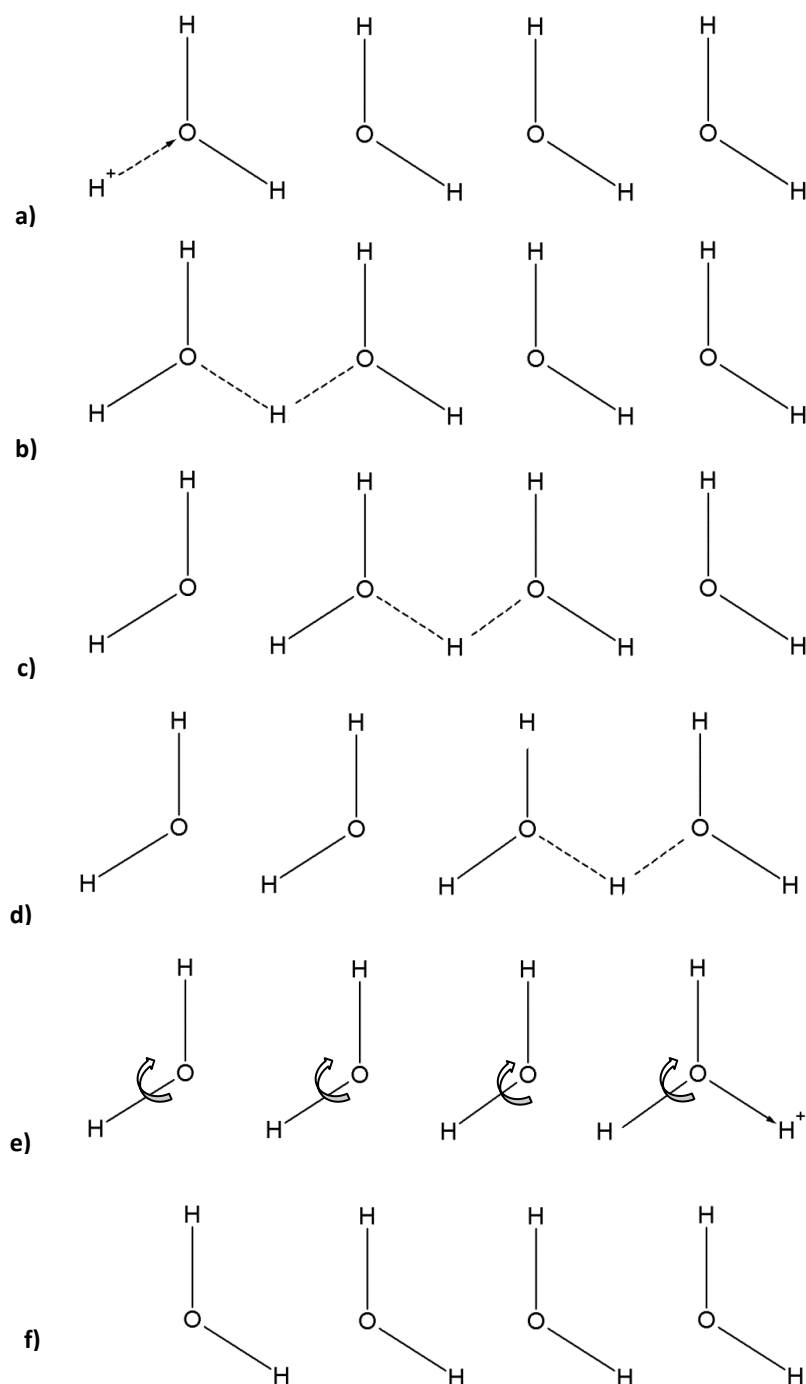


Fig. 6.11. Schematic representation of proton transfer along an H-bonded water chain via the Grotthuss Mechanism.

An H^+ gets closer to the oxygen atom of a molecule of water in the chain forming a covalent O-H bond (a). As a consequence, one of the former hydrogen atoms is now shared with a neighbouring water molecule forming a dimer, known as Zundel's cation (b).^{[B7] [68] [69]} The proton hopping is propagated along the chain (b-d) and finally the H^+ leaves the chains. Note that due to the proton transfer, the dipole moment of the water molecules is reverted, so at the end a rotation that leaves the system in an indistinguishable conformation is needed (e). Then the water chains are ready to transport another H^+ in the same direction (f).

In some studies, proton transfer is described as an isomerization between two water cations (protonated clusters). The Eigen cations present the more stable configuration while Zundel's cations are transition states. The process can be called "EZE transition."^{[B7] [70] [71] [72]} These protonated states of water are embedded in a complex net of hydrogen bonds.

Recent studies on the mechanism postulate that the rate limiting step depends on the dynamics of the solvation shell of water cations. It is suggested that the cleavage of a hydrogen bond in the second solvation shell of Zundel's cation produces electrostatic modifications in its environment that favour the "jump" of the proton from the donor water molecule to the acceptor.^{[66] [73] [74]} It is obvious that when a proton is transferred, a local re-arrangement of the H-bonds is required. There is an H-bond cleavage in the environment of the donor water molecule and a subsequent H-bond formation around the acceptor water molecule. This mechanism is known as the "Moses Mechanism."^{[75] [70]}

Calculations show that the energy of the H-bond broken at the second solvation shell of the Zundel cation is about 2.5 kcal/mol, which is approximately the value of the activation energy for H^+ mobility in bulk water. Note that in bulk water, an H^+ takes about 1 ps to cover 2.5 Å, which is in the range of the H-O distance in an H-bond.^[73]

It has been proved that any substance that could interact with the protonated clusters (*i.e.*, HCl) obstructs or blocks the transfer of protons. The intercalation of an ion or molecule between water chains will affect the transmission of protons. It has been suggested that the mobility of the protons is determined by a combination of two factors, the Grotthuss mechanism and the hydrodynamic diffusion of the water cations.^{[76] [77]}

As a final remark, it can be said that independently of the correct mechanism operating within a sample, what is clear is that the geometric arrangement of the water molecules in the chain and also in their surroundings should be appropriate for the proton transfer to take place.^{[78] [79] [80] [81] [82]}

- Modelling Proton Transport

Most studies on the Grotthuss Mechanism are theoretical or need some calculations to compare experimental data with results obtained by simulation. There are not many cases in which a direct empirical observation of this mechanism has been obtained.^[83] An additional problem is that calculations on proton transport are not accurate enough. That is because the small mass of protons means that quantum effects have a significant influence on the microscopic mechanism and on the calculated values. Besides, the differences in energy values are of a few kcal/mol, so it is hard to design a description of the potential energy surface (PES) that gives accurate values of energy for the rupture and formation of H-bonds. The commonest methods used in these calculations are Car-Parrinello Dynamic Simulations (CPDS)^[84] and the Empirical Valence Bond (EVB) method^[85] which provide information on the geometry, formation energies, energy barriers, etc.

Proton transfer has been observed in a variety of materials. Of special importance are those present in biological systems, as the understanding of these processes may aid in the development of new techniques in medicine. Aquaporins are a class of trans-membrane proteins formed by four identical monomers containing water channels. Their high water selectivity is due to the size of the pore. Its narrowest section corresponds to the size of a molecule of water (about 2.8 Å). In addition, there is an arginine residue that impedes the entrance of charged water or other cations. Finally, positively charged dipoles in the middle of the channel provoke the reorientation of the water molecules.^{[86] [87] [88] [89]} From the point of view of industrial applications, Polymer Electrolyte Membranes (PEMs) are one of the most significant representatives. They are present for instance in polymer electrolyte fuel cells. They are involved in the transport of the protons generated during the oxidation of the fuel at the anode of the cell. Some examples of commercial membranes used in industry are perfluorinated sulfonated polymers such as Nafion (DuPont), Acipex and Gore (Asahi) or Dow (Dow Chemicals).^{[90] [91] [92]} New materials such as Metal Organic Frameworks (MOFs) have recently been demonstrated to undergo proton transfer. A nice example is based on a porous 3-D MOF in whose pores large ionic water clusters have been trapped. The compound shows a high mobility for the aqueous protons due to the rich H bond net around a central $\text{H}(\text{H}_2\text{O})_{28}^+$ core.^[93]

References

- [1] H. Manohar, *Journal of the Indian Institute of Science* **1975**, *57*, 468-488.
- [2] B. Kirchner, *Chemphyschem* **2007**, *8*, 41-43.
- [3] D. Braga, F. Grepioni, *Angewandte Chemie-International Edition* **2004**, *43*, 4002-4011.
- [4] L. R. MacGillivray, G. S. Papaefstathiou, *Encyclopedia of Supramolecular Chemistry*, **2004**.
- [5] G. M. J. Schmidt, *Vol. 27*, *Pure Appl. Chem.*, **1971**, pp. 647-678.
- [6] K. Tanaka, F. Toda, *Chemical Reviews* **2000**, *100*, 1025-1074.
- [7] V. Enkelmann, *Advances in Polymer Science* **1984**, *63*, 91-136.
- [8] I. C. Paul, D. Y. Curtin, *Science* **1975**, *187*, 19-26.
- [9] P. A. Ramachandran, L. K. Doraiswamy, *Aiche Journal* **1982**, *28*, 881-900.
- [10] R. H. Spitzer, F. S. Manning, Philbroo.Wo, *Transactions of the Metallurgical Society of Aime* **1968**, *242*, 618-&.
- [11] S. C. Tseng, S. S. Tamhankar, C. Y. Wen, *Chemical Engineering Science* **1981**, *36*, 1287-1294.
- [12] Q. T. Tsay, W. H. Ray, J. Szekely, *Aiche Journal* **1976**, *22*, 1064-1079.
- [13] Anastasi.Lj, Alfredso.Pg, Steindle.Mj, *Industrial & Engineering Chemistry Process Design and Development* **1971**, *10*, 150-&.
- [14] L. K. Doraiswamy, H. C. Bijawat, M. V. Kunte, *Vol. 55*, *Chemical Engineering Progress*, **1959**, pp. 80-88.
- [15] P. A. Ramachandran, M. H. Rashid, R. Hughes, *Chemical Engineering Science* **1975**, *30*, 1391-1398.
- [16] M. Hartman, R. W. Coughlin, *Aiche Journal* **1976**, *22*, 490-498.
- [17] J. Szekely, C. I. Lin, *Metallurgical Transactions B-Process Metallurgy* **1976**, *7*, 493-495.
- [18] M. A. Fahim, J. D. Ford, *Canadian Journal of Chemical Engineering* **1978**, *56*, 730-734.
- [19] R. W. Bartlett, H. H. Haung, *Jom-Journal of Metals* **1973**, *25*, 28-34.
- [20] Bourgeoi.Sv, F. R. Groves, A. H. Wehe, *Aiche Journal* **1974**, *20*, 94-103.
- [21] S. S. Tamhankar, M. Hasatani, C. Y. Wen, *Chemical Engineering Science* **1981**, *36*, 1181-1191.
- [22] Y. K. Rao, *Transactions of the Institution of Mining and Metallurgy Section C-Mineral Processing and Extractive Metallurgy* **1981**, *90*, C47-C52.
- [23] A. Orita, L. S. Jiang, T. Nakano, N. C. Ma, J. Otera, *Chemical Communications* **2002**, 1362-1363.
- [24] I. Tsukushi, O. Yamamuro, H. Suga, *Thermochimica Acta* **1992**, *200*, 71-86.
- [25] F. Toda, K. Tanaka, A. Sekikawa, *Journal of the Chemical Society-Chemical Communications* **1987**, 279-280.
- [26] F. Toda, H. Miyamoto, *Chemistry Letters* **1995**, 861-861.
- [27] A. J. Schultz, G. D. Stucky, R. H. Blessing, P. Coppens, *Journal of the American Chemical Society* **1976**, *98*, 3194-3201.
- [28] Rosenber.B, L. Vancamp, J. E. Trosko, V. H. Mansour, *Nature* **1969**, *222*, 385-&.
- [29] V. P. Balema, J. W. Wiench, M. Pruski, V. K. Pecharsky, *Chemical Communications* **2002**, 1606-1607.
- [30] G. W. Wang, K. Komatsu, Y. Murata, M. Shiro, *Nature* **1997**, *387*, 583-586.
- [31] K. Komatsu, G. W. Wang, Y. Murata, T. Tanaka, K. Fujiwara, K. Yamamoto, M. Saunders, *Journal of Organic Chemistry* **1998**, *63*, 9358-9366.
- [32] G. Kaupp, *Current Opinion in Solid State & Materials Science* **2002**, *6*, 131-138.
- [33] V. Kohlschütter, P. Haenni, *Vol. 105*, *Zeitschrift für anorganische und allgemeine Chemie*, **1918**, pp. 121-144.
- [34] M. D. Cohen, G. M. J. Schmidt, *Journal of the Chemical Society* **1964**, 1996-&.

- [35] M. D. Cohen, G. M. J. Schmidt, F. I. Sonntag, *Journal of the Chemical Society* **1964**, 2000-&.
- [36] G. M. J. Schmidt, *Journal of the Chemical Society* **1964**, 2014-&.
- [37] V. Ramamurthy, K. Venkatesan, *Chemical Reviews* **1987**, *87*, 433-481.
- [38] M. A. Collins, D. P. Craig, *Chemical Physics* **1981**, *54*, 305-321.
- [39] D. P. Craig, C. P. Mallett, *Chemical Physics* **1982**, *65*, 129-142.
- [40] D. P. Craig, R. N. Lindsay, C. P. Mallett, *Chemical Physics* **1984**, *89*, 187-197.
- [41] K. Norris, P. Gray, D. P. Craig, C. P. Mallett, B. R. Markey, *Chemical Physics* **1983**, *79*, 9-19.
- [42] M. D. Cohen, *Angewandte Chemie-International Edition in English* **1975**, *14*, 386-393.
- [43] M. D. Cohen, *Molecular Crystals and Liquid Crystals* **1979**, *50*, 1-10.
- [44] G. Wegner, *Zeitschrift Fur Naturforschung Part B-Chemie Biochemie Biophysik Biologie Und Verwandten Gebiete* **1969**, *B 24*, 824-&.
- [45] J. W. Lauher, F. W. Fowler, N. S. Goroff, *Accounts of Chemical Research* **2008**, *41*, 1215-1229.
- [46] Soderqui.R, B. Dickens, *Journal of Physics and Chemistry of Solids* **1967**, *28*, 823-&.
- [47] J. F. Goodman, *Proceedings of the Royal Society of London Series a-Mathematical and Physical Sciences* **1958**, *247*, 346-&.
- [48] K. Lonsdale, E. Nave, J. F. Stephens, *Philosophical Transactions of the Royal Society of London Series a-Mathematical and Physical Sciences* **1966**, *261*, 1-&.
- [49] P. Pfeiffer, E. Breith, E. Lubbe, T. Tsumaki, *Justus Liebigs Annalen Der Chemie* **1933**, *503*, 84-130.
- [50] Z. Yin, M. Zeng, *Science China-Chemistry* **2011**, *54*, 1371-1394.
- [51] Z. Su, M. Chen, T.-a. Okamura, M.-S. Chen, S.-S. Chen, W.-Y. Sun, *Inorganic Chemistry* **2011**, *50*, 985-991.
- [52] T. Zhang, Y. Lu, Z. Zhang, Q. Lan, D. Liu, E. Wang, *Inorganica Chimica Acta* **2014**, *411*, 128-133.
- [53] G. Kaupp, *Angewandte Chemie-International Edition in English* **1992**, *31*, 592-595.
- [54] G. Kaupp, *Angewandte Chemie-International Edition in English* **1992**, *31*, 595-598.
- [55] M. Kawano, M. Fujita, *Coordination Chemistry Reviews* **2007**, *251*, 2592-2605.
- [56] M. P. Suh, Y. E. Cheon, *Australian Journal of Chemistry* **2006**, *59*, 605-612.
- [57] G. J. Halder, C. J. Kepert, *Australian Journal of Chemistry* **2006**, *59*, 597-604.
- [58] C. Dellago, M. M. Naor, G. Hummer, *Physical Review Letters* **2003**, *90*.
- [59] J. Halding, P. S. Lomdahl, *Physical Review A* **1988**, *37*, 2608-2613.
- [60] K. D. Kreuer, A. Rabenau, W. Weppner, *Angewandte Chemie-International Edition in English* **1982**, *21*, 208-209.
- [61] G. A. Luduena, T. D. Kuehne, D. Sebastiani, *Chemistry of Materials* **2011**, *23*, 1424-1429.
- [62] B. Jaselskis, C. E. Moore, A. Von Smolinski, *Abstracts of Papers of the American Chemical Society* **2007**, *233*, 651-651.
- [63] S. Cukierman, *Biochimica Et Biophysica Acta-Bioenergetics* **2006**, *1757*, 876-885.
- [64] O. Markovitch, H. Chen, S. Izvekov, F. Paesani, G. A. Voth, N. Agmon, *Journal of Physical Chemistry B* **2008**, *112*, 9456-9466.
- [65] A. A. Kornyshev, A. M. Kuznetsov, E. Spohr, J. Ulstrup, *Journal of Physical Chemistry B* **2003**, *107*, 3351-3366.
- [66] T. J. F. Day, U. W. Schmitt, G. A. Voth, *Journal of the American Chemical Society* **2000**, *122*, 12027-12028.
- [67] J. F. Nagle, H. J. Morowitz, *Proceedings of the National Academy of Sciences of the United States of America* **1978**, *75*, 298-302.
- [68] M. Eigen, *Angewandte Chemie-International Edition* **1964**, *3*, 1-&.
- [69] M. L. Huggins, *Journal of Physical Chemistry* **1936**, *40*, 723-731.
- [70] N. Agmon, *Chemical Physics Letters* **1995**, *244*, 456-462.

- [71] N. Agmon, S. Y. Goldberg, D. Huppert, *Journal of Molecular Liquids* **1995**, *64*, 161-195.
- [72] N. Agmon, *Israel Journal of Chemistry* **1999**, *39*, 493-502.
- [73] N. Agmon, *Journal De Chimie Physique Et De Physico-Chimie Biologique* **1996**, *93*, 1714-1736.
- [74] J. Lobaugh, G. A. Voth, *Journal of Chemical Physics* **1996**, *104*, 2056-2069.
- [75] M. Tuckerman, K. Laasonen, M. Sprik, M. Parrinello, *Journal of Chemical Physics* **1995**, *103*, 150-161.
- [76] S. Cukierman, *Biophysical Journal* **2000**, *78*, 1825-1834.
- [77] E. P. Quigley, P. Quigley, D. S. Crumrine, S. Cukierman, *Biophysical Journal* **1999**, *77*, 2479-2491.
- [78] S. Lengyel, J. Tamas, J. Giber, *Acta Chimica Academiae Scientiarum Hungaricae* **1962**, *32*, 429-&.
- [79] D. A. Lown, H. R. Thirsk, *Transactions of the Faraday Society* **1971**, *67*, 132-&.
- [80] D. A. Lown, H. R. Thirsk, *Transactions of the Faraday Society* **1971**, *67*, 149-&.
- [81] B. B. Owen, F. H. Sweeton, *Journal of the American Chemical Society* **1941**, *63*, 2811-2817.
- [82] A. Chernyshev, R. Pomes, S. Cukierman, *Biophysical Chemistry* **2003**, *103*, 179-190.
- [83] U. W. Schmitt, G. A. Voth, *Journal of Physical Chemistry B* **1998**, *102*, 5547-5551.
- [84] R. Car, M. Parrinello, *Physical Review Letters* **1985**, *55*, 2471-2474.
- [85] U. W. Schmitt, G. A. Voth, *Journal of Chemical Physics* **1999**, *111*, 9361-9381.
- [86] M. Amiry-Moghaddam, O. P. Ottersen, *Nature Reviews Neuroscience* **2003**, *4*, 991-1001.
- [87] C. Maurel, *Annual Review of Plant Physiology and Plant Molecular Biology* **1997**, *48*, 399-429.
- [88] C. Maurel, L. Verdoucq, D.-T. Luu, V. Santoni, in *Annual Review of Plant Biology*, Vol. 59, **2008**, pp. 595-624.
- [89] A. S. Verkman, *Journal of Cell Science* **2005**, *118*, 3225-3232.
- [90] P. Commer, A. G. Cherstvy, E. Spohr, A. A. Kornyshev, *Fuel Cells* **2003**, *2*, 127-136.
- [91] R. S. Yeo, *Journal of the Electrochemical Society* **1983**, *130*, 533-538.
- [92] S. J. Paddison, R. Paul, *Physical Chemistry Chemical Physics* **2002**, *4*, 1158-1163.
- [93] C. Duan, M. Wei, D. Guo, C. He, Q. Meng, *Journal of the American Chemical Society* **2010**, *132*, 3321-3330.
- [P7] IUPAC. Compendium of Chemical Terminology, 2nd ed. (the "Gold Book"). Compiled by A. D. McNaught and A. Wilkinson. Blackwell Scientific Publications, Oxford (1997). XML on-line corrected version: <http://goldbook.iupac.org> (2006-) created by M. Nic, J. Jirat, B. Kosata; updates compiled by A. Jenkins. ISBN 0-9678550-9-8. doi:10.1351/goldbook.
- [B6] Kearsley, S.K. The Prediction of Chemical Reactivity within Organic Crystals Using Geometric Criteria. In *Organic Solid State Chemistry*; Desiraju, G.R., Ed.; Elsevier: New York, 1987; 69-115.
- [B7] Zundel, G. The Hydrogen Bond, Recent DeVelopments in Theory and Experiments; Schuster, P., Zundel, G., Sandorfy, C., Eds.; North Holland: Amsterdam, 1976; pp 687-766.

7

0-D Manganese citrate cubanes*

A Discrete Neutral Transition-Metal Citrate Cubane with a New Core Geometry.

This chapter is focused on the first derivative of a series of manganese citrate compounds ranging from 0D to 2D. This is the first reported example of a derivative with formula $[M_8(\text{citr})_4]$, that is, a discrete, neutral complex with a cubane core, peripheral metal atoms and, except for water of crystallization, no further diversity in its composition (note that compounds 1 and 2 are also discrete neutral compounds) Neutral compounds with general formula $[M^{\text{II}}_x(\text{citrate})_y(\text{H}_2\text{O})_z]$ where the citrate can be in any of its states of deprotonation have been reported. Those which have been structurally characterized present a polymeric structure. To date there is no report of a discrete neutral derivative. Three compounds were found in the Cambridge Database V5.31 with neutral discrete structures (*i.e.* compounds $[M^{\text{II}}_2(\text{H}_2\text{citrate})_2(\text{H}_2\text{O})_4] \cdot \text{N-N} \cdot 2\text{H}_2\text{O}$ ($M = \text{Zn}, \text{Mn}$, $\text{N-N} = 4\text{-}4'\text{-ethene-1,2-diyldipyridine}$; $M = \text{Mn}$, $\text{N-N} = 1,2\text{-bis(pyridin-4-yl)ethane}$)). However, a re-refinement of the structures reveals that the citrate is clearly anionic, $[M^{\text{II}}_2(\text{Hcitrate})_2(\text{H}_2\text{O})_4]^{2-}$, in two cases while for the remaining case there is strong evidences of that. (For further details see supplementary material)

In this case, the compound is based in the same basic unit as the previously described cobalt citrate cubanes, with a spatial distribution of the rings around the cube corresponding to isomer B.

First, we will describe in detail the crystal structure of this monomer. (As before, we use one entire cubane as the structural building block, so the term monomer is applied to a compound with one complete cubane.) An uncommon coordination of the additional Mn(II) centres to the periphery of the cube has been observed, as a consequence of which the resulting molecular structure is polar (as is the overall crystal structure, with space group $I2$). Finally, a reversible transformation of the compound under mild conditions has been observed. Despite the fact that there are no channels through the structure, there are

evidences that the observed transformation is a dehydration-rehydration process. That is in accord with results obtained for other compounds that will be presented further on.

7.1. Experimental

7.1.1 Synthesis

All reactants were used as received from commercial sources. No further purification of the reagents was considered necessary.

The neutral monomer $\{[\text{Mn}_4(\text{C}_6\text{H}_4\text{O}_7)_4][\text{Mn}(\text{H}_2\text{O})_4]_2 [\text{Mn}(\text{H}_2\text{O})_5]_2\} \cdot (\text{H}_2\text{O})$, **9**, was obtained as a white to pale-pink powder or as large colourless single crystals depending on the details of the synthetic procedure.

The reaction mixture was prepared by adding MnCO_3 (5.18 g, 45.1 mmol) to a stirred solution of citric acid monohydrate (250 mL, 0.095 M). The mixture was heated to reflux under a stream of Ar for 5 h. and filtered. The solution was cooled under ambient conditions for several days, upon which it became orange, and crystals of the known compound - not a cubane - $(\text{C}_{12}\text{H}_{22}\text{Mn}_3\text{O}_{20})_n \cdot 4n(\text{H}_2\text{O})$ ^[1] were obtained. The suspension was filtered and the resulting supernatant was heated to reflux for 3 h. At this point, a white precipitate appeared; reflux was detained while maintaining the heating, allowing evaporation of the solvent down to a volume of 50 mL. The suspension was filtered, giving a white to pale-pink powder of **9**. The supernatant, placed in a closed vial in an oven at 90 °C, yielded large, colourless crystals of **9**.

7.1.2 Single Crystal X-Ray diffraction

Single crystal X-Ray diffraction data were collected using an Xcalibur S3 CCD-based four-circle diffractometer (Oxford Diffraction and Agilent Technologies). The program CrysAlis Pro^[P1] controlled data collection and processing. The structure was solved *ab initio* by direct methods^[2] and refined by full-matrix least-squares analysis.^[3] Non-hydrogen atoms were refined with anisotropic displacement parameters. The methylene H atoms of the citrate ligands were placed at idealized positions and refined as riders on their respective parent C atoms with isotropic displacement parameters set to 1.2 times the equivalent isotropic U of the C atom. The hydrogen atoms of the coordinated water molecules were found as q peaks in the difference map, setting their isotropic displacement parameter to 1.2 times the equivalent isotropic U of the O atom. Those for the only free molecule of water could not be found. The program Diamond^[P2] was used in the preparation of graphics. Data collection and structure solution and refinement details are shown in Table 7.1.

Table 7.1. Crystallographic data for **9**.

Formula	^a C ₂₄ H ₅₄ Mn ₈ O ₄₇	Crystal size (mm³)	0.50 x 0.31 x 0.13
fw (g mol⁻¹)	1534.19	θ (min,max) (°)	4.36, 28.85
Radiation	X-Rays (Mo Kα)	Reflns collected	13682
Wavelength (Å)	0.71073	Indep reflns	5597
Crystal system	monoclinic	R(int), R(σ)	0.0144, 0.0218
Space group	I2	Completeness (θ)	0.985 (27.50)
temp (K)	100(1)	Abs corr	multi-scan
a (Å)	11.7817(2)	T(min,max)	0.4162, 0.7696
b (Å)	9.9864(3)	restraints/parms	3, 415
c (Å)	21.2165(3)	Goodness-of-fit	1.059
β (°)	101.519(2)	R1, wR2 (obs)^b	0.0168, 0.0426
V (Å³), Z	2445.99(9), 2	R1, wR2 (all)	0.0168, 0.0426
ρ_{calc} (Mg/m³)	2.083	Δσ(max,mean)	0.004, < 0.001
μ (mm⁻¹)	2.126	Δρ range (e Å⁻³)	0.658, -0.532
F (000)	1548.0	Flack parameter	0.007(7)
^a {[Mn ₄ (C ₆ H ₄ O ₇) ₄][Mn(H ₂ O) ₄] ₂ [Mn(H ₂ O) ₅] ₂ }·(H ₂ O)			
^b threshold I > 2σ(I).			
^c Flack, 1983. ^[4]			

7.1.3 Powder X-Ray diffraction

Powder X-Ray data were collected by the X-Ray Diffraction and Fluorescence Analysis Service of the University of Zaragoza using a RIGAKU D/max 2500 diffractometer equipped with a copper rotating anode, operating at 40 kV and 100 mA with a graphite monochromator (Cu Kα). Measurements were made from 2θ equals to 5° to 50° in steps of 0.03° with a rate of 1s/step.

7.1.4 FT-IR spectroscopy

The FT-IR spectrum of compound **9** was measured on a Perkin-Elmer Spectrum 100 FT-IR Spectrophotometer with ATR accessory in the range of 4000 - 350 cm⁻¹ (Figure 7.1).

IR (neat compound, cm⁻¹): ν(OH) 3166.19 (w); ν(C=O) 1549.00 (w); ν(C-H) 1414.30 (w) and 1371.94 (n); ν(CH) 1242.45 (n); ν(CO) 1106.84, 1081,37 and 1051.22 (t).

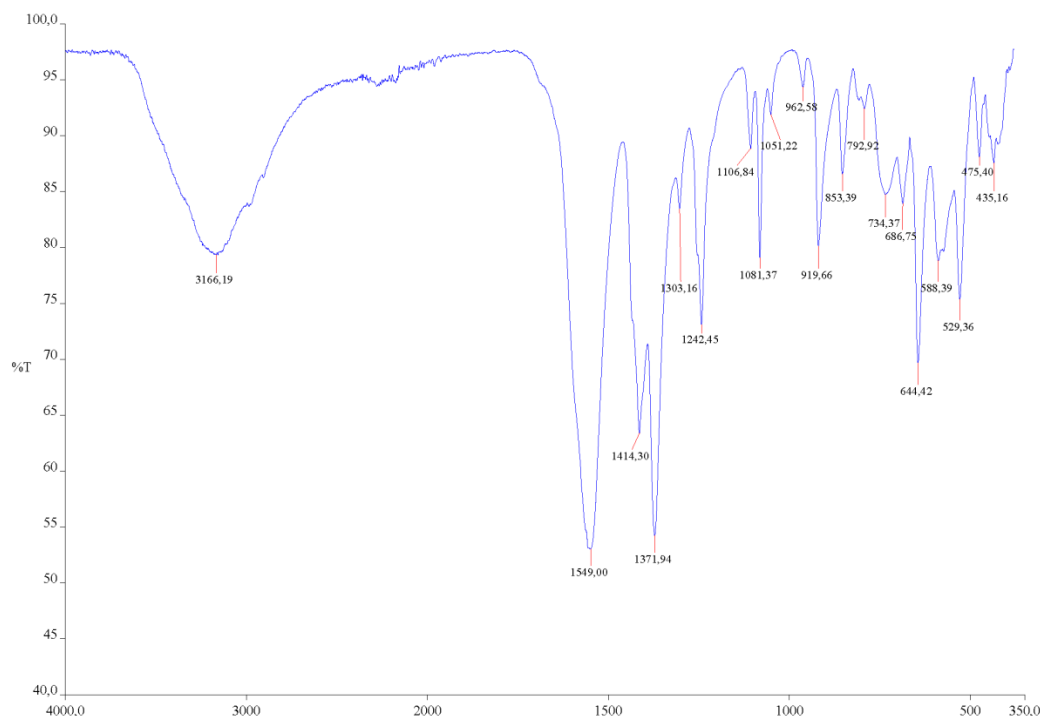


Fig. 7.1. IR spectrum of 9

7.1.5 Elemental analysis

Elemental analysis was performed on a Perkin Elmer 2400 CHNS/O analyser. Calculated analysis for (C₂₄H₅₄Mn₈O₄₇) is: C, 18.79%; H, 3.55%. Results obtained were C, 18.85%; H, 3.65%.

7.1.6 Thermogravimetric analysis (TGA)

Thermogravimetric analysis (TGA) was carried out in a Universal V4.5A TA Instrument, model 2960 SDT V3.0F in the range of 25 - 500 °C (Figure 7.2). No accurate quantitative results can be obtained from this analysis, as the compound decomposes during the process, due to the organic nature of the ligand and also because most of the water molecules present are covalently bonded to metal atoms and involved in an H-bond net. The crystal structure is not a rigid covalent grid with guest molecules hosted in its voids, in which case it would be possible to study solvent loss processes with this technique. However, useful qualitative information arises from this experiment. There are three steps involving loss of mass. The first one, between 58 - 155 °C (aprox.), corresponds to a loss of 17.57% of the molecular weight. At this range of temperature, this loss can be related to a dehydration process. As the molecular weight of compound 9 is 1534.16, (molecular weight calculated for a complete cubane with a free molecule of water), 15 molecules of water would have been lost at this point. The remaining 4 molecules of water could be involved in the formation of stable products with other fragments in the structure, allowing decomposition. There is a small shoulder at low

temperature (at around 80 °C) that could be associated with of the unique unligated molecule of water. The two remaining steps are at temperatures higher than 250 °C. Those could be caused by the formation of decomposition products as a result of the high temperature.

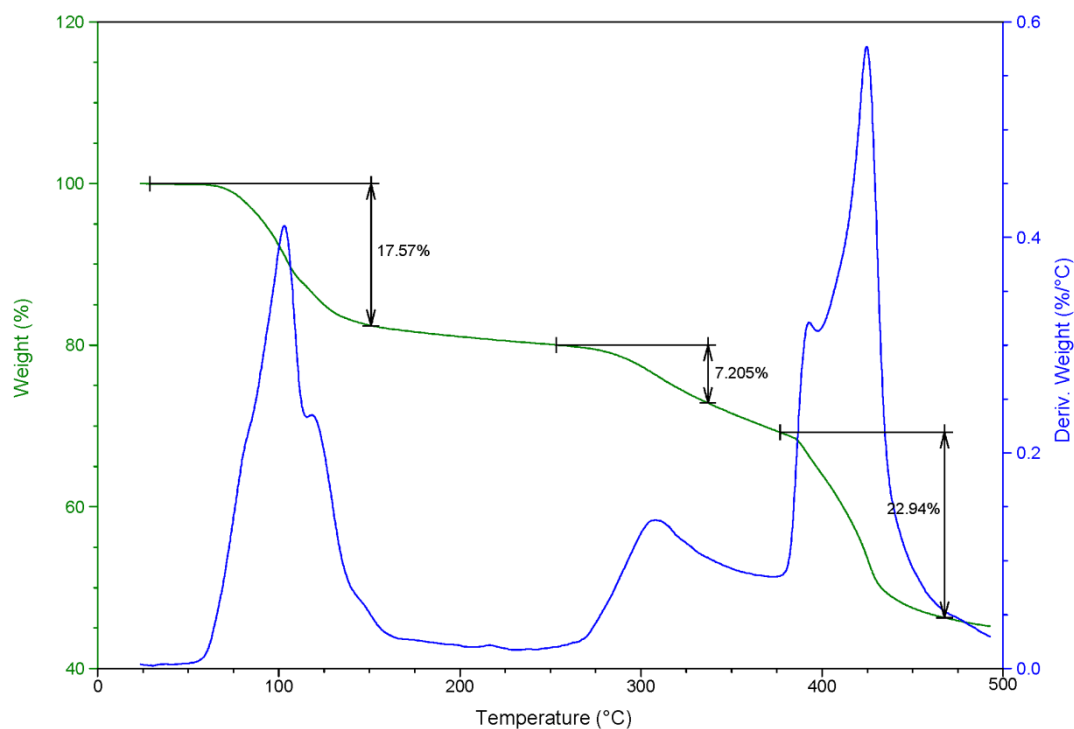


Fig. 7.2. TGA for **9**

The conclusion obtained from the TGA is that the compound is almost stable below 50 - 60 °C, at which temperature a dehydration process takes place in which most of the water molecules are lost. After that, the compound is stable below 250 °C, the temperature at which decompositions starts.

7.2 Results and discussion

7.2.1 Synthesis

For the preparation of **9**, manganese carbonate is added to a stirred aqueous solution of citric acid, and then the solution is heated under reflux. CO₂ is formed in the reaction, so an Ar stream is used to extract that product, thus favouring the reaction. After 5 h, the reaction mixture is filtered and the supernatant is cooled to ambient temperature and left for several days. During that time it becomes orange and the pH changes from 5.5 to 6. Crystals of a subproduct with Mn/citrate ratio of 3/2 are obtained.^[1] The mixture is filtered and heated again to reflux for 3 h., after which the heating is maintained but without reflux allowing the solvent to evaporate. With volume reduction, a white precipitate of compound **9** appears. It is

the only compound of the as many as six different compounds obtained from this reaction mixture that precipitates as a powder and also the only one obtained under heating. The others crystallize when the mixture is cool. After the white to pale-pink solid is isolated by filtering the hot suspension, the colourless solution is placed inside a closed vial in an oven at 90 °C. After few days, large colourless crystals of **9** are obtained. In contrast, if the colourless supernatant obtained when the white to pale-pink solid is filtered is allowed to cool down under room conditions inside an open flask, it becomes orange and the pH changes from 5.5 to 6.5. Crystals of four different species have been isolated from this reaction medium. The quantities of these derivatives vary with the pH. At low pH values (5.5 - 6) crystals of a series of derivatives in which the citric acid is not completely deprotonated (the OH group retains its hydrogen atom) and with a Mn/citrate ratio of 3/2 are obtained.^[1, 5] As the pH reaches higher values (6.5) the amount of these derivatives decreases and a 1D manganese polymer based on cubanes crystallizes. Another compound in this series of products is a derivative with an Mn/citrate ratio of 1/1 in which citric acid only has lost two protons.^[6] This is a minor product but it was possible to isolate it a few times. For further details on the synthetic procedure, see chapter 8.

7.2.2 Single Crystal X-Ray diffraction

Compound **9** crystallizes in the monoclinic system, space group I2. The use of this setting is in accord with the IUCr rules,^[7] with the *a*- and *c*-axes of the unit cell chosen as the two shortest axes perpendicular to the two-fold symmetry direction *b*. There is one-half cubane per asymmetric unit, with the full cubane sitting astride a crystallographic two-fold axis.

The compound is based on a $[\text{Mn}_4(\text{citr})_4]^{8-}$ cubane core, isomer B. The isomerism for the asymmetric C atoms of the citrate ligands in the reference asymmetric unit is R. Balancing the charge of the cube and attached to its periphery there are two crystallographically independent, chemically distinct Mn(II) units, each with two congeners related by the two-fold axis. The first one, $[\text{Mn}(\text{H}_2\text{O})_4]^{2+}$, is doubly bridged to two internal oxygen atoms from long arms (κ^2 -Lxi, *i.e.* O9, O13), while the second, $[\text{Mn}(\text{H}_2\text{O})_5]^{2+}$, is a pendant unit bonded to a peripheral oxygen atom from a long arm (Lxi, O8). There is also a free water site, partitioned into O10w, which resides on a two-fold axis, and O10a, on a general position at roughly 0.4 Å from O10w. The structural model assigned a total (Shelx) occupancy of 0.5 to this split site, for a stoichiometry of one water per cubane. The occupancies do not require any two of the partially occupied sites to be occupied simultaneously, and so no impossibly close contacts arise from the model. (Figure 7.3).

The pendant Mn(II) unit is attached to O8, one of the external carboxylate oxygen atom, as expected. However, the chelated Mn(II) unit is bonded to inner oxygen atoms, each of which is also bonded to a manganese atom of the cube (O9 and O13) (Figure 7.3) in an unprecedented coordination mode for these units. *N.b.*, O9 and O13 belong to distinct citrate ligands. The resulting fragment is a four-membered ring in which each of two carboxylate groups bridges two transition-metal centers through one of its oxygen atoms. The geometry around the two different Mn(II) units is presented in Table 7.2a,b.

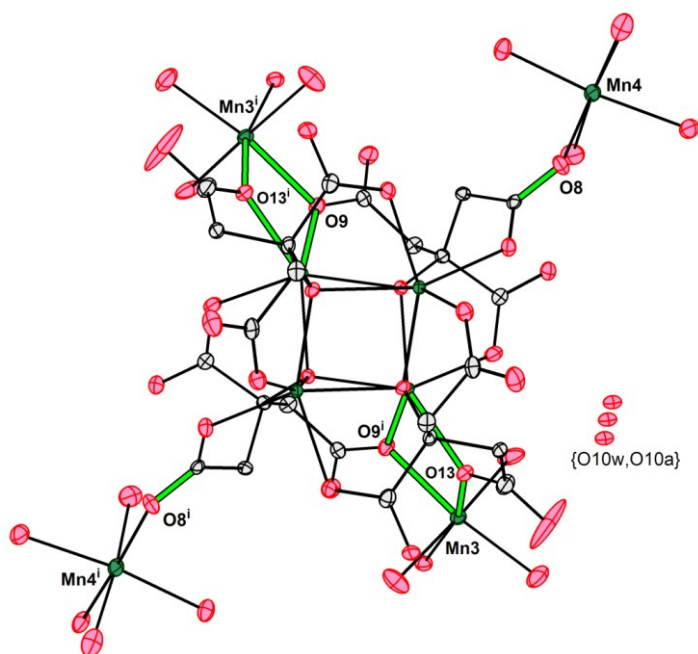


Fig. 7.3. A complete cubane unit with four Mn(II) cations and a free molecule of water. Thermal ellipsoids (probability 60%). i: (1-x, y, -z). Coordination of Mn3 and Mn4 are shown (green).

Table 7.2a. Coordination environment for Mn3						
Mn3	Distance (Å)	Angles (°)				
O13	2.1676 (13)					
O3w	2.1762 (15)	102.06 (6)				
O1w	2.1862 (15)	93.67 (6)	91.59 (6)			
O2w	2.1868 (14)	84.05 (5)	172.57 (7)	92.25 (6)		
O9 (-x+1, y, -z)	2.2042 (13)	76.36 (5)	86.55 (5)	169.21 (6)	90.84 (6)	
O4w	2.2059 (13)	162.84 (5)	90.83 (6)	97.27 (6)	82.36 (5)	93.38 (5)
	Mn3	O13	O3w	O1w	O2w	O9 (-x+1, y, -z)

Mn4	Distance (Å)	Angles (°)				
O7w	2.1583 (14)					
O8	2.1592 (13)	87.55 (5)				
O8w	2.1601 (13)	94.60 (5)	175.09 (6)			
O6w	2.1711 (16)	100.54 (6)	88.74 (5)	86.53 (6)		
O9w	2.1869 (17)	83.71 (6)	94.62 (5)	90.00 (6)	174.71 (6)	
O5w	2.2167 (14)	168.06 (6)	90.05 (5)	88.72 (6)	91.10 (6)	84.83 (6)
	Mn4	O7w	O8	O8w	O6w	O9w

Another interesting aspect of the peripheral Mn(II) units is their preferential coordination to just one end (which we will call the upper side or the top face) of the cube. They point to the same side of the cubane unit, so the molecular structure is polar.

There is a strong hydrogen-bonding network which extends through the entire structure. As most of the water molecules are coordinated to manganese atoms, their disposition around the cube directly affects the directionality of the H-bonds. These manganese units directed to the bases of the neighbouring cubes, as seen in Figure 7.4. All the molecules in the structure have the same orientation, in keeping with the polarity of the molecule and the directionality of the H-bonding. The result is a polar crystal structure in the hemimorphic (polar) space group I2.

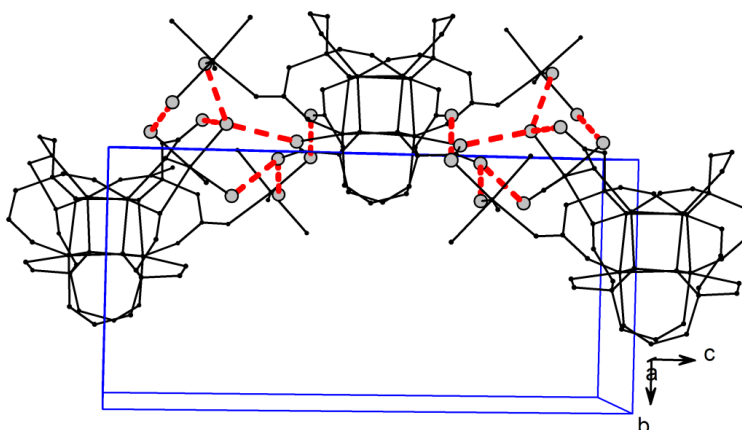


Fig. 7.4. Hydrogen bonds between three cubane-units showing the directionality of the interaction.

There are no voids or channels within the structure in agreement with the values of the Kitaigorodskii packing index,^[B1] calculated using Platon^[8]. The K.P.I. gives the percentage of "filled space" for a crystal structure. A typical structure with no significant voids or channels

presents a K.P.I of about 65 - 70%. We note here that the calculation of the K.P.I. is complicated by the presence of disorder; for the calculation of the K.P.I. of this structure we used a structural model in which O10w was given full occupancy while its congener (O10a) was omitted. This represents one of the local atomic arrangements described by our disorder model. The K.P.I value thus calculated is 76.8%, so we can conclude that water does not exit the structure through channels or voids. A different mechanism should be present to allow this dehydration process to take place.

7.2.3 Powder X-Ray diffraction

Most of the metal citrate based compounds presented in this work undergo reversible transformations under mild conditions in which solvent molecules, water for all of them, are involved.

The study of adsorption isotherms for gases such as N₂, H₂ or CO₂ is widely used in experiments which aim is to determine the quantity of guest molecules than can be hosted by the starting material. However, this is not our objective. Our sample is not suitable at all for sorption measurements using for example gravimetric sorption techniques. That is because there is not a porous material. In those experiments, samples are composed by a rigid grid acting as a host with some solvent molecules occupying its pores or channels. The experiments consist in removing every solvent molecule preserving the integrity of the framework and then calculate how much of the free space is available for the inert gas molecules. Our samples not only are not porous but they present more special features. Solvent molecules are mostly coordinated to the rigid grid so that, its egress is not straightforward. In addition, is it not recommended to use the high temperatures used commonly for this stage in these techniques because as it will be soon shown, crystalline samples lose their crystallinity below 100 °C. This is a really low temperature for such experiments. Finally, the last difference is that probably, the quantity of inert gas molecules that could enter the sample would be insignificant because the processes expected would involve some kind of host-guest interaction. That hypothesis will be clearly demonstrated in the next chapter.

An “*in situ*” thermal analysis of the evolution of **9** was conducted, using X-Ray powder diffraction.

When the compound was heated at a constant temperature for about 8 hours on the powder diffractometer, no changes were observed for constant temperatures lower than 60 °C (T1 = 30 °C, T2 = 40 °C, T3 = 50 °C) (Figure 7.5a-d). However, when T = 60 °C there is a clear

evolution of **9** in a few hours. That suggests that the evolution is time-independent below a critical temperature and has an energy barrier which requires temperatures of 60 °C or higher. In order to get a full study of the process, a ramp from 20 °C to 180 °C in 10-degree steps was performed, with data measured after 30 minutes of heating at each temperature (Figure 7.6). The evolution takes place between 60 °C and 70 °C, and at 90 °C the compound loses its crystallinity. A second ramp was made, in the limited range of 60 °C to 76 °C in 2-degree steps, collecting data after 30 minutes of heating at each temperature (Figure 7.7). With these data, we were able to characterise the transition temperature more accurately. It takes place between 64-66 °C under these specific experimental conditions.

In order to check the reversibility of the process, after this last experiment the sample was placed in a humid atmosphere for a weekend. Then data were collected at 20 °C. Figure 7.8 shows the reversibility of the transformation. The fact that the initial diffractogram was regenerated after exposure to a humid atmosphere indicates that the transformation observed at 64 - 66 °C can be correlated with a dehydration-rehydration process. That supports the information obtained from the TGA, in which there was a significant weight loss starting at 60 °C that was associated with a dehydration process. Two factors should be taken into account to explain the decomposition temperature. In powder X-Ray diffraction experiments we see that at 100 °C the material starts losing crystallinity, but this does not necessarily involve a decomposition process. At this temperature, the crystalline network is destroyed; but for irreversible destruction of the compound itself we need temperatures above 250 °C. The other fact to consider is that the heating rates in both experiments are different. For the powder experiment, by the time the starting material loses crystallinity it has been heated for more than four and a half hours, while the heating rate in TGA was 10°/min. It is not only a matter of temperature, once the critical temperature is exceeded; it is also necessary to consider the time the sample has been heated.

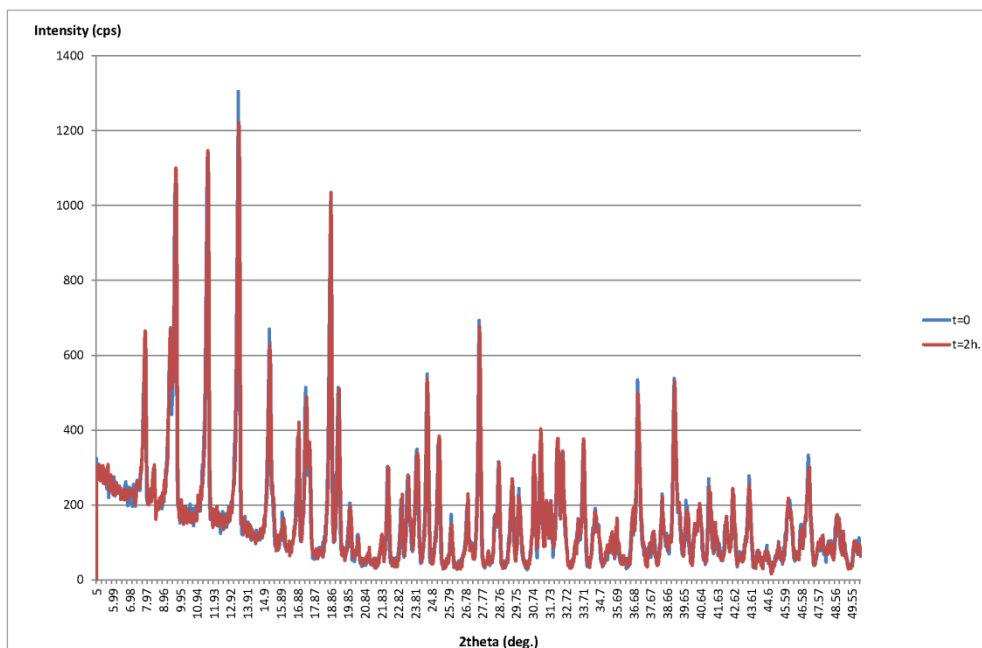


Fig. 7.5a. Powder X-Ray diffractogram for the evolution of **9** at constant temperature $T=30\text{ }^{\circ}\text{C}$. Time=0 (blue) and time=2 hours (red).

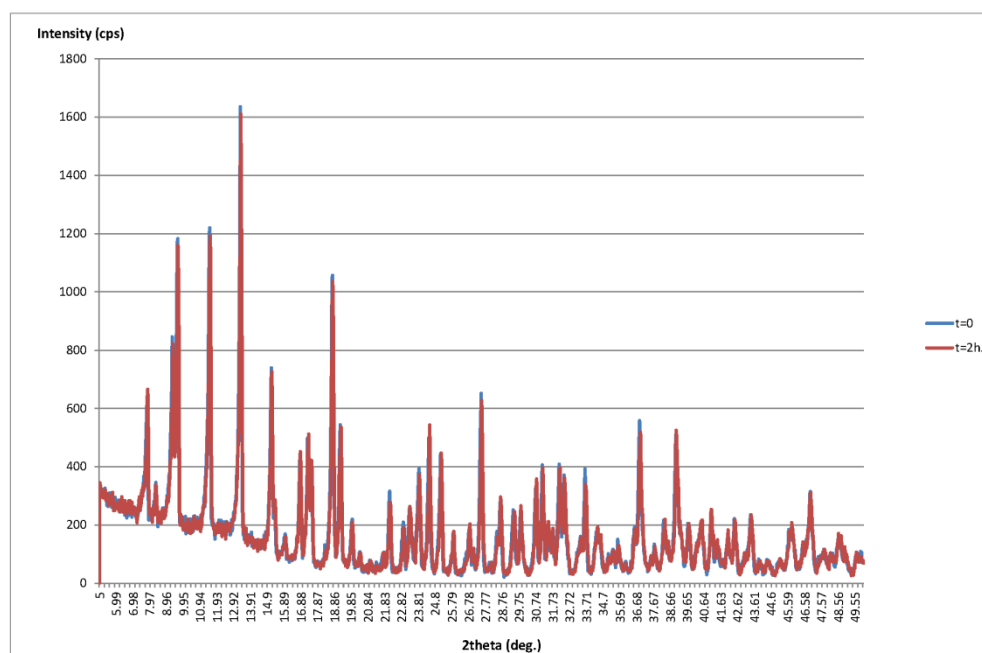


Fig. 7.5b. Powder X-Ray diffractogram for the evolution of **9** at constant temperature $T=40\text{ }^{\circ}\text{C}$. Time=0 (blue) and time=2 hours (red).

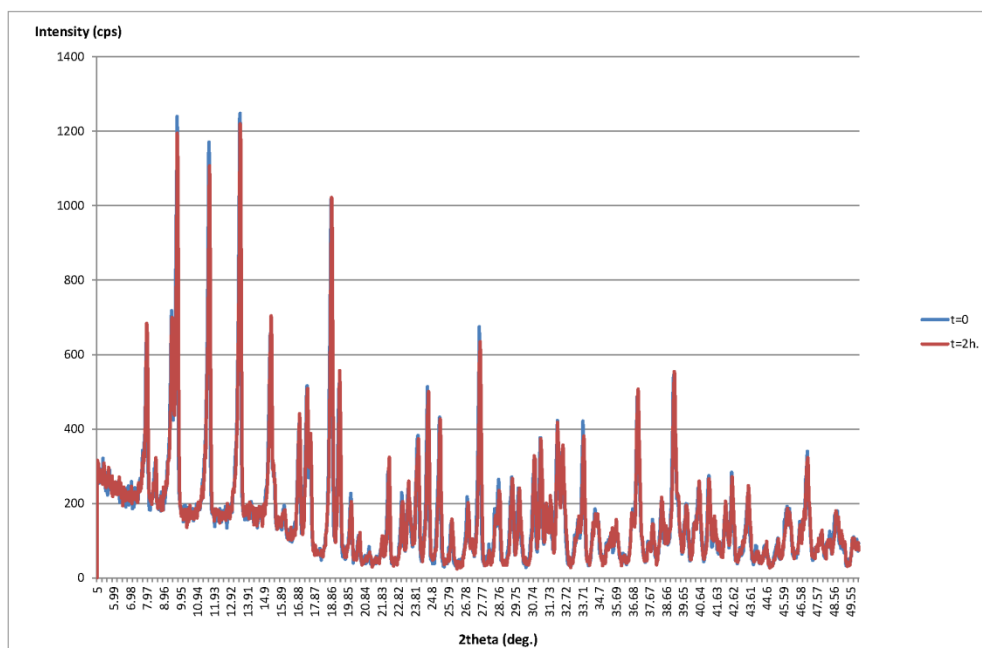


Fig. 7.5c. Powder X-Ray diffractogram for the evolution of **9** at constant temperature $T=50^{\circ}\text{C}$. Time=0 (blue) and time=2 hours (red).

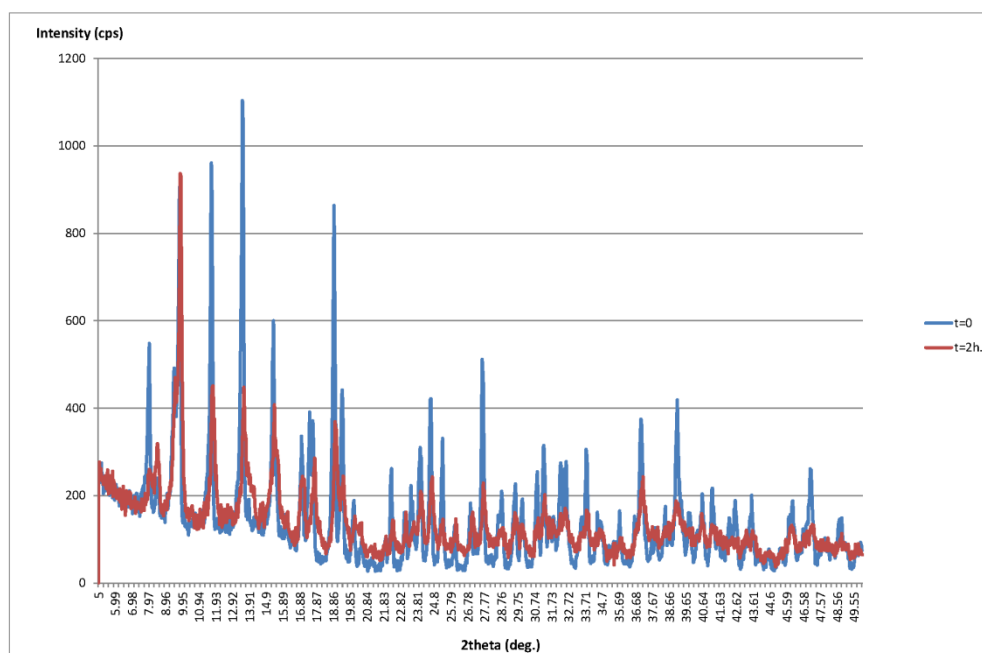


Fig.7.5d. Powder X-Ray diffractogram for the evolution of **9** at constant temperature $T=60^{\circ}\text{C}$. Time=0 (blue) and time=2 hours (red).

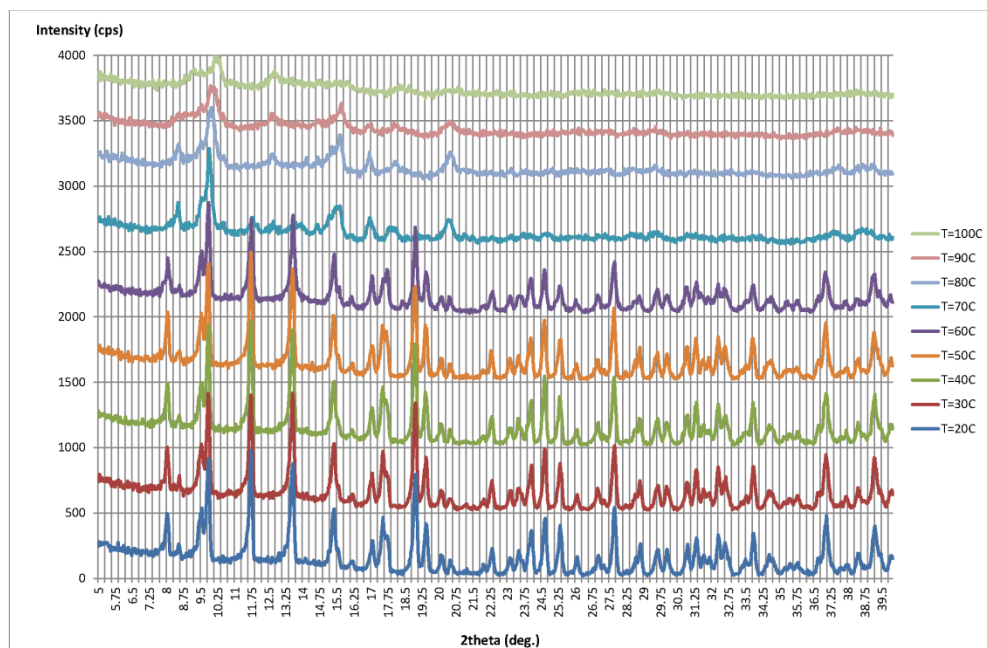


Fig.7.6. Powder X-Ray diffractograms for the evolution of 9 from 20 °C. to 100 °C. The sample was heated at each temperature 30 minutes before data collection.

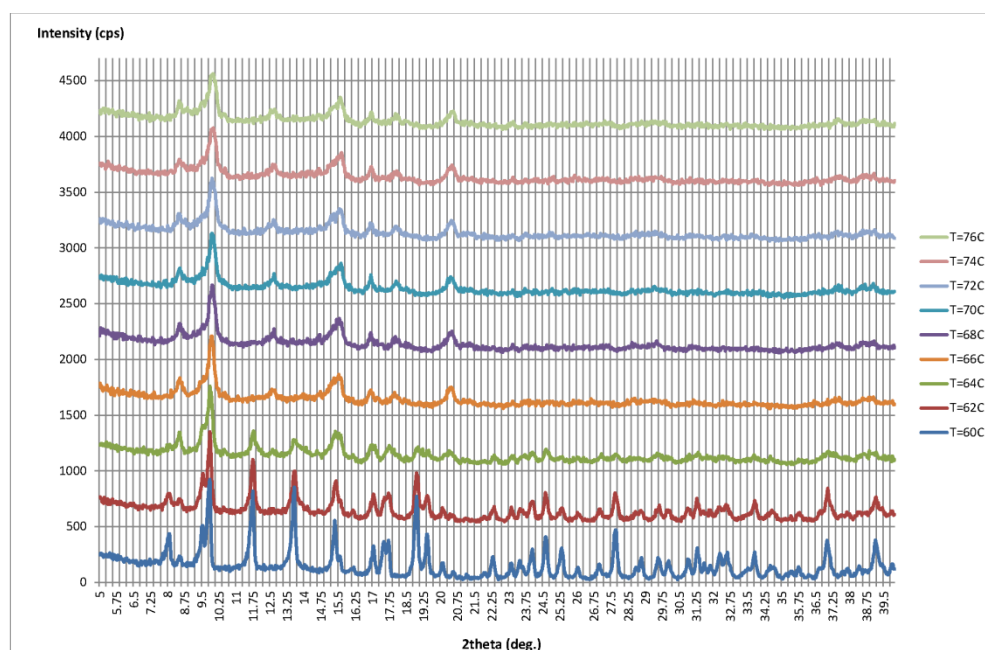


Fig.7.7. Powder X-Ray diffractograms for the evolution of 9 from 60°C to 76 °C. The sample was heated at each temperature 30 minutes before data collection.

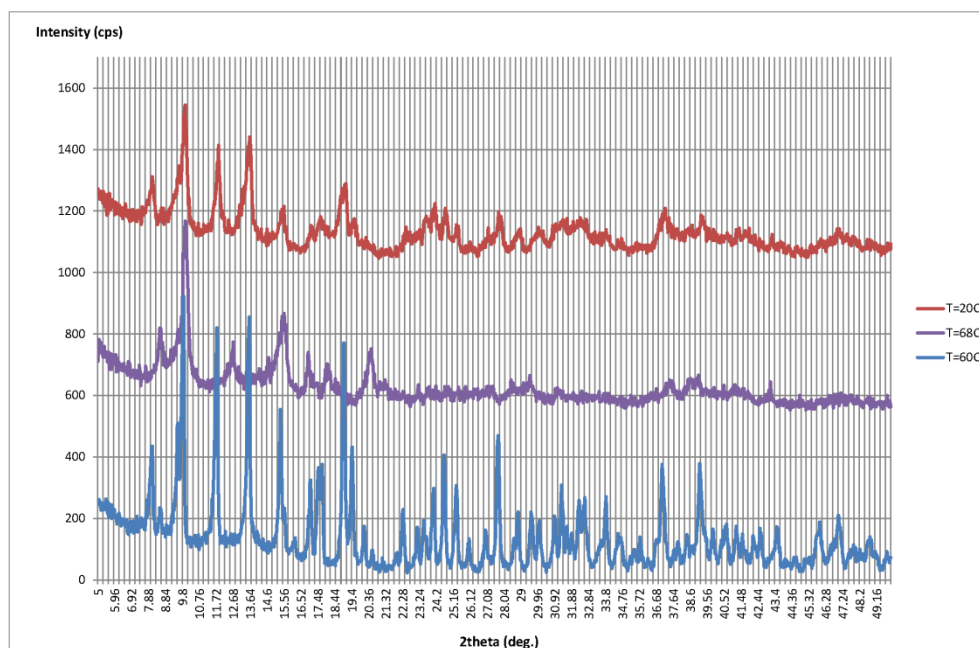


Fig. 7.8. Comparison of powder X-Ray diffractograms of **9** before transformation (blue, T=60°C), after dehydration (violet, T=68°C) and after rehydration (red, T=20°C).

7.3 Conclusions

A compound based on a Mn-citrate cubane is presented in this chapter. This is the first reported example of a neutral discrete TM citrate compound. A detailed study of its crystal structure shows an unprecedented coordination mode of the unit, which acts as a bidentate ligand chelating at a Mn(II) center through two inner oxygen atoms. In addition, the striking distribution of the Mn(II) units around the cube with a preferential orientation to the top face of the cube (according with the arbitrary definition of top used in this chapter), confers a directionality on the H-bond network, making the entire crystal structure polar.

Thermal studies using powder X-Ray diffraction reveal that the compound undergoes a reversible transformation under mild conditions. The transformation is inactive at any temperature below 60 °C and above this temperature it is controlled by kinetic effects. Under mild conditions (those used in the X-Ray powder studies) it takes place between 64 - 66 °C and involves molecules of water, since exposure of the compound to a humid atmosphere after the initial transformation restores the original sample. That is in agreement with results obtained from TGA, which show a massive loss of weight starting at the same threshold temperature found in the powder X-Ray

diffraction studies. We also know that the compound itself is stable up to 250 °C for a fast heating procedure; however, crystallinity is only preserved below 100 °C. We can conclude that the dehydration process needs an activation temperature of 60 °C, above which water molecules, most of them bonded to the main structure do not leave the sample. In addition, if heating is stopped before the crystallinity is lost, the process is reversible by simply leaving the sample at room temperature in the presence of humidity. The initial powder diffractogram is restored. This is an important feature as there are no pores or channels in this structure; nevertheless, water molecules can exit and enter the sample under mild conditions. This behaviour, the movement of solvent molecules within non porous materials is commonly known as the “vehicle mechanism”.

References

- [1] W. G. Wang, X. F. Zhang, F. Chen, C. B. Ma, C. N. Chen, Q. T. Liu, D. Z. Liao, L. C. Li, *Polyhedron* **2005**, *24*, 1656-1668.
- [2] A. Altomare, G. Cascarano, C. Giacovazzo, A. Guagliardi, *Journal of Applied Crystallography* **1993**, *26*, 343-350.
- [3] G. M. Sheldrick, *Acta Crystallographica Section A* **2008**, *64*, 112-122.
- [4] H. D. Flack, *Acta Crystallographica Section A* **1983**, *39*, 876-881.
- [5] H. L. Carrell, J. P. Glusker, *Acta Crystallographica Section B-Structural Science* **1973**, *B* *29*, 638-640.
- [6] Y. F. Deng, Z. H. Zhou, H. L. Wan, S. W. Ng, *Acta Crystallographica Section E-Structure Reports Online* **2003**, *59*, M310-M312.
- [7] O. Kennard, J. C. Speakman, J. D. H. Donnay, *Acta Crystallographica* **1967**, *22*, 445-&.
- [8] A. L. Spek, *Acta Crystallographica Section D-Biological Crystallography* **2009**, *65*, 148-155.

- [B1] A.I. Kitaigorodskii, *Molecular Crystals and Molecules*, Academic Press, New York, 1973.

- [P1] CrysAlisPro, Oxford Diffraction Ltd., Version 1.171.33.31

- [P2] Diamond. Klaus Brandenburg, Crystal Impact GbR, Bonn, Germany. Version 3.2i.

Supplementary Material

Re-refinement of the crystal structures of $M^{II}_2(H_2citrate)_2(H_2O)_4 \cdot N-N \cdot 2H_2O$ $M = Zn$ (CEFHUS),^{S1} Mn (EDUJUK),^{S2} $N-N = 4-4'$ -ethene-1,2-diyl dipyridine; $M = Mn$, $N-N = 1,2$ -bis(pyridin-4-yl)ethane (LEHPAR).^{S3} Reproduced from Falvello *et al.* 2014.^{S4}

To date the vast majority of discrete molecular transition-metal (TM) citrate complexes have been found to be ionic, while neutral complexes have been found largely to be polymeric. We are aware of only three TM citrate complexes that have been reported as neutral, discrete molecules. These are $[M^{II}_2(H_2citrate)_2(H_2O)_4] \cdot N-N \cdot 2H_2O$ [$M = Zn$ (CEFHUS in the Cambridge Database), Mn (EDUJUK), $N-N = 4-4'$ -ethene-1,2-diyl dipyridine; $M = Mn$, $N-N = 1,2$ -bis(pyridin-4-yl)ethane (LEHPAR)]. As the reduced diffraction data are available at the journal web site, we have reconsidered the nature of these structures and have performed new refinements in light of discrepancies between our findings and the original reports.

We tested the possibility that in the following structures the hydrogen atom assigned to O5 of a citrate carboxyl group might in reality reside on pyridyl atom N11 of the base.

CEFHUS: We calculated an omit map, omitting H5, using all other parameters as found in the published refinement. This showed a double well between O5 and N11A.

We performed an ab initio re-determination of the positions and displacement parameters of H1O and H5 (which we ended up calling H5N, since it appeared near N11). First, H1O was located in a difference map and refined freely. Its displacement parameter, which was convergent, had a too-small value of about 0.006 \AA^2 . A subsequent difference map revealed H1N near N11, as the first non-Zn-ghost peak in the difference map, Q7. This H atom refined to nearly ideal geometry and Uiso. The refinement was convergent. An omit map at this point showed slight density near the O5 position but nearly all of the positive density was at the new position of H1N, near N11.

EDUJUK: First, a difference map using the original model as published showed negative difference density over the region of the H atom in question, H5O, and pronounced positive difference density in the region that would be occupied by a putative H atom attached to N11. An omit map, omitting H5N from the original model, showed a double well pattern, but with the difference maximum in the region of O5 located very close to O5, about half-way along the O5---H5O bond.

We removed H1O (as a control atom) and H5O from the original model and refined the remainder. A difference map gave two peaks well differentiated from the others in density. The top peak had ideal geometry for the position of H1O, and the second peak had ideal

geometry for a hydrogen atom attached to N11. These two atoms were incorporated into the model and refined freely -- both positions and Uiso. The refinement converged with good Uiso and nearly ideal geometries for the two H atoms, with the second now called H5N. An omit map following convergence, with H5N omitted, showed a clear one-well pattern for H attached to N11. A difference map, without omitting H5N, was nearly flat.

LEHPAR: For LEHPAR, we re-examined the data and the refinement using files downloaded from the Acta Cryst., Section E web site. Using the atoms from the original CIF, we observed what appeared to be a double well between O5 and N11c (1-x,1-y,2-z), with stronger difference density near N11c. Upon re-refining the structure, when H5 is freed from riding behavior it migrates toward N11c. When its Uiso is freed, H5 moves completely to a geometrically correct position bonded to N11c. Its Uiso refines convergently to a value of 0.068(8) Å². At this point an omit map does not show significant density near O5. A difference map does not show significant negative difference density near the new position of H5. We conclude that the original double-well with a minor component near O5 was caused by leverage affecting other parameters when H5 was included in the incorrect position bonded to O5. A final test was to remove H1 and H5 completely from their reported positions and find them anew in a difference map following refinement of all of the other parameters, exactly as previously done by Kim *et al.* The two H atoms appeared as the top peaks in a difference map and were refined freely -- positions and Uiso. The resulting geometries and Uiso values were ideal.

We conclude that the H atom originally attributed to the carboxylate group O atom O5 is really located on the pyridyl nitrogen atom N11.

Refinement details are shown in Table S1.

Table S1. Comparison of the refinement details for compounds $M^{II}_2(H_2citrate)_2(H_2O)_4 \cdot N-N \cdot 2H_2O$ [M = Zn (CEFHUS),^{S1} Mn (EDUJUK),^{S2} N-N = 4-4'-ethene-1,2-diylpyridine; M = Mn, N-N = 1,2-bis(pyridin-4-yl)ethane (LEHPAR)].^{S3}

	CEFHUS		EDUJUK		LEHPAR	
	^a Original	^b New	Original	New	Original	New
Restraints/parms	7 / 239	0 / 224	8 / 241	0 / 225	7 / 239	0 / 225
Goodness-of-fit	1.092	1.072	1.084	1.025	1.051	1.059
R1, wR2 (obs)^c	0.0514, 0.1342	0.0506, 0.1319	0.0381, 0.0946	0.0364, 0.0896	0.0327, 0.0910	0.0307, 0.0846
R1, wR2 (all)	0.0604, 0.1395	0.0597, 0.1374	0.0482, 0.0975	0.0463, 0.0925	0.0351, 0.0924	0.0330, 0.0858
Δ/σ(max,mean)	0.000, <0.001	0.005, <0.001	0.001, <0.001	0.004, <0.001	0.001, <0.001	0.000, <0.001
$\Delta\rho$ range (e Å⁻³)	0.766, - 1.356	0.770, - 1.357	0.472, - 0.632	0.279, - 0.427	0.517, - 0.417	0.361, - 0.310

^aData for the refinement reported in the original publication, with one carboxylate protonated and the N atom from the N-N ligand unprotonated.

^bData for our re-refinement in which the H atom originally bonded to the carboxylate group of the citrate ligand has been located in the difference map and placed and refined freely coordinated to the N atom of the N-N ligand. That makes the three discrete compounds anionic instead of neutral as reported in the original publication.

^cthreshold $I > 2\sigma(I)$.

- S1 I. H. Hwang, P.-G. Kim, C. Kim, Y. Kim, Acta crystallographica. Section E, Structure reports online 2012, 68, m1305-1306.
- S2 I. H. Hwang, P.-G. Kim, J.-C. Lee, C. Kim, Y. Kim, Acta crystallographica. Section E, Structure reports online 2012, 68, m1516-1517.
- S3 I. H. Hwang, P.-G. Kim, C. Kim, Y. Kim, Acta crystallographica. Section E, Structure reports online 2012, 68, m1116-1117.
- S4 L. R. Falvello, E. Forcén-Vázquez, F. Palacio, S. Sanz and M. Tomás, Dalton Transactions 2014, 43, 10700-10704

8

1-D Manganese citrate cubanes.

Proton Cascade in a Molecular Solid.*

Water transport within confined spaces is of great interest in many areas of science and technology. As described in this chapter, neutron diffraction experiments have revealed proton transport in a non-porous crystal of a manganese citrate compound. We report a crystal of a manganese cubane complex that when it is exposed to an atmosphere of D₂O a total exchange of the hydrogen atoms by deuterium is observed for both coordinated and unbound molecules of water. The notable contrast in the scattering length of hydrogen and deuterium makes the neutron technique a conclusive tool for the study of isotope exchange. This is the first case in which a proton cascade has been observed in a molecular crystal. There is no ambiguity in the description of the steps involved in the mechanism.

The compound that undergoes this exchange, with formula $[\text{Mn}(\text{H}_2\text{O})_6]_{2n}\{[\text{Mn}_4(\text{C}_6\text{H}_4\text{O}_7)_4]\mu\text{-}[\text{Mn}(\text{H}_2\text{O})_4][\text{Mn}(\text{H}_2\text{O})_5]\}_n \cdot 8n(\text{H}_2\text{O})$, **10**, has been fully characterised by single crystal X-Ray diffraction, IR and other techniques. It also undergoes a reversible partial dehydration when it is exposed to air, through a single-crystal to single-crystal transformation. In presence of humidity, the initial compound is fully restored, preserving its crystallinity. The three steps of this process have been characterised by single crystal X-Ray diffraction.

8.1. Experimental

8.1.1 Synthesis

Reagents and solvents for the preparation of the compounds presented in this chapter were used as received. No further purification was needed.

The 1-D polymer $[\text{Mn}(\text{H}_2\text{O})_6]_{2n}\{[\text{Mn}_4(\text{C}_6\text{H}_4\text{O}_7)_4]_{\mu\mu}[\text{Mn}(\text{H}_2\text{O})_4][\text{Mn}(\text{H}_2\text{O})_5]\}_n \cdot 8n(\text{H}_2\text{O})$ **10**, was obtained as block-shaped colourless crystals in the same reaction system that produces compound **9**, presented in the preceding chapter. Only slight modifications in the last step of the synthesis are required to produce the present product. To a stirred solution of citric acid monohydrate (250 mL, 0.095 M) was added MnCO_3 (5.18 g, 45.1 mmol). The brownish mixture was heated to reflux for 5 h. under a stream of Ar and then filtered. The supernatant was cooled at room temperature for several days. It became orange and crystals of a subproduct with formula $(\text{C}_{12}\text{H}_{22}\text{Mn}_3\text{O}_{20})_n \cdot 4n(\text{H}_2\text{O})$ ^[1] and a ratio Mn/citrate of 3/2 were isolated. The solution was filtered and heated to reflux for 3 hours. Then boiling was continued without reflux until the volume was reduced to 50 mL. A white to pale-pink powder of compound **9** precipitated during the heating process. The mixture was filtered and cooled to ambient temperature before being placed into a closed vial. After several weeks, a mixture of crystals of **10** along with two subproducts with Mn/citrate ratio of 3/2 and formulas $(\text{C}_{12}\text{H}_{22}\text{Mn}_3\text{O}_{20})_n \cdot 4n(\text{H}_2\text{O})$ and $(\text{C}_{12}\text{H}_{26}\text{Mn}_3\text{O}_{22})_n \cdot 6n(\text{H}_2\text{O})$,^[1] respectively, were obtained.

The other compounds presented throughout this chapter were obtained from compound **10**. Compound **11** is the result of the exposure of a crystal of **10** to the atmosphere, it loses three molecules of water through a SC-SC transformation. If a crystal of **11** is exposed to a humid atmosphere, compound **10** is fully restored, preserving the crystallinity of the sample (compound **10b**).

In addition, in order to trace the pathway through which water molecules exit and enter the structure, neutron diffraction studies were performed for a suitable crystal of **10** (compound **10n**) and for the compound when the rehydration process was conducted under D_2O atmosphere (compound **12**). Details for their preparation are given in section 8.2.1.

8.1.2 Single Crystal X-Ray diffraction

Single crystal X-Ray diffraction data were collected in an Xcalibur S3 CCD-based four-circle diffractometer (Oxford Diffraction and Agilent Technologies). The program CrysAlis Pro^[P1] controlled data collection and processing. The structures were solved *ab initio* by direct methods^[2] and refined by full-matrix least-squares analysis.^[3] Non-hydrogen atoms were

refined with anisotropic displacement parameters. The methylene H atoms of the citrate ligands were placed at idealized positions and refined as riders on their respective parent C atoms with isotropic displacement parameters set to 1.2 times the equivalent isotropic U of the C atom. Hydrogen atoms of the water molecules were not found at the difference map due to the disorder and the background noise. The program Diamond^[P2] was used in the preparation of graphics. Data collection and structure solution and refinement details for both X-Ray and neutron experiments are shown in Table 8.1.

	10	11	10b	10n	12
Formula	^a (C ₂₄ H ₇₄ Mn ₈ O ₅₇) _n	^b (C ₂₄ H ₆₈ Mn ₈ O ₅₄) _n	^a (C ₂₄ H ₇₄ Mn ₈ O ₅₇) _n	^a (C ₂₄ H ₇₄ Mn ₈ O ₅₇) _n	^c (C ₂₄ H ₁₆ D ₅₈ Mn ₈ O ₅₇) _n
fw (g mol⁻¹)	1714.3	1660.3	1714.3	1714.3	1772.6
Radiation	X-Rays (Mo K α)	X-Rays (Mo K α)	X-Rays (Mo K α)	neutron	neutron
Wavelength (Å)	0.71073	0.71073	0.71073	1.4554	1.4554
Crystal system	monoclinic				
Space group	P2 ₁ /n				
Temp (K)	100(1)	100(1)	100(1)	20(1)	20(1)
a (Å)	12.6047(2)	12.6911(3)	12.5952(3)	12.6151(6)	12.6288(19)
b (Å)	21.2473(5)	20.3286(5)	21.2551(6)	21.2745(15)	21.2383(27)
c (Å)	22.3681(4)	22.2341(5)	22.3719(6)	22.3944(11)	22.4022(28)
β (°)	93.321(2)	93.128(2)	93.412(2)	93.359(3)	93.351(8)
V (Å³), Z	5980.5(3), 4	5727.7(3), 4	5978.6(4), 4	6000(3), 4	5998.3(14), 4
ρ calc (Mg/m³)	1.904	1.925	1.905	1.898	1.963
μ (mm⁻¹)^d	1.761	1.832	1.762	0.4016	0.0999
F (000)	3496	3376	3496	735	25304
Crystal size (mm³)	0.18 x 0.12 x 0.09	0.18 x 0.12 x 0.09	0.18 x 0.12 x 0.09	0.18 x 0.12 x 0.09	0.18 x 0.12 x 0.09
θ (min,max) (°)	3.76,27.50	3.75, 28.97	3.72,27.50	2.71,59.99	2.71,46.48
Refins collected	33051	38048	50521	16654	13746
Indep reflns	13315	13435	13402	8484	4863
R(int), R(σ)	0.0471, 0.0864	0.0547, 0.0998	0.0723, 0.0726	0.1435, 0.1539	0.2670, 0.2036
Completeness (θ)	0.996 (26.00)	0.995 (26.00)	0.995 (26.00)	0.878 (50.00)	0.781 (46.48)
Abs corr	multi-scan			for V can	

T(min,max)	0.8545,1.000 0	0.7876, 1.0000	0.4243, 1.0000	-	-
Restraints/pa rms	0/829	42/812	0/811	0/733	4/697
Goodness-of- fit	1.059	1.083	1.128	1.945	2.092
R1, wR2(obs)^e	0.0723, 0.1882	0.0771, 0.1867	0.0934, 0.2205	0.1265, 0.1583	0.1659, 0.2525
R1, wR2 (all)	0.1077, 0.1999	0.1307, 0.2014	0.1243, 0.2325	0.2004, 0.1703	0.2481, 0.2688
Δ/σ(max,mea n)	0.001, < 0.001	0.002, < 0.001	0.001, < 0.001	0.001, < 0.001	0.003, < 0.001
$\Delta\rho$ range^f	2.464, -0.833	3.964, -1.187	2.399, -1.009	1.691, -1.291	1.468, -1.114
<p>^a $[(\text{Mn}(\text{H}_2\text{O})_6)]_{2n}\{[\text{Mn}_4(\text{citr})_4]\mu\text{-}[\text{Mn}(\text{H}_2\text{O})_4][\text{Mn}(\text{H}_2\text{O})_5]\}_n \cdot 8n(\text{H}_2\text{O})$</p> <p>^b $[(\text{Mn}(\text{H}_2\text{O})_6)]_{2n}\{[\text{Mn}_4(\text{citr})_4]\mu\text{-}[\text{Mn}(\text{H}_2\text{O})_4][\text{Mn}(\text{H}_2\text{O})_5]\}_n \cdot 5n(\text{H}_2\text{O})$</p> <p>^c $[(\text{Mn}(\text{D}_2\text{O})_6)]_{2n}\{[\text{Mn}_4(\text{citr})_4]\mu\text{-}[\text{Mn}(\text{D}_2\text{O})_4][\text{Mn}(\text{D}_2\text{O})_5]\}_n \cdot 8n(\text{D}_2\text{O})$</p> <p>^dWavelength-specific linear attenuation factors for neutron radiation were calculated using the form available at http://www.ncnr.nist.gov/instruments/bt1/neutron.html using data from Sears.^{P6}</p> <p>^ethreshold $I > 2\sigma(I)$.</p> <p>^fFor the X-Ray analyses 10, 11 and 10b, the difference density has units of ($\text{e} \text{ \AA}^{-3}$). For the neutron analyses 10n and 12, the units of difference density are ($\text{fm} \text{ \AA}^{-3}$).</p>					

8.1.3 Neutron diffraction

Neutron diffraction data were collected at the Institut Laue-Langevin in Grenoble (France), on the D19 single-crystal thermal-neutron diffractometer equipped with a large-area position-sensitive detector based on Multi-Wire Chamber technology (120 by 30 deg. detection angle).^[P5] Data were measured at 20 K for the two data sets, using a wavelength of 1.4554(4) Å (Cu(220) monochromated).

Two data sets were collected, the first one for a pristine crystal of **10** (**10n**) and the second one for the crystal after rehydration conducted under a D₂O atmosphere (**12**). Data collection and structure solution and refinement details are shown in Table 8.1.

Data were processed in a similar manner using standard software to establish the unit cell and the symmetry. Integration of the data was performed using the program Retreat.^[P8] Only a geometrical correction for the absorption of the vanadium screens of the cryostat was applied due to the small size of the crystal. The refinement of the structures started from the coordinates of the non-hydrogen atoms of compound **10** from the single crystal X-Ray diffraction data collected at 100 K. All atoms had isotropic displacement parameters, which were permitted to vary freely at the beginning of the refinement. After the initial refinement,

hydrogen and deuterium atoms were located in a difference map, including those with half occupancy, distinguished without ambiguity by their different scattering lengths (-3.739 fm for protium and +6.669 fm for deuterium), even with the weaker diffraction data obtained for the rehydrated structure.

The final refinement of the model of **10n** led to a convergent refinement with reasonable displacement parameters for all the sites with a data-to-parameter ratio of 13. Restraints were not needed.

For **12**, it was necessary to apply a 2θ cutoff of 93° for a resolution of 1.0 Å due to the quality of the data after two phase transitions. The final refinement was convergent with some mild convergence problems due to the resolution of 1 Å; for instance, some O atoms moved away from their positions until the D atoms in their surroundings were located. However, the geometry and thermal parameters were as expected. Restraints were used only for the D geometry of three of the nine free water sites. The hydrogen atoms of the CH₂ groups of the citrate ligands were found as negative peaks. They were used as a control group to test the ability of the analysis to distinguish H from D. Tests were conducted for mixed H/D populations at the H positions of the citrates as well as for the water sites. Physically meaningless results were obtained for populations higher than 10% D at the citrate groups or H at the water sites. Sixty-nine D sites were found and refined with acceptable anisotropic displacement parameters. Seven of them, located in disordered regions, present larger but reasonable values.

The atom names in **12** are based as far as possible on the names of the corresponding atoms in **10** in order to have a measure of concordance between the structures for comparative purposes.

8.1.4 FT-IR spectroscopy

FT-IR spectra of compound **10** and **11** were measured on a Perkin-Elmer Spectrum 100 FT-IR Spectrophotometer with ATR accessory in the range of 4000 - 350 cm⁻¹ (Figures 8.1a,b).

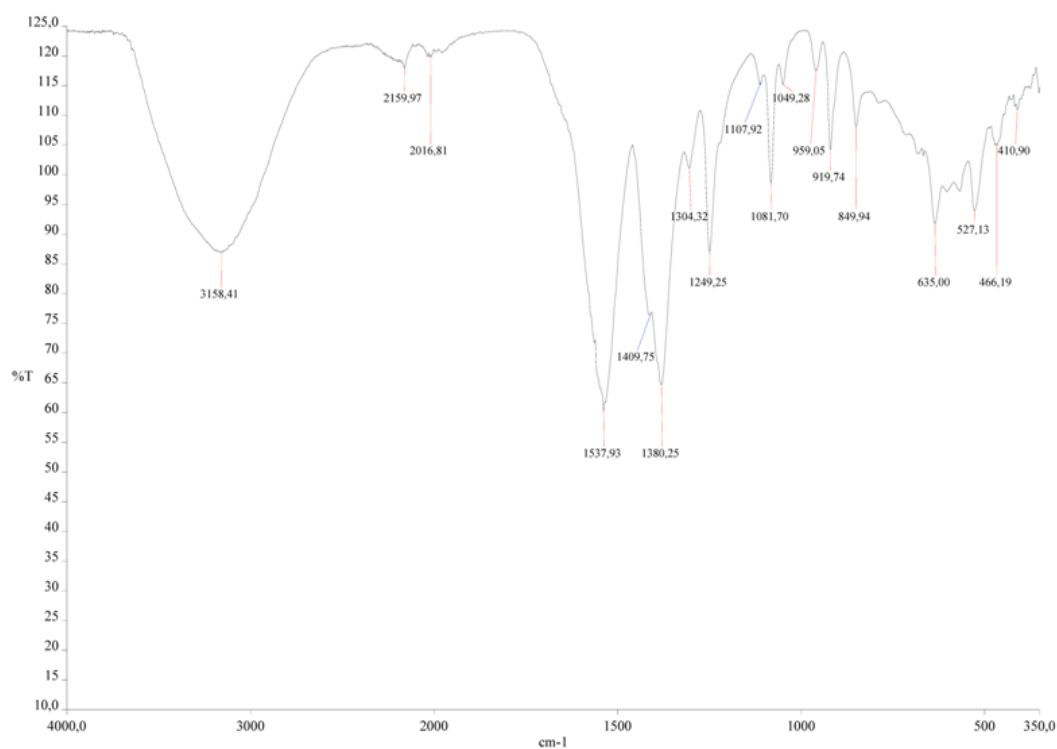


Fig. 8.1a. IR spectrum of **10**.

IR of **10** (neat compound, cm⁻¹): $\nu(\text{OH})$ 3158.41 (w); $\nu(\text{C=O})$ 1537.93 (w); $\nu(\text{C-H})$ 1380.25 (w); $\nu(\text{C-H})$ 1249.25 (n); $\nu(\text{CO})$ 1107.92, 1081,70 and 1049.28 (t).

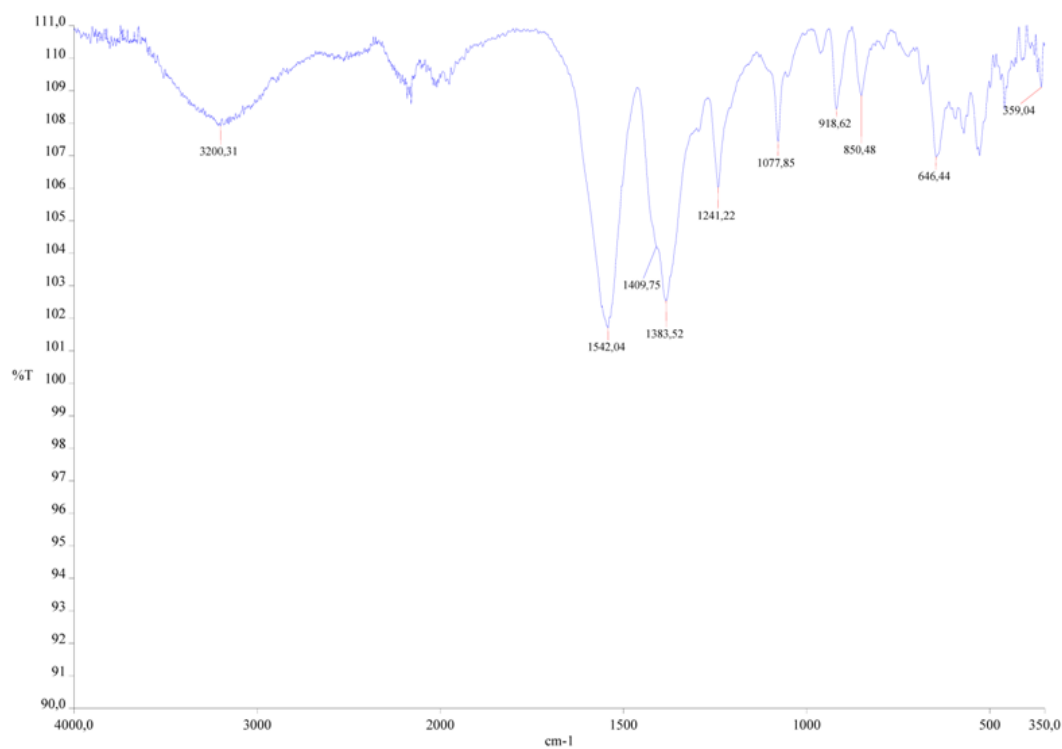


Fig. 8.1b. IR spectrum of **11**.

IR of **11** (neat compound, cm^{-1}): $\nu(\text{OH})$ 3200.31 (w); $\nu(\text{C}=\text{O})$ 1542.04 (w); $\nu(\text{C}-\text{H})$ 1383.52 (w); $\nu(\text{CH})$ 1241.22 (n); $\nu(\text{CO})$ 1077.85 (t).

8.1.5 Elemental analysis

Elemental analysis was performed on a Perkin Elmer 2400 CHNS/O analyser. Results obtained were C, 17.15%; H, 3.97%.

Calculated for 8 molecules of free water (compound **10**): $(\text{C}_{24}\text{H}_{74}\text{Mn}_8\text{O}_{57})_n$, MW: 1714.3 %C 16.81, %H 4.35; Calculated for 6 molecules of free water (water loss of 2 molecules): $(\text{C}_{24}\text{H}_{70}\text{Mn}_8\text{O}_{55})_n$, MW: 1678.3 %C 17.18, %H 4.20; Calculated for 5 molecules of free water (compound **11**): $(\text{C}_{24}\text{H}_{68}\text{Mn}_8\text{O}_{54})_n$, MW: 1660.3 %C 17.36, %H 4.13.

The elemental analysis was done with a sample composed of single crystals selected and cleaned carefully one by one in order to prevent contamination. So, as expected, we can conclude that under the experimental conditions (room conditions) the compound suffers a water loss of 2 - 3 molecules of water.

8.2. Results and discussion

8.2.1 Synthesis

Compound **10** is the fourth compound of a series of four species obtained from the same reaction. The first product is compound **9**, presented in the previous chapter. It appears when the final solution is heated at about 90 °C. However, if the solution is left at room temperature crystals of two different subproducts, both polymers with a Mn/citrate ratio of 3/2 are obtained, as single crystals. In these products, the hydroxyl group of the citrate ligand is protonated. As time passes, the formation of those compounds decreases at the same time that crystals of **10** appear. If the mixture is then filtered and placed again into a closed vial, crystals of **10** are obtained as the major product with minor impurities of the above mentioned compounds. This suggests that compound **10** is the thermodynamically favoured product. Other compounds have also been isolated and characterised. However they do not emerge consistently from the reaction. The first one is obtained after several months; it has an Mn/citrate ratio of 3/2 and the hydroxyl group protonated.^[4] The other was only obtained one time when the reaction went to dryness under heating. This product has an Mn/citrate ratio of 1/1 and the hydroxyl group and one methylenecarboxylate are protonated.^[5]

The abundance and variety of products makes it clear that there is a subtler equilibrium of many species in solution. Slight modification of the reaction conditions may displace the

equilibrium for the obtainment of a certain compound or maybe for the crystallization of a different derivative, not existing in solution.

The structure of a single crystal of **10** was also determined by neutron diffraction. We will refer to this analysis as **10n**.

The second derivative presented in this chapter is $[\text{Mn}(\text{H}_2\text{O})_6]_{2n}\{[\text{Mn}_4(\text{C}_6\text{H}_4\text{O}_7)_4]_{\mu-}[\text{Mn}(\text{H}_2\text{O})_4][\text{Mn}(\text{H}_2\text{O})_5]\}_n \cdot 5n(\text{H}_2\text{O})$ **11**. It is obtained by partial dehydration of **10**. When a single crystal of **10** covered by a thin layer of perfluorinated oil is exposed to the atmosphere under ambient conditions for three days, it undergoes a single-crystal to single-crystal transformation in which it loses three molecules of water to give a crystal of compound **11**. It is the same compound as **10**, with three fewer molecules of free water in the crystal.

When this crystal is enclosed in a sealed tube with a piece of wet cotton at its bottom for several hours, compound **10** is completely restored. The crystal reabsorbs three molecules of water per formula unit, and these return to the same positions that they occupied in the pristine sample of **10**. This product will be called **10b**.

If a crystal of compound **11** is exposed to a humid atmosphere of D_2O instead of H_2O for 3 days at room temperature, a new derivative in which all of the hydrogen atoms, with the exception those of the citrate CH_2 groups, have been substituted by deuterium (compound **12**). *N. b.*, during the rehydration process, the crystal is not in contact with the wet cotton at any moment and it is covered with a thin layer of perfluorinated oil. The wet cotton is only used to create the humid atmosphere.

8.2.2 Single Crystal X-Ray diffraction

Compound **10** crystallises in the monoclinic system, space group $\text{P}2_1/n$. The cubane corresponds to isomer B. For the reference asymmetric unit there are three central C atoms from the citrates which are not chiral and the fourth one is S. The asymmetric unit includes a complete cubane fragment. A bridging Mn(II) centre (Mn5) is attached to its periphery through an external oxygen atom of a short arm (S1e), and the polymer is propagated through this bridge by binding to an external oxygen atom from a short arm of a neighbouring cubane unit (S3e). The carboxylate oxygen atoms coordinated to the bridging Mn(II) centre are mutually trans. Mn5 completes its coordination sphere with 4 molecules of water. Attached to an external oxygen atom of a long arm (L1e) there is a pendant penta-aquo manganese (II) unit (Mn6) (Figure 8.2a). The cubanes form 1-D chains propagated by the n -glide plane perpendicular to the crystallographic b -axis. The negative charge of the polymer is balanced by

two $[\text{Mn}(\text{H}_2\text{O})_6]^{2+}$ cations residing in the space between the polymeric chains (Mn7 and Mn8) (Figures 8.3 and 8.4).

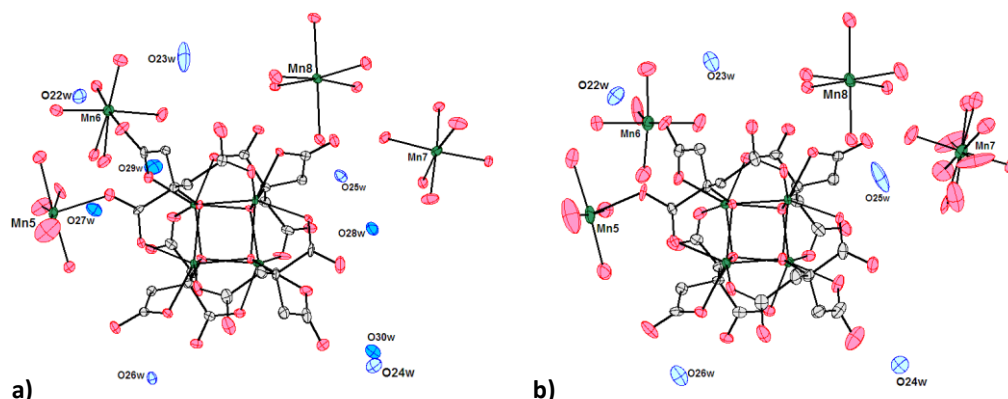


Fig. 8.2. A complete cubane unit for **10** (a) and **11** (b) with their bridging and pendant Mn(II) units and two hexaquo manganese (II) cations balancing the charge of the polymer. Water molecules are represented in blue. Those that exit the structure during the dehydration process are in dark blue (note that these are not present in **11** as it is the dehydrated species), while the others are drawn in light blue. Thermal ellipsoids (probability 50%).

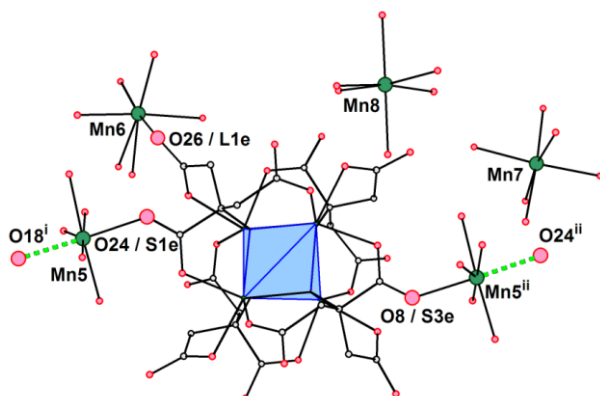


Fig. 8.3. A complete cubane unit of **10** with its two Mn(II) bridges showing the propagation of the polymer, a pendant Mn(II) unit and the two counterions. i: $(0.5+x, 1.5-y, 0.5+z)$, ii: $(-0.5+x, 1.5-y, -0.5+z)$.

There is a total of 21 molecules of water coordinated to the Mn(II) units and 8 free water molecules per formula unit, distributed over 9 crystallographic sites. O1w (coordinated to Mn5) and O7w (coordinated to Mn6) are disordered over two sites with half occupancy each (O1wa,b and O7wa,b). One of the half-occupied molecules of free water (O27w) can coexist with the congeners O1wa and O7wb but not with the others. No restraints were needed for these sites.

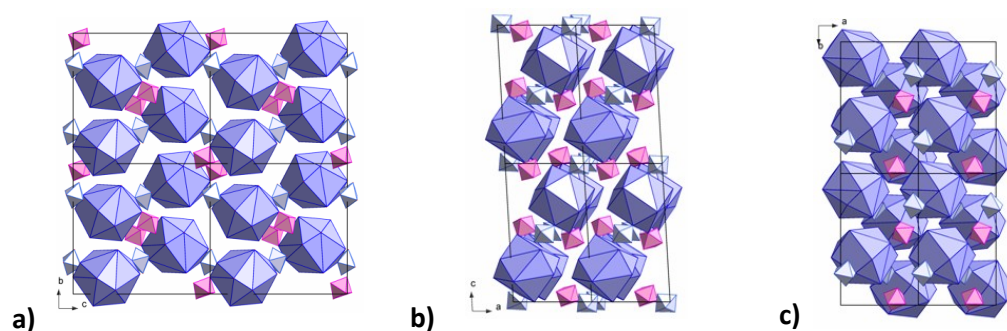


Fig. 8.4. Representation of **10** showing the polyhedra formed by the 12 peripheral oxygen atoms of the cube (blue), including the bridging (light blue) and pendant (pink) Mn(II) units as tetrahedra; views along the *a*-, *b*- and *c*-axes (*a*, *b* and *c* respectively). Counterions and free molecules of water have been omitted for clarity.

There is an extended net of strong hydrogen bonds throughout the structure due to the high number of molecules of water and partially negative oxygen atoms from the methylenecarboxylate and carboxylate groups.

There are no significant voids or channels in the crystal so that there is no clear pathway for the water molecules to exit the sample. Those molecules have one of their shortest H-bond contacts with an oxygen atom of either a citrate ligand or a Mn-bound molecule of water. The four sites occupied by the molecules of water lost are not embedded in a free water environment but are close to the polymer.

The structure of compound **11** is almost identical to that of compound **10** (Figure 8.2b). The only significant difference is that four crystallographic sites are vacated as a result of the egress of three molecules of water. There is a rotational disorder around one of the free Mn(II) units (Mn7). The rotation is around the axis O11w-Mn7-O13w in such a way that both congeners (a and b) share these two axial molecules of water. The equatorial plane is occupied by four molecules of water disordered over two sites each (O10wa, O12wa, O13wa and O15wa and O10wb, O12wb, O13wb and O15wb). The final occupancies of the congeners result in a ratio *a*/*b* of 2/1. For this disorder assembly (using IUCr terminology defined in the Core CIF Dictionary: http://www.iucr.org/__data/iucr/cifdic_html/1/cif_core.dic/index.html), the two disorder groups were refined with geometrical similarity restraints, and the anisotropic displacement parameters of the partially occupied O atoms were restrained to similarity for any pair of O sites within 1.7 Å of each other. No further restraints or constraints were used for this refinement.

It is observed that in the structure of **10**, three of the molecules which become disordered in **11** (O10w, O12w and O14w) form hydrogen bonds with two of the mobile molecules of water that exit the structure when **10** is transformed to **11** (O28w and O30w) (Table 8.2).

Table 8.2. Hydrogen bond distances for the disordered water molecules around Mn7 and two of the free water molecules that will exit the sample in the transformation of compound **10** to compound **11**.

Atom 1	Atom 2	d (Å)	Symm op.
O12w	O28w	3.013(12)	x, y, z
O14w	O28w	2.778(11)	-x, 1-y, -z
O10w	O30w	2.758(7)	-x, 1-y, -z
O14w	O30w	2.795(7)	-x, 1-y, -z

8.2.3 Neutron diffraction

A well-formed crystal of compound **10** was selected and used as a seed in a new fresh solution. The partial evaporation of the solution in air together with the addition of fresh solution over a period of two months produced a crystal of **10** with dimensions of approximately 1 x 1 x 1 mm. A glass tube was prepared with wet cotton at its bottom and a dab of grease on its side. The crystal was then transferred directly from the solution to the tube, still humid. It was pressed into the dab of grease, avoiding contact with the wet cotton. The tube was sealed in order to preserve the humidity and assure the retention of **10** without formation of **11**.

The first data set was collected from that crystal at 20 K. After that, the sample was brought to room temperature and the crystal was taken out of the tube and dried with lint-free tissue paper to remove external moisture. The crystal was fixed to the wall of a dry tube with dry cotton at its bottom, using perfluorinated oil. The tube was kept inside a desiccator for 18 h. after which a dab of colourless grease was used to hold the crystal more firmly to the wall of the tube. The system was left inside the desiccator for a total of 36 h., after which the crystal was opaque. An attempt to collect data from this crystal at 20 K did not succeed. As previous experiments done with smaller crystals using X-Ray diffraction had shown that the quality of the dehydrated crystal is worse than that of the hydrated one, it was concluded that the derivative formed by the dehydration process was compound **11**.

A syringe was used to wet the cotton with D₂O while the dehydrated crystal was still attached to the wall of the tube. The system was sealed and the crystal was kept in this atmosphere for 24 h. After that, the tube was placed back on the diffractometer and the temperature was lowered to 20 K. The tube broke and the temperature had to be raised to room temperature, after which the crystal and the wet cotton were placed in a new tube. The crystal was not in contact with the cotton at any time. The temperature was lowered to 20 K again and data were collected. After the experiment, a drop of condensed water, considerably

smaller than the crystal, was observed in contact with the grease holding the crystal. We do not think that this fact could affect the result because of the size of the drop, and also because grease was present to protect the crystal. In addition, other experiments confirm the rehydration process in the presence of only a humid atmosphere. Possibly, the drop was formed during the warming-up process after the data collection.

8.2.4 A model for the proton wire

Isotopic substitution of protium for deuterium has been widely used for the study of a variety of processes, some of the most important of which involve water movement in biological systems. The marked difference in their scattering lengths makes neutron diffraction a convenient tool for these studies.

The initial motivation of these studies was the observation of a reversible dehydration-rehydration process preserving the crystallinity of the sample in the absence of pores or channels. As there was not a clear pathway for the water molecules to exit and enter the structure, it was thought that another mechanism must be operative in the crystal. With the aim of clarifying the paths for the water egress and reuptake, the rehydration process was conducted under D_2O atmosphere. As expected, the H atoms from the citrate groups were still hydrogen (*i.e.*, protium). However, surprisingly, the remaining H atoms in the structure, namely those of the free and coordinated water molecules had been substituted by deuterium. The same hydrogen disorder as in the pristine sample was observed. As three molecules of water (4 crystallographic sites) leave the structure during the dehydration, these water molecules should enter the structure from the D_2O vapour as complete water fragments. Nevertheless, the fact that 26 H_2O moieties, 21 of which are bonded to Mn atoms, have had their H substituted by D, preserving the crystallinity of the sample with no channels, obviates the consideration of this mechanism for the complete interchange, as it is sufficiently remote on energetic and steric grounds. A proton cascade could explain the complete interchange and the H/D disorder around the water molecules.

There are 30 water sites, 8 of which present an oxygen atom surrounded by three deuterium atoms, one fully occupied and the others with half occupancy. That corresponds to two possible congeners of the water moiety sharing the oxygen atom and the deuterium with complete occupancy. The O---D distances as well as the D-O-D angles are in the expected ranges. This has been observed in compounds where a water molecule is disordered over two sites with the O atom and one H atom common to the two congeners.

In addition, 2 of the 30 formula units are formed by an oxygen atom bonded to 4 deuterium atoms, all half occupied. It is possible to describe two water fragments sharing the central oxygen atom, with good geometries. This type of disorder is commonly observed in neutron diffraction studies of cyclodextrins and is the result of a flip-flop of the water molecules.

In order to understand the mechanism through which the complete interchange of H by D takes place when the crystal is exposed to a humid atmosphere of D_2O , a detailed explanation of the water molecules in structures **10n** and **12** is given in Table 8.3.

Table 8.3. Comments on the disorder and geometry of the water molecules in **10n** and **12**. s.o.f. values in brackets. s.o.f of the oxygen atoms is omitted for complete occupancies.

Compound 10n	
Mn5	
O1wa/O1wb	both with half occupancy
O18a/O18b	both with half occupancy (O18a coexists with O1wa and O18b with O1wb)
Mn6	
O7wa/O7wb	both with half occupancy
O6W	H6a (1.0), H6b (0.5), H6c (0.5)
O7WA	H7a (1.0), H7b (0.5)
O7WB	H7a (1.0), H7c (0.5)
Mn7	
O10W	H10a (1.0), H10b (0.5), H10c (0.5)
O12W	H12a (1.0), H12b (0.5), H12c (0.5)
O14W	H14a and H14c (all 0.5) coexist H14b and H14d (all 0.5) coexist
Unligated water molecules	
O23w (0.5)	H23c, H23d (0.5)
O23z (0.5)	H23y, H23z (0.5)
O24w	no disorder
O25w	no disorder
O26w	no disorder
O27w	half occupied (coexists only with O1wb due to the short contact with O1wa (O1wa...H27b, 1.34 Å)
O28w	half occupied
O29w (0.5) / O29z (0.5).	H29a (0.5), H29b (0.5), H29c (0.5) Any combination of two H sites is nearly acceptable. Better geometry: O29w/H29a/H29c and O29z/H29b/H29c Displacement parameters of H29c suggest more occupancy. That is dismissed due to the impossible contact H29c... H1b (1-x, 1-y, 1-z) 1.05 Å and the possible but short contact H29c...O1wb (1-x, 1-y, 1-z) (2.04(3) Å)
H30w	H30a (0.5), H30b (0.5), H30c (0.5)
Compound 12	
Mn5	
*O1wa/O1wb Similar refinement as in 10n	D1a (1.0) / O1wa / D1c (0.5): sort contact of O1wa with D27b (0.5), they do not coexit. D1a (1.0) / O1wb / D1b (0.5)
Mn6	
O5w	D5c (1.0), D5d (1.0)
O6w	D6a (1.0), D6b (0.5), D6c (0.5). Angles D6a-O6w-D6b and D6a-O6w-D6c tight, no

	restraints used.
O7w Not split	D7a (0.5) / O7w / D7c (0.5) D7b (0.5) / O7w / D7d (0.5) D7a and D7c have large displacement parameters but acceptable geometry
O8w	D8a (1.0) and D8b (1.0) – Geometry OK
O9w	D9c (1.0) and D9d (1.0) – Geometry OK
Mn7	
** O10w	D10a (1.0) / O10w / D10b (1.0 – shared with O30w) D10a (1.0) / O10w / D10c (0.5)
O11w	D11c (1.0) and D11d (1.0) – Geometry OK
O12w	D12a (1.0) / O12w / D12b (0.5) – Geometry OK D12a (1.0) / O12w / D12d (0.5) – Geometry OK
O13w	D13a (1.0) and D13b (1.0) – Geometry OK
O14w	D14b (2/3) / O14w / D14c (2/3) D14c (2/3) / O14w / D14d (2/3) There are four half occupied sites in the original H-containing compound. The three D found here match three of those in the original structure. A possible fourth site was found, but the refinement showed instability. Restraints: sadi O14w D14b O14w D14c O14w D14d (Similarity restraints on the three O---D distances.)
O15w	D15a (1.0) and D15b (1.0) – Geometry OK
Mn8	
O16w	D16a (1.0) and D16b (1.0) – Geometry OK
O17w	D17c (1.0) and D17d (1.0) – Geometry OK
O18w	D18a (1.0) and D18b (1.0) – Geometry OK
O19w	D19a (1.0) and D19b (1.0) – Geometry OK
O20w	D20a (1.0) and D20b (1.0) – Geometry OK
O21w	D21c (1.0) and D21d (1.0) – Geometry OK
Unligated water molecules	
O22w	D22a (1.0) and D22b (1.0) – Geometry OK
O23w Not split	D23y (1.0) and D23z (1.0) – Geometry OK
O24w	D24a (1.0) and D24b (1.0) – Geometry OK
O25w	D25a (1.0) and D25b (1.0) – Geometry OK (angle 94°)
O26w	D26a (1.0) and D26b (1.0) – Geometry OK
O27w (0.5)	D27a (0.5) and D27b (0.5 – short contact with O1wa)
O28w (0.5)	D28a (0.5) and D28b (0.5) – disordered around an inversion center. O-D distance are OK, D-O-D angle is 86° (In the H-containing structure the angle is 116°)
* O29w	D27a (1.0), D29b (0.5), D29c (0.5) D29c collides with a symmetry relative of D1b
** O30w	D30a (1.0) and D30b (0.5)

	O30w contacts a symmetry relative of D10b
* See further notes on region 1	
** See further notes on region 2	

Further explanation of the water disordered in selected areas due to their importance in the interpretation of the results:

Region 1:

The coordinated water molecule O1wa/O1wb and the free, half occupied O27w are involved in this disordered region (Figure 8.5). Half occupied D1b collides with a half occupied symmetry relative of D29c (1-x, 1-y, 1-z). They occupy the space between the half occupied O1wb and the fully occupied O29w at a distance of 1 Å. This implies that O29w must have two disordered orientations, D29a/O29w/D29b and D29a/O29w/D29c (as D29a is fully occupied). Despite the fact that D29b is consistent in the difference map and refines stably, the angle formed with O29w and D20a is almost linear. Although the results are indubitable, we are not able to provide a chemically reasonable explanation for this region. However, we prefer to attribute this unacceptable geometry to either the low resolution of the data or to an as-yet unexplained structural feature, instead of overriding the data, even at 1 Å resolution.

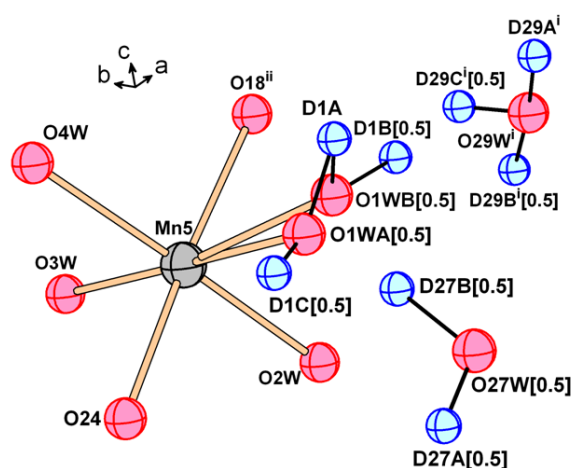


Fig. 8.5. Disordered zone 1. Complete Mn5 fragment coordinated by O1wa/O1wb and the free molecule of water O29w. O27w is also present in this region. i: (1-x, 1-y, 1-z), ii: (0.5+x, 1.5-y, 0.5+z). Reproduced from Falvello *et al.* 2014.^[6]

Region 2:

This zone affects O10w and O30w (Figure 8.6). D1b is slightly displaced from the midpoint of the line segment connecting O10w and O30wⁱⁱⁱ (iii: -x, 1-y, -z). It was refined with full occupancy. O10w has two additional D atoms (D10a (1.0) and D10c (0.5)). The same is found for O30w; it is bonded to D30a (1.0) and D30b (0.5). All atoms were refined freely, all were stable, and all have displacement parameters within expected ranges of values. D10b presented a large U_{iso} value (0.11 Å²). The distance O10w-D10b is longer than expected (1.390 Å) as is the distance O30wⁱⁱⁱ-D10b is 1.256 Å. The angles D10a-O10w-D10b, D10a-O10w-D10c, D30aⁱⁱⁱ-O30wⁱⁱⁱ-D10b and D30a-O30w-D30b are all close to the expected tetrahedral value.

This situation has been interpreted as a two-way disorder at both O10w and O30w. The two half-occupied congeners of the water at O10w will be D10a/O10w/D10b and D10a/O10w/D10c; and those at O30w are D30a/O30w/D30b and D30a/O30w/D10bⁱⁱⁱ. We assume that the site found for D10b is an average position, and that would place one congener of D10b closer to O10w and another closer to O30w. Anisotropic refinement of D10b would ratify (or otherwise) this interpretation, although the quality of the data did not permit this. The distance O10w-O30wⁱⁱⁱ (2.64(3) Å), is consistent with potential wells nearer the middle of the H-bond, which is also consistent with the long O-D distances.

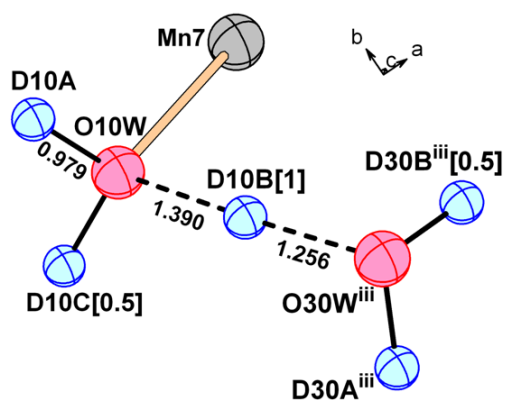


Fig. 8.6 Disordered zone 2. Only Mn5, its coordinated water molecule O10w and the free molecule of water O30w have been represented. iii: $(-x, 1-y, -z)$. Reproduced from Falvello *et al.* 2014.^[6]

The proposed model for proton transport, based on the hydrogen disorder in the initial compound **10** is in accord with the Grotthuss mechanism. It is based on the concerted hopping of a proton from one molecule of water to a neighbouring one, followed by the reorientation of the molecule to restore the initial situation; this leaves the system ready for a new hopping-reorientation cycle. The hydrogen disorder observed can be interpreted as the superposition of two different positions of a water molecule, frozen at the low temperature of the diffraction measurements and averaged over the whole crystal. We can identify a chain of double-minimum hydrogen potentials which fit the two canonical states of a Grotthuss mechanism involving the movement of hydrogen atoms of both coordinated and free water, and which traverse the crystal parallel to the crystallographic *a*-axis.

The initial indication of the Grotthuss mechanism as the most likely means of proton transport in the crystal was the identification of a sophisticated H-bonding network through the crystal. Water molecules, both bonded and free, are connected forming H-bonded patterns that traverse the crystal. Figure 8.7a shows a linear aggregate parallel to the *a*-axis (red). There are other pathways such as the cyclic motif shown in Figure 8.7b formed by a linear chain parallel to the *b*-axis (blue).

In Figure 8.7a a repeat unit of a chain is shown. O28w and O30w are unligated water. O28w (half-occupied) lies at 1.94(3) Å from its inversion-related congener, O28wⁱ. O10wⁱ and O14wⁱ are the O atoms of aqua ligands coordinated to a $[\text{Mn}(\text{H}_2\text{O})_6]^{2+}$ cation, Mn7ⁱ. With reference to the figure (symmetry operations defined in the caption), O28w and its congener O28wⁱⁱ are separated by the lattice repeat [100]. The repeat unit of the chain is O28w ... O14wⁱ

... O30w ... O10wⁱ ... O10wⁱⁱ ... O30wⁱⁱⁱ ... O14wⁱⁱ ... O28wⁱⁱⁱ (there are eight water sites with a center of symmetry in the middle, between O10wⁱ and O10wⁱⁱ). O28w is surrounded by two H atoms half-occupied as is O28w itself. Three H sites are found for O10w and O30w, one of the H sites has full occupancy and the other two are half-occupied. Four half occupied H atoms are found for O14w. At all of the water sites, two geometrically acceptable water fragments can be described with a total stoichiometry of one full aqua unit. Table S8.1 and S8.2 show the H-bonds formed between the atoms forming the chain shown in Figure 8.7a for compounds **10n** and **12**.

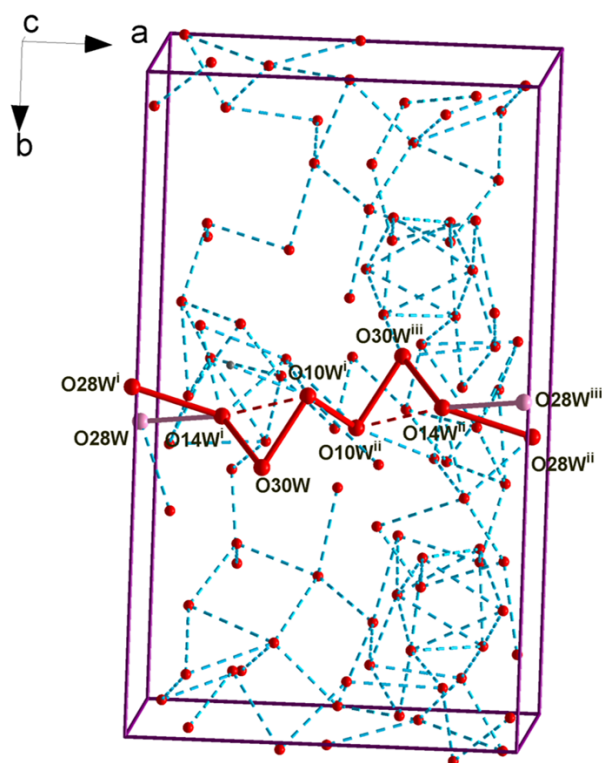


Fig. 8.7a. Unit-cell water content, showing one of the hydrogen-bonded water chains. O28w is half-occupied. O28w-O28wⁱ 1.92(3); O28w-O14wⁱ 2.766(19); O28wⁱ-O14wⁱ 3.094(19); O14wⁱ-O30w 2.803(14); O14wⁱ...O10wⁱ 3.190(12); O30w-O10wⁱ 2.753(13); O10wⁱ-O10wⁱⁱ 2.788(12). i: (-x, 1-y, -z), ii: (1+x, y, z), iii: (1-x, 1-y, -z). Reproduced from Falvello *et al.* 2014.^[6]

According to the disorder observed in the atomic sites occupied by oxygen and hydrogen atoms in structure **10n**, three different pathways for proton transfer can be described. They represent three different ways through which a proton can be transferred from one molecule to other (Figures 8.8 and 8.9).

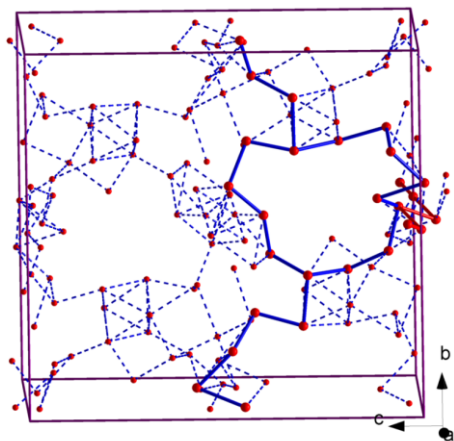


Fig. 8.7b. Linear H-bonded chain propagated parallel to [010], with an attached cyclic motif joining this chain to that shown in (a). Reproduced from Falvello *et al.* 2014.^[6]

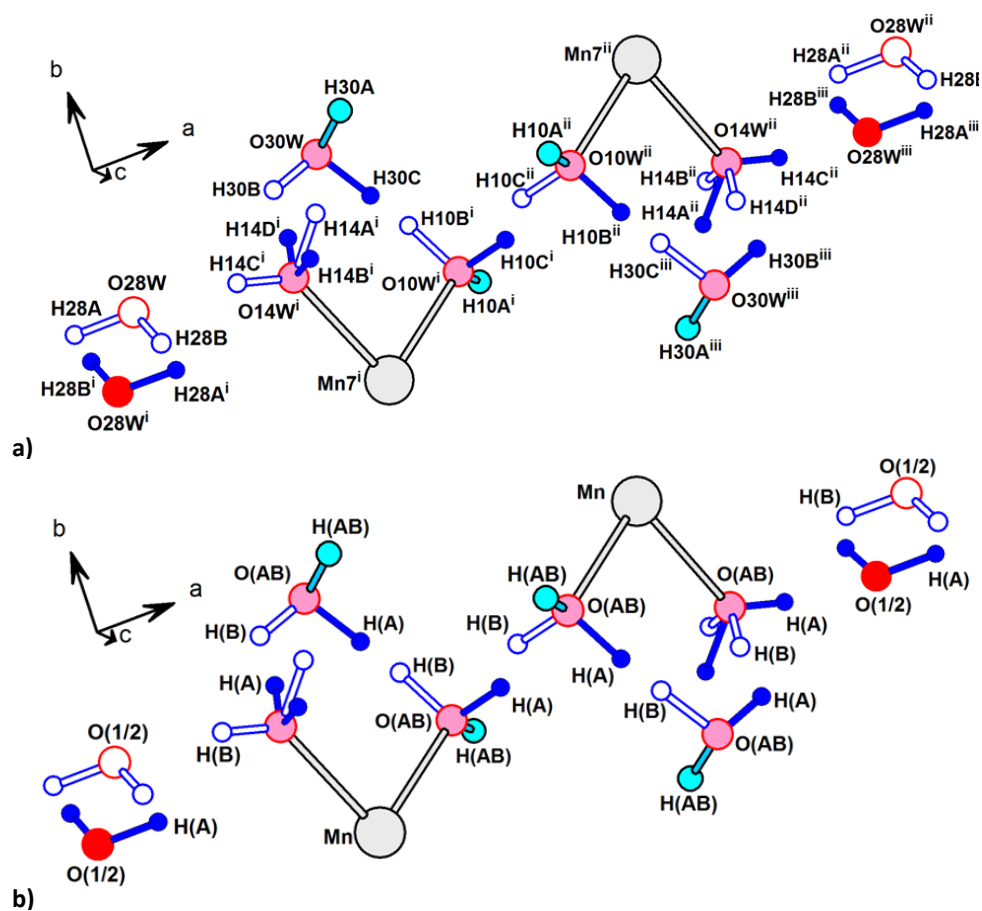


Fig. 8.8. One repeat unit of a water chain along the crystallographic a -axis, showing disorder. (a) Original crystallographic nomenclature and symmetry designations. Because of the disorder of O28w, alternative bounds for the repeat unit are O28wⁱ and O28wⁱⁱ. Proton hopping distances (Å) are: H28aⁱ...H14cⁱ and H14cⁱⁱ...H28aⁱⁱ, 1.55(4); H14dⁱ...H30b and H30bⁱⁱⁱ...H14dⁱⁱ, 1.39(4); H30c...H10bⁱ and H10bⁱⁱ...H30cⁱⁱⁱ, 0.73(3); H10cⁱ...H10cⁱⁱ, 0.98(4). A crystallographic inversion center is located between H10cⁱ and H10cⁱⁱ. (b) Decomposition into two canonical forms for the Grotthuss proton transport mechanism. The two endpoints are identified as congeners A and B. Atoms labeled "AB" are present in both congeners. The local movement of protons implied by this mechanism does not adhere to crystallographic symmetry. i: (-x, 1-y, -z), ii: (1+x, y, z), iii: (1-x, 1-y, -z). Reproduced from Falvello *et al.* 2014.^[6]

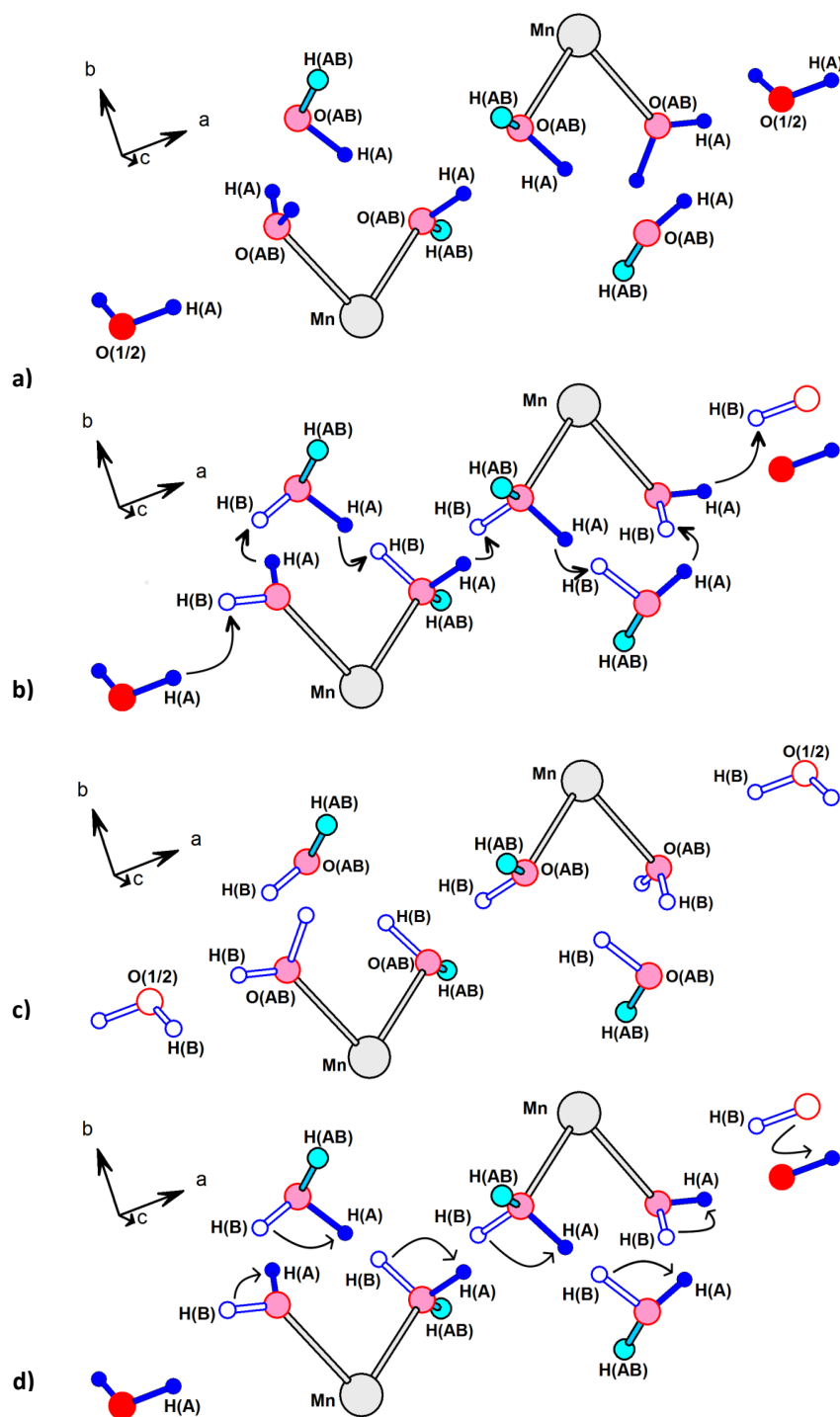


Fig. 8.9. (a) One of the valid H-atom structures, congener A (solid blue) through the length of one unit cell along the a -direction. (b) First stage of the Grotthuss mechanism, consisting of short hops between neighboring water molecules, from positions in congener A (solid blue) to the positions of congener B (open blue). (c) The second valid H-atom structure, congener B (open blue). (d) Second stage of the Grotthuss mechanism, consisting of rotations of the H₂O molecules of congener B to return the system to its initial condition (congener A, (a)). Reproduced from Falvello *et al.* 2014.^[6]

1) Proton transfer through two mutually *cis*- aqua ligands mediated by a free molecule of water.

Mn7ⁱ, its coordinated water molecules O10wⁱ and O14wⁱ and the free water O30w are involved in this mechanism (symmetry codes are as in Figure 8.8a). A view of the region in which this first pathway takes place is shown in Figure 8.10a.

In the average structure considering the disorder, O10w is bonded to H10a(1.0), H10b(0.5) and H10c(0.5), O14w is found to be surrounded by 4 hydrogen atoms, all of them with half occupancy. Good geometry is obtained for H14a-O14w-H14c and H14b-O14w-H14d. O30w bonds H30a(1.0), H30b(0.5) and H30c(0.5).

In the initial situation there are O10w (with H10a and H10c), O14w (H14b and H14d) and O30w (with H30a and H30c).

A description of our proposed model begins with the transfer of H14d to O30w. The distance H14d-O30w is 1.93(3) Å which is within the range given for a putative Grotthuss mechanism. H14d would occupy the site of H30b. That involves a hop of 1.39(4) Å.

As H14d occupies the position of H30b, H30c should be transferred to another molecule. It bonds O10w at the site of H10b, 0.73(3) Å away from the initial position.

H10c leaves O10w and bonds O14w, occupying the position of H14c and balancing the loss of the initial H14d. Note that in order to geometrically accommodate H14c, H14b should rotate to the position of H14a. This rotation is favoured by the formation of an H-bond of H14a with an oxygen atom of a citrate ligand.

To restore the initial situation and to prepare the system for a new concerted hopping, some rearrangement must be done (Figure 8.10b).

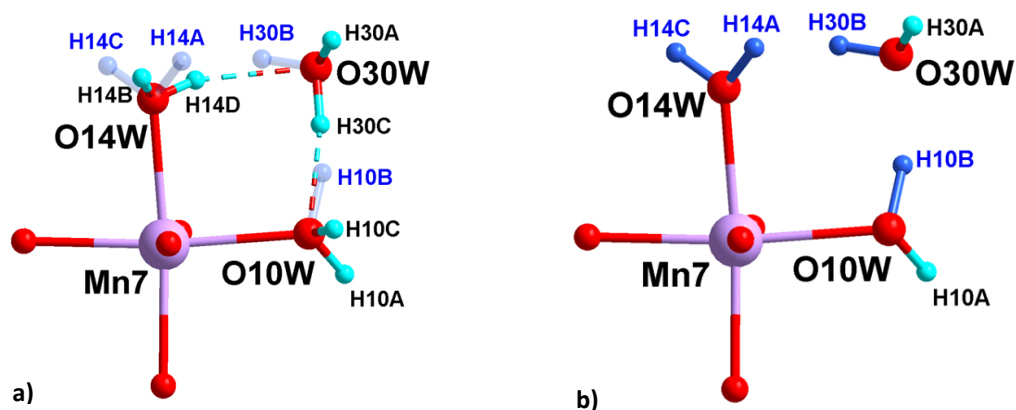


Fig. 8.10. Proton transfer between two H₂O ligands coordinated to the same Mn center, with free water as a shuttle. (a) View showing all of the disordered H-atom sites. (b) H-atom positions following proton transfer. Reproduced from Falvello *et al.* 2014.^[6]

A simple rotation of 90° about the Mn7-O14w axis will transform H14a into H14d and a somewhat larger angular displacement of 104° carries H14c to H14b. A rotation of 109° about the O30w-H30a axis will restore the initial congener of O30w. An analogous rotation of 111° about O10w-H10a will transform H10b into H10c.

2) Direct proton transfer between two Mn(II) units.

The two manganese atoms and the two molecules of water taking place in this mechanism are symmetry related by an inversion centre. Figure 8.11a shows the complete coordination sphere of Mn7ⁱ and Mn7ⁱⁱ and in Figure 8.11b only the most important atoms are represented for clarity.

The pathway described in what follows would be subsequent to the previous one. When H30c occupies the position of H10b, H10c should leave the molecule. In this case, H10bⁱ enters the molecule and then H10cⁱ is transferred to a neighbouring molecule related by symmetry in a hop of 0.98(4) Å, where it occupies the position H10cⁱⁱ (symmetry codes are referred to Figure 8.11).

In Figure 8.11c,d, the arrangement of the species involved in the process before and after the hop are represented. The coordination of H10bⁱ to O10wⁱ is coordinated with the exit of H10bⁱⁱ, which bonds O14wⁱⁱ through O30wⁱⁱⁱ in a mechanism analogous to the shuttle described above, but in the opposite direction.

To restore the initial situation for a new hopping stop a simple rotation about the O10w-H10a axis will transform H10bⁱ into H10cⁱ and H10cⁱⁱ into H10bⁱⁱ. Although the O...O and Mn...Mn distances between the complexes related by the centre of symmetry are quite large (2.830(13) and 6.069(18) Å, respectively) the hopping distance for the hydrogen atoms is much shorter as noted above.

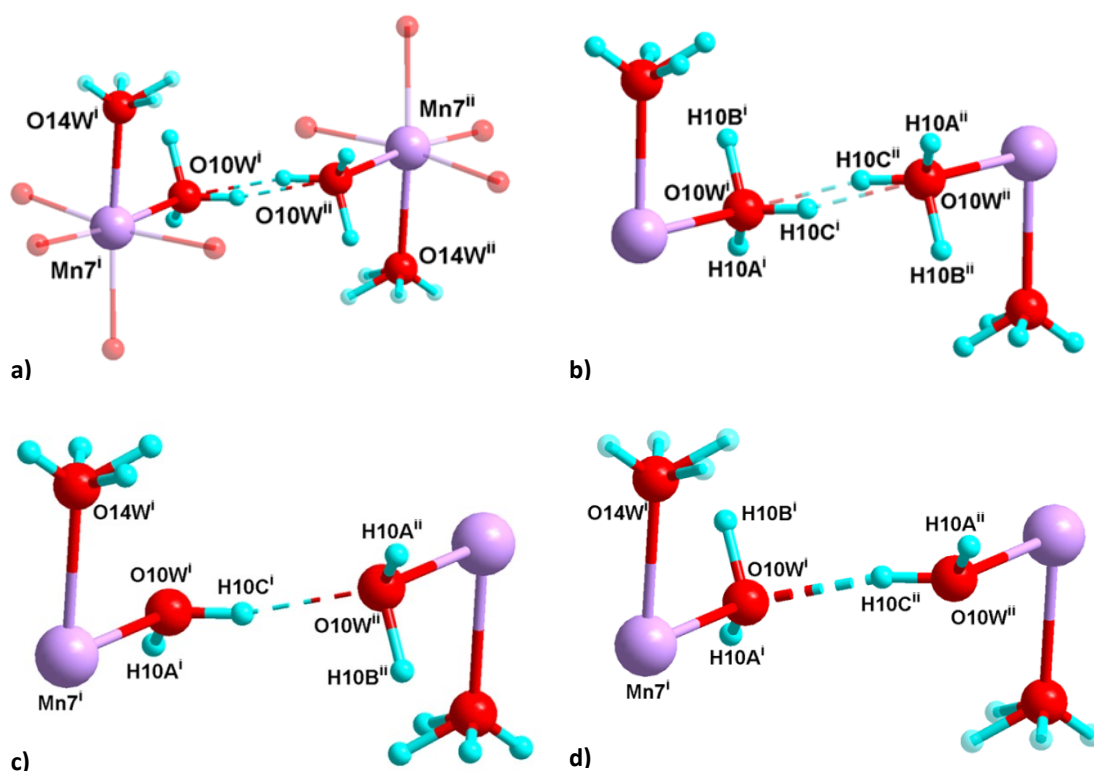


Fig. 8.11. Proton transfer between aqua ligands of two different $[\text{Mn}(\text{H}_2\text{O})_6]^{2+}$ units. (a) Coordination spheres of Mn7ⁱ and Mn7ⁱⁱ. (b) Close-up view showing the H atoms involved in the transfer. (c) Arrangements at O10wⁱ and O10wⁱⁱ before this transfer. (d) H positions at O10wⁱ and O10wⁱⁱ after this transfer. i: (-x, 1-y, -z), ii: (1+x, y, z). Reproduced from Falvello *et al.* 2014.^[6]

3) Proton transfers between two Mn(II) units with a free molecule of water acting as a shuttle.

Disorder across an inversion centre has been observed for some water molecules with half occupancy. Figure 8.12a shows O28wⁱⁱ and O28wⁱⁱⁱ related by a centre of symmetry at (1, 0.5, 0) at a distance of 1.94(3) Å from each other. Note that O28w is one of the molecules that exits the crystal during the dehydration process. To give a complete analysis of the proton transfer in this compound it is necessary to describe a pathway by which a single proton can traverse at least one lattice repeat.

The disorder observed could be due to the fact that both dispositions are equally probable at every such site in the crystal. It can be that a particular congener is necessary for the movement of protons in one direction and the other for transfer in the opposite direction, which would further mean that the conduction of protons can take place in opposite directions in different regions of the crystal.

It could also be the case that the molecule varies its position between the two sites observed in the disordered pattern as a part of the transport mechanism, a possible substitute for the reorientation steps of the molecules after proton hopping. In this case, it would be called vehicle transport.^[7]

In the proposed mechanism, a simple transfer of H14cⁱⁱ to O28wⁱⁱⁱ takes place with a hopping distance of 1.94(3) Å, followed by the coordination of H28aⁱⁱⁱ to O14wⁱⁱⁱ which substitutes H14cⁱⁱⁱ (H28aⁱⁱⁱ-H14cⁱⁱⁱ distance is 1.55(4) Å) (Figure 8.12a). The full details are masked by the disorder in that zone of the structure, so no further speculation will be offered here. The proposed mechanism is favoured by steric features as there is enough space around the inversion centre that relates the congeners of O28w to allow any reorientation or reallocation needed.

The transfer of H14cⁱⁱ to O28wⁱⁱⁱ is coordinated with the entrance of H30bⁱⁱⁱ (Figure 8.8) which occupies the site of H14dⁱⁱ. Then, there is a reorientation of O14wⁱⁱ to allocate H14aⁱⁱ into the position of H14bⁱⁱ (Figure 8.12b).

The coordination of H28aⁱⁱⁱ to O14wⁱⁱⁱ at the site of H14cⁱⁱⁱ is coordinated with the hopping of H14dⁱⁱⁱ to O30w (Figure 8.10a) and provokes the rotation of O14w to transform H14bⁱⁱⁱ into H14aⁱⁱⁱ (Figure 8.12b).

Finally, a rotation of H14bⁱⁱ and H14dⁱⁱ to produce H14cⁱⁱ and H14aⁱⁱ and of H14aⁱⁱⁱ and H14cⁱⁱⁱ to give the other possible orientation of O14wⁱⁱⁱ leaves the system ready for a new hopping step.

In summary: the situation before and after of any of the three pathways proposed above can be superposed to obtain the atomic positions derived from single crystal neutron diffraction data. A plausible model for the proton transfer based on the Grotthuss mechanism can thus be deduced from the data.

However, the substitution of H by D has been explained only for 2 coordinated and two free molecules of water. It would be necessary to find more pathways to describe the

substitution at the 52 hydrogen positions per asymmetric unit (72 sites if disorder is considered).

8.3. Conclusions

In this chapter a 1-D polymer based on Mn-citrate cubanes has been presented. The one-dimensional anionic polymer has its negative charge balanced by two hexaquo manganese (II) units located in the space between the chains. There are 29 molecules of water per unit of the polymer, 8 of which are unbound, occupying 9 crystallographic sites.

The compound undergoes a reversible dehydration under ambient conditions, preserving the crystallinity of the sample. This process is commonly called single-crystal to single-crystal transformation (SC-SC). In spite of the absence of pores or voids, three molecules of water (occupying four crystallographic sites) exit the structure when the compound is left exposed to the atmosphere for several hours. When the dehydrated crystal is placed inside a closed vial under a humid atmosphere, the initial structure is fully restored. Looking for an explanation for that observation, neutron diffraction analyses were performed. The rehydration was conducted under a D₂O atmosphere in an attempt to trace the route followed by the molecules of water to exit and re-enter the crystal.

However, the results of this experiment were unexpected. A complete interchange of H by D was observed, not only for the three water molecules involved in the dehydration process but also for the remaining 26 water molecules. The hydrogen atoms coordinated to the CH₂ of the citrate were used as a control group to check the validity of the neutron analysis. Although the marked difference in the scattering length between H and D makes the results unambiguous, some efforts were extended in order to confirm the absence of H and the validity of the study.

Despite the fact that there is no a clear pathway for the water to egress the compound, what is clear is that when the rehydration take place, these molecules enter the crystal as whole molecules. However, the possibility that this mechanism is the one operating in the substitution of H by D for all thirty water sites is remote enough to suggest that an alternative mechanism is operative.

In the crystal there were zones of considerable disorder involving a large number of molecules of water. The nature of this part of the structure can be understood by first partitioning the disordered sites into two groups. The disorder at some sites consists of water oxygen atoms surrounded by 4 hydrogen atoms with half occupancy, or of oxygen surrounded by three hydrogen atom sites, one of them fully occupied and the remaining half occupied. This division of the disorder was done on the basis of geometry around the water oxygen atoms.

The disorder can then be explained as the superposition of the structure as it exists at energy minima between two steps of a concerted proton transfer mechanism. The first step is a concerted hopping of hydrogen atoms between successive water molecules along the chain. The second step is a reorganization and reallocation of the molecules to restore the initial

situation, allowing a new cycle of proton transport. That is a canonical representation of the Grotthuss mechanism. The superposition of these two situations is the disorder observed.

This is the first example in which the Grotthuss mechanism has been inferred from experimental data for molecular crystals.

However, the water egress and reuptake observed throughout this study remains unexplained. Further effort is needed in order to characterize this system fully.

References

- [1] W. G. Wang, X. F. Zhang, F. Chen, C. B. Ma, C. N. Chen, Q. T. Liu, D. Z. Liao, L. C. Li, *Polyhedron* **2005**, *24*, 1656-1668.
- [2] A. Altomare, G. Cascarano, C. Giacovazzo, A. Guagliardi, *Journal of Applied Crystallography* **1993**, *26*, 343-350.
- [3] G. M. Sheldrick, *Acta Crystallographica Section A* **2008**, *64*, 112-122.
- [4] H. L. Carrell, J. P. Glusker, *Acta Crystallographica Section B-Structural Science* **1973**, *B 29*, 638-640.
- [5] Y. F. Deng, Z. H. Zhou, H. L. Wan, S. W. Ng, *Acta Crystallographica Section E-Structure Reports Online* **2003**, *59*, M310-M312.
- [6] S. C. Capelli, L. R. Falvello, E. Forcen-Vazquez, G. J. McIntyre, F. Palacio, S. Sanz, M. Tomas, *Angewandte Chemie (International ed. in English)* **2013**, *52*, 13463-13467.
- [7] G. A. Luduena, T. D. Kuehne, D. Sebastiani, *Chemistry of Materials* **2011**, *23*, 1424-1429.
- [P1] CrysAlisPro, Oxford Diffraction Ltd., Version 1.171.33.31
- [P2] Diamond. Klaus Brandenburg, Crystal Impact GbR, Bonn, Germany. Version 3.2i.
- [P5] <http://www.ill.eu/instrumentssupport/instrumentgroups/instruments/d19/description/instrument-layout/>
- [P6] a) NIST Center for Neutron Research, <http://www.ncnr.nist.gov/instruments/bt1/neutron.html>. b) V. F. Sears, *Neutron News* 1992, *3*, 26-37.
- [P8] Program Retreat: Wilkinson, C., Khamis, H. W., Stansfield, R. F. D. & McIntyre, G. J. (1988). *J. Appl. Cryst.* **21**, 471-478.

Supplementary Material

Table S8.1. Hydrogen bonds for **10n** from the neutron analysis. Reproduced from Falvello *et al.* 2014.^[6]

D-H...A	d(D-H), Å	d(H...A), Å	d(D...A), Å	<(DHA), (°)	acceptor coords
O1WB-H1A...O8#1	0.95(2)	1.769(18)	2.653(15)	154.1(15)	#1 -x+1,-y+1,-z+1
O1WB-H1B...O29Z#1	1.04(3)	1.51(3)	2.49(3)	154(3)	#1 -x+1,-y+1,-z+1
O1WB-H1B...O29W#1	1.04(3)	1.67(4)	2.68(3)	163(3)	#1 -x+1,-y+1,-z+1
O1WA-H1C...O26	0.98(4)	2.37(3)	3.350(15)	173(3)	
O2W-H2A...O23	0.941(16)	1.943(13)	2.771(9)	145.6(9)	
O2W-H2B...O24W#2	0.926(15)	1.845(13)	2.769(10)	175.4(12)	#2 x+1/2,-y+3/2,z+1/2
O3W-H3C...O25W#3	0.90(2)	1.942(16)	2.818(13)	164.4(12)	#3 -x+1/2,y+1/2,-z+1/2
O3W-H3D...O19#2	1.14(3)	2.20(2)	3.329(12)	169.4(19)	#2 x+1/2,-y+3/2,z+1/2
O3W-H3E...O28W#2	1.05(4)	2.10(4)	3.14(2)	167(3)	#2 x+1/2,-y+3/2,z+1/2
O4W-H4A...O22W	0.993(15)	1.836(14)	2.823(9)	172.2(11)	
O4W-H4B...O17#2	0.913(17)	2.009(14)	2.798(9)	143.8(11)	#2 x+1/2,-y+3/2,z+1/2
O5W-H5C...O22#4	0.958(16)	1.825(15)	2.771(10)	168.7(12)	#4 x-1/2,-y+3/2,z+1/2
O5W-H5D...O23W	0.980(17)	1.72(2)	2.685(17)	165.4(14)	
O5W-H5D...O23Z	0.980(17)	1.70(2)	2.66(2)	166.6(14)	
O6W-H6A...O11	0.939(17)	1.971(14)	2.905(10)	172.6(12)	
O6W-H6B...O6W#5	0.92(3)	2.39(3)	3.168(15)	143(2)	#5 -x,-y+1,-z+1
O6W-H6B...O5W#5	0.92(3)	2.40(3)	3.116(11)	136(2)	#5 -x,-y+1,-z+1
O6W-H6C...O29W	1.28(4)	1.80(5)	3.03(3)	158(2)	
O6W-H6C...O29Z	1.28(4)	1.86(4)	3.04(2)	149(2)	
O6W-H6C...O23W#5	1.28(4)	2.38(4)	3.15(2)	115.6(17)	#5 -x,-y+1,-z+1
O7WA-H7A...O27W#1	0.89(3)	1.79(2)	2.65(2)	161.1(17)	#1 -x+1,-y+1,-z+1
O7WA-H7B...O25	0.96(3)	1.78(3)	2.686(18)	156(2)	
O7WB-H7C...O29Z	0.97(4)	1.86(3)	2.76(2)	155(2)	
O7WB-	0.97(4)	2.13(4)	3.03(3)	155(2)	

H7C...O29W					
O8W-H8A...O21W#2	0.996(15)	1.659(14)	2.652(9)	174.1(12)	#2 $x+1/2, -y+3/2, z+1/2$
O8W-H8B...O8#1	0.924(14)	1.862(13)	2.774(8)	168.8(12)	#1 $-x+1, -y+1, -z+1$
O9W-H9C...O10#1	0.954(16)	1.791(14)	2.716(10)	162.5(10)	#1 $-x+1, -y+1, -z+1$
O9W-H9D...O12#5	0.952(15)	1.718(13)	2.641(9)	162.5(11)	#5 $-x, -y+1, -z+1$
O10W-H10A...O5#6	1.001(15)	1.774(13)	2.757(9)	166.5(11)	#6 $x-1, y, z$
O10W-H10B...O30W#7	1.03(4)	1.76(4)	2.760(10)	163(2)	#7 $-x, -y+1, -z$
O10W-H10C...O10W#8	0.98(2)	1.878(18)	2.830(13)	163.9(18)	#8 $-x-1, -y+1, -z$
O11W-H11C...O13#7	0.940(16)	1.765(14)	2.693(9)	168.5(12)	#7 $-x, -y+1, -z$
O11W-H11D...O28#9	0.998(18)	1.693(15)	2.678(10)	168.5(12)	#9 $x-1/2, -y+3/2, z-1/2$
O12W-H12A...O14#7	0.978(17)	1.772(15)	2.745(10)	172.7(12)	#7 $-x, -y+1, -z$
O12W-H12B...O24#9	0.95(4)	2.34(4)	3.218(11)	153(3)	#9 $x-1/2, -y+3/2, z-1/2$
O12W-H12C...O4W#9	0.91(3)	2.22(3)	3.076(11)	157(2)	#9 $x-1/2, -y+3/2, z-1/2$
O12W-H12C...O4W#9	0.91(3)	2.22(3)	3.076(11)	157(2)	#9 $x-1/2, -y+3/2, z-1/2$
O12W-H12C...O3W#9	0.91(3)	2.59(2)	3.200(12)	125.2(18)	#9 $x-1/2, -y+3/2, z-1/2$
O13W-H13A...O6#6	0.980(14)	1.682(12)	2.660(9)	174.8(10)	#6 $x-1, y, z$
O13W-H13B...O16	0.958(15)	1.685(13)	2.625(9)	166.1(10)	
O14W-H14A...O19#7	1.12(2)	1.85(2)	2.969(11)	174.9(15)	#7 $-x, -y+1, -z$
O14W-H14A...O19#7	1.12(2)	1.85(2)	2.969(11)	174.9(15)	#7 $-x, -y+1, -z$
O14W-H14B...O13#7	0.93(3)	2.24(3)	3.087(10)	150(2)	#7 $-x, -y+1, -z$
O14W-H14C...O28W#7	0.86(3)	1.94(3)	2.760(15)	158(2)	#7 $-x, -y+1, -z$
O14W-H14C...O28W	0.86(3)	2.38(3)	3.057(15)	136(2)	
O14W-H14D...O30W#7	0.92(4)	1.93(3)	2.813(11)	162(2)	#7 $-x, -y+1, -z$
O15W-H15C...O22W#9	0.950(18)	1.772(16)	2.714(11)	170.7(11)	#9 $x-1/2, -y+3/2, z-1/2$
O15W-H15D...O20#6	0.957(18)	1.825(16)	2.763(9)	165.9(15)	#6 $x-1, y, z$
O16W-H16A...O9#6	0.990(14)	1.716(12)	2.699(8)	171.9(10)	#6 $x-1, y, z$

O16W- H16B...O16	1.004(15)	1.689(14)	2.690(9)	174.2(11)	
O17W- H17C...O21#6	0.973(14)	1.793(14)	2.758(8)	171.1(12)	#6 x-1,y,z
O17W- H17D...O25W#10	0.948(19)	1.852(16)	2.792(10)	170.7(12)	#10 -x- 1/2,y+1/2,- z+1/2
O18W- H18A...O30W#4	1.064(14)	1.679(14)	2.742(9)	176.7(10)	#4 x-1/2,- y+3/2,z+1/2
O18W- H18B...O28	0.956(15)	1.717(13)	2.672(9)	177.6(11)	
O19W- H19A...O27	0.979(14)	1.756(13)	2.726(9)	170.7(11)	
O19W- H19B...O8#3	0.959(18)	1.899(15)	2.852(10)	172.4(10)	#3 - x+1/2,y+1/2,- z+1/2
O20W- H20A...O10#6	1.001(15)	1.673(14)	2.669(9)	173.0(11)	#6 x-1,y,z
O20W- H20B...O15	0.996(14)	1.660(13)	2.654(8)	175.2(11)	
O21W- H21C...O26W#3	0.992(16)	1.646(14)	2.637(10)	176.5(11)	#3 - x+1/2,y+1/2,- z+1/2
O21W- H21D...O22#6	0.978(13)	1.643(12)	2.613(9)	170.6(11)	#6 x-1,y,z
O22W- H22A...O26	0.961(19)	1.865(16)	2.804(11)	164.8(11)	
O22W- H22B...O16W#2	0.926(15)	2.035(14)	2.865(9)	148.4(12)	#2 x+1/2,- y+3/2,z+1/2
O23W- H23C...O9W#5	0.93(4)	1.90(3)	2.835(18)	179(3)	#5 -x,-y+1,- z+1
O23W- H23D...O24W#4	0.85(5)	1.89(4)	2.75(2)	178(3)	#4 x-1/2,- y+3/2,z+1/2
O23Z- H23D...O24W#4	0.96(4)	1.89(4)	2.73(2)	145(3)	#4 x-1/2,- y+3/2,z+1/2
O23Z- H23Z...O9W#5	0.87(5)	2.05(4)	2.93(2)	175(3)	#5 -x,-y+1,- z+1
O24W- H24A...O20	0.95(2)	1.837(16)	2.775(11)	168.6(11)	
O24W- H24B...O20W#11	0.943(16)	1.895(14)	2.766(10)	152.6(12)	#11 x+1/2,- y+3/2,z-1/2
O25W- H25A...O26W#6	0.953(18)	1.994(15)	2.907(10)	160.0(12)	#6 x-1,y,z
O25W- H25B...O14	0.963(15)	1.775(13)	2.722(9)	167.3(11)	
O26W-H26A...O6	0.949(16)	1.745(14)	2.683(9)	169.0(11)	
O26W- H26B...O12#12	0.961(16)	1.754(14)	2.704(9)	169.6(12)	#12 x+1,y,z
O27W- H27A...O25	0.92(3)	1.78(3)	2.681(14)	167(2)	

O27W-H27B...O1WA	1.10(4)	1.34(4)	2.38(2)	154(3)	
O27W-H27B...O1WB	1.10(4)	1.67(4)	2.77(2)	172(3)	
O28W-H28A...O14W	0.93(4)	2.19(3)	3.057(15)	155(3)	
O28W-H28A...O12W	0.93(4)	2.49(3)	3.054(18)	119(2)	
O28W-H28B...O14	0.78(4)	2.27(3)	2.997(18)	156(2)	
O29Z-H29A...O7	0.83(3)	1.96(2)	2.78(2)	168.8(19)	
O29W-H29B...O23W#5	0.74(7)	2.22(5)	2.88(3)	148(4)	#5 -x,-y+1,-z+1
O29W-H29B...O6W	0.74(7)	2.53(5)	3.03(3)	126(4)	
O29W-H29C...O18A#13	0.95(5)	2.04(3)	2.95(3)	160(3)	#13 -x+1/2,y-1/2,-z+1/2
O29W-H29C...O1WB#1	0.95(5)	2.04(3)	2.68(3)	123(3)	#1 -x+1,-y+1,-z+1
O29W-H29C...O18B#13	0.95(5)	2.55(4)	3.45(4)	158(2)	#13 -x+1/2,y-1/2,-z+1/2
O30W-H30A...O20	0.977(19)	1.677(16)	2.653(10)	176.7(13)	
O30W-H30B...O14W#7	0.87(3)	2.30(3)	2.813(11)	118(2)	#7 -x,-y+1,-z
O30W-H30B...O25W#7	0.87(3)	2.38(3)	3.057(10)	135(2)	#7 -x,-y+1,-z
O30W-H30C...O10W#7	1.03(4)	1.74(4)	2.760(10)	169(2)	#7 -x,-y+1,-z

Table S8.2. Hydrogen bonds for **12** from the neutron analysis.

D-H...A	d(D-H), Å	d(H...A), Å	d(D...A), Å	<(DHA), (°)	acceptor coords
C3-H3B...O18W#1	1.13(4)	2.56(3)	3.62(3)	156.4(19)	#1 -x+1/2,y-1/2,-z+1/2
C5-H5B...O8W#2	1.21(5)	2.59(4)	3.60(3)	141(2)	#2 -x+1,-y+1,-z+1
C11-H11B...O26W#3	1.01(4)	2.52(4)	3.36(3)	140.5(19)	#3 x-1,y,z
C17-H17A...O29W#4	1.08(4)	2.48(4)	3.542(18)	167(3)	#4 -x+1/2,y+1/2,-z+1/2
C17-H17B...O27	1.13(4)	2.63(4)	3.68(2)	154(2)	
O1WB-D1A...O8#2	0.94(4)	1.81(3)	2.69(4)	153(5)	#2 -x+1,-y+1,-z+1
O1WB-D1B...O29W#2	1.23(6)	1.65(4)	2.77(5)	148(4)	#2 -x+1,-y+1,-z+1
O1WA-D1C...O26	0.83(9)	2.46(9)	3.28(8)	173(9)	

O2W-D2A...O23	1.04(2)	1.87(3)	2.75(3)	140(3)	
O2W-D2A...O17W#5	1.04(2)	2.63(3)	3.31(3)	122(2)	#5 $x+1,y,z$
O2W-D2B...O24W#6	0.96(3)	1.84(3)	2.79(4)	171(2)	#6 $x+1/2,-y+3/2,z+1/2$
O3W-D3C...O25W#4	0.89(2)	1.84(3)	2.72(3)	171(3)	#4 - $x+1/2,y+1/2,-z+1/2$
O3W-D3D...O19#6	1.10(3)	2.25(4)	3.34(3)	173(3)	#6 $x+1/2,-y+3/2,z+1/2$
O3W-D3E...O28W#6	1.08(5)	2.06(6)	3.09(5)	158(4)	#6 $x+1/2,-y+3/2,z+1/2$
O4W-D4A...O22W	1.00(3)	1.88(3)	2.86(3)	164(2)	
O4W-D4B...O17#6	0.95(2)	1.94(3)	2.74(3)	141(3)	#6 $x+1/2,-y+3/2,z+1/2$
O5W-D5C...O22#7	1.00(2)	1.76(2)	2.75(2)	171(2)	#7 $x-1/2,-y+3/2,z+1/2$
O5W-D5D...O23W	0.97(2)	1.80(3)	2.75(3)	165(3)	
O6W-D6A...O11	1.01(2)	1.98(2)	2.97(3)	166(2)	
O6W-D6C...O23W#8	1.06(7)	2.57(7)	3.20(4)	118(5)	#8 $-x,-y+1,-z+1$
O6W-D6C...O29W	1.06(7)	1.95(7)	2.84(3)	140(6)	
O7W-D7A...O27W	0.96(6)	1.63(6)	2.20(5)	113(6)	
O7W-D7A...O27W#2	0.96(6)	1.50(6)	2.28(5)	134(6)	#2 $-x+1,-y+1,-z+1$
O7W-D7B...O25	1.17(4)	1.88(4)	3.02(3)	162(4)	
O7W-D7B...O26	1.17(4)	2.54(4)	3.19(3)	113(3)	
O7W-D7D...O29W	1.25(5)	2.01(4)	3.05(3)	138(3)	
O8W-D8A...O21W#6	0.99(2)	1.65(2)	2.64(3)	174(3)	#6 $x+1/2,-y+3/2,z+1/2$
O8W-D8B...O8#2	0.98(3)	1.89(3)	2.86(3)	170(3)	#2 $-x+1,-y+1,-z+1$
O9W-D9C...O10#2	1.02(2)	1.78(2)	2.77(2)	165(2)	#2 $-x+1,-y+1,-z+1$
O9W-D9D...O12#8	0.92(2)	1.73(3)	2.63(3)	168(2)	#8 $-x,-y+1,-z+1$
O10W-D10A...O5#3	0.98(2)	1.79(2)	2.75(2)	165(2)	#3 $x-1,y,z$
O11W-D11C...O13#9	1.02(2)	1.72(3)	2.73(3)	174(2)	#9 $-x,-y+1,-z$
O11W-D11D...O28#10	0.920(18)	1.80(2)	2.71(2)	170.8(19)	#10 $x-1/2,-y+3/2,z-1/2$
O12W-D12A...O14#9	1.02(2)	1.83(2)	2.84(3)	170(2)	#9 $-x,-y+1,-z$
O12W-	0.94(5)	2.62(6)	3.28(4)	128(4)	#10 $x-1/2,-$

D12B...O3W#10					$y+3/2, z-1/2$
O12W- D12B...O4W#10	0.94(5)	2.12(5)	2.99(3)	153(5)	#10 $x-1/2, -y+3/2, z-1/2$
O12W- D12C...O24#10	1.18(6)	2.12(6)	3.27(3)	167(5)	#10 $x-1/2, -y+3/2, z-1/2$
O12W- D12B...O4W#10	0.94(5)	2.12(5)	2.99(3)	153(5)	#10 $x-1/2, -y+3/2, z-1/2$
O13W- D13A...O6#3	0.95(2)	1.77(3)	2.71(3)	170(2)	#3 $x-1, y, z$
O13W- D13B...O16	0.97(2)	1.69(2)	2.63(3)	162(2)	
O14W- D14B...O13#9	0.95(2)	2.47(3)	3.08(3)	122(3)	#9 $-x, -y+1, -z$
O14W- D14B...O19#9	0.95(2)	2.07(3)	2.97(3)	158(3)	#9 $-x, -y+1, -z$
O14W- D14C...O28W	0.92(3)	2.39(6)	3.06(6)	130(6)	
O14W- D14C...O28W#9	0.92(3)	1.86(6)	2.76(6)	167(6)	#9 $-x, -y+1, -z$
O14W- D14D...O30W#9	0.91(2)	2.08(4)	2.94(4)	157(4)	#9 $-x, -y+1, -z$
O15W- D15C...O22W#10	1.07(3)	1.66(3)	2.69(3)	161(3)	#10 $x-1/2, -y+3/2, z-1/2$
O15W- D15D...O20#3	0.96(3)	1.86(3)	2.76(4)	157(3)	#3 $x-1, y, z$
O16W- D16A...O9#3	0.98(2)	1.76(3)	2.74(2)	174(2)	#3 $x-1, y, z$
O16W- D16B...O16	0.96(2)	1.69(3)	2.65(3)	174(2)	
O17W- D17C...O21#3	0.98(2)	1.81(3)	2.78(3)	173(2)	#3 $x-1, y, z$
O17W- D17D...O25W#11	1.00(2)	1.80(3)	2.78(3)	170(2)	#11 $-x-1/2, y+1/2, -z+1/2$
O18W- D18A...O30W#7	0.95(2)	1.71(3)	2.66(3)	179(3)	#7 $x-1/2, -y+3/2, z+1/2$
O18W- D18B...O28	0.95(3)	1.85(3)	2.80(3)	178(2)	
O19W- D19A...O27	1.05(2)	1.75(3)	2.80(3)	176(2)	
O19W- D19B...O8#4	1.00(2)	1.91(2)	2.92(2)	178(2)	#4 $-x+1/2, y+1/2, -z+1/2$
O20W- D20A...O10#3	1.02(2)	1.73(3)	2.74(3)	176(2)	#3 $x-1, y, z$
O20W- D20B...O15	1.00(2)	1.76(3)	2.75(3)	171(2)	
O21W- D21C...O26W#4	0.98(2)	1.67(3)	2.65(2)	178(2)	#4 $-x+1/2, y+1/2, -z+1/2$

O21W-D21D...O22#3	1.05(3)	1.64(3)	2.68(3)	170(2)	#3 x-1,y,z
O22W-D22A...O26	1.06(2)	1.88(2)	2.91(2)	163(2)	
O22W-D22B...O16W#6	1.00(2)	1.96(3)	2.81(2)	141(2)	#6 x+1/2,-y+3/2,z+1/2
O23W-D23Y...O24W#7	0.92(3)	1.74(3)	2.62(3)	158(3)	#7 x-1/2,-y+3/2,z+1/2
O23W-D23Z...O9W#8	0.97(3)	1.93(3)	2.85(3)	159(3)	#8 -x,-y+1,-z+1
O24W-D24A...O20	1.00(2)	1.87(2)	2.83(2)	160(2)	
O24W-D24B...O20W#12	1.01(2)	1.83(3)	2.73(2)	147(2)	#12 x+1/2,-y+3/2,z-1/2
O25W-D25A...O26W#3	0.92(2)	2.00(3)	2.87(3)	158(2)	#3 x-1,y,z
O25W-D25B...O14	1.05(3)	1.79(3)	2.82(3)	165(2)	
O26W-D26B...O12#5	1.00(2)	1.82(3)	2.81(2)	169(2)	#5 x+1,y,z
O26W-D26A...O6	1.02(2)	1.72(3)	2.70(3)	160(2)	
O27W-D27A...O25	0.93(5)	1.97(6)	2.80(5)	149(5)	
O27W-D27B...O1WA	1.16(5)	1.16(5)	2.27(6)	159(7)	
O27W-D27B...O1WB	1.16(5)	1.53(6)	2.66(6)	164(5)	
O28W-D28A...O14W	0.84(6)	2.30(7)	3.06(6)	151(6)	
O28W-D28B...O14	0.91(5)	2.24(5)	3.11(5)	159(6)	
O29W-D29A...O7	1.03	1.89	2.92(2)	172.2	
O29W-D29B...O23W#8	1.06	2.07	3.01(3)	147.3	#8 -x,-y+1,-z+1
O29W-D29C...O18#1	0.78	2.45	3.21(3)	167.9	#1 -x+1/2,y-1/2,-z+1/2
O29W-D29C...O1WB#2	0.78	2.31	2.77(5)	118.6	#2 -x+1,-y+1,-z+1
O30W-D30A...O20	0.94(2)	1.74(2)	2.68(3)	173(3)	
O30W-D30B...O14W#9	0.90(4)	2.33(4)	2.94(4)	124(3)	#9 -x,-y+1,-z
O30W-D30B...O25W#9	0.90(4)	2.38(5)	3.08(4)	135(3)	#9 -x,-y+1,-z

9

2-D Manganese citrate cubanes.*

This is the last of a series of chapters devoted to a family of derivatives based on manganese citrate cubanes. The compound presented in what follows is a 2-D polymer with a close structural relationship with the 1-D derivatives described in the preceding chapter.

Compound **13**, with formula $[(\text{Mn}(\text{H}_2\text{O})_6)]_{2n}\{[\text{Mn}_4(\text{C}_6\text{H}_4\text{O}_7)_4]_{\mu_3}[\text{Mn}(\text{H}_2\text{O})_3(\text{C}_2\text{H}_6\text{O}_2)_{0.5}][\text{Mn}(\text{H}_2\text{O})_4(\text{C}_2\text{H}_6\text{O}_2)_{0.5}]\}_n \cdot 6.5n(\text{H}_2\text{O})$, is obtained by a procedure similar to the one used for the other compounds containing Mn-citrate cubanes described in this part of the thesis, with the main difference that ethylene glycol was added to the reaction media. This is a good example of how it is possible to tune the environment of the cubanes just by subtle changes in the reaction media. There is evidence that **13** undergoes a reversible SC-SC transformation. Unfortunately, that process has not been further characterised. A strong H-bonded network is observed in this compound, which suggests that it could present the same reactivity as compound **10**.^[1]

9.1 Experimental

9.1.1. Synthesis

Reagents were obtained commercially and were used with no further purification.

The 2-D polymer with formula $[(\text{Mn}(\text{H}_2\text{O})_6)]_{2n}\{[\text{Mn}_4(\text{C}_6\text{H}_4\text{O}_7)_4]\mu_3[\text{Mn}(\text{H}_2\text{O})_3(\text{C}_2\text{H}_6\text{O}_2)_{0.5}][\text{Mn}(\text{H}_2\text{O})_4(\text{C}_2\text{H}_6\text{O}_2)_{0.5}]\}_n \cdot 6.5n(\text{H}_2\text{O})$ (**13**) was obtained by a procedure similar to the one used in the synthesis of compounds **9** through **12**. MnCO_3 (5.18 g, 45.1 mmol) was added to a stirred solution of citric acid monohydrate (250 mL, 0.095 M). The mixture was heated to reflux under a stream of Ar for 5 h. and filtered. The supernatant was cooled to room temperature for several days and filtered again to remove the crystals of a subproduct with a Mn/citrate ratio of 3/2 and formula $(\text{C}_{12}\text{H}_{22}\text{Mn}_3\text{O}_{20})_n \cdot 4n(\text{H}_2\text{O})$.^[2] The supernatant was heated to reflux for 3h. The reflux was stopped, maintaining the heating to allow the solvent to evaporate until a final volume of approximately 50 mL was reached. Then the mixture was filtered. As described previously, a white to pale-pink powder of **9** precipitates during the heating process. An aqueous solution of CsOH (~1.2 M) was added dropwise to the supernatant until a pH of 7.5 was attained. Ethylene glycol was added to the resulting solution ($\text{H}_2\text{O}/\text{Ethylene glycol}$ 2/1), and the mixture was placed in a closed vial and kept in a refrigerator at 18 °C. After several months block-like colourless crystals of **13** were obtained.

9.1.2. Single Crystal X-Ray diffraction

Single crystal X-Ray diffraction data were measured using an Xcalibur S3 CCD-based four-circle diffractometer (Oxford Diffraction and Agilent Technologies). The program CrysAlis Pro^[P1] was used for data collection and processing. The structure was solved *ab initio* by direct methods^[3] and refined by full-matrix least-squares analysis.^[4] Non-hydrogen atoms were refined with anisotropic displacement parameters. The methylene H atoms of the citrate ligands were placed at idealized positions and refined as riders on their respective parent C atoms with isotropic displacement parameters set to 1.2 times the equivalent isotropic U of the C atom. Hydrogen atoms of the water molecules were not seen in a difference map. Material for publication was prepared using Diamond.^[P2] Data collection and structure solution information and refinement details are shown in Table 9.1.

9.1.3. FT-IR spectroscopy

FT-IR spectra of **13** were measured in the range of 4000 - 350 cm^{-1} using a Perkin-Elmer Spectrum 100 FT-IR Spectrophotometer with ATR accessory (Figure 9.1).

IR (neat compound, cm^{-1}): $\nu(\text{OH st})$ 3289.90 (w) and 2949.77 (w); $\nu(\text{C=O})$ 1541.58 (w); $\nu(\text{C-H})$ 1378.71 (w); $\nu(\text{CO})$ 1080.58 (t).

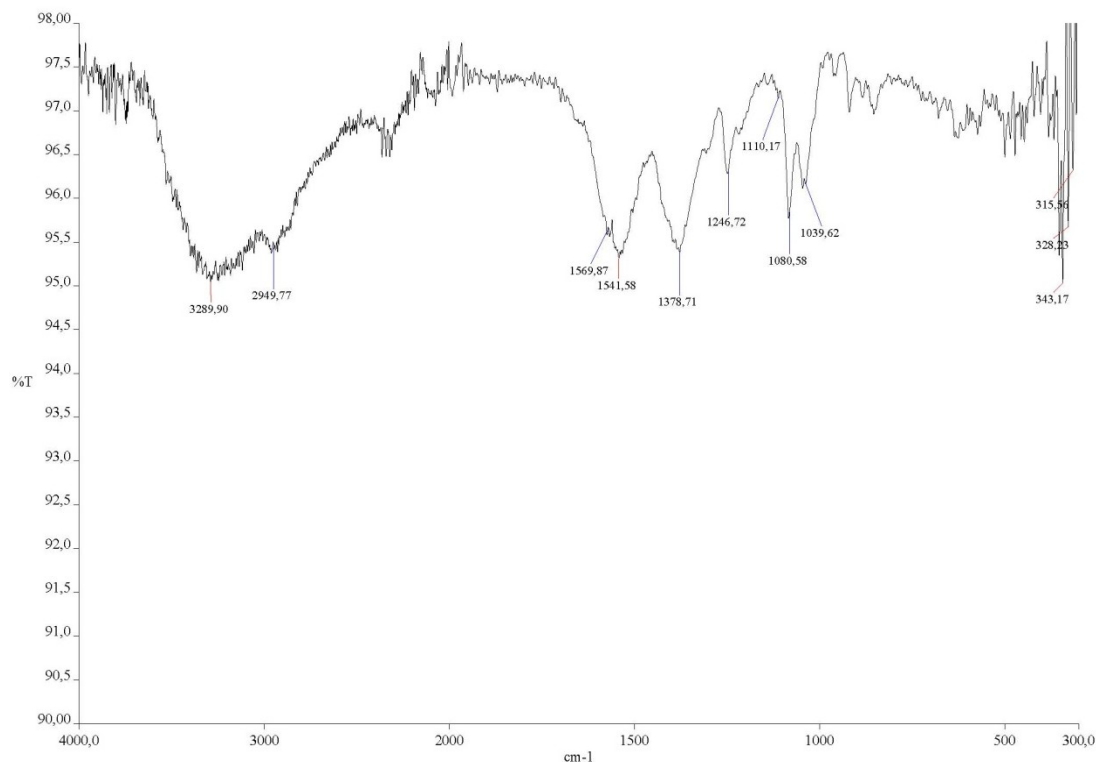


Fig. 9.1. IR spectrum of 13.

Formula	${}^a\text{C}_{26}\text{H}_{73}\text{Mn}_8\text{O}_{55.5}$	Crystal size (mm^3)	0.34 x 0.20 x 0.09
fw (g mol^{-1})	1715.38	θ (min,max) ($^\circ$)	4.20, 28.85
Radiation	X-Rays (Mo k_α)	Reflns collected	52932
Wavelength (Å)	0.71073	Indep reflns	14064
Crystal system	monoclinic	R(int), R(σ)	0.0304, 0.0265
Space group	P 2 ₁ /n	Completeness (θ)	0.976 (27.50)
temp (K)	110	Abs corr	multi-scan
a (Å)	12.6192(2)	T(min,max)	0.5880, 0.8646
b (Å)	21.1904(3)	restraints/parms	0 / 811
c (Å)	22.3694(3)	Goodness-of-fit	1.110
β ($^\circ$)	93.536(2)	R1, wR2 (obs)^b	0.0571, 0.1513
V (Å^3), Z	5970.32(15), 4	R1, wR2 (all)	0.0634, 0.1559
ρ_{calc} (Mg/m^3)	1.908	Δ/σ(max,mean)	0.001, <0.001
μ (mm^{-1})	1.763	$\Delta\rho$ range ($\text{e } \text{Å}^{-3}$)	2.173, -0.856
F (000)	3500.0		
^a $[(\text{Mn}(\text{H}_2\text{O})_6)]_{2n}\{[\text{Mn}_4(\text{C}_6\text{H}_4\text{O}_7)_4]\mu_{\text{T}}[\text{Mn}(\text{H}_2\text{O})_3(\text{C}_2\text{H}_6\text{O}_2)_{0.5}][\text{Mn}(\text{H}_2\text{O})_4(\text{C}_2\text{H}_6\text{O}_2)_{0.5}]\}_n \cdot 6.5n(\text{H}_2\text{O})$			
^b threshold $I > 2\sigma(I)$.			

9.2 Results and discussion

9.2.1 Synthesis

The synthetic procedure for compound **13** is exactly the same as that which yields crystals of compounds **9** and **10**. The differences are introduced once an appropriate solution of citric acid and manganese carbonate with a pH of about 5.5 - 6 has been prepared. At that point, a powder of compound **9** has already been isolated. If crystals of **9** are needed, the solution is placed inside a closed vial in an oven at 90 °C. For crystals of **10**, the solution is left at room temperature for several months. Finally, for the obtainment of **13**, CsOH is added to the solution in order to get a pH high enough to prevent the formation of subproducts not based on cubanes. In addition, ethylene glycol is added in a ratio solution/ethylene glycol of 2/1.

Note that the procedure is exactly the same as that used in the preparation of compounds **3** and **4**.^[5] Schematically, after obtaining a solution that yields subproducts with a Mn/citrate ratio of 3/2 (pH < 7), MOH is added to attain a pH of 7.5 - 8 and then ethylene glycol is added (solution/ethylene glycol 2/1).

There are two significant aspects to the synthesis of this compound. The first is that despite the fact that another counterion is introduced in the reaction medium, presumably prior to the formation of the cubane, it does not enter the structure as happens with the cobalt based derivatives. The compound still preserves the hexa-aquo manganese (II) units observed in the related 1-D polymer, acting as counterions.

It is observed that when ethylene glycol is used, 2-D arrays of cubanes are obtained. However, this is the first example where this diol is crucial for the formation of the bidimensional net. In the case of compounds **3** and **4**, the ethylene glycol does not propagate the net; it only chelates the bridging Co(II) units, favouring the square arrangement of the cubanes in the polymeric layers. On the contrary, in compound **13**, the cubanes and the bridging Mn(II) units form 1-D chains, which are connected through ethylene glycol molecules. The presence of this diol is of great structural importance in the 2-D layers.

9.2.2 Single Crystal X-Ray diffraction

Compound **13** crystallises in the monoclinic system, space group $P2_1/n$. The cubane core corresponds to isomer B. Per asymmetric unit there are a complete cubane unit, bridging $[\text{Mn}(\text{H}_2\text{O})_3(\text{C}_2\text{H}_6\text{O}_2)_{0.5}]$ and $[\text{Mn}(\text{H}_2\text{O})_4(\text{C}_2\text{H}_6\text{O}_2)_{0.5}]$ units, two hexa-aquo manganese (II) counterions and 6.5 molecules of water, with the latter distributed over 7 crystallographic sites (Figure 9.2). Three of the central C atoms of the citrate ligands are not chiral. The fourth one

has an S configuration. To the periphery of the polymer are attached two bridging Mn(II) units. The first is Mn5, coordinated to an external oxygen atom through a short arm (Sx2 -S2e in this case) which acts as a triple bridge. It bonds a neighbouring cubane through an external oxygen atom from a long arm (Lxe - L5e in this example). This coordination gives the same 1-D chains as observed in compound **10**, propagated by the *n*-glide plane perpendicular to [0 1 0]. To this point, the two structures are comparable. However, the differences arise from the coordination of Mn6 to the periphery of the cube and from the distinct coordination environment of the two bridging units. The structure will be described here in contrast to that of **10**. Mn6 is attached to an external oxygen atom of a long arm (Lxe - L6e in this case). This coordination point is different from the one in **10**. Mn6 in **13** has migrated from its original anchor site to another farther away from Mn5, which allows the propagation of the 2-D net. Note that the new coordination site of Mn6 in **13** was a prolate oxygen atom in **10**, which suggests a higher reactivity in comparison with the remaining peripheral oxygen atoms.

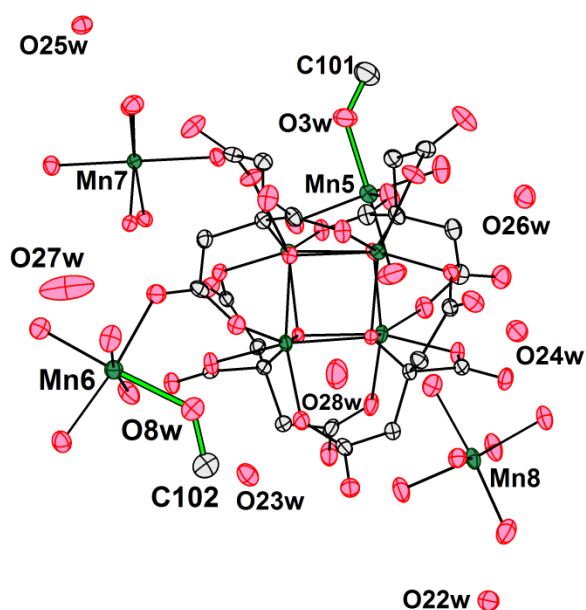


Fig. 9.2. A complete cubane unit with the two bridging Mn(II) units, counterions and free water for compound **13**. Bonds connecting each external Mn unit to ethylene glycol are represented in green. Thermal ellipsoids (probability 60%).

About the coordination of Mn5, instead of completing its coordination sphere with 4 molecules of water, one has been substituted by an oxygen atom of an ethylene glycol molecule. The other oxygen atom of this molecule of ethylene glycol has substituted another water molecule coordinated to Mn6 attached to a cubane in a neighbouring chain. Mn5 coordinates 3 cubane units in a *mer*- configuration (Figure 9.3). (Note that O3w and O8w are

from ethylene glycol despite the fact that "w" means water as we decided to maintain the names used for compound **10** on the basis of their coordinates for comparative purposes.

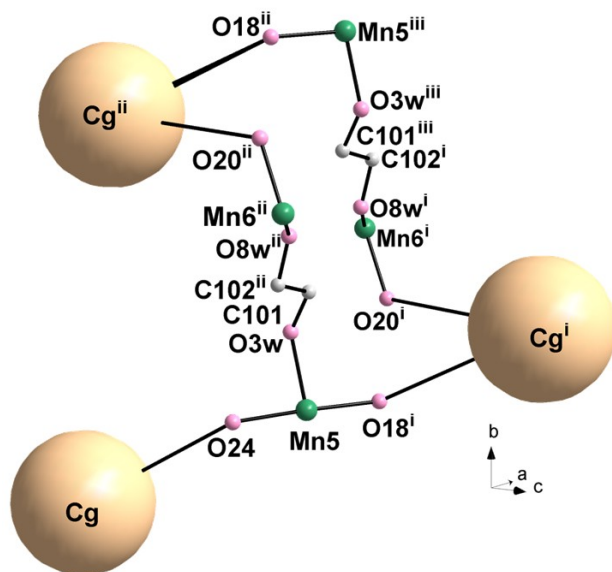


Fig. 9.3. Coordination environment of Mn5 bridging three cubane units with a *mer*- configuration. Cubanes are represented as orange spheres around their centers of gravity for the sake of simplicity. i: $(0.5+x, 1.5-y, 0.5+z)$, ii: $(0.5-x, 0.5+y, 0.5-z)$, iii: $(1-x, 2-y, 1-z)$.

The cubane residing at (x, y, z) (coordinates of its center of gravity) is connected to a neighbouring cubane at $(0.5+x, 1.5-y, 0.5+z)$ through a Mn5 unit (x, y, z) which bonds an external oxygen atom from a long arm (O24 (x, y, z)) and an external oxygen atom from a short arm (O18 $(0.5+x, 1.5-y, 0.5+z)$) mutually trans. That forms 1-D chains propagated by the *n*-glide plane perpendicular to $[0\ 1\ 0]$, analogous to that observed in **10**. In addition, this Mn5 unit bonds another cubane unit located at $(0.5-x, 0.5+y, 0.5-z)$ through an ethylene glycol molecule. This ethylene glycol molecule has substituted two water molecules coordinated to two different Mn(II) units -- one at Mn5 (x, y, z) and the other at Mn6 $(0.5-x, 0.5+y, 0.5-z)$. In the same way, the cubane unit at $(0.5-x, 0.5+y, 0.5-z)$ is connected to the cubane placed at $(0.5+x, 1.5-y, 0.5+z)$ through Mn5 $(1-x, 2-y, 1-z)$ and Mn6 $(0.5+x, 1.5-y, 0.5+z)$ (Figure 9.3). That generates 2-D layers of covalently bonded 1-D chains. In general terms, the structure of **13** is almost the same as that of **10** but with the 1-D chains bonded by a double bridge that involves Mn5, Mn6 and ethylene glycol molecules (Figures 9.4 and 9.5).

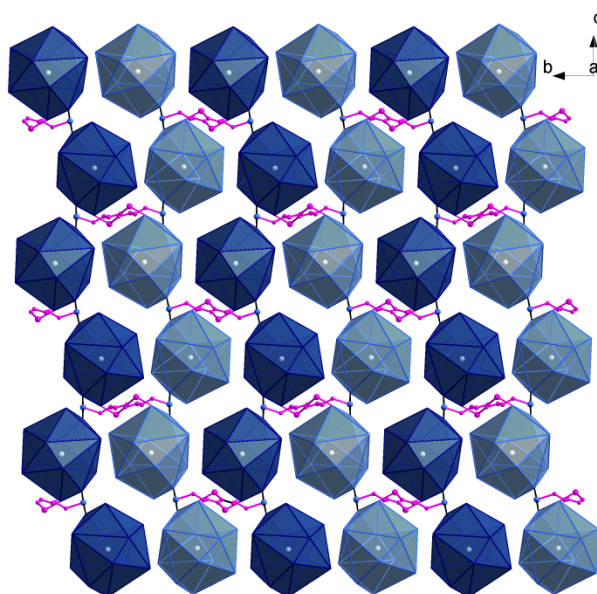


Fig. 9.4. View of a single layer of compound **13** perpendicular to the a -axis. The layers are formed by the linkage of the same chains that constitute compounds **10**, **11** and **12**. Chains are represented alternately in dark and light blue. The double bridges between chains are plotted in fuschia.

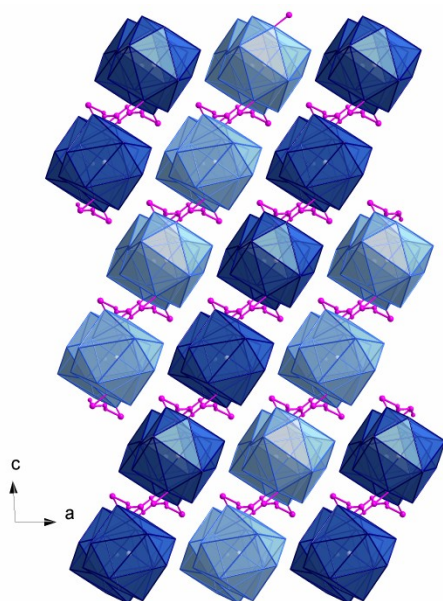


Fig. 9.5. View of packing of the layers in the (1,0,-1) family planes. Layers are represented alternately in dark and light blue. The double bridge between chains are plotted in fuschia.

The 19 coordinated water molecules and the 6.5 free waters form a rich H-bonded net within the crystal. There are 3 different motifs (Figure 9.6). When extended by symmetry, this H-bonded net traverses the unit cell through different pathways (Figure 9.7). That makes this

compound a candidate for proton transport via the Grotthuss mechanism, as previously described for compound **10**.

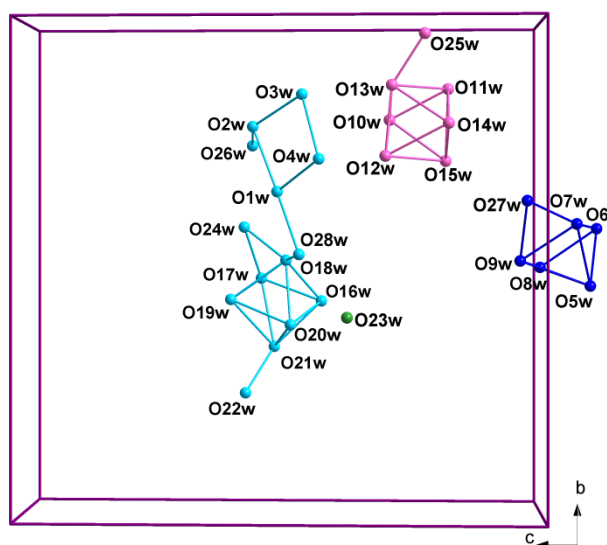


Fig. 9.6. Representation of the H-bonded chains of one asymmetric unit. Four independent motifs are found.

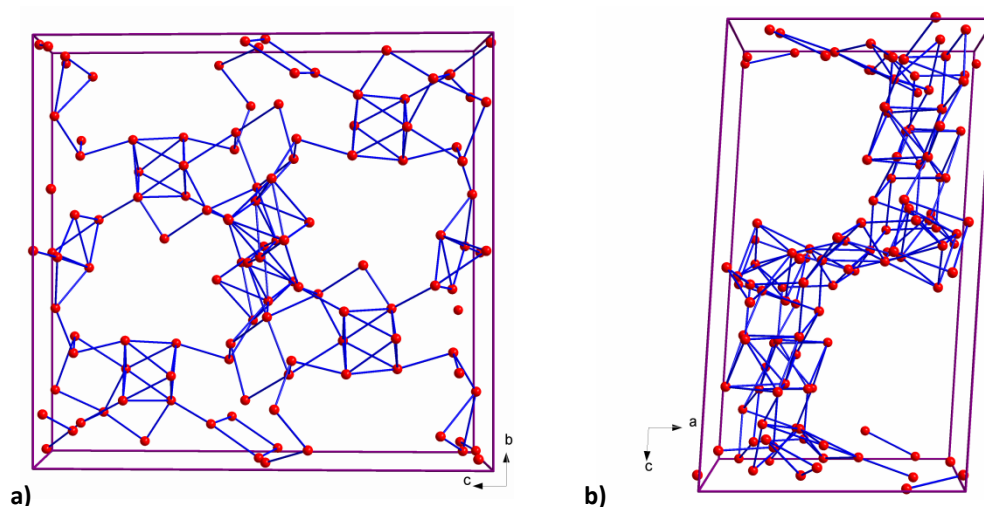


Fig. 9.7 H-bonded water chains within a complete unit cell viewing along the a -axis (a) and the b -axis (b). They form a unique motif where the 28 water molecules are connected forming several routes to cross the crystal.

The Kitaigorodskii Packing Index (K.P.I.)^[B1] calculated using Platon,^[6] is 71.1%. As the calculation is complicated for disordered structures, the input to Platon (Shelx .res file) was modified giving full occupancy to the half occupied water molecule O28w. When the 6.5 free molecules of water were removed from the input file, a K.P.I. of 64.6% was obtained. The K.P.I.

value for a structure with no pores or channels is in the range of 65 - 70%, so we can conclude that the compound is not porous even when the species within the layers are removed.

There is evidence for a reversible dehydration process through a SC-SC transformation; nevertheless, its characterization has not been possible yet. Crystals of **13** do not undergo dehydration at room temperature as do those of **10**. A thermal treatment or another alternative system to provoke dehydration, such as a desiccator or a dry flux of N₂, is needed for the process to take place. After that the unit cell suffers a reduction of 286.8 Å³ in volume which is in accord with the volume change observed for compound **10**. When the crystal is exposed to a humid atmosphere, the initial cell is restored.

9.3 Conclusions

This chapter concludes the synthesis and characterization of a family of compounds possessing different arrangements of the same secondary building unit (SBU). The results show how cubanes are optimal SBUs for the construction of a wide variety of related compounds with dimensionalities ranging from discrete molecules to 3-D structures with different properties and behaviours.

In light of the results obtained for compound **10**, described in the preceding chapter, the rich H-bonding network in **13**, with its varied pathways through the crystal, suggests that compound **13** may also display proton transport. In addition, for compound **10** a previous partial dehydration coexists with the complete interchange of H by D. The present compound **13** does not undergo the dehydration at room temperature; and if it displays proton transport, that phenomenon could be studied on its own in the absence of the dehydration. There is evidence for a reversible dehydration of **13** at higher temperatures; some further work is needed for a complete characterization of compound **13**.

References

- [1] S. C. Capelli, L. R. Falvello, E. Forcen-Vazquez, G. J. McIntyre, F. Palacio, S. Sanz, M. Tomas, *Angewandte Chemie (International ed. in English)* **2013**, *52*, 13463-13467.
- [2] W. G. Wang, X. F. Zhang, F. Chen, C. B. Ma, C. N. Chen, Q. T. Liu, D. Z. Liao, L. C. Li, *Polyhedron* **2005**, *24*, 1656-1668.
- [3] A. Altomare, G. Cascarano, C. Giacovazzo, A. Guagliardi, *Journal of Applied Crystallography* **1993**, *26*, 343-350.
- [4] G. M. Sheldrick, *Acta Crystallographica Section A* **2008**, *64*, 112-122.
- [5] E. Burzuri, J. Campo, L. R. Falvello, E. Forcen-Vazquez, F. Luis, I. Mayoral, F. Palacio, C. Saenz de Pipaon, M. Tomas, *Chemistry-a European Journal* **2011**, *17*, 2818-2822.
- [6] A. L. Spek, *Acta Crystallographica Section D-Biological Crystallography* **2009**, *65*, 148-155.

- [P1] CrysAlisPro, Oxford Diffraction Ltd., Version 1.171.33.31

- [P2] Diamond. Klaus Brandenburg, Crystal Impact GbR, Bonn, Germany. Version 3.2i.

- [B1] A.I. Kitaigorodskii, *Molecular Crystals and Molecules*, Academic Press, New York, 1973.

Spanish summary and conclusions

SMM basados en Cubanos Metálicos
con el Ligando Citrato: Obtención,
Caracterización y Propiedades

Resumen y conclusiones de la memoria de tesis

Resumimos aquí los aspectos más importantes del trabajo llevado a cabo en esta Tesis Doctoral y descrito en los capítulos anteriores, junto con sus conclusiones.

La tesis, titulada "Cubanos Metálicos con el Ligando Citrato: Obtención, Caracterización y Propiedades," se basa en el estudio de compuestos conocidos comúnmente como cubanos, formados por el ligando citrato (tetra anión del ácido cítrico) y cobalto o manganeso. El trabajo se ha dividido en tres partes para una exposición más clara de los resultados obtenidos.

En la primera parte se ha llevado a cabo un completo estudio de la unidad cubano. En él, aspectos importantes de dicha unidad tales como su estructura, quiralidad y topología de su periferia han sido descritos y comparados. Así mismo, se ha propuesto un sistema de nomenclatura para el sistema cubano con el objetivo de simplificar futuras descripciones de su estructura y coordinación y de unificar los resultados. Finalmente, se ha revisado y clasificado los modos de coordinación de las diferentes unidades cubano obtenidas así como los de los ejemplos previamente publicados.

La segunda parte de la tesis se centra en el estudio de los cubanos de citrato y cobalto. Se ha comprobado que estos compuestos son capaces de comportarse como "Single Molecule Magnets" (SMMs), exhibiendo interesantes propiedades magnéticas. Se ha logrado la síntesis de una familia de compuestos relacionados entre sí que presentan diferentes dimensionalidades. El primer capítulo de esta parte es una introducción al magnetismo y a los SMMs desde una aproximación química. El capítulo 3 está dedicado al estudio de una pareja de compuestos relacionados a través de una transformación reversible de monocristal a monocristal (SC-SC, por sus siglas en inglés). Ambas especies son moléculas discretas. Una de ellas presenta una estructura cristalina modulada. Los capítulos 4 y 5 constan de un conjunto de citrato-cubanos de cobalto con estructuras 2-D y 3-D respectivamente.

Finalmente, la tercera y última parte de la tesis se centra en los compuestos de citrato y manganeso cuya unidad básica es el cubano. Estos compuestos, a pesar del evidente parecido estructural con los compuestos de cobalto, no presentan comportamiento de SMM. Sin embargo, se ha observado que son capaces de dar lugar a reacciones de pérdida y ganancia de agua de forma reversible en condiciones ambiente a pesar de tratarse de materiales no porosos. Además, este proceso tiene lugar manteniendo la cristalinidad de las muestras lo que nos ha permitido su estudio mediante difracción de Rayos X. Esto ha aportado valiosa información acerca del mecanismo que opera en cada caso. Así pues, el primer capítulo de esta parte es una introducción a la química y reactividad en estado sólido así como al transporte de protones en diferentes materiales. Los siguientes capítulos, números 7, 8 y 9 se centran en el estudio y propiedades de compuestos 0-D, 1-D y 2-D respectivamente basados en cubanos de citrato y manganeso.

Parte I: Citrato-cubanos de metales de transición.

Esta parte consta de un único capítulo (Capítulo 1) que combina introducción y revisión bibliográfica con resultados experimentales de todos los compuestos que serán tratados en detalle en los siguientes capítulos. Es importante remarcar que si bien los compuestos presentados en la tesis se dividen en función del átomo metálico que los constituye, en esta parte, al tratarse de un capítulo que pretende dar una visión general de los cubanos de citrato con metales de transición, se encuentran resultados obtenidos para todos ellos, sin distinción en función del átomo metálico.

El capítulo comienza con una breve introducción a cerca del origen del uso del término cubano para describir estructuras basadas en un cubo en cuyos vértices se encuentran diferentes átomos. El primer compuesto al que se le asignó dicho nombre es el Pentaciclo [4.2.0.02,5.03,8.04,7] octano, un hidrocarburo sintetizado por primera vez en 1964 por P. E. Eaton.^[1] A continuación se prosigue con una presentación de los ejemplos más representativos de sustancias que presentan cubanos en su estructura, a destacar los cubanos $[\text{Fe}_4\text{S}_4]$ presentes en las ferredoxinas (proteínas encargadas de la transferencia electrónica en procesos metabólicos),^[2] proteínas Fe-S de alto potencial (HiPIP, por sus siglas en inglés)^[3] y las nitrogenasas.^[4]

Por otro lado, se presenta al ligando citrato empleado en la síntesis de nuestros compuestos. Esta sustancia, a parte de su gran importancia biológica en procesos tan conocidos como el ciclo de Krebs (o ciclo del ácido cítrico) es un ligando muy versátil en la química de coordinación.^[5, 6] Presenta un grupo -OH, un grupo -COOH y dos -CH₂COOH, así pues, puede experimentar hasta 4 desprotonaciones. Existen valores tabulados de pH para las desprotonaciones correspondientes a los grupos carboxilato y metil carboxilato, sin embargo no para el grupo -OH. Se ha observado a lo largo de este trabajo que la coordinación del este grupo a un átomo metálico, favorece la salida del protón enlazado. Para valores de pH entre 7-8 en presencia de un metal de la primera serie de transición, el ácido cítrico se encuentra totalmente desprotonado con el oxígeno del grupo -OH coordinado a dicho átomo. Se cree que esta coordinación da lugar a una estructura estable que hace que su desprotonación sea favorable.

En términos generales, la estructura de un cubano de citrato y metal de transición, $[\text{MT}_4(\text{citrato})_4]^{n-}$, está formado por un cubo en cuyos vértices encontramos de forma alterna los 4 MT y los 4 O de los grupos -OH de los 4 ligandos citrato. Uno de los oxígenos del carboxilato y de los metil carboxilatos de cada citrato coordinan un MT en los vértices del cubo

formando anillos quelato de 5 y 6 miembros respectivamente. De este modo tenemos el núcleo cubano, rodeado en primer lugar por una capa de anillos quelato y en segunda instancia por un envoltorio de 12 átomos de oxígeno parcialmente negativos (los que no quelatan el cubo). Esto da lugar a una unidad muy estable como grupo con una alta reactividad y versatilidad en cuanto a coordinación a otras especies externas.

- **Parte experimental**

El ácido cítrico es un reactivo proquiral, es decir, la coordinación de dos grupos diferentes a los dos grupos metil carboxilato deja al carbono central rodeado de 4 grupos químicamente distinguibles. Así se ha estudiado la quiralidad de todos los ligandos citrato presentes en cada uno de los compuestos de la tesis con resultados muy variables de uno a otro. Por otro lado, la formación de estructuras cubano, con simetría S_4 , pone de manifiesto la simetría latente del citrato, ya que a partir de un ligando poco simétrico se consiguen estructuras de simetría mayor.

En el estudio de los cubanos obtenidos en este trabajo hemos encontrado que algunos de ellos presentaban una estructura diferente a la de todos los ejemplos publicados hasta la fecha.^[6-10] Así pues, estas estructuras son isómeros de coordinación con una distribución de los anillos de 5 y 6 miembros en torno al cubo diferente. Dadas estas diferencias se ha llevado a cabo un estudio de la distorsión tanto del cubo como de su periferia en términos de sus parámetros de elongación cuadrática. Para ello, el cubo se ha considerado como compuesto por dos tetraedros interpenetrados (uno formado por los 4 MT y otro por los 4 O) y la periferia se ha descompuesto en 3 tetraedros formados por 4 átomos de oxígeno relacionados por simetría. Los resultados muestran que para los dos isómeros (A y B a partir de ahora) el núcleo cubano es prácticamente regular mientras que en la periferia tenemos un tetraedro regular, uno elongado y otro achatado.^[11]

A continuación se pasa a describir las diferencias en la periferia de los dos isómeros formada por los 12 átomos de oxígeno no coordinados. Para el isómero A (correspondiente a los previamente publicados, también encontrado para algunas de nuestras muestras) la periferia puede ser descrita como un icosaedro con 12 vértices y 20 caras. Sin embargo para el nuevo isómero (isómero B) dos pares de caras (relacionadas por simetría con otras dos) presentan un ángulo diedro suficientemente pequeño como para considerarlas una sola cara, así pues se describe como un octakaidecaedro con 12 vértices y 18 caras.

Como se ha comentado brevemente, la unidad cubano es muy reactiva y versátil en cuanto a modos de coordinación. Por este motivo se propone un sistema de nomenclatura que asigna un nombre diferente a cada uno de los oxígenos que rodean al núcleo, los 12 internos (formando los anillos quelato) y los 12 externos (no coordinados al núcleo). Los nombres están formados por una combinación de 2 letras y un número.

Primera letra (mayúscula): L o S en función de si es un oxígeno perteneciente a un metil carboxilato (pata larga, Long) o a un carboxilato (pata corta, Short).

Número: dada una orientación concreta del cubano se numeran los oxígenos de los citratos siguiendo un orden predefinido. Como resultado tenemos que las 4 patas cortas tienen números del 1 al 4 (S1 a S4) y las patas largas de 1 a 8 (L1 a L8). Nota que para las patas largas L1 y L2 corresponden a un mismo citrato. Lo mismo ocurre con L3-L4, L5-L6 y L7-L8 respectivamente.

Segunda letra (minúscula): “e” o “i” dependiendo de si se trata de un oxígeno externo (no coordinado al cubo, e) o interno (coordinado al cubo, i).

Así pues, la información que podemos extraer directamente del nombre de un oxígeno es:

- 1) La naturaleza de la pata a la que pertenece el oxígeno, larga o corta y si es un oxígeno formando un anillo quelato o se encuentra no coordinado a los metales del cubo.
- 2) En el caso de más de un oxígeno, permite saber si corresponden o no al mismo citrato.
- 3) Para polímeros, nos dice si los puntos de propagación del polímero son análogos, relacionados por simetría o simplemente diferentes.

Por último, se presenta una revisión de todos los modos de coordinación para las especies cubano de MT y citrato. Este análisis se divide en dos, por un lado cómo las especies externas se coordinan a la superficie del cubo y por otro lado como el cubo, actuando como un ligando en sí mismo, coordina a dichas especies.

- **Conclusiones**

En esta primera parte se pretende poner en contexto al lector y hacer más sencilla la toma de contacto con estos compuestos. Con este objetivo se han revisado las estructuras previas y se han comparado con las obtenidas en este trabajo. Se ha dado también un detallado estudio y descripción de sus estructuras comenzando desde lo más elemental y llegando a aspectos

más generales. Con este estudio previo, se intenta que la descripción de las estructuras presentadas en los siguientes capítulos sea lo más sencilla y menos repetitiva posible, ya que al haber introducido los aspectos generales en un capítulo anterior, solamente han de remarcar las individualidades características de cada compuesto en concreto. Finalmente, el sistema de nomenclatura propuesto para estas unidades cubano MT-citrato será empleado para describir la coordinación de todos los compuestos presentados a lo largo de la tesis.

Parte II: Citrato-cubanos de cobalto.

A lo largo de esta parte, el estudio se centra en aquellos compuestos obtenidos basados en cobalto. Esta parte se divide en 4 capítulos, el primero de ellos es una introducción sobre SMMs y los restantes capítulos están dedicados a una familia de compuestos, todos ellos basados en cubanos de citrato y cobalto clasificados en función de sus dimensionalidades, yendo desde moléculas discretas (capítulo 3) hasta polímeros 3-D (capítulo 5).

- **Capítulo 2: Introducción II**

Se ha comprobado que los cubanos de Co(II) son capaces de comportarse como Single Molecule Magnets (SMMs). En esta parte se hace una revisión completa sobre este tipo de nuevos materiales magnéticos con un enfoque químico. La introducción comienza con una parte general de magnetismo en la que se explican brevemente los diferentes tipos de comportamientos magnéticos. Se describen los conceptos de paramagnetismo, ferro-, ferri- y antiferromagnetismo, metamagnetismo, antiferromagnetismo no colineal, que puede dar lugar a débil ferromagnetismo y vidrio de espín o “spin glass” (características, ejemplos y aplicaciones).^{[B3] [12]}

A continuación nos centramos en el magnetismo de los iones Co(II). En esta breve sección se explica por qué los compuestos basados en cubanos de Co(II) presenta una lenta relajación magnética y por tanto comportamiento de SMM. Este comportamiento se debe a la anisotropía que presenta el Co(II), que es un ion d^7 . Los iones con esta configuración que se encuentran en un entorno octaédrico de alto spin tienen 5 electrones en los orbitales T_{2g} (dos de ellos con 2 electrones apareados cada uno y el tercero con sólo un electrón) y 2 electrones en los orbitales E_g . Para los iones Co(II) se ha comprobado que el momento magnético orbital tiene una gran influencia en el momento magnético total. Esta anisotropía de los iones individuales es trasladada al complejo formado por el acoplamiento de los 4 iones cobalto en los vértices del cubo.^[13, 14]

En general los imanes pueden encontrarse en cualquier material de uso cotidiano como pueden ser memorias magnéticas, altavoces, micrófonos o motores y generadores. Así pasamos a hablar de los imanes moleculares. Estos nuevos materiales magnéticos son descritos en detalle y comparados con los ejemplos convencionales. En este caso el magnetismo no procede del ordenamiento a lo largo de la estructura de los pares de electrones desapareados en orbitales d o f como en los imanes convencionales sino que los electrones desapareados también se pueden encontrar en orbitales s y p o incluso en el ligando empleado. Son imanes en los que la unidad básica no es un átomo sino un conjunto de ellos. Las interacciones entre las moléculas pueden darse por varias vías, comúnmente por acoplamiento dipolar, orbitales ortogonales no solapados o acoplamiento ferromagnético.

Los imanes moleculares presentan varias ventajas con respecto a los imanes convencionales como por ejemplo baja densidad, transparencia o aislamiento eléctrico. Su procesado también es ventajoso ya que evita las extremas condiciones necesarias en la industria metalúrgica que se encarga de la preparación de imanes convencionales.

Dentro de los diferentes tipos de imanes moleculares, los más significativos son los compuestos organometálicos como el $[\text{FeCp}^*_2]^{+}[\text{TCNE}]^{-}$ (Cp^* = pentametil ciclopentadienilo; TCNE = tetraciano etileno),^[15] los compuestos puramente orgánicos como la fase ferromagnética beta del p-nitro-fenil nitrosil nítróxido, descrito por Nakazawa *et al.*,^[16] el antiferromagneto no colineal descrito por Banister *et al.*,^[17] y Palacio *et al.*,^[18] los compuestos híbridos orgánicos/inorgánicos,^[19] los compuestos inorgánicos basados en redes de cianuros,^[20] los ferromagnetos moleculares como el caso del complejo basado en Fe(III) con fórmula $\text{Fe}(\text{Cl})\text{S}_2\text{CN}(\text{C}_2\text{H}_5)_2$ ^[21] y por último los Single Molecule Magnets.^[7-9, 22, 23]

Los SMMs son compuestos polinucleares de MT que presentan un comportamiento superparamagnético. Estos MT están unidos a través de ligandos no inocentes formando clústeres de tal manera que los iones metálicos se acoplan dotando al clúster de spin propio. Pueden verse como un estado intermedio entre un ion paramagnético aislado y las redes extendidas de óxidos o hidróxidos. El interés en ellos radica en que sus propiedades combinan características de la física clásica con la física cuántica.

Para que un complejo se comporte como SMM tiene que cumplir varios requisitos. Entre ellos está tener un alto valor de espín y de anisotropía, aunque estas condiciones no se aplicarían de la misma forma en el caso de los Single Ion Magnets (SIM), en los que una molécula formada por un único ión, en general de lantánido, presenta un comportamiento análogo al de los SMM. Los efectos de relajación en estos compuestos han puesto de

manifiesto la extrema importancia que desempeña la anisotropía magnética del ión.^[24] Este spin debe de estar aislado de los estados excitados. La separación entre el estado fundamental y los estado excitados depende de la fuerza de la interacción de intercambio. Cuanto mayor es ésta, mayor será la separación entre niveles. Otro requisito es la anisotropía. La mayor contribución a la anisotropía global del clúster es el tensor suma de las anisotropías de los iones individuales que lo forman. Cuanto mayor sea la anisotropía del compuesto más alta será la temperatura de bloqueo del material. Lo deseado es que el compuesto presente un estado fundamental con un valor de spin lo más elevado posible y que al mismo tiempo presente una gran anisotropía. La evidencia experimental que revela el comportamiento de un material como SMM son las medidas de susceptibilidad en AC (corriente alterna). Al aplicar un campo magnético alterno a diferentes frecuencias bajando la temperatura se observa la aparición de un pico dependiente de la frecuencia que corresponde a un bloqueo de la muestra. La temperatura a la que dicho bloqueo tiene lugar se llama temperatura de bloqueo, T_b .^{[25] [26]}

Tras esta parte introductoria más teórica, se pasa a una parte más química en la que se muestran las diferentes aproximaciones químicas para la preparación de SMMs.

La mayoría de trabajos para la obtención de nuevos SMM se centran en el aumento de la nuclearidad del clúster, lo que produce en principio sustancias con mayores valores de spin en el estado fundamental. Sin embargo se ha observado que esto no siempre es así y que las predicciones sobre estos materiales no son del todo precisas ni para el magnetismo ni para su síntesis. Detalles como el ligando usado, el estado de oxidación del metal, la proporción metal/ligando y las condiciones de reacción (pH, temperatura, tiempo, etc.) son factores importantes a tener en cuenta. La mayoría de investigación en síntesis de SMM emplea técnicas aleatorias en lugar de rutas sintéticas detalladamente estudiadas debido a esta aleatoriedad en los resultados.^[B4]

Sin embargo es cierto que el uso de ciertos ligandos o metales favorecen la obtención de unas estructuras frente a otras. Este es el caso del ligando 1,4,8,11-tetraaza ciclotetradecano (cyclam) que se emplea para bloquear la posiciones ecuatoriales del átomo metálico, favoreciendo la reactividad en las posiciones axiales.

A pesar de que es sabido que los ligandos carboxilato producen una interacción magnética débil, son sustancias que se emplean comúnmente debido a su versatilidad en modos de coordinación y la facilidad con la que se pueden modificar los sustituyentes de las cadenas laterales. En este punto se muestran no sólo los modos de coordinación propios de un ligando carboxilato genérico sino que se han estudiado todos los modos de coordinación del ácido

cítrico en cualquiera de sus desprotonaciones a MT que se han encontrado en la Base de Datos de Cambridge (Cambridge Database System V.1.15).

El capítulo prosigue con una clasificación de los SMM más comunes. Entre ellos tenemos el conocido Mn₁₂ (el primer ejemplo identificado como SMM) y sus múltiples derivados o los clústeres de Fe₈.^[27]

Especial mención reciben los SMMs basados en Co(II). Existe un gran número de ejemplos debido a las interesantes propiedades del Co(II). En esta sección se comentan brevemente varios ejemplos de estos compuestos como son los cubanos Co₄ (los 4 átomos de cobalto en los vértices de un cubo que es completado por átomos correspondientes al ligando empleado),^[6-10, 13, 23, 28, 29] cuadrados Co₄ (4 átomos de cobalto formando un cuadrado),^[30] pirámides Co₅ (pirámide de base cuadrada donde el entorno de los Co de la base es octaédrico mientras que para el que está en el ápice es de prisma trigonal),^[31] discos Co₇ (compuestos de valencia mixta donde un átomo de cobalto se encuentra en el centro de un hexágono formado por los restantes 6 Co)^[32] y por último clústeres Co₁₂ (3 cubanos conectados por puentes μ_6 -nitrate).^[33]

Por otro lado se ha hecho una búsqueda en la Web of Science (WOS Versión 5.13.1) de todos los compuestos basados en la unidad cubano con comportamiento de SMM. Se han encontrado ejemplos para Co(II),^[13] Dy(III),^[34] Fe(II),^[35] Ni(II),^[36] Zn(II),^[6] Cu(II),^[37] compuestos homometálicos de valencia mixta^[38] y derivados heterometálicos que contienen Mn(III)Ni(II), Mn(III)Zn(II),^[39] Cu(II)Y(III) y Cu(II)Gd(III).^[40]

La siguiente parte del capítulo está dedicada a la deposición de SMMs en superficies. Este paso es de crucial importancia para la futura aplicación de estos materiales en la creación de dispositivos tales como memorias magnéticas o sensores. Sin embargo este proceso presenta un desafío ya que no es tan sencillo como aparenta en un principio. En primer lugar se debe escoger el sustrato adecuado, generalmente silicio u oro dada su importancia en aplicaciones tecnológicas. Una vez escogido, éste debe preservar las propiedades de SMM y el aislamiento de una molécula con respecto a sus vecinas. Además debe haber algún tipo de interacción que permita transferir la información contenida en una molécula a otro dispositivo a través de la superficie. Por su parte el proceso de deposición no puede ser aleatorio, se han de poder dirigir las moléculas de una forma controlada y ordenada al sustrato de tal modo que sea un proceso homogéneo y reproducible. Con este fin, se han desarrollado y probado (sin éxito a día de hoy) numerosas técnicas que se detallan en el texto principal y que sólo se enumeraran aquí.

- Películas Langmuir-Blodgett de polioxometalatos (POMs), derivados del Mn12 y ferritina.^{[41] [42]}
- Ablación laser^[43]
- Auto ensamblaje por deposición directa o mediante la pre-funcionalización del sustrato.^[44]

A continuación, se detallan en el texto todos los soportes empleados para la deposición de sustancias, así como las moléculas utilizadas para la pre-funcionalización de dichos soportes. Entre otros, los sustratos empleados son Au (111) (110), Si (100), Sílica (MCM41), Cu(100), AgO, Al₂O₃, CuO, etc.

Finalmente, una pequeña sección de aplicaciones concluye esta primera introducción. Actualmente, los usos de los SMM se basan en el estudio de nuevos comportamientos magnéticos y en la postulación y comprobación de nuevas teorías. Sin embargo, la dificultad para su deposición en superficies está retrasando sus aplicaciones tecnológicas. Dentro de las múltiples aplicaciones potenciales están los dispositivos magnéticos de almacenaje de información, los materiales híbridos que combinen la relajación magnética lenta con otras propiedades (como propiedades ópticas o eléctricas), imanes interconvertibles o incluso materiales innovadores como los imanes en capas o imanes líquidos.

- [Capítulo 3: Citrato cubanos de cobalto 0-D](#)

En este capítulo se presentan dos compuestos discretos basados en cubanos de citrato y cobalto, como todos los presentados en esta parte de la tesis. Estos dos compuestos están relacionados por una transición de monocristal a monocristal (Single Crystal to Single Crystal, SC-SC) reversible a temperatura ambiente. Ambos productos se han podido caracterizar por difracción de Rayos X.

El primero de los productos presenta una complicación añadida al tratarse de una estructura modulada. Esto consiste en una estructura desordenada en la que las partes implicadas en dicho desorden presentan periodicidad a lo largo de la estructura. Esto se observa en la propia difracción, en la que además de los picos Bragg procedentes de la estructura principal, tenemos unos picos satélites a una cierta distancia de los picos principales. Si dicha distancia es un número racional, hablamos de una modulación conmensurable y si se trata de un valor irracional, como es el caso, tenemos una estructura inconmensurable. El llamado vector \mathbf{q} es el vector que relaciona la difracción satélite con la principal. Como es lógico, los picos satélites, que sólo se deben a la porción de átomos en

desorden tienen muchísima menos intensidad que los picos principales, así que la toma de datos deberá realizarse de tal modo que permita tener suficiente intensidad en los picos satélites para poder proceder posteriormente a su uso en el refinado de la estructura.

Así pues, para resolver este tipo de estructuras el primer paso es resolver lo que se denomina la estructura media. Es decir, resolver el problema como si se tratase de un desorden sencillo. A continuación, se determina el valor del vector \mathbf{q} y a partir de ahí se ha de buscar una explicación con sentido químico al desorden y su periodicidad. El último paso es algo más complejo (debido a la poca intensidad de los picos satélite) y requiere el uso de software especial para el refinado final del desorden.

En este capítulo se ha refinado la estructura con desorden inconmensurable de la primera especie discreta y se ha propuesto una explicación y modelo para el desorden de dicha molécula (compuesto **1**).

Por otro lado se ha observado que, cuando esta especie se deshidrata en condiciones suaves, es capaz de perder moléculas de agua dando lugar a una especie ordenada (**2**), también discreta, preservando la cristalinidad de la muestra. La reversibilidad de este proceso es muy alta, en condiciones ambiente el compuesto **2** se transforma rápidamente en **1**.

Ambos compuestos se han caracterizado magnéticamente y se confirma su comportamiento como SMM. El mayor desorden en torno al cubano de la especie modulada hace que la temperatura de bloqueo de **1** sea mayor que la de **2**. De este modo se tiene una pareja intercambiable de SMMs relacionados a través de un simple proceso de deshidratación que puede ser provocado de forma controlada.

Por último, se ha observado que si las condiciones necesarias para la deshidratación de **1** se mantienen tras haberse formado el derivado **2**, aparece un tercer derivado, fruto de una masiva deshidratación que mantiene también la cristalinidad de la muestra. Este proceso sigue siendo reversible. Desafortunadamente, no ha sido posible la caracterización de esta tercera especie mediante difracción de Rayos X de monocristal ya que la calidad de los datos no era lo suficientemente buena como para tener un refinado final. Sin embargo la comparación de los difractogramas de polvo experimental y calculado confirma la existencia de este tercer derivado.

Conclusiones: se ha obtenido y caracterizado química y magnéticamente una pareja interconvertible de derivados con diferencias en su comportamiento SMM. La transformación de uno en otro se puede llevar a cabo de una forma controlada lo que permite su uso en

múltiples aplicaciones tales como sensor de humedad. La observación de un tercer derivado deja una puerta abierta a la continuación del estudio de este complejo sistema.

- [Capítulo 4: Citrato cubanos de cobalto 2-D^{\[9, 29\]}](#)

El siguiente capítulo de la tesis se centra en citratos cubanos de cobalto con estructuras bidimensionales. Está dividido en 3 apartados en los cuales se presentan 4 compuestos diferentes.

La primera parte describe las estructuras y propiedades de 2 compuestos isoestructurales, basados en la misma red 2-D aniónica pero cristalizados con diferentes contraiones, Rb^+ para el compuesto **3** y Cs^+ para el **4**. Ambos compuestos están formados por capas bidimensionales formadas por cubanos unidos entre sí a través de unidades magnéticamente activas de Co(II) . Este Co(II) completa su esfera de coordinación con 2 moléculas de agua y un etilenglicol. Cada cubano está unido a otros 4 cubanos formando una malla cuadrada. Las capas aniónicas se apilan perpendiculares al eje cristalográfico c de la celda tetragonal, siguiendo un patrón ABAB. Los cubanos dentro de una capa residen sobre los nodos de las dos capas vecinas logrando un empaquetamiento más eficiente. Entre las capas se encuentran los contraiones, moléculas de agua libre y etilenglicol empleados en la síntesis. Estas especies se encuentran en desorden y ésta es la diferencia más destacable entre los dos compuestos. Para el caso del derivado con Rb^+ , el catión está distribuido entre dos posiciones cristalográficas y presenta por parte asimétrica un total de 2.375 moléculas de agua distribuidas en 8 posiciones y 0.5 moléculas de etilenglicol. En el compuesto **4**, el Cs^+ está distribuido en 3 posiciones distintas y tiene por parte asimétrica 1.125 moléculas de agua en 3 posiciones cristalográficas y 0.625 moléculas de etilenglicol. Además, el espacio entre capas es ligeramente mayor para el compuesto con Cs^+ debido a que el eje c de la celdilla es ligeramente mayor (el espaciado entre capas es $0.5c$). Para los dos compuestos se han observado canales a lo largo de los ejes a y b que ocupan un 38.6% y 39.2% del volumen de la estructura respectivamente.

Para ambos compuestos se observa a aproximadamente 4 K el bloqueo característico de los SMMs. Sin embargo, tras el bloqueo se observa que el valor de la magnetización sigue aumentando, así que se llevaron a cabo medidas magnéticas a muy baja temperatura en un refrigerador de dilución. Los resultados muestran un segundo pico, independiente de la frecuencia, que puede ser debido o bien al bloqueo de la sub-red formada por los Co(II) que conectan los cubanos o a un ordenamiento colectivo del material.

En la segunda parte del capítulo encontramos un derivado formado por capas rómbicas aniónicas de la misma composición que las anteriores (un cubano unido a otros 4 mediante puentes Co(II) que en este caso completan su esfera de coordinación con moléculas de agua ya que en la síntesis no se emplea etilenglicol) que se apilan siguiendo un patrón ABAB perpendicular al eje *b*. En este caso los cubanos de una red yacen sobre los cubanos de las adyacentes de manera que el espacio se ocupa menos eficientemente que los ejemplos previos. El compuesto se ha cristalizado con Cs⁺ como contraión que se aloja entre las capas junto con moléculas de agua de cristalización. La mayor diferencia con los anteriores derivados es que el entorno del cubano no es simétrico debido a la formación de la red rómbica.

La caracterización magnética de este compuesto ha resultado ser análoga a la de los anteriores con una mayor energía de bloqueo debido a un entorno menos regular de este cubano.

En la tercera y última sección de este capítulo tenemos un derivado (compuesto **6**) cuya estructura es muy similar a la de los compuestos **3** y **4**, cristalizado con Cs⁺. En lugar de añadir etilenglicol se ha añadido 3,3'-tiodipropanol, especie que no entra a formar parte de la estructura. El resultado es un compuesto formado por capas 2-D aniónicas con una estructura cuadra casi idéntica a la de los compuestos **3** y **4**. La única diferencia es que la unidad Co(II) que une los cubanos completa su esfera de coordinación únicamente con moléculas de agua. Estas capas se apilan en la dirección del eje *c* de la celda tetragonal, siguiendo un patrón ABAB de manera que los cubanos de una red eclipsan los nodos de las vecinas. Compensando la carga negativa de la red polimérica tenemos 2 Cs⁺ y un [Co(H₂O)₆]²⁺ por cubano.

Tras la caracterización magnética de esta muestra se observa que la barrera de energía es 2 veces mayor a la de los otros dos compuestos con redes cuadradas. Se cree que esta diferencia se debe a la interacción de los contraiones con el campo magnético molecular del cubo.

Conclusiones: en este trabajo se ha sintetizado una serie de compuestos que presentan la misma red magnética con pequeñas modificaciones. Esto permite estudiar como las alteraciones del entorno de las redes magnéticas pueden influir en sus propiedades, mostrando las claves para el diseño de nuevos derivados.

El hecho de que estos compuestos estén formados por capas 2-D abre la posibilidad de utilizar una capa de estos materiales como una monocapa depositada sobre un soporte. Por otro lado, la presencia de canales entre capas llenos de especies en desorden sugiere que

dichos compuestos pueden dar lugar a reacciones de intercambio iónico o captura de disolventes o pequeñas moléculas huésped, procesos que harían de estos materiales sustancias multifuncionales.

Los experimentos realizados con los dos primeros derivados constituyen el primer caso en el que se lleva a cabo la caracterización magnética de cubanos con comportamiento de SMM?? a tan baja temperatura con el objetivo de elucidar lo que ocurre tras el bloqueo de los cubanos. Se ha observado que para estas muestras la señal que se observa antes de dicho bloqueo es el resultado de la suma de dos procesos. A 4 K los cubanos quedan bloqueados y a partir de ahí la señal observada es debida solamente al segundo de los procesos operantes en la muestra.

A pesar de que de forma cualitativa los resultados entre los dos derivados son análogos, no es así su análisis cuantitativo. Existe una diferencia de 0.05 K en la temperatura crítica para el segundo proceso de bloqueo observado a bajas temperaturas que puede atribuirse a pequeñas diferencias en el alineamiento del eje fácil de anisotropía del cubano y las unidades Co(II) anexas.

En los dos siguientes ejemplos se observa como pequeñas modificaciones tanto en el entorno directo del cubano como la introducción de nuevas especies dentro de la estructura del material son capaces de introducir cambios en el comportamiento magnético del material preservando su comportamiento como SMMs.

Este capítulo sirve también para mostrar la gran versatilidad de la unidad cubano y como cambios en principio poco trascendentes en el proceso sintético dan lugar a una variedad de compuestos, lo que hace óptimo su uso en la búsqueda de nuevos materiales.

- [Capítulo 5: Citrato cubanos de cobalto 3-D](#)

Este es el último capítulo dedicado a los cubanos de citrato y cobalto. Consta de dos partes en las que se presentan dos compuestos muy diferentes, ambos con una estructura polimérica tridimensional.

En la primera parte tenemos un derivado formado por una red tridimensional de alta simetría con una estructura tipo diamante. Estas redes aniónicas están formadas al igual que las de los capítulos anteriores por cubanos conectados a través de unidades Co(II). Cada cubo se encuentra unido a 4 vecinos. La diferencia es que los vecinos en lugar de encontrarse dentro del mismo plano se sitúan en los vértices de un tetraedro si consideramos a este cubo

colocado en el centro de dicho tetraedro. Así pues, el entorno de cada cubano es análogo a los de los carbonos sp^3 en la estructura del diamante. En estado sólido, el compuesto está formado por interpenetración de estas redes aniónicas. A pesar de que la interpenetración tiene lugar en la naturaleza para lograr un empaquetado más eficiente, el compuesto presenta canales a lo largo de su estructura donde se encuentran alojados los K^+ que actúan como contraiones y varias moléculas de agua libre.

Este compuesto se ha caracterizado magnéticamente, comprobándose su comportamiento como SMM. Se observa que tras el bloqueo de los cubanos a una temperatura próxima a los 4 K, la magnetización continúa creciendo dando lugar a un nuevo pico independiente de la temperatura a 2.9 K. Este comportamiento se asemeja al observado para los compuestos **3** y **4**, sin embargo, es la primera vez que este segundo pico se observa íntegramente dentro del rango de temperaturas habitual para este tipo de medidas. El análisis de estas medidas muestran que dicho pico es debido a una transición de fase.

Dada a la presencia de canales a lo largo de la estructura en donde se encuentran moléculas de agua libre, se lleva a cabo el estudio de la evolución de la muestra frente a la temperatura mediante difracción de Rayos X en polvo. Los resultados muestran que las moléculas de agua no abandonan la estructura fácilmente, conservándose el patrón de difracción hasta unos 80 °C. A partir de ahí, la cristalinidad se pierde y el compuesto pasa de un color fucsia a morado. Si la muestra se coloca dentro de una atmósfera húmeda durante una semana, recupera el color fucsia y el difractograma inicial se restaura por completo, por lo que la deshidratación masiva experimentada es un proceso reversible.

La segunda sección de este capítulo trata sobre otro polímero 3-D con una estructura altamente irregular. En este caso la propagación del polímero no se da a través de puentes sencillos sino que cada unidad Co(II) conecta 3 cubanos diferentes con una configuración *mer*- (en forma de T). Una forma sencilla de ver la estructura es como capas perpendiculares al eje *c* con un apilamiento ABAB conectadas a través de enlaces covalentes. Compensando la carga del polímero aniónico tenemos iones Ca^{2+} que se encuentran muy próximos a la red formando interacciones con los oxígenos de los carboxilatos. Este compuesto es isoestructural con el primer polímero tridimensional publicado por Murrie *et al.* en 2010 con una sustitución catiónica de Na^+ por Ca^{2+} .^[8]

Conclusiones: con este capítulo se concluye una parte en la que se ponen de manifiesto varios comportamientos generales de los citrato cubanos de cobalto. Entre los más importantes tenemos la gran estabilidad de la unidad cubano en sí misma, su alta reactividad y

versatilidad, la observación de que cambios en el entorno de los cubanos ya sea por coordinación o por proximidad, producen modificaciones en el magnetismo preservando el comportamiento de SMM y la posibilidad de emplear estos derivados para la preparación de materiales multifuncionales.

Por otro lado, el compuesto con la estructura tipo diamante presenta dos características que en principio parecen mutuamente excluyentes, interpenetración y porosidad. Además es el primer caso en el que existen claras evidencias de la coexistencia de un bloqueo y una transición de fase en estos compuestos. Esto se atribuye a la fuerte interacción entre las entidades magnéticamente activas debido a que la interpenetración hace que los segundos vecinos de un cubano dado pertenezcan a redes vecinas y no a su propia red. Normalmente se considera que el tener canales en una estructura de este tipo se traduce en un alejamiento de las unidades magnéticas y por tanto en una menor interacción. Este es un ejemplo de como una mayor interacción entre las mismas se puede conseguir al mismo tiempo que se tiene un material poroso. Esto deja abierta la puerta de experimentos de intercambio iónico.

Por su parte el polímero cristalizado con Ca^{2+} constituye el primer ejemplo en el que un compuesto de este tipo es obtenido empleando un metal alcalino térreo como contraión. Resulta sorprendente que pese a la diferente composición y síntesis este derivado sea estructuralmente equivalente a una sustitución isomorfa del catión de la primera y única estructura tridimensional de cubanos de citrato y cobalto. A pesar de que no se ha podido medir el magnetismo de esta muestra, se espera que sea análogo al de los ejemplos anteriores y al publicado por Murrie *et al.* para la muestra con Na^+ ,^[8] con modificaciones cuantitativas del orden de las observadas a lo largo de esta parte de la tesis.

Parte III: Citrato-cubanos de manganeso.

Esta tercera parte de la tesis se centra en el estudio de una serie de derivados basados en cubanos de citrato y manganeso. Como se ha dicho anteriormente, estos compuestos no se comportan como SMM, debido a que el Mn(II) es un ión muy isótropo y por tanto no se cumple uno de los requisitos necesarios para la observación de dicho comportamiento. Sin embargo se han observado interesantes propiedades para esta familia de compuestos cuyas dimensionalidades van desde moléculas discretas (capítulo 7) hasta polímeros 2-D (capítulo 9). Al igual que la parte anterior, ésta comienza con una introducción a cerca de aspectos que se tratarán en los siguientes capítulos.

- [Capítulo 6: Introducción III](#)

En el capítulo 3 se ha hablado de que el compuesto **1** experimenta una transición SC-SC. Debido a que el aspecto más interesante de las muestras que contienen cobalto es el comportamiento magnético no se ha querido entrar en detalle en ese otro fenómeno. Sin embargo, esta reactividad en estado sólido observada para dicha muestra cobra gran importancia en el estudio de los compuestos de manganeso. Así pues, este capítulo introductorio tratará entre otros temas los aspectos más interesantes de esta inusual reactividad.^[45, 46]

La introducción comienza con los aspectos más generales de la reactividad en estado sólido. Estos se presentan intentando respetar en la medida de lo posible la cronología de los avances en este campo con el objetivo de entender más en profundidad este área de la química.

Cuando se habla de reacciones químicas en estado sólido, se piensa en reacciones en las que la disposición de los grupos reactivos se encuentra fija y las moléculas no pueden moverse libremente como ocurre en disolución. La reactividad de dichas muestras no depende solo de las entidades que las forman sino también de su ensamblaje periódico en el sólido. Por lo general, se necesita un estímulo externo que desencadene la reacción, como puede ser luz o calor. Estas reacciones presentan numerosas ventajas con respecto a la química en disolución. Permiten, en primer lugar, un estereó control de los productos finales mucho más sencillo que en disolución y en numerosas ocasiones la obtención de productos que no pueden prepararse por ninguna otra vía, dando por lo general buenos rendimientos y un sólo producto en periodos de tiempo bastante aceptables. También se evita la formación de subproductos de solvatación. Otra ventaja está también relacionada con el no uso de disolventes. Desde el punto de vista de la química verde y la sostenibilidad, el no emplear disolventes evita los problemas de almacenaje y desecho que éstos conllevan. Por último, el equipamiento para llevar a cabo estas reacciones suele ser muy simple, una lámpara de ultravioleta (UV) o una fuente de calor que en ocasiones puede ser el propio sol son empleadas normalmente.

Las reacciones en estado sólido pueden implicar reactivos y productos en forma de monocristales, polvo microcristalino o sólido amorfo. Existe cierta controversia para aquellos casos en los que se forman fases líquidas intermedias como fundidos o fases eutécticas. Las reacciones que implican la completa destrucción de la estructura cristalina por fuerzas mecánicas no se suelen considerar reacciones en estado sólido genuinas ya que la energía mecánica puede causar la fusión local de la muestra. Las reacciones en las que se emplean

cantidades catalíticas de disolvente se consideran reacciones sin disolvente pero no reacciones en estado sólido.

A continuación, el capítulo prosigue con las técnicas empleadas en el estudio de estas reacciones como son la Resonancia Magnética en estado sólido (RMN), la calorimetría de barrido diferencial (DSC por sus siglas en inglés), el análisis termogravimétrico (TGA por sus siglas en inglés), la espectroscopía de infrarrojo (IR) y la difracción de Rayos X de polvo (XRPD por sus siglas en inglés (y muchas veces sencillamente XRD)) o de monocristal (XSCD por sus siglas en inglés) entre otras.

Tras estos aspectos generales, se continúa con una detallada descripción, ilustrada con ejemplos de los diferentes tipos de reacciones en estado sólido. Por motivos de brevedad, sólo se enumeran brevemente en esta parte.

Tipo de reacciones en estado sólido:

- Reacciones Gas-Sólido.^[47, 48]
- Reacciones intersólido: son reacciones entre diferentes muestras cristalinas. El proceso suele ser algo tan sencillo como mezclar los reactivos sólidos y aplicar el estímulo externo correspondiente. Ejemplos de este tipo de reacciones son la preparación de sólidos de inclusión o reacciones entre cristales.^[49]
- Reacciones intrasólido: estas reacciones implican solamente moléculas dentro de un mismo sólido. La mayoría de ejemplos son reacciones topotácticas. A pesar de que según el libro de Gold de la IUPAC^[48] reacciones topotácticas son aquellas reacciones reversibles o irreversibles que implican la introducción de especies huésped dentro de la estructura de un hospedador dando lugar a modificaciones en este último como por ejemplo la ruptura de enlaces, clásicamente se entiende como reacción topotáctica aquella que ocurre con el mínimo movimiento atómico o molecular y suele producirse cuando en un sólido los grupos reactivos están a distancias próximas a las de enlace.^[46, 50, 51]

Así pues, se introduce en este punto el “Postulado Topoquímico” enunciado por Kohlschutter en 1918 que establece que las reacciones en cristales tienen lugar con el mínimo movimiento atómico y molecular.^[52] Los puntos más importantes son:

- La reactividad intrínseca de una molécula es menos importante que la naturaleza del empaquetamiento de las moléculas vecinas que la rodean.

- La distancia de separación, la orientación relativa y la simetría espacial de los grupos reactivos es crucial.
- En sólidos cristalinos, hay pocas (o a veces sólo 1) conformaciones que puedan ser adquiridas por las moléculas.
- Los cristales moleculares presentan una amplia gama de formas polimórficas en las cuales un conformero en concreto o una simetría particular y la separación de los grupos funcionales prevalece.

El capítulo prosigue con la evolución histórica de estas reacciones, lo que nos lleva a la búsqueda un una explicación para todas aquellas reacciones que violan estas reglas. Se observó que este postulado obvia dos aspectos fundamentales como son los efectos de la excitación molecular y la influencia de las moléculas vecinas.

Craig *et al.* introducen el término “preformación dinámica” para explicar los efectos de la excitación electrónica en las moléculas.^[53] Por su parte, Cohen *et al.* acuñan el término “cavidad de reacción” que tiene en cuenta el entorno de los grupos reactivos.^[54] Así pues el postulado se puede reformular diciendo que “las reacciones que tienen lugar bajo el control de la red ocurren provocando los cambios o distorsiones mínimos en la superficie de la cavidad de reacción”.

Tras esta revisión de la evolución de las reacciones topotácticas, se presenta una serie de ejemplos en los que se pone de manifiesto la multitud de procesos que pueden tener lugar en estado sólido. Entre ellos tenemos las foto ciclo adiciones [2+2], polimerizaciones, polimorfismo, deshidratación, descomposición y transferencia electrónica (redox).^[55]

Esta sección del capítulo termina con un apartado dedicado a aquellas reacciones que tienen lugar conservando la cristalinidad de la muestra en un proceso monocristal a monocristal (SC-SC, por sus siglas en inglés).^[50, 56] Es importante destacar que no existe ningún tipo de reacción típica para las transformaciones SC-SC, esto es simplemente una característica propia de la reacción que puede observarse en cualquier proceso. Al contrario de lo que se creía en un principio, este fenómeno se puede observar incluso cuando tenemos movimiento molecular de largo alcance dentro del cristal. De algún modo, la red cristalina es capaz de cooperar de forma conjunta para adoptar la nueva situación. Esto es de especial importancia en las reacciones de pérdida y captura de disolvente en muestras no porosas.^[57]

Uno de los aspectos más deseables de estos procesos es que permiten la caracterización completa de las especies inicial y final por técnicas como la difracción de Rayos X de

monocristal, lo que es de vital importancia para la elucidación del mecanismo de reacción así como en la explicación de los cambios ocurridos. Avances recientes han hecho posible la obtención de datos de alta calidad en periodos razonables de tiempo, lo que ha permitido el estudio de estos procesos “in situ”.

Tras esta introducción al campo de la reactividad en estado sólido, en la segunda parte de la introducción se trata el tema del transporte protónico haciendo especial hincapié en el mecanismo de Grotthuss. A pesar de la antigüedad de este mecanismo y del gran número de ejemplos encontrados en diferentes campos de investigación, sigue sin tener una explicación clara y su observación directa es complicada, necesiándose cálculos teóricos y simulación para la confirmación de dicho fenómeno.^[58]

El apartado comienza con una discusión acerca del transporte protones. Un posible mecanismo es aquel en el que un protón extra salta de una molécula de agua a otra a distancia de puente de hidrógeno dispuestas en una cadena. Este fenómeno se conoce hoy en día como el “Mecanismo de Grotthuss” y se observa por ejemplo en membranas. Otro mecanismo es el llamado “Transporte de Vehículo” en el que el protón no salta sino que es transportado por un portador como pueden ser los iones H_3O^+ o el NH_4^+ .^[59]

A continuación se hace un repaso al estudio de Grotthuss sobre pilas galvánicas que sirvió de precursor de lo que hoy conocemos como el “Mecanismo de Grotthuss”.^[60] Esto viene seguido de su reinterpretación actual y de una descripción del mecanismo acuñado con dicho nombre.^[61] Se establece que el salto protónico de una molécula de agua a otra vecina tiene lugar a través de los llamados cationes del agua (Zundel e Eigen)^[62] siendo de vital importancia las esferas de solvatación de dichos cationes así como la geometría de la molécula de agua implicada y la de sus vecinas en la primera y segunda esfera de solvatación.^[63]

Como se ha mencionado antes, la simulación y los cálculos teóricos son necesarios en la mayoría de casos para la confirmación del mecanismo operante en las muestras. Las técnicas más habituales son las Simulaciones Dinámicas de Car y Parrinello (CPDS por sus siglas en inglés)^[64] y el Método Empírico de Enlace de Valencia (EVB por sus siglas en inglés).^{[65] [66]}

El capítulo acaba con una revisión de los ejemplos más significativos entre los que destacan las acuaporinas,^[67] las membranas comerciales como el NAFION (DuPont)^[68] o los MOFs.^[69]

- Capítulo 7: Citrato cubanos de manganeso 0-D^[70]

Al igual que en la anterior parte, esta comienza con los derivados discretos. En este caso se trata de un sólo compuesto cuya estructura consta de un cubano de citrato y manganeso que compensa su carga negativa gracias a la presencia de 4 Mn(II) por cubano que se encuentran coordinados a su periferia de modos distintos 2 a 2 (están relacionados por simetría). La primera de estas unidades es un penta-aquo manganeso (II) que se coordina a través de un enlace sencillo a un oxígeno de carboxilato externo (los que no forman los anillos quelato con el cubo). La segunda unidad es un tetra-aquo manganeso (II), coordinado a dos átomos de oxígeno de carboxilato internos, pertenecientes a diferentes citratos. Si se tratasen de oxígenos del mismo citrato, el hecho de que un carboxilato coordine a más de un centro o a uno mismo varias veces no sería nada remarcable. Sin embargo al tratarse de citratos diferentes estamos frente a modo de coordinación poco frecuente para estas unidades y que convierte al cubano, como entidad completa, en un ligando bidentado al centro de Mn(II). Además hay una molécula de agua libre en desorden por cubano.

Otro aspecto interesante de la estructura es que la distribución de las cuatro unidades Mn(II) que compensan la carga no es homogénea en torno al cubo sino que apuntan todas en una misma dirección. Debido a que la mayoría de las moléculas de agua se encuentran coordinadas a estas unidades, la red de puentes de hidrógeno formada presenta polaridad.

Por otro lado, se ha observado que el compuesto experimenta una deshidratación reversible cuando es calentado a pesar de no presentar canales o poros en su estructura. Esta transformación no se ha podido caracterizar por difracción de Rayos X de monocristal por lo que la estructura de la especie final es desconocida por el momento. Sin embargo, sí que se han realizado varios estudios de dicho proceso "in situ" a través difracción de Rayos X de polvo y TGA. Éstos muestran que la especie es estable a temperaturas inferiores a 60 °C. Por encima de esta temperatura se produce un cambio en la estructura a una temperatura de entre 64-66 °C para las condiciones de medida empleadas. A temperaturas superiores a 90 °C se produce la destrucción de la red cristalina. Si se coloca la muestra tras la transformación (antes de que se destruya la red) dentro de una atmósfera húmeda durante unos días, el producto inicial es restaurado completamente.

Conclusiones: se ha presentado el primero de una serie de compuestos basados en citrato cubanos de manganeso. Este derivado neutro, con una estructura discreta representa el primer ejemplo publicado de un complejo de MT-citrato con una estructura neutra y discreta. Al igual que los compuestos **1** y **2** no necesitan ningún otro elemento para cristalizar, los propios iones Mn(II) son capaces de actuar también como contraiones además de formar el

cubano y no es necesaria la introducción de elementos adicionales. Además de esto, el modo de coordinación del cubano como entidad única a los Mn(II) no tiene precedentes. El cubano se comporta en su totalidad como un ligando bidentado que se enlaza a un átomo de manganeso para formar un anillo quelato de 4 miembros.

A parte de esto, el compuesto experimenta una deshidratación reversible que conlleva la ruptura de enlaces covalentes que permite la salida de las aguas coordinadas a los contraiones. Esto tiene lugar en ausencia de canales o poros y preservando la integridad de la muestra. Este proceso tiene una temperatura de activación de 60 °C, por encima de la cual, solamente actúan efectos cinéticos.

- [Capítulo 8: Citrato cubanos de manganeso 1-D^{\[71\]}](#)

En línea con lo expuesto hasta ahora, en este capítulo se muestra un nuevo derivado de citrato cubanos de manganeso con una estructura polimérica 1-D formada por cadenas de cubanos unidos a través de unidades Mn(II) que completa su coordinación con moléculas de agua. Estas cadenas poliméricas aniónicas se propagan a lo largo del plano deslizador n . Hay una unidad $[\text{Mn}(\text{H}_2\text{O})_5]^{2+}$ por cubano que cuelga de un oxígeno de carboxilato. Entre las cadenas poliméricas encontramos 2 unidades $[\text{Mn}(\text{H}_2\text{O})_6]^{2+}$ compensando la carga negativa y 8 moléculas de agua libre distribuidas en 9 sitios cristalográficos.

Se observa que cuando este compuesto (**10**) se deja expuesto al aire pierde 3 moléculas de agua conservando la cristalinidad y dando lugar a la especie deshidratada **11**. Si ese mismo cristal de **11** se coloca dentro de una atmósfera húmeda durante unos días, el compuesto **10** es restaurado completamente manteniendo la cristalinidad de la muestra. Estas 3 especies se han caracterizado a través de difracción de Rayos X de monocristal empleando el mismo cristal para las 3 estructuras.

Esto es algo muy sorprendente pues no existen canales, poros o ruta posible para que estas moléculas de agua libre puedan abandonar la estructura sin dañar el cristal. Con el objetivo de averiguar el mecanismo que estaba teniendo lugar, se analizó la muestra inicial **10** mediante difracción de neutrones en el Instituto Laue-Langevin en Grenoble (France) (análisis **10n**). Tras esto, el cristal se deshidrató para llevar a cabo la rehidratación bajo una atmósfera de D₂O. El resultado de este análisis (**12**) fue todavía más sorprendente al verse que todos los H de la estructura (52, 2 por cada una de las 26 moléculas de agua inmóviles) habían sido sustituidos por D. Es obvio que las moléculas de agua que abandonan la estructura en la deshidratación entran como entidades D₂O completas, sin embargo este proceso es lo

suficientemente remoto tanto estérica como energéticamente como para no ser considerado en la explicación del intercambio de los 52 H restantes.

Estudiando la estructura **10n** en detalle se observa la presencia de cadenas de puentes de hidrógeno que corren a lo largo del cristal. Así pues, los átomos tanto de H como de D pueden saltar de una a otra, atravesando el cristal completo. Este proceso se conoce como el mecanismo de Grotthuss, el cual consta de dos pasos fundamentales, el salto de un protón de una molécula a otra y la posterior reorientación de las moléculas implicadas que deje al sistema listo para un segundo salto. Cuando se mira en detalle la estructura de la especie inicial tomada mediante difracción de neutrones se puede ver que las moléculas de agua se encuentran en desorden. Algunos átomos de oxígeno de las aguas se encuentran rodeados por 3 átomos de hidrógeno, uno de ellos con ocupación completa y los dos restantes con media ocupación. Otros, están enlazados a 4 hidrógenos, todos ellos con media ocupación. Así pues, es posible desdoblar cada molécula en dos congéneres en lo que sería una representación de las dos disposiciones que adopta la molécula de agua cuando el mecanismo de Grotthuss es operante.

El texto detalla cuidadosamente varias zonas en las que se ve de forma inequívoca como es el salto de un protón de una molécula a otra y las subsiguientes reorientaciones de las moléculas implicadas.

Conclusiones: la especie presentada en este capítulo constituye el primer ejemplo de un polímero 1-D presentado en esta tesis. A pesar de no contar con las propiedades magnéticas de los cubanos de cobalto, ha resultado presentar una característica igual o más interesante que la de sus análogos de cobalto. Al igual que la especie discreta de Mn descrita anteriormente, ésta experimenta una deshidratación reversible en condiciones suaves a temperatura ambiente. Esto tiene lugar en ausencia de canales o poros a través de los cuales el agua pueda salir o entrar en la muestra. Afortunadamente en este caso la reacción tiene lugar a través de un proceso SC-SC reversible lo que ha permitido la observación de un fenómeno totalmente inesperado.

El estudio de difracción de neutrones antes y después de la rehidratación llevada a cabo bajo atmósfera de D₂O mostró un intercambio total de H por D. Solamente los H de los grupos CH₂ de los citratos mantuvieron su identidad. Este fenómeno se explica a través del mecanismo de Grotthuss por el cual los H (o D) saltan de una molécula a otra. La reorientación de dichas moléculas tras el salto deja el sistema listo para acoger un nuevo salto. El desorden observado en torno a las aguas es el resultado de la superposición de las dos formas canónicas

del mecanismo de Grotthuss. La existencia de cadenas de puentes de hidrógeno atravesando la estructura avala esta explicación. Este es el primer ejemplo donde se observa de forma experimental e inequívoca, sin necesidad de cálculos teóricos, la manifestación de dicho mecanismo en cristales moleculares.

- **Capítulo 9: Citrato cubanos de manganeso 2-D**

Este último capítulo muestra un compuesto con una estructura bidimensional de cubanos de citrato y manganeso. La estructura del compuesto se puede describir en términos de la del compuesto anterior (**10**). Las capas aniónicas 2-D están formadas por cadenas idénticas a las presentes en el compuesto **10** unidas mediante enlaces covalentes. La especie encargada de unir las cadenas es una molécula de etilenglicol, empleado en la síntesis. La unidad terminal $[\text{Mn}(\text{H}_2\text{O})_5]^{2+}$ se coordina a un oxígeno de carboxilato diferente al que lo hace en la estructura **10**. Las moléculas de etilenglicol van desde una unidad Mn(II) puente hasta una terminal de un cubano de una cadena adyacente. La unidad Mn(II) puente entre los cubanos que propaga las cadenas 1-D, actúa como puente a 3 con una conformación *mer-*, uniendo a su vez, cadenas vecinas en el mismo plano dentro de la familia de planos (1 0 -1). En el espacio entre las capas encontramos 2 unidades hexa aquo manganeso (II) y varias moléculas de agua libre en desorden.

Se ha observado una rica red de puentes de hidrógeno entre las moléculas de agua (19 coordinadas y 6.5 libres). Todas las moléculas de agua de una celdilla unidad están conectadas a través de puentes de hidrógeno. Así pues, es posible trazar una infinidad de rutas por las cuales un átomo de H o D podría atravesar el cristal al igual que lo hacen en el compuesto **10**.

Conclusiones: El objetivo de este último capítulo es mostrar un vez más la versatilidad de los cubanos a la hora de formar nuevas estructuras, habiéndose conseguido ejemplos de prácticamente todas las dimensionalidades tanto para Mn como para Co.

A pesar de que en condiciones ambiente este compuesto no experimenta deshidratación espontánea como ocurre en el caso del compuesto **10**, existen indicios de que este derivado experimenta una transformación reversible causada por deshidratación cuando la muestra inicial es calentada. Esta especie es regenerada al colocar la muestra dentro de una atmósfera húmeda. Sin embargo los datos obtenidos son muy preliminares y no se ha obtenido información sobre la especie deshidratada.

La presencia de cadenas de puentes de hidrógeno a lo largo del cristal hacen que este derivado sea un buen candidato para continuar con los estudios de transporte protónico

iniciados con el compuesto **10**. Estos estudios podrían aportar nuevos datos ya que al no experimentar deshidratación a temperatura ambiente, los resultados nos permitirían averiguar entre otras cosas, si esta deshidratación parcial previa al intercambio es necesaria para desencadenar o no el proceso.

REFERENCIAS

- [1] P. E. Eaton, T. W. Cole, *Journal of the American Chemical Society* **1964**, *86*, 3157-&; P. E. Eaton, T. W. Cole, *Journal of the American Chemical Society* **1964**, *86*, 962-&.
- [2] L. E. Mortenson, J. E. Carnahan, R. C. Valentine, *Biochemical and Biophysical Research Communications* **1962**, *7*, 448-&.
- [3] S. Ciurli, F. Musiani, *Photosynthesis Research* **2005**, *85*, 115-131.
- [4] L. M. Rubio, P. W. Ludden, *Annual Review of Microbiology* **2008**, *62*, 93-111.
- [5] H. D. Krebs, *Biochemical Journal* **1940**, *34*, 460-463.
- [6] T. A. Hudson, K. J. Berry, B. Moubaraki, K. S. Murray, R. Robson, *Inorganic Chemistry* **2006**, *45*, 3549-3556.
- [7] M. Murrie, S. J. Teat, H. Stoeckli-Evans, H. U. Gudel, *Angewandte Chemie-International Edition* **2003**, *42*, 4653-4656.
- [8] K. W. Galloway, M. Schmidtman, J. Sanchez-Benitez, K. V. Kamenev, W. Wernsdorfer, M. Murrie, *Dalton Transactions* **2010**, *39*, 4727-4729.
- [9] E. Burzuri, J. Campo, L. R. Falvello, E. Forcen-Vazquez, F. Luis, I. Mayoral, F. Palacio, C. Saenz de Pipaon, M. Tomas, *Chemistry-a European Journal* **2011**, *17*, 2818-2822.
- [10] J. Campo, L. R. Falvello, I. Mayoral, F. Palacio, T. Soler, M. Tomas, *Journal of the American Chemical Society* **2008**, *130*, 2932-2933.
- [11] K. Robinson, G. V. Gibbs, P. H. Ribbe, *Science* **1971**, *172*, 567-&; K. Isele, F. Gigon, A. F. Williams, G. Bernardinelli, P. Franz, S. Decurtins, *Dalton Transactions* **2007**, 332-341.
- [12] J. S. Miller, A. J. Epstein, *Mrs Bulletin* **2000**, *25*, 21-28.
- [13] M. Murrie, *Chemical Society Reviews* **2010**, *39*, 1986-1995.
- [14] F. Lloret, M. Julve, J. Cano, R. Ruiz-Garcia, E. Pardo, *Inorganica Chimica Acta* **2008**, *361*, 3432-3445; J. S. Miller, A. J. Epstein, in *Materials Chemistry: an Emerging Discipline, Vol. 245* (Eds.: L. V. Interrante, L. A. Caspar, A. B. Ellis), **1995**, pp. 161-188; D. Gatteschi, *Advanced Materials* **1994**, *6*, 635-645; P. Day, A. E. Underhill, *Philosophical Transactions of the Royal Society a-Mathematical Physical and Engineering Sciences* **1999**, *357*, 2851-2853.
- [15] J. S. Miller, P. J. Krusic, A. J. Epstein, W. M. Reiff, J. H. Zhang, *Molecular Crystals and Liquid Crystals* **1985**, *120*, 27-34; J. S. Miller, J. C. Calabrese, A. J. Epstein, R. W. Bigelow, J. H. Zhang, W. M. Reiff, *Journal of the Chemical Society-Chemical Communications* **1986**, 1026-1028; J. S. Miller, *Pramana-Journal of Physics* **2006**, *67*, 1-16.
- [16] M. Tamura, Y. Nakazawa, D. Shiomi, K. Nozawa, Y. Hosokoshi, M. Ishikawa, M. Takahashi, M. Kinoshita, *Chemical Physics Letters* **1991**, *186*, 401-404.
- [17] A. J. Banister, N. Bricklebank, I. Lavender, J. M. Rawson, C. I. Gregory, B. K. Tanner, W. Clegg, M. R. J. Elsegood, F. Palacio, *Angewandte Chemie-International Edition in English* **1996**, *35*, 2533-2535.
- [18] F. Palacio, G. Antorrena, M. Castro, R. Burriel, J. Rawson, J. N. B. Smith, N. Bricklebank, J. Novoa, C. Ritter, *Physical Review Letters* **1997**, *79*, 2336-2339.
- [19] K. Awaga, E. Coronado, M. Drillon, *Mrs Bulletin* **2000**, *25*, 52-57; V. Laget, C. Hornick, P. Rabu, M. Drillon, R. Ziessel, *Coordination Chemistry Reviews* **1998**, *178*, 1533-1553.
- [20] E. Coronado, C. Marti-Gastaldo, E. Navarro-Moratalla, A. Ribera, *Inorganic Chemistry* **2010**, *49*, 1313-1315.
- [21] G. C. Defotis, F. Palacio, C. J. Oconnor, S. N. Bhatia, R. L. Carlin, *Journal of the American Chemical Society* **1977**, *99*, 8314-8315.
- [22] R. Sessoli, D. Gatteschi, A. Caneschi, M. A. Novak, *Nature* **1993**, *365*, 141-143.
- [23] B. Moubaraki, K. S. Murray, T. A. Hudson, R. Robson, *European Journal of Inorganic Chemistry* **2008**, 4525-4529; K. W. Galloway, A. M. Whyte, W. Wernsdorfer, J. Sanchez-

- Benitez, K. V. Kamenev, A. Parkin, R. D. Peacock, M. Murrie, *Inorganic Chemistry* **2008**, *47*, 7438-7442.
- [24] R. Sessoli, A. K. Powell, *Coordination Chemistry Reviews* **2009**, *253*, 2328-2341.
- [25] G. Christou, D. Gatteschi, D. N. Hendrickson, R. Sessoli, *Mrs Bulletin* **2000**, *25*, 66-71; G. S. Papaefstathiou, A. Escuer, R. Vicente, M. Font-Bardia, X. Solans, S. P. Perlepes, *Chemical Communications* **2001**, 2414-2415; E. C. Yang, W. Wernsdorfer, L. N. Zakharov, Y. Karaki, A. Yamaguchi, R. M. Isidro, G. D. Lu, S. A. Wilson, A. L. Rheingold, H. Ishimoto, D. N. Hendrickson, *Inorganic Chemistry* **2006**, *45*, 529-546.
- [26] A. Ferguson, J. Lawrence, A. Parkin, J. Sanchez-Benitez, K. V. Kamenev, E. K. Brechin, W. Wernsdorfer, S. Hill, M. Murrie, *Dalton Transactions* **2008**, 6409-6414; G. Chaboussant, A. Sieber, S. Ochsenbein, H. U. Gudel, M. Murrie, A. Honecker, N. Fukushima, B. Normand, *Physical Review B* **2004**, *70*; O. Waldmann, *Inorganic Chemistry* **2007**, *46*, 10035-10037; E. Ruiz, J. Cirera, J. Cano, S. Alvarez, C. Loose, J. Kortus, *Chemical Communications* **2008**, 52-54; N. Ishikawa, M. Sugita, W. Wernsdorfer, *Angewandte Chemie-International Edition* **2005**, *44*, 2931-2935; C.-I. Yang, W. Wernsdorfer, G.-H. Lee, H.-L. Tsai, *Journal of the American Chemical Society* **2007**, *129*, 456-457; C. J. Milios, A. Vinslava, W. Wernsdorfer, S. Moggach, S. Parsons, S. P. Perlepes, G. Christou, E. K. Brechin, *Journal of the American Chemical Society* **2007**, *129*, 2754-+.
- [27] T. Lis, *Acta Crystallographica Section B-Structural Science* **1980**, *36*, 2042-2046; R. Bagai, G. Christou, *Chemical Society Reviews* **2009**, *38*, 1011-1026; P. Artus, C. Boskovic, J. Yoo, W. E. Streib, L. C. Brunel, D. N. Hendrickson, G. Christou, *Inorganic Chemistry* **2001**, *40*, 4199-4210; M. Soler, P. Artus, K. Folting, J. C. Huffman, D. N. Hendrickson, G. Christou, *Inorganic Chemistry* **2001**, *40*, 4902-4912; N. E. Chakov, W. Wernsdorfer, K. A. Abboud, G. Christou, *Inorganic Chemistry* **2004**, *43*, 5919-5930; C. Boskovic, M. Pink, J. C. Huffman, D. N. Hendrickson, G. Christou, *Journal of the American Chemical Society* **2001**, *123*, 9914-9915; H. B. Heersche, Z. de Groot, J. A. Folk, H. S. J. van der Zant, C. Romeike, M. R. Wegewijs, L. Zobbi, D. Barreca, E. Tondello, A. Cornia, *Physical Review Letters* **2006**, *96*; A. Caneschi, D. Gatteschi, C. Sangregorio, R. Sessoli, L. Sorace, A. Cornia, M. A. Novak, C. Paulsen, W. Wernsdorfer, *Journal of Magnetism and Magnetic Materials* **1999**, *200*, 182-201; M. Soler, W. Wernsdorfer, K. A. Abboud, J. C. Huffman, E. R. Davidson, D. N. Hendrickson, G. Christou, *Journal of the American Chemical Society* **2003**, *125*, 3576-3588; E. Coronado, A. Forment-Aliaga, A. Gaita-Arino, C. Gimenez-Saiz, F. M. Romero, W. Wernsdorfer, *Angewandte Chemie-International Edition* **2004**, *43*, 6152-6156; A. Forment-Aliaga, E. Coronado, M. Feliz, A. Gaita-Arino, R. Llusar, F. M. Romero, *Inorganic Chemistry* **2003**, *42*, 8019-8027; K. Wieghardt, K. Pohl, I. Jibril, G. Huttner, *Angewandte Chemie-International Edition in English* **1984**, *23*, 77-78; C. Delfs, D. Gatteschi, L. Pardi, R. Sessoli, K. Wieghardt, D. Hanke, *Inorganic Chemistry* **1993**, *32*, 3099-3103; E. Ruiz, J. Cano, S. Alvarez, *Chemistry-a European Journal* **2005**, *11*, 4767-4771.
- [28] G. P. Guedes, S. Soriano, N. M. Comerlato, N. L. Speziali, P. M. Lahti, M. A. Novak, M. G. F. Vaz, *European Journal of Inorganic Chemistry* **2012**, 5642-5648; E. C. Yang, D. N. Hendrickson, W. Wernsdorfer, M. Nakano, L. N. Zakharov, R. D. Sommer, A. L. Rheingold, M. Ledezma-Gairaud, G. Christou, *Journal of Applied Physics* **2002**, *91*, 7382-7384.
- [29] L. R. Falvello, E. Forcen-Vazquez, I. Mayoral, M. Tomas, F. Palacio, *Acta Crystallographica Section C-Crystal Structure Communications* **2011**, *67*, M359-M363.
- [30] D. Wu, D. Guo, Y. Song, W. Huang, C. Duan, O. Meng, O. Sato, *Inorganic Chemistry* **2009**, *48*, 854-860.
- [31] F. Kloewer, Y. Lan, J. Nehr Korn, O. Waldmann, C. E. Anson, A. K. Powell, *Chemistry-a European Journal* **2009**, *15*, 7413-7422.

- [32] Y.-Z. Zhang, W. Wernsdorfer, F. Pan, Z.-M. Wang, S. Gao, *Chemical Communications* **2006**, 3302-2006.
- [33] M.-H. Zeng, M.-X. Yao, H. Liang, W.-X. Zhang, X.-M. Chen, *Angewandte Chemie-International Edition* **2007**, *46*, 1832-1835.
- [34] Y. Gao, G.-F. Xu, L. Zhao, J. Tang, Z. Liu, *Inorganic Chemistry* **2009**, *48*, 11495-11497; D. Savard, P.-H. Lin, T. J. Burchell, I. Korobkov, W. Wernsdorfer, R. Clerac, M. Murugesu, *Inorganic Chemistry* **2009**, *48*, 11748-11754.
- [35] H. Oshio, N. Hoshino, T. Ito, M. Nakano, *Journal of the American Chemical Society* **2004**, *126*, 8805-8812.
- [36] D. Venegas-Yazigi, J. Cano, E. Ruiz, S. Alvarez, *Physica B-Condensed Matter* **2006**, *384*, 123-125; S. Hameury, L. Kayser, R. Pattacini, G. Rogez, W. Wernsdorfer, P. Braunstein, *Dalton Transactions* **2013**, *42*, 5013-5024.
- [37] C. Aronica, Y. Chumakov, E. Jeanneau, D. Luneau, P. Neugebauer, A.-L. Barra, B. Gillon, A. Goujon, A. Cousson, J. Tercero, E. Ruiz, *Chemistry-a European Journal* **2008**, *14*, 9540-9548.
- [38] S. M. J. Aubin, M. W. Wemple, D. M. Adams, H. L. Tsai, G. Christou, D. N. Hendrickson, *Journal of the American Chemical Society* **1996**, *118*, 7746-7754.
- [39] P. L. Feng, C. C. Beedle, W. Wernsdorfer, C. Koo, M. Nakano, S. Hill, D. N. Hendrickson, *Inorganic Chemistry* **2007**, *46*, 8126-8128.
- [40] C. Aronica, G. Chastanet, G. Pilet, B. Le Guennic, V. Robert, W. Wernsdorfer, D. Luneau, *Inorganic Chemistry* **2007**, *46*, 6108-6119.
- [41] M. Clemente-Leon, H. Soyer, E. Coronado, C. Mingotaud, C. J. Gomez-Garcia, P. Delhaes, *Angewandte Chemie-International Edition* **1998**, *37*, 2842-2845; M. Clemente-Leon, E. Coronado, A. Soriano-Portillo, C. Mingotaud, J. M. Dominguez-Vera, *Advances in Colloid and Interface Science* **2005**, *116*, 193-203; M. Cavallini, M. Facchini, C. Albonetti, F. Biscarini, *Physical Chemistry Chemical Physics* **2008**, *10*, 784-793; M. Clemente-Leon, E. Coronado, C. L. Gomez-Garcia, C. Mingotaud, S. Ravaine, G. Romualdo-Torres, P. Delhaes, *Chemistry-a European Journal* **2005**, *11*, 3979-3987.
- [42] D. G. Kurth, P. Lehmann, D. Volkmer, H. Colfen, M. J. Koop, A. Muller, A. Du Chesne, *Chemistry-a European Journal* **2000**, *6*, 385-393; D. G. Kurth, P. Lehmann, D. Volkmer, A. Muller, D. Schwahn, *Journal of the Chemical Society-Dalton Transactions* **2000**, 3989-3998; D. Volkmer, A. Du Chesne, D. G. Kurth, H. Schnablegger, P. Lehmann, M. J. Koop, A. Muller, *Journal of the American Chemical Society* **2000**, *122*, 1995-1998; M. Clemente-Leon, E. Coronado, A. Soriano-Portillo, E. Colacio, J. M. Dominguez-Vera, N. Galvez, R. Madueno, M. T. Martin-Romero, *Langmuir* **2006**, *22*, 6993-7000; D. W. Britt, D. Mobius, V. Hlady, *Physical Chemistry Chemical Physics* **2000**, *2*, 4594-4599.
- [43] J. Means, V. Meenakshi, R. V. A. Srivastava, W. Teizer, A. Kolomenskii, H. A. Schuessler, H. Zhao, K. R. Dunbar, *Journal of Magnetism and Magnetic Materials* **2004**, *284*, 215-219; V. Meenakshi, W. Teizer, D. G. Naugle, H. Zhao, K. R. Dunbar, *Solid State Communications* **2004**, *132*, 471-476.
- [44] A. Cornia, A. C. Fabretti, M. Pacchioni, L. Zobbi, D. Bonacchi, A. Caneschi, D. Gatteschi, R. Biagi, U. Del Pennino, V. De Renzi, L. Gurevich, H. S. J. Van der Zant, *Angewandte Chemie-International Edition* **2003**, *42*, 1645-1648; M. Cavallini, G. Aloisi, R. Guidelli, *Langmuir* **1999**, *15*, 2993-2995; A. Cornia, A. C. Fabretti, M. Pacchioni, L. Zobbi, D. Bonacchi, A. Caneschi, D. Gatteschi, R. Biagi, U. del Pennino, V. De Renzi, L. Gurevich, H. S. J. Van der Zant, *Journal of Magnetism and Magnetic Materials* **2004**, *272*, E725-E726; C. D. Bain, E. B. Troughton, Y. T. Tao, J. Evall, G. M. Whitesides, R. G. Nuzzo, *Journal of the American Chemical Society* **1989**, *111*, 321-335; D. M. Seo, V. Meenakshi, W. Teizer, H. Zhao, K. R. Dunbar, *Journal of Magnetism and Magnetic Materials* **2006**, *301*, 31-36; R. E. Holmlin, X. X. Chen, R. G. Chapman, S. Takayama, G. M. Whitesides, *Langmuir* **2001**, *17*, 2841-2850; E. Coronado, A. Forment-Aliaga, F. M. Romero, V. Corradini, R. Biagi, V. De Renzi, A. Gambardella, U. del Pennino, *Inorganic Chemistry*

- 2005**, *44*, 7693-7695; G. G. Condorelli, A. Motta, I. L. Fragala, F. Giannazzo, V. Raineri, A. Caneschi, D. Gatteschi, *Angewandte Chemie-International Edition* **2004**, *43*, 4081-4084; B. Fleury, L. Catala, V. Huc, C. David, W. Z. Zhong, P. Jegou, L. Baraton, S. Palacin, P. A. Albouy, T. Mallah, *Chemical Communications* **2005**, 2020-2022; R. V. Martinez, F. Garcia, R. Garcia, E. Coronado, A. Forment-Aliaga, F. M. Romero, S. Tatay, *Advanced Materials* **2007**, *19*, 291-+; L. Zobbi, M. Mannini, M. Pacchioni, G. Chastanet, D. Bonacchi, C. Zanardi, R. Biagi, U. Del Pennino, D. Gatteschi, A. Cornia, R. Sessoli, *Chemical Communications* **2005**, 1640-1642.
- [45] D. Braga, F. Grepioni, *Angewandte Chemie-International Edition* **2004**, *43*, 4002-4011.
- [46] L. R. MacGillivray, G. S. Papaefstathiou, *Encyclopedia of Supramolecular Chemistry*, **2004**.
- [47] I. C. Paul, D. Y. Curtin, *Science* **1975**, *187*, 19-26.
- [48] P. A. Ramachandran, L. K. Doraiswamy, *Aiche Journal* **1982**, *28*, 881-900.
- [49] A. Orita, L. S. Jiang, T. Nakano, N. C. Ma, J. Otera, *Chemical Communications* **2002**, 1362-1363; I. Tsukushi, O. Yamamuro, H. Suga, *Thermochimica Acta* **1992**, *200*, 71-86; F. Toda, K. Tanaka, A. Sekikawa, *Journal of the Chemical Society-Chemical Communications* **1987**, 279-280; F. Toda, H. Miyamoto, *Chemistry Letters* **1995**, 861-861; A. J. Schultz, G. D. Stucky, R. H. Blessing, P. Coppens, *Journal of the American Chemical Society* **1976**, *98*, 3194-3201; Rosenber.B, L. Vancamp, J. E. Trosko, V. H. Mansour, *Nature* **1969**, *222*, 385-&; V. P. Balema, J. W. Wiench, M. Pruski, V. K. Pecharsky, *Chemical Communications* **2002**, 1606-1607; G. W. Wang, K. Komatsu, Y. Murata, M. Shiro, *Nature* **1997**, *387*, 583-586; K. Komatsu, G. W. Wang, Y. Murata, T. Tanaka, K. Fujiwara, K. Yamamoto, M. Saunders, *Journal of Organic Chemistry* **1998**, *63*, 9358-9366.
- [50] G. Kaupp, *Current Opinion in Solid State & Materials Science* **2002**, *6*, 131-138.
- [51] K. Tanaka, F. Toda, *Chemical Reviews* **2000**, *100*, 1025-1074.
- [52] V. Kohlschütter, P. Haenni, *Vol. 105, Zeitschrift für anorganische und allgemeine Chemie*, **1918**, pp. 121-144; V. Ramamurthy, K. Venkatesan, *Chemical Reviews* **1987**, *87*, 433-481.
- [53] M. A. Collins, D. P. Craig, *Chemical Physics* **1981**, *54*, 305-321; D. P. Craig, C. P. Mallett, *Chemical Physics* **1982**, *65*, 129-142; D. P. Craig, R. N. Lindsay, C. P. Mallett, *Chemical Physics* **1984**, *89*, 187-197; K. Norris, P. Gray, D. P. Craig, C. P. Mallett, B. R. Markey, *Chemical Physics* **1983**, *79*, 9-19.
- [54] M. D. Cohen, *Angewandte Chemie-International Edition in English* **1975**, *14*, 386-393; M. D. Cohen, *Molecular Crystals and Liquid Crystals* **1979**, *50*, 1-10.
- [55] M. D. Cohen, G. M. J. Schmidt, F. I. Sonntag, *Journal of the Chemical Society* **1964**, 2000-&; G. M. J. Schmidt, *Journal of the Chemical Society* **1964**, 2014-&; G. Wegner, *Zeitschrift Fur Naturforschung Part B-Chemie Biochemie Biophysik Biologie Und Verwandten Gebiete* **1969**, *B 24*, 824-&; J. W. Lauher, F. W. Fowler, N. S. Goroff, *Accounts of Chemical Research* **2008**, *41*, 1215-1229; H. Manohar, *Journal of the Indian Institute of Science* **1975**, *57*, 468-488; Soderqui.R, B. Dickens, *Journal of Physics and Chemistry of Solids* **1967**, *28*, 823-&; J. F. Goodman, *Proceedings of the Royal Society of London Series a-Mathematical and Physical Sciences* **1958**, *247*, 346-&; K. Lonsdale, E. Nave, J. F. Stephens, *Philosophical Transactions of the Royal Society of London Series a-Mathematical and Physical Sciences* **1966**, *261*, 1-&; P. Pfeiffer, E. Breith, E. Lubbe, T. Tsumaki, *Justus Liebigs Annalen Der Chemie* **1933**, *503*, 84-130.
- [56] Z. Yin, M. Zeng, *Science China-Chemistry* **2011**, *54*, 1371-1394; Z. Su, M. Chen, T.-a. Okamura, M.-S. Chen, S.-S. Chen, W.-Y. Sun, *Inorganic Chemistry* **2011**, *50*, 985-991; T. Zhang, Y. Lu, Z. Zhang, Q. Lan, D. Liu, E. Wang, *Inorganica Chimica Acta* **2014**, *411*, 128-133; G. Kaupp, *Angewandte Chemie-International Edition in English* **1992**, *31*, 592-595; G. Kaupp, *Angewandte Chemie-International Edition in English* **1992**, *31*, 595-598.

- [57] M. Kawano, M. Fujita, *Coordination Chemistry Reviews* **2007**, *251*, 2592-2605; M. P. Suh, Y. E. Cheon, *Australian Journal of Chemistry* **2006**, *59*, 605-612; G. J. Halder, C. J. Kepert, *Australian Journal of Chemistry* **2006**, *59*, 597-604.
- [58] B. Kirchner, *Chemphyschem* **2007**, *8*, 41-43; C. Dellago, M. M. Naor, G. Hummer, *Physical Review Letters* **2003**, *90*; J. Halding, P. S. Lomdahl, *Physical Review A* **1988**, *37*, 2608-2613.
- [59] K. D. Kreuer, A. Rabenau, W. Weppner, *Angewandte Chemie-International Edition in English* **1982**, *21*, 208-209; G. A. Luduena, T. D. Kuehne, D. Sebastiani, *Chemistry of Materials* **2011**, *23*, 1424-1429.
- [60] B. Jaselskis, C. E. Moore, A. Von Smolinski, *Abstracts of Papers of the American Chemical Society* **2007**, *233*, 651-651; S. Cukierman, *Biochimica Et Biophysica Acta-Bioenergetics* **2006**, *1757*, 876-885.
- [61] O. Markovitch, H. Chen, S. Izvekov, F. Paesani, G. A. Voth, N. Agmon, *Journal of Physical Chemistry B* **2008**, *112*, 9456-9466; A. A. Kornyshev, A. M. Kuznetsov, E. Spohr, J. Ulstrup, *Journal of Physical Chemistry B* **2003**, *107*, 3351-3366; T. J. F. Day, U. W. Schmitt, G. A. Voth, *Journal of the American Chemical Society* **2000**, *122*, 12027-12028; J. F. Nagle, H. J. Morowitz, *Proceedings of the National Academy of Sciences of the United States of America* **1978**, *75*, 298-302.
- [62] M. Eigen, *Angewandte Chemie-International Edition* **1964**, *3*, 1-&; M. L. Huggins, *Journal of Physical Chemistry* **1936**, *40*, 723-731.
- [63] N. Agmon, *Chemical Physics Letters* **1995**, *244*, 456-462; N. Agmon, S. Y. Goldberg, D. Huppert, *Journal of Molecular Liquids* **1995**, *64*, 161-195; N. Agmon, *Israel Journal of Chemistry* **1999**, *39*, 493-502; N. Agmon, *Journal De Chimie Physique Et De Physico-Chimie Biologique* **1996**, *93*, 1714-1736; J. Lobaugh, G. A. Voth, *Journal of Chemical Physics* **1996**, *104*, 2056-2069; M. Tuckerman, K. Laasonen, M. Sprik, M. Parrinello, *Journal of Chemical Physics* **1995**, *103*, 150-161; S. Cukierman, *Biophysical Journal* **2000**, *78*, 1825-1834; S. Lengyel, J. Tamas, J. Giber, *Acta Chimica Academiae Scientiarum Hungaricae* **1962**, *32*, 429-&; D. A. Lown, H. R. Thirsk, *Transactions of the Faraday Society* **1971**, *67*, 132-&; D. A. Lown, H. R. Thirsk, *Transactions of the Faraday Society* **1971**, *67*, 149-&; B. B. Owen, F. H. Sweeton, *Journal of the American Chemical Society* **1941**, *63*, 2811-2817; A. Chernyshev, R. Pomes, S. Cukierman, *Biophysical Chemistry* **2003**, *103*, 179-190.
- [64] R. Car, M. Parrinello, *Physical Review Letters* **1985**, *55*, 2471-2474.
- [65] U. W. Schmitt, G. A. Voth, *Journal of Chemical Physics* **1999**, *111*, 9361-9381.
- [66] U. W. Schmitt, G. A. Voth, *Journal of Physical Chemistry B* **1998**, *102*, 5547-5551.
- [67] M. Amiry-Moghaddam, O. P. Ottersen, *Nature Reviews Neuroscience* **2003**, *4*, 991-1001; C. Maurel, *Annual Review of Plant Physiology and Plant Molecular Biology* **1997**, *48*, 399-429; C. Maurel, L. Verdoucq, D.-T. Luu, V. Santoni, in *Annual Review of Plant Biology*, Vol. 59, **2008**, pp. 595-624; A. S. Verkman, *Journal of Cell Science* **2005**, *118*, 3225-3232.
- [68] P. Commer, A. G. Cherstvy, E. Spohr, A. A. Kornyshev, *Fuel Cells* **2003**, *2*, 127-136; R. S. Yeo, *Journal of the Electrochemical Society* **1983**, *130*, 533-538; S. J. Paddison, R. Paul, *Physical Chemistry Chemical Physics* **2002**, *4*, 1158-1163.
- [69] C. Duan, M. Wei, D. Guo, C. He, Q. Meng, *Journal of the American Chemical Society* **2010**, *132*, 3321-3330.
- [70] L. R. Falvello, E. Forcen-Vazquez, F. Palacio, S. Sanz, M. Tomas, *Dalton transactions (Cambridge, England : 2003)* **2014**, *43*, 10700-10704.
- [71] S. C. Capelli, L. R. Falvello, E. Forcen-Vazquez, G. J. McIntyre, F. Palacio, S. Sanz, M. Tomas, *Angewandte Chemie (International ed. in English)* **2013**, *52*, 13463-13467.

[B3] R. L. Carlin, *Magnetochemistry*, Springer-Verlag, Berlin Heidelberg New York Tokio 1986

[B4] D. Gatteschi, R. Sessoli, J. Villain, Oxford University Press, 2006. ISBN: 9780199602261

